CONSTITUTIVE MODELING FOR BIODEGRADABLE POLYMERS

FOR APPLICATION IN ENDOVASCULAR STENTS

A Dissertation

by

JOÃO FILIPE DA SILVA SOARES

Submitted to the Office of Graduate Studies of
Texas A&M University
in partial fulfillment of the requirements for the degree of

DOCTOR OF PHILOSOPHY

May 2008

Major Subject: Mechanical Engineering

CONSTITUTIVE MODELING FOR BIODEGRADABLE POLYMERS

FOR APPLICATION IN ENDOVASCULAR STENTS

A Dissertation

by

JOÃO FILIPE DA SILVA SOARES

Submitted to the Office of Graduate Studies of
Texas A&M University
in partial fulfillment of the requirements for the degree of

DOCTOR OF PHILOSOPHY

Approved by:

Co-Chairs of Committee,	Kumbakonam R. Rajagopal
	James E. Moore, Jr.
Committee Members,	Jay D. Humphrey
	Joseph E. Pasciak
Head of Department,	Dennis O'Neal

May 2008

Major Subject: Mechanical Engineering

ABSTRACT

Constitutive Modeling of Biodegradable Polymers

for Application in Endovascular Stents. (May 2008)

João Filipe da Silva Soares, Licenciatura, Universidade Técnica de Lisboa

Co-Chairs of Advisory Committee: Dr. K. R. Rajagopal

Dr. James E. Moore, Jr.

Percutaneous transluminal balloon angioplasty followed by drug-eluting stent implantation has been of great benefit in coronary applications, whereas in peripheral applications, success rates remain low. Analysis of healing patterns in successful deployments shows that six months after implantation the artery has reorganized itself to accommodate the increase in caliber and there is no purpose for the stent to remain, potentially provoking inflammation and foreign body reaction. Thus, a fully biodegradable polymeric stent that fulfills the mission and steps away is of great benefit.

Biodegradable polymers have a widespread usage in the biomedical field, such as sutures, scaffolds and implants. Degradation refers to bond scission process that breaks polymeric chains down to oligomers and monomers. Extensive degradation leads to erosion, which is the process of mass loss from the polymer bulk. The prevailing mechanism of biodegradation of aliphatic polyesters (the main class of biodegradable polymers used in biomedical applications) is random scission by passive hydrolysis and results in molecular weight reduction and softening.

In order to understand the applicability and efficacy of biodegradable polymers, a two pronged approach involving experiments and theory is necessary. A constitutive model involving degradation and its impact on mechanical properties was developed through an extension of a material which response depends on the history of the motion and on a scalar parameter reflecting the local extent of degradation and depreciates the mechanical properties. A rate equation describing the chain scission process confers characteristics of stress relaxation, creep and hysteresis to the material, arising due to the

entropy-producing nature of degradation and markedly different from their viscoelastic counterparts.

Several initial and boundary value problems such as inflation and extension of cylinders were solved and the impacts of the constitutive model analyzed. In vitro degradation of poly(L-lactic acid) fibers under tensile load was performed and degradation and reduction in mechanical properties was dependent on the mechanical environment. Mechanical testing of degraded fibers allowed the proper choice of constitutive model and its evolution. Analysis of real stent geometries was made possible with the constitutive model integration into finite element setting and stent deformation patterns in response to pressurization changed dramatically as degradation proceeded.

To my dearest Filipa Arinto

ACKNOWLEDGMENTS

I am truly indebted to Dr. Rajagopal, the Abbé Faria of my Chateau d'If, for granting me this unique opportunity of learning from him. He is the utmost contributor to my development, not only on the academic level but also from a personal standpoint. During my five years being his apprentice, mechanics, mathematics, their history and intricate connections were presented to me in novel ways, either at his insightful lectures or during meetings in his office. Most important of all is his ability to present himself as a followable role model and his uncharacteristic stance of "always question authority". I am sure that I will not find such anywhere else.

Dr. Moore and his pragmatic knowledge helped me to look at my research from the practical standpoint, functioning almost as the perfect balance between theory and practice. I thank him for all the important opportunities for the development of an academic career with all the posters, presentations, and grant writing. I am also grateful for all the resources needed for my research, and most of all, his teachings on his savvy of the academic world. My courtesy should also be extended to his family for making times away from mine so much more bearable.

I must thank Dr. Jay Humphrey and Dr. Joe Pasciak for serving on my committee. I also thank Dr. Luís Faria and Dr. Adélia Sequeira for all the support needed to seize this opportunity. My thanks should also be extended to Dr. Luoyi Tao, Dr. Arun Srinivasa, Dr. John Criscione, Dr. Theofanis Strouboulis and Dr. Raytcho Lazarov for the useful discussions. The experimental part of my work would never be possible without Dr. Melissa Grunlan, Yaping You and Dirk Rosenstock. Thanks must also be extended to Dr. Jay Walton for substituting for my defense.

I am grateful to my parents, sister and friends for offering their kind words of encouragement and support. I thank Dr. Moore's lab mates Mike Moreno, Clark Meyer, Julian Bedoya, Luke Timmins, Shiva Yazdani, Ellie Rahbar as well as other journal club members; and Dr. Rajagopal's fellow graduate students, Krishna Kannan, Sharat Prasad, Anand Mohan, Wakar Malik, Parag Ravindran, Sai Krishna and all others not listed but

not forgotten. Finally, I thank Timothy Forrest and his family for serving as such outstanding hosts of the United States of America.

TABLE OF CONTENTS

LIST OF FIGURES

Page

LIST OF TABLES

CHAPTER I

INTRODUCTION

Since the introduction of balloon angioplasty by Dotter in the 1960s [1], catheter-based technologies have improved health care for atherosclerosis. Well over a million balloon dilatations were performed by the early 1990s and as of today more than 600,000 a year are carried out in coronary arteries alone [2]. Yet by 1980, after more than 20 years of clinical experience and many catheter designs, angioplasty was far from being perfect and the incidence of restenosis remained unchanged. Many studies reported acute thrombogenic complications in 3 to 5% of the patients and restenosis rates at 3 to 6 months between 25 to 50% [3,4]. Restenosis seemed to be largely independent of the technique, device, or the clinician's skill [5-7]. The pathophysiology of restenosis is complex and incompletely understood. Early events in restenosis are thought to consist of immediate elastic recoil, platelet deposition, and thrombus formation, followed by smooth muscle cell proliferation and extra cellular matrix formation [8-10].

A. Cardiovascular stents

Percutaneous implantation of metallic stents in the coronary vessels was first performed in humans in 1987 by Sigwart et al. [11]. During the late 1990s, stents revolutionized the field of interventional cardiology and stent implantation has become the new standard in angioplasty procedure [12]. The expansion of the artery with the balloon, followed by the implantation of the permanent, metallic scaffolding provided by the stent, results in a treatment option that is much less invasive, and requires much less recovery time. Since its first inception, stent technology advancement has led to stents that are more easily delivered in tortuous arteries through better flexibility and larger expansion ratios. There have been 21 balloon expandable stents and 28 self-expanding

This dissertation follows the style of International Journal of Non-Linear Mechanics.

stents approved by the FDA for human use since 1994. Stents account for more than $4 billion per year in sales, with that number expected to double by 2010.

The major design concept behind cardiovascular stents was to prevent post-traumatic vasospasm [11]. Besides keeping the artery patent immediately after intervention, a stent also tackles injured flaps of the lumen preventing downstream embolic complications [13,14]. Although the concept seemed to be flawless and a significant reduction of the incidence of restenosis was promptly reported [15,16], all cardiovascular stents have two distinct and significant modes of chronic failure. Immediately after deployment acute thrombosis can occur due to the thrombogenic aspect of the stent promoting a foreign body response, but it can be promptly treated with anticoagulant drug therapy [17]. Also the most critical failure mode is in-stent restenosis which still occurs at intolerable rates. Despite the success and growth of stent implantation procedures, there are patients in whom in-stent restenosis is a chronic and recurrent problem [18]. The mechanism of in-stent restenosis can be obviously related with restenosis after angioplasty and has been shown to be neointimal proliferation in response to an non-homeostatic mechanical environment [19] and not chronic stent recoil [20].

Other common mode of stent failure is through strut fracture. Especially in peripheral applications the stent is subjected to cyclic deformations of large amplitude and its stability is becoming increasingly critical [21]. In coronary applications, fracture is less common but still occurs [22].

1. Responses to stenting

The reaction of the artery to a stent is a multistage process [23]. First, the exposure of the sub-endothelium and the stent material to the blood stream activates platelets and leads to thrombus formation. This process is initiated immediately after deployment and the extent to which the thrombus deposition occurs is highly correlated not only with the surface characteristics of the stent but also with its design. Areas of flow stagnation, which depend heavily on strut spacing design, influence the degree of

platelet adhesion [24]. The second stage is inflammation. Stenting overstretches and may even rupture the internal elastic membrane inducing leukocyte adhesion and consequent inflammatory reaction [25]. The peak of this process occurs approximately one week after deployment. Deposits of surface adherent and tissue infiltrating monocytes can be seen around stent struts, demonstrating the degree to which the struts are injuring the wall. These monocytes release cytokines, mitogens, and tissue growth factors that further increase neointimal formation [26]. The third stage is the proliferation of vascular smooth muscle cells in the media and neointima. This process can be thought as the short-term response to the change in hemodynamics and to the new mechanical environment the artery wall experiences after stent placement [27,28]. Cellular proliferation and extracellular matrix production provides additional tissue to shore up stress concentration due to stent deployment [29,30]. The final stage of arterial adaptation is remodeling. One can think of this phase as the artery's attempt to reach a new homeostatic state in the presence of the persistent injury and change in the normal environment caused by the stent [31].

Systematically administered pharmaceutical agents, besides pre- and post-interventional anticoagulant therapies, fail to prevent restenosis because the tolerated dose for such agents is too low to achieve a sufficient drug concentration at the targeted site [32]. The problem of in-stent restenosis is currently being addressed by coating stents with polymers in which drugs can be impregnated and locally delivered. Polymers provide a stable medium into which drugs can be either uniformly distributed or surface layered and then locally released over a specific and controlled period of time, usually between weeks to months [33]. The first reports of local drug delivery in the cardiovascular system date back only to the mid 1990s with forskolin [34] and heparin [35]. Success with anti-inflammatory dexamethasome was reported by Lincoff et al. in 1997 [36]. Suppression of restenotic proliferative stimuli was achieved by Yamawaki et a. in 1998 [37]. Successful gene transfer and expression following implantation of polymer stents impregnated with a recombinant adenovirus gene was demonstrated by Ye et a. in 1998 [38].

The objective of the pharmacological agents used in drug eluting stents is to address a particular stage of the restenotic cascade: heparin is loaded into stents in order to inhibit the thrombus formation [35] and inflammation is usually prevented with dexamethasome [36]. The most effective drugs are antimitotic agents that minimize the proliferation stage. As of now, the two most effective and well-studied pharmacological agents for this outcome are paclitaxel and sirolimus. Paclitaxel inhibits microtubule depolymerization, and thereby has potent effects in cell division and migration [39]. Sirolimus is a macrolide antibiotic with potent antiproliferative effects on vascular smooth muscle cells preventing the initiation of DNA synthesis [40,41].

2. Drug eluting stents

The use of drug eluting stents generally improves the success of coronary stenting. In fact, drug eluting stents are now considered general practice [42]. Several randomized studies have been carried out and are still ongoing with the objective of evaluating the efficacy of the drugs with regard to their release kinetics, effective dosage, and the benefit of such particular pharmacological approach [43]. Two major randomized trials have been carried out: the RAVEL randomized trial (with several follow up SIRIUS studies) employed sirolimus eluting stents initially showed a promising zero restenosis at six months in 238 patients [44,45], and good results all across the most common subsets of patients and lesion types [45-47]; the TAXUS series of randomized trials with a paclitaxel eluting stent also exhibited good restenosis results [48-50]. As of today, only two polymer-coated drug eluting stents (Cypher[TM] Sirolimus eluting stent from Cordis, Johnson & Johnson, Miami Lake, FL, USA, and the Taxus[TM] paclitaxel eluting stent, Boston Scientific, Natick, MA, USA) are commercially available in the US. Several registries are in effect in several European countries [51-53] (less data is available on the paclitaxel eluting stent: Cypher[TM] was introduced in 2002 and Taxus[TM] in 2003) and show similar results with regard to the two stents and good "real world" success rates ($\approx$ 1% stent thrombosis, $\approx$ 10% angiographic restenosis, $\approx$ 7% target lesion revascularization) [54].

More recently, two more drugs were added to the list of smooth muscle cell proliferation inhibitors used with drug eluting stents: everolimus and ABT-578. Everolimus traces back to the start of the drug eluting stent as being a sirolimus analog [55], was initially developed by Guidant, Santa Clara, CA, USA [56], and is currently being clinically investigated by Abbot Vascular, Santa Clara, CA, USA, with the XIENCE V^{TM} everolimus eluting coronary stent [57]. The interesting fact about this drug is that it has been used in conjunction with a new biodegradable polymer coating and gave promising results in initial clinical studies [58,59]. The FUTURE I and II trials reported the common improved results of the everolimus eluting stent when compared with bare metal stents [60]. Recently, Ormiston et al. reported the first-in-human implantation of a fully bioabsorbable everolimus eluting stent with a poly-L-lactic acid backbone [61]. Although the properties of the stent are usually inferior when compared with a metal counterpart, there were no adverse events in-hospital or by 1-month. The ABSORB trial with 54 patients undergoing the deployment of the fully biodegradable stent showed that the in vivo stent recoil is slightly larger but insignificantly different from that of the coated stent, implying that the fully biodegradable may have good radial strength similar to the metallic stent [62].

ABT-578, more commonly known by zotarolimus, is another pharmacological agent with both antiproliferative and anti-inflammatory properties and is being advocated as the promising successor of sirolimus and paclitaxel [63]. The Endeavor^{TM} drug eluting stent (Medtronic Vascular, Santa Rosa, CA, USA) represents the combination of zotarolimus, a low-profile cobalt alloy stent platform, and a phosphorylcholine drug carrier system [64]. Two randomized trials have been reported with this stent: although one case of subacute thrombosis following implantation was reported [65], the ENDEAVOR II trial suggest that the usage of this stent might reduce the rates of clinical and angiographic restenosis and stent thrombosis at 9, 12 and 24 months when compared with bare metal counterparts [66], but slightly worse results were observed when compared with sirolimus eluting stents [67]. Recent news report

that the Endeavor[TM] zotarolimus eluting stent was recently approved by the FDA in February of 2008.

Despite these impressive numbers, drug eluting stents are not without their problems. Delayed stent thrombosis due to incomplete endothelialization of the stent struts is still a problem with stents, either drug eluting or not [68-70], where problems are exacerbated on the former because of the inherent antiproliferative agents being delivered [71]. The "catch-up" effect after the complete elution of the drug raised some concerns [72], and the lack of long-term follow up studies still haunts this technology. Another limitation is the emphasis given to drug eluting stents in coronaries; only a limited amount of data exists on their application in peripheral arteries. The SIROCCO trials, with sirolimus eluting stents deployed in long lesions in peripheral arteries, showed promising short-term results (6% restenosis at 6 months) but no difference relative to bare metal stents after 18 months [73,74]. Thus, the drug eluting stent revolution has not translated into clinical success for peripheral applications. The fact that current drug eluting stents employ cytostatic agents may be partially responsible. These agents can delay re-endothelialization of the stented artery, which is more important in peripheral arteries.

The physiologic situation in peripheral arteries is quite different from the coronary arteries. The arteries of the legs, for example, feature flows that oscillate strongly between forward and retrograde. Distal runoff can also be poor (low mean flow). These factors result in low and oscillating wall shear stress, conditions that have been linked to early, focal atherogenesis in every commonly diseased artery [75-77]. There is also evidence that low and oscillating wall shear stress correlates with intimal hyperplasia development in by-pass graft anastomoses [78]. There are also unique solid mechanical challenges in the leg arteries that result from the large deformations that occur due to limb movements such as hip and knee flexion [79]. These deformations have in fact been linked to fractures of stent struts and associated clinical failures. This, along with the clinical evidence that current drug eluting stents do not perform well in peripheral applications, suggests that alternative strategies are required.

B. Biodegradable stents

There are some theoretical concerns with metallic stents: (i) most metals are positively charged, resulting in high thrombogenicity [80]; (ii) in addition, metal stents remain in the body indefinitely and many interfere with future clinical procedures [81]; and (iii) due to their microstructural properties, metals are not feasible materials to act as loadable drug carriers. All these problems have encouraged significant efforts in the development of new stent materials, either used in coatings [82] or in stents completely made of polymeric materials [83]. Polymers can also act as optimal carriers for the controlled release of drugs [84].

1. Polymeric stents

One possible objective of coating a metal stent is to diminish its thrombogenic properties [85]. Experience with Nylon™, silicone, polyurethane, and other materials have been reported in the literature since the beginning of the 1990s [86]. Either naturally occurring polymers (fibrin [87]) or pharmacological agents (heparin [88], dexamethasome [36], and others [89]) relevant to the local biochemistry of the lesion were tested in vivo as coatings. The use of polymers in stent coatings requires less mechanical requisites from the polymer by itself and shifts the attention mostly to biocompatibility and to manufacturability. Still, poor adherence of the coating to the metal, possible delamination with strain, or damage during implantation are problems that still occur [90].

Interest in polymeric stents started in the 1990s. Significant progress has been achieved in increasing the level of biocompatibility of polymers tailoring surface characteristics and mechanical strength through advancements in polymerization procedures and processing techniques [84]. In 1992, Murphy et al. [91] demonstrated the technical feasibility of polyethylene terephthalate stents but obtained poor results in porcine coronaries, particularly an intense proliferative neointimal response that resulted in complete vessel occlusion. On the other hand, around the same time, van der Giessen et al. [92] showed acceptable results with stents made of the same material deployed in

the same animal model. The extent of neointimal proliferation was similar to that observed after the placement of bare metal stents (obviously, compared with the standards of that time prior to the drug eluting stent revolution), despite the presence of a more pronounced inflammatory reaction [93]. Later in 1996, van der Giessen et al. [94] investigated the biocompatibility of an array of both biodegradable and non-biodegradable polymers (poly(glycolic acid), poly (lactic acid), polycaprolactone, poly(hydroxybutyrate valerate), polyorthoester, poly(ethylene oxide), and poly(butylene terephthalate)) for stent coating and found a marked inflammatory reaction with subsequent neointimal thickening in all of them. The experimental procedure used was inappropriate, in that stents were not sterilized before implantation [95]. The biocompatibility of these polymers has been proven in other in vivo and in vitro tests [85,96].

Because of this general disagreement on the cardiovascular biocompatibility of polymers, the idea of either biodegradable or biostable polymers, which had considerable appeal during the early 1990s, was set aside. The interest peaked in 1994 with Zidar's chapter included in the 2nd edition of the Textbook of Interventional Cardiology dedicated in full to the topic of biodegradable stents [97]. Later in 2000, Tamai et al. should be credited with rekindling the resurgence of the interest in employing fully biodegradable stents. They provided the first report on the immediate and six-month results after implantation of biodegradable poly(L-lactic acid) stents in humans [98]. With their good initial results (obviously, compared with the standards before the drug eluting stents era), the motivation for fully biodegradable stents was flourishing once again [99].

2. Concept of biodegradable stents

The rationale behind biodegradable stents can be simply explained in the wonderful allegory by Colombo and Karvouni in their 2000 Circulation editorial [100]: "in 458 BC, a prominent Roman leader named Lucius Quinctius Cincinnatus was unique in his behavior. Cincinnatus served his country when he was needed and, after fulfilling

his duty, he returned to his private life". More than 2000 years after, George Washington is parallelized with Cincinnatus when he withdrew from politics and returned to his farm [101]. Like Cincinnatus or Washington, "a biodegradable stent fulfills the mission and steps away" [100]. Because the development of restenosis usually happens during the first six months after deployment [102,103], a permanent stent that is in place beyond this initial period has no clear function.

However, it is worth recognizing that besides leading to unpredictable complications (e.g. stent failure due to fatigue, obstacles for other treatments, and infection due to the presence of a foreign body inside the lumen and after re-endothelialization inside the artery wall), there are no demonstrable clinical complications with a permanent endovascular stent.

Thus, the question should be turned around and one should ask what the advantages of a temporary stent are [100]. The answer is manyfold: (i) if a stent degrades and is absorbed by the body it will not be an obstacle for future treatments; (ii) if a stent degrades in a controlled manner, its desired failure can be predicted and prescribed; (iii) also, the gradual softening of the stent would permit a smooth transfer of the load from the stent to the healing wall; (iv) because of the inherent viscoelastic behavior of most polymers, a less-chronic deployment could be designed, preventing artery injury characteristic of balloon angioplasty; (v) the degradation of the polymeric material may act as an optimal vehicle for specific therapy with drugs or genes, and (vi) a response to pulsatile flow closer to the physiological response of an healthy artery can be achieved with the inherent softness of a biodegradable stent.

Also, there are some drawbacks with regard to permanent metal stents that biodegradable stents would not have. Metal stents remain inside the body indefinitely, becoming a potential nidus for infection [104], and can be an adverse obstacle for subsequent treatments making bypass surgery almost the only hope for treatment of in-stent restenosis [81].

3. Design of biodegradable stents

A significant challenge in the development of a novel biodegradable stent is the lack of precise engineering modeling tools [105]. Essentially, three different steps are usually taken in the design of such devices.

Firstly, only a limited number of biodegradable materials have been tried, and in many cases the materials are picked based on designer's past experience [106,107]. Scant data is available on the mechanical behavior of biodegradable polymers undergoing degradation. In most studies, emphasis is given to chemical quantities or phenomenological measurements. Examples are the temporal evolution of molecular weight (either averages or distributions) and quantification of mass loss over time. This results in a considerable amount of uncertainty with regard to the design of a biodegradable stent.

Secondly, the usual procedure is to pick pre-existing metallic stent designs and manufacture them with biodegradable materials. There are some concerns with manufacturing and sterilization of these polymeric devices when compared with stainless steel counterparts because polymers cannot usually be processed using metal stent techniques [108]. Also, the usual forms of solid polymers are fibers, films, or matrices. From these building blocks, the stent must be woven or assembled. The sophistication of the existing designs is variable, ranging from the simplest single fiber helicoidal stents [109] to the more complex interwoven stents [108,110,111].

The last step is then to conduct experiments, either in vivo [112,113] or in vitro [114,115], analyze the results, and draw conclusions. Computational simulations with biodegradable stents are either non-existent or simplistic in virtue of the inability to account for the complexity of the constitutive modeling of the biodegradable material. Grabow et al. [116] used a finite element analysis to investigate the mechanical properties of a balloon-expandable poly(L-lactic acid) stent under various load conditions, whereas Nuutinen et al. [117] used an analytical method for calculating the mechanical properties of braided stents. Both models consider the polymer as being a linearized elastic material with no effect due to degradation being taken into account.

Because of this inductive way of dealing with the problem, the number of materials and designs used in biodegradable stents is as large as the number of people working in the field. Certain main trends can be identified: (i) biodegradable stents made of bioerodible metals, for example, magnesium [118,119] (a choice that evolved from corrodible iron [120]), are currently under study and have shown encouraging results, especially in below-the-knee applications; (ii) natural polymers such as type I collagen were used to make tubes [121] and chitosan, a polysaccharide present in the exoskeleton of crustaceans, was employed in a self-expanding helical coil stent [122]; and lastly, (iii) a somewhat large number of biodegradable polymers were tried, more commonly aliphatic polyesters (e.g. poly(glycolic acid) or poly(lactic acid)) [84,123].

Poly(L-lactic acid) is the most commonly used of all these polymers. It was used in the Duke stent [81,114,124], and is being used in the Igaki-Tamai stent [98,125-127], by Eberhart et al. in their biodegradable stent [38,111,115,128], and in the Tampere stent for urethral applications [110,129-131].

Unfortunately, almost all of these previous studies focused on the chemical aspects of degradation and not in the mechanical changes occurring during degradation. Regardless of the material that the stent is made of, the issue of structural integrity is the most important factor for its performance. Structural collapse can take place if weakness occurs in particular regions, so understanding the impact of degradation on local mechanical properties should be the ultimate goal of biodegradable stent design. Obviously, this question does not have an easy answer. Lastly, drug delivery modeled with diffusion kinetics is another important aspect that needs to be addressed and is closely related with degradation, erosion, and mechanical response.

C. Polymer degradation

The number, availability, and utilization of synthetic biodegradable polymers have increased dramatically over the last 50 years, with applications ranging from the field of agriculture to biomedical devices. The first reported biomedical application of biodegradable polymers was absorbable sutures in the 1970s [132], and this remains

today to be the most widespread use of this family of materials. After 30 years of growth and development, many other absorbable internal fixation devices have become available to the practicing surgeon, such as pins, screws, suture anchors, and osteosynthesis plates [133]. Biodegradable polymers have been chosen to be the optimal carries for local drug delivery [134] and are widely used in tissue engineering applications [135]. The interest in these applications continues to increase as the number of biodegradable polymers evaluated with respect to the concept of biomaterials increases [136]. However, the number of compounds having reached the stage of clinical and commercial applications is still very small [137].

Basically, one can distinguish between the two major applications for biodegradable polymers in the medical field. When used for prosthetic purposes in orthopedics, the contribution of the polymer is required for a limited period of time, notably the healing time, and the polymer can be engineered to degrade at a rate that will transfer load to the healing bone [138]. Also, there is no need for a second surgical event for removal [139]. To accomplish all of these requirements, the main concern behind the design of the device is its load-bearing capability as well as its evolution during degradation over time. On the other hand, for drug delivery implants, the attention is shifted to delivery kinetics and their changes during the course of degradation. The case of a biodegradable drug eluting stent is a bridge connecting the two approaches: the stent must perform mechanically, maintaining the artery patent and restoring the blood flow immediately after deployment and during degradation, and at the same time be capable of effective drug delivery.

1. Terminology

Longman Dictionary of Contemporary English defines degradation as "the change from a chemical compound to a simpler one". The prefix bio- is defined as "concerning living things". It is important to make distinctions between the different terminologies often encountered in the literature. Biodegradable polymers are polymers that are decomposed in the living body but whose degradation products remain in the

tissues long-term. On the other hand, bioresorbable polymers can be defined as polymers that degrade after implantation into non-toxic products which are then eliminated from the body or metabolized therein. Although this last term is more precise, it is often used interchangeably with other terms, including absorbable, resorbable, bioabsorbable, and biodegradable [107].

In their book, Biodegradable Polymers and Plastics, Ottenbrite et al. [140] present a discussion aimed at settling the terminology for such class of polymers. The conclusion of the discussion board was a set of working definitions. Polymer degradation is a deleterious change in properties due to a change in its chemical structure. A biodegradable polymer is a polymer in which the degradation is mediated at least partially by a biological system. Also, a distinction between degradation and erosion was made. Degradation, defined as the change in chemical structure, is a process different from erosion, defined to be the process of dissolution or wearing away of a polymer. Thus, a bioabsorbable polymer automatically implies degradation mediated by a biological system as well as its erosion into non-toxic products that will be then absorbed by the body.

More precisely, polymer degradation is the chain scission process that breaks polymer chains down to oligomers and finally monomers, ultimately resulting in a decrease of molecular weight. Degradation leads to erosion, which is the process of material loss from the polymer bulk. Such materials can be monomers, oligomers, parts of the polymer backbone, or even parts of the polymer bulk.

Thus, degradation and erosion are distinct but related processes [141]. It is worth noting that all polymers undergo backbone scission; that is, all polymers "degrade". Only the time they require for degradation is different, and it can range from hours in the case of the hydrolytic degradation of poly-anhydrides, to many years for poly-amines [142]. The relationship between the actual life of the polymer and the intended life to perform its function will ultimately dictate the distinction between a polymer being degradable or non-degradable.

2. Mechanisms of polymer degradation

Polymers degrade by several different mechanisms, depending on their inherent chemical structure and on the environmental conditions to which they are subjected. Degradation results from an irreversible change in the material which eventually leads to its breakdown or failure. There are five major mechanisms of polymer degradation: thermal, radiation induced, mechanical, enzymatic, and chemical [143].

Covalent bonds of the backbone chain of the polymer have a limited strength. In thermal degradation, scission is due to the highly excited vibrational state of bonds attained with increases in temperature. When energy associated with the vibrational state overcomes the bond dissociation energy, scission, i.e. degradation, occurs. Although these processes cause rapid decomposition of polymers only at elevated temperatures (around 500 ºC), the pronounced temperature dependence of the rates of chemical reactions can cause a significant and rather rapid degradation already under milder conditions [144]. Radiation induced degradation occurs when polymers undergo chemical reactions upon irradiation with ultraviolet or gamma radiation [145]. In generally isothermal biomedical applications, such as endovascular biodegradable stents, thermal degradation and radiation induced degradation are assumed not to be relevant.

Mechanical degradation of polymers comprises a large number of different phenomena, ranging from fracture to chemical changes induced by the mechanical environment. Mechanical degradation has been utilized for processing natural rubber since the middle of the 19th century in a process called mastication and usually carried out on roll mills or in plasticators. In the presence of air it leads to a marked decrease in the average molecular weight of the rubber thus increasing its plasticity [146]. Degradation of polymers in solution can be obtained with high-speed stirring, shaking, flowing through capillaries, turbulent flow, or ultrasonic treatment.

Before discussing various important aspects of mechanical degradation of polymers, it should be pointed out that under the influence of mechanical stress low molecular weight compounds generally exhibit a different behavior to polymers, i.e. normally they do not undergo chemical changes if subjected to stress. Assemblies of low

molecular weight molecules respond to applied stress by loosening intermolecular bonds resulting, macroscopically, in a deformation, and microscopically, in a displacement of molecules. Under the influence of shearing forces, intermolecular interactions between certain molecules at certain sites are disrupted and new interactions become operative after the displacement [145]. Cracking crystals or amorphous specimens of low molecular weight compounds generally does not lead to the formation of free radicals, whereas free radicals are detected in polymers after the mechanical treatment indicating rupture of chemical bonds [147].

Mechanical energy transferred to a polymeric system can be dissipated via two main relaxation processes: enthalpy relaxation, defined to be the slippage of chains relative to surrounding molecules and entropy relaxation, changes in chain conformation. These relaxations are harmless to the polymer because they do not induce chemical changes and are the microstructural mechanism behind the classical theory of rubber elasticity [148]. In competition with these relaxation mechanisms, the scission of chemical bonds can occur. Obviously, the probability for bond scission should increase as relaxation is impeded. A single, generally applicable mechanism of stress-induced chemical reactions does not appear to exist. It seems that different bond scission mechanisms are operative depending on the state of the polymer (glass, rubbery, or molten) and the mode of imposition of stress. In solid polymers, fracture planes and voids might give rise to the rupture of chemical bonds. In the rubbery state or molten in solution, inter- and intra-chain entanglements might cause stretching of parts of the macromolecules, resulting eventually in bond scission. Strain is a prerequisite for bond rupture in polymer chains regardless of the state of the material; that is, bond rupture occurs when sufficient energy is concentrated in a certain segment of a macromolecule as a consequence of a non-uniform distribution of internal stresses [145].

Enzymatic degradation in the human body is mainly relevant for natural polymers such as proteins, polysaccharides, or poly(β-hydroxy esters), for which specific enzymes exist [142]. Chemical degradation is a general classification of molecular weight reduction due to chemical reactions that start spontaneously when certain low

molecular weight compounds are brought into contact with the polymer [145]. Oxidation and hydrolysis are classic examples of chemical degradation.

3. Degradation of aliphatic polyesters

The prevailing mechanism of biological degradation for synthetic biodegradable aliphatic polyesters is scission of the hydrolytically unstable backbone chain by passive hydrolysis, because for most of them, no specific enzymes exist [149]. By tailoring the polymer backbone with hydrolysable functional groups, the polymer chains become labile to an aqueous environment and their ester linkages are cleaved by absorbed water [150]. For semi-crystalline polymers, hydrolysis occurs in two distinct stages: initially, water penetrates the polymer, preferentially attacking the more accessible chemical bonds in the amorphous phase and converting long polymer chains into shorter, ultimately water soluble fragments [143]. Because the amorphous phase is degraded in the first place, there is a reduction in molecular weight without a loss of apparent physical properties as the polymer matrix is still held together by the crystalline regions. The reduction in molecular weight is soon followed by a reduction in physical properties as water begins to fragment the polymer bulk [151,152].

There two key factors that influence the rate of this reaction: co-polymer composition and water uptake [143]. Water adsorption, the first step of degradation, is dependent on the polymer hydrophilicity. Poly(lactic acid) degrades slower compared to poly(glycolic acid) due to its pendant methyl groups, which makes the ester bonds less susceptible to hydrolysis and diminishes water adsorption. Increasing the content of lactic acid in poly(lactic/glycolic acid) copolymers has also been shown to decrease the rate of biodegradation [153]. Morphology similarly controls degradation due to its influence on water adsorption and bond availability. Because water is less able to penetrate crystalline regions, these tend to degrade slower than the amorphous regions. Poly(glycolic acid) is highly crystalline (~50%) as is the stereoregular poly(L-lactic acid) (~40% crystalline), but crystallinity is disrupted in copolymers and its amorphous

nature produces faster rates of biodegradation. For instance, a copolymer of 50% glycolic acid and 50% D,L-lactic acid degrades faster than either homopolymer [154].

Other factors can also be relevant: (i) residual monomer concentration was found to enhance hydrolytic degradation of poly(DL-lactic acid) [155]; (ii) lower pH and autocatalysis by residual monomers increase the rate of degradation, especially inside polymer matrixes where acidic byproducts of degradation are trapped [156]; (iii) higher temperatures leading to transition to the rubbery state or simply by increasing chain flexibility promoting water penetration [144]; (iv) the chemical environment obtained through the encapsulation of ionic salts that will impart changes in the water uptake and rate of hydrolysis [157]; and (v) higher molecular weights have a higher probability of undergoing hydrolytic bond scission than lower molecular weight polymers [153,158].

On the other hand, although the number of factors that influence degradation might be large, under the conditions of interest only a few might be relevant. Moreover, inherent chemical and physical changes to the polymer and to the surrounding environment might have a substantial feedback on the degradation rate [142].

4. *Influence of the mechanical environment on degradation*

The influence of the mechanical environment in the rates of degradation of stable polymers has long been understood and addressed by the polymer physics and chemistry community, especially for dilute polymers under solution with application as drag reducers in turbulent flows or as viscosity index improvers for motor oils [159]. Shear degradation seems to be the best understood: chain scission appears to be a non-random process with higher probability of breakage of the bond at the midpoint of the chain. It shows narrowing of the poly-dispersity index principally through the degradation of the larger molecules. Shear stress was found to be the controlling parameter for degradation and an undegradable molecular weight, at which molecules will not degrade any further, is also observed for a broad class of polymers [160-162].

On the other hand, the application of these concepts to biodegradable medical polymers, which per se show unquestionably chain scission by chemical degradation and

are designed to perform under mild to severe loading conditions, the research has been scant.

Miller and Williams [163] in 1984 reported one of the initial studies on the effect of imposed strain on the degradability of a commercially available poly(glycolic acid) used for surgical sutures. A special device (suited either for in vitro, in aqueous media, and in vivo, implanted subcutaneously in rabbits) was designed such that the sutures could be maintained under a state of strain. 25% and 50% of the breaking strain of the non-degraded material were applied uniaxially and stress relaxation was observed during degradation – after 14 to 21 days all tension had been lost in both in vivo and in vitro experiments. Degradation was accessed by measurements of the load at break and it was found that the rate of hydrolysis was affected by the magnitude of the imposed strain. They also noticed an initial increase in breaking load in both experiments.

It seems that Chu [164] in 1985 was the first to portrait a coupling the between mechanical environment and the hydrolytic degradation rate of aliphatic polyesters. The development of synthetic biodegradable sutures (made of poly(glycolic acid)), a common practice since late 1960s, prompted a series of investigations on their biodegradable phenomena both in in vivo and in vitro situations. Sutures can be subjected to various degrees of external stress and strain when surgeons pull them taut during tying knots, when patients cough, or when wounds develop severe edema. Chu reported that strained fibers degraded faster than unstrained ones, and the magnitude of degradation depended on the level of the strain applied and the duration of immersion [164]. Moreover, a possible microstructural mechanism for semi-crystalline polymers was proposed: as stress or strain is applied to the material, the segments of long chain that transverse the amorphous phase in between two crystalline blocks become uncoiled and taut; not only taut segments have an higher probability of being broken, but when degradation occurs it creates void spaces in the amorphous regions that allow more water to penetrate and accelerate hydrolytic degradation [164].

Zhong et al. [165] in 1993 followed the same procedure, i.e. imposing a 4% strain, with a slightly different suture material (90-10% poly(glycolic-lactic acid)) and

more experimental resources. After two weeks of accelerated degradation in hydrogen peroxide (which allows hydrolysis and oxidation mechanisms to coexist), they concluded that the degradation of the suture under strain was much faster than without strain. Furthermore, the applied strain itself, in the absence of a chemical environment, did not change the mechanical properties of the suture. More recently, Deng et al. [166] investigated the effect of stress in the rate of hydrolysis in a similar 90%-10% poly(glycolic-lactic acid) co-polymer. In a creep experiment, they subjected 0.3 mm diameter fibers to uniaxial extension by prescribing constant loads of 0.2 N, 0.4 N, and 0.8 N that corresponded to 0.25%, 0.5% and 1% of the non-degraded tensile breaking strength. Contrary to the previous studies, they found that external loading did not affect degradation, quantified by decrease in breaking strength, Young's modulus and breaking strain, but it can surely be attributed to the very small differences in the amounts of loads used. With a completely different polymer, polyurethane (on which the degradation mechanism is oxidation), Wiggins et al. [167] found that the degradation rate of polyurethane increased with increasing cyclic strain rate, whereas strain magnitude had essentially no effect. Their experiments employed a circular membrane device in which pressure was applied to one side of the membrane, causing it to deflect into a well. This deformation applies bi-axial strain to the membrane in the middle region, and largely uniaxial strain in the outer region. In a separate study, the same group demonstrated that polymer in the cyclic uniaxial strain region degraded at the same rate as unstressed and constant stress controls. However, polymer from the biaxial strain region degraded at a much higher rate [168].

D. Erosion and elimination

The diffusion of water into the polymer bulk and polymer degradation compete against each other in the process of polymer erosion. Erosion is the process of dissolution or wearing away of a polymer and is by far much more complex than degradation inasmuch as the number of parameters that potentially might influence the process is considerably larger.

Two different main types of erosion can be distinguished. If degradation is fast, the diffusing water is absorbed quickly by hydrolysis and hindered from penetrating deep into the polymer bulk. In this case, degradation and consequently erosion are restricted to the surface of the polymer, a phenomenon referred to as heterogeneous or surface erosion [169]. This type of erosion changes if degradation is slower than the rate of diffusion of water though the polymer. In this case water cannot be absorbed quickly enough to be hindered from reaching deep into the polymer and the polymer degrades and erodes through its entire swollen cross-section, a behavior which has been termed homogeneous or bulk erosion [169]. It must be stressed, however, that surface or bulk erosion are two extremes and the erosion mechanism in a degradable polymer usually shows characteristics of both. In addition to water diffusion and bond stability, other factors such as polymer morphology (crystalline or amorphous) or water uptake which depend on the hydrophilicity of the polymer affect the hydrolysis rate or the swelling rate and consequently the erosion behavior substantially [170].

As should be expected, many different types of morphological changes occur upon erosion. An increase in surface roughness and the formation of cracks, macropores and micropores are common phenomena observed in degrading polymers. Erosion fronts, which separate eroded from non-eroded polymer, have been reported for surface eroding polymers such as polyanhydrides [171]. In contrast, inversely moving erosion fronts have been observed in poly(DL-lactic acid) [172], where hydrolysis rate is dramatically increased inside eroding polymer matrices due to the autocatalytic activity of monomers that have been created and are trapped inside [156]. Due to the preference for the amorphous phase, the degree of crystallinity of degradable polymers can change tremendously during erosion [173]. Additional changes in crystallinity are a consequence of the recrystallization of small chain oligomers and monomers [174].

Elimination is the concluding stage of the complete function of a biodegradable implant. The obvious requirement is to have a polymer that is biocompatible during the whole time of permanence inside the body as well as its breakdown products being eliminated through normal metabolic pathways in a non-toxic manner [97]. The

biocompatibility of aliphatic polyesters, especially poly(lactic acid) and poly(glycolic acid), is well established in the literature [175-177]. On the other hand, the elimination of byproducts of degradation and erosion appears to follow different mechanisms for different polymers. Ultimately, the elimination involves the solubilization of the degradation products which are then carried away from the implantation site and eliminated [171]. The surrounding tissue (in the case of a biodegradable stent, the artery wall) must be capable of absorption, digestion, and elimination of the resulting oligomers and monomers [178]. The last step is the removal of these waste products from the blood. Lysosomal digestion is the major pathway for elimination of polymers that cannot be excreted directly via the kidney [179].

E. Models of degradation and erosion

Theoretical models to predict polymer degradation and erosion would seem to be important tools for a number of different applications. If drug elution is to be part of the therapy, drug delivery profiles should be programmable at the design stage. For orthopedic applications, load-bearing capabilities as well as their evolution with time must be determined. A drug eluting biodegradable stent should ideally be designed accounting for all these criteria.

1. Models for polymer degradation

Hydrolysis degradation is the breakage of backbone bonds caused by incoming water and is a phenomenon that occurs at the molecular level [180]. It is a very intricate process, as a variety of different degradation mechanisms can occur simultaneously and concurrently. Also, the reactivity of each bond might be equal when considered individually, but the large number of repeating units and their inherent steric environment, weak links, and branches may influence the local rate of reaction. Experiments with gel permeation chromatography provide data to model the mechanism of degradation [181,182].

The task of obtaining kinetic parameters from a change in molecular weight distribution is not trivial and has been tackled since the beginning of polymer chemistry. Basically, three approaches have been applied to resolve this problem. The first, pioneered by Kuhn [183] and Montroll and Simha [184], used combinatorial statistics to derive analytical solutions of the change in the dispersity index as a function of the extent of degradation. The probability of hydrolysis of a particular bond is expressed as a distribution function (commonly random scission, central Gaussian, or parabolic) and for some limited initial distributions exact solutions for the whole molecular weight distribution can be obtained [184-186]. Unfortunately, the applicability of such elegant exact solutions to real systems is limited essentially due to simplifying assumptions necessary for the analytical treatment of the problem.

The second technique relies on the system of differential equations which describe the depolymerization rates of individual bonds during the degradation process. In principle, any chemical reaction could be described by a set of differential kinetic equations that upon integration yield the time evolution of the molecular weight distribution for any arbitrary degradation scheme. Such a procedure, however, is impracticable in view of the enormous number of coupled differential equations which is necessarily involved in a macromolecular system. First-order degradation rates with respect to reactant concentrations and the absence of recombination reactions are necessary requirements to obtain a linear system and hence the existence of a general analytical solution of the system of kinetic equations [187]. The former hypothesis usually holds for many systems whereas the latter is usually excessively strong for most of degradation schemes. Nevertheless, a complete kinetic scheme includes all the individual rate constants for each reacting bond, which represents thousands of differential equations even for modest size macromolecules; for practical purposes a lumping procedure is commonly used, i.e. the maximum degree of polymerization is divided into a set of equidistant molecular weights, each set with an associated depolymerization rate and a kinetic differential equation [181].

A third method employing Monte Carlo techniques is used in order to overcome the simplifying assumptions of the previous approaches [188]. Although the use of Monte Carlo method to solve chemical kinetics problems dated back to the 50s, only with the advent of the computer its application to the polymer field saw a dramatic increase. Monte Carlo or other more complex techniques are applied to populations of simple polymers to predict the theoretical evolution of molecular weight averages or distributions [189,190]. While being a versatile tool capable of handling complex reactions in a straightforward manner, however realistic simulations require excessive amount of computational resources. Furthermore, due to computational limits, Monte Carlo results are subjected to large statistical errors [182].

Other degradation models sharing characteristics of the methods above have been reported [191-193]. Lastly, complex degradation schemes depicting possible mechanisms can be developed and computationally solved to obtain realistic molecular weight distribution evolutions [194,195].

2. *Models for polymer erosion*

Erosion is the dissolution of oligomers and monomers resulting from degradation and is a much more complex phenomenon to model, not only because of the interplay between different physical mechanisms as well as due to the dramatic changes that occur upon erosion. Two main approaches can be currently identified: models based on differential equations that consider the erodible material as a continuum where species dissolve and diffuse; and models based on statistics that describe degradation and erosion as a probabilistic event.

Joshi and Himmelstein first proposed a reaction-diffusion model for degradation and drug release, consisting of Fick's law of diffusion coupled with a reaction equation describing the kinetics of the degradation mechanism [196]. Theoretical results for drug release, water penetration, and erosion were obtained as a consequence of degradation and were corroborated with experimental results [196,197]. One drawback of this model is that it did not take into account changes in the microstructure caused by the

preferential degradation and consequent degradation of the amorphous phase compared with the crystalline phase. Similar methods based on diffusion equations that account degradation, erosion and drug release in more complex systems have been developed [198-200]

Gopferich and Langer developed different models for erosion [201]. They describe erosion as being a probabilistic event and the polymer matrix as a grid of pixels. Monte Carlo simulations coupled with a reaction equation describing random scission were performed. Different properties can be assigned to each pixel, so a distinction between the crystalline and amorphous phase was considered [202]. By removing eroded pixels continuously from the grid, temporal evolutions of a degradable polymer matrix can be determined stochastically. From such simulations, many experimentally measurable parameters can be calculated, such as porosity or weight loss. Erosion fronts and erosion modes can also be inferred from the results of the simulation [203]. The fit of experimental data allows the determination of the erosion rate constants and demonstrates that the stochastic model is quite well able to adjust the experimental data. Later models by the same group included diffusion equations to obtain results on the release of drugs through the pores [204].

3. Models for mechanical properties reduction

Up until now, most of the research efforts on biodegradable polymers were directed experiments and product development. A fair amount of experimental data concerning biodegradable polymers exists, ranging from evolutions of molecular weight averages or distributions, mass loss, and amount of drug eluted. Because of the complexity of these materials and the variety of processes to which they are subjected, the modeling effort has been very limited. The existing models are based on widely different approaches, certainly driven by the field of application. Erosion and drug elution for drug delivery implants and are far better understood when compared to the impact of degradation on the load-bearing performance in orthopedic applications, usually based on phenomenological models with data from in vitro and in vivo

experiments. Any previous study of the impact of degradation and erosion on the mechanical response of polymers seems not to exist.

As can be expected, the biodegradation of the polymers that constitute a stent depend on two classes of factors: the mechanical environment and the biochemical environment. One could easily imagine an astonishingly large number of parameters in these broad categories that potentially could influence the degradation, ranging from the local states of stress or strain the material is subjected to, to the concentration of a particular compound present in the degradation environment. Besides degradation modeling (how the polymer chains are broken) and erosion modeling (how monomeric and oligomeric products are washed out), the modeling of the mechanical response is equally relevant. To know how degradation influences the mechanical response and how the mechanical environment influences the degradation and erosion mechanisms requires a significant effort. This dissertation reports the development of constitutive models for biodegradable polymeric materials, which are aimed at developing a tool for biodegradable stent design.

CHAPTER II

PRELIMINARIES

In this chapter the notation and terminology that is used in this dissertation is introduced. While initially its main objective was to render this dissertation self-contained with the least amount of space and time consumed, it soon became a personal review of the formalism of the field, which was imbibed by me during the recent years.

Motions, measures of strain and Cauchy's stress theory are summarized and balance laws stated. The restrictions imposed on constitutive relations by the second law of thermodynamics and material frame indifference are referred. Some important inequalities restricting the response functions of elastic materials are listed. To conclude the chapter, simple materials and some classical particularizations are recorded.

The program presented here draws heavily from [205] and [206]. Its results will be presented without derivation and can be found in [205-209]. Mathematical terminology, tensor calculus, and analysis are presented extensively in introductory books [210,211].

A. Kinematics

Kinematics is defined as the study of changes in positions with time. Motions can only be defined with the aid of some reference, as bodies should always be referred to be in motion relative to other bodies. Kinematics comprises not only the study of the current state of a body and its time rates of change, but also its history up to some current time.

1. Bodies, motions and configurations

A body $\mathcal{B}$ is set that has topological structure and a measure structure. The elements of the body are called particles. Usually bodies are mapped onto regions of the three-dimensional Euclidean space $\mathcal{E}$. An image of $\mathcal{B}$ is called a configuration $\kappa(\mathcal{B})$

and the mapping is called a placer κ. A necessary condition is that placers are one-to-one in the correspondence between members of $\mathcal{B}$ and members of $\kappa(\mathcal{B})$, i.e. particles onto places in the Euclidean space.

A one-to-one mapping $\chi: \mathcal{B} \times \mathcal{I} \rightarrow \mathcal{E}$, where $\mathcal{I} = (-\infty, t_0)$ for some t_0,

$$\mathbf{x} = \chi(X, t),\tag{2.1}$$

is called a motion of $\mathcal{B}$. X is the particle, t the time, and $\mathbf{x}$ the place in Euclidean space that particle X occupies at time t. The configuration of body $\mathcal{B}$ and part $\mathcal{P} \subseteq \mathcal{B}$ at time t are $\kappa_t(\mathcal{B})$ and $\kappa_t(\mathcal{P})$. Only smooth motions in the sense that χ is differentiable with respect to X and t as many times as needed will be considered.

The velocity $\mathbf{v}$ and the acceleration $\mathbf{a}$ of the particle X at time t are defined as the 1st and 2nd material time derivative of the motion, i.e.

$$\mathbf{v} = \dot{\mathbf{x}} = \frac{\mathrm{d}}{\mathrm{d}t}\mathbf{x} = \frac{\partial}{\partial t}\chi(X, t),\tag{2.2}$$

$$\mathbf{a} = \ddot{\mathbf{x}} = \frac{\mathrm{d}}{\mathrm{d}t}\dot{\mathbf{x}} = \frac{\partial^2}{\partial t^2}\chi(X, t).\tag{2.3}$$

It is convenient to select one particular configuration and refer everything concerning the body to that configuration. This configuration is called the reference configuration $\kappa_R(\mathcal{B})$, and κ_R is the placer that maps the body to the reference configuration. Then, the mapping

$$\mathbf{X} = \kappa_R(X)\tag{2.4}$$

gives the place $\mathbf{X}$ occupied by the particle X in the reference configuration $\kappa_R(\mathcal{B})$. Since mapping (2.4) is smooth, its inverse exists and the particle X that is at place $\mathbf{X}$ in the reference configuration is given by

$$X = \kappa_R^{-1}(\mathbf{X}).\tag{2.5}$$

Hence, the motion (2.1) may be written in the form

$$\mathbf{x} = \chi(\kappa_R^{-1}(\mathbf{X}),t) \equiv \chi_{\kappa_R}(\mathbf{X},t) . \tag{2.6}$$

The 2nd term of equation (2.6) considers motions in a slightly different way, i.e. as mappings of places of $\kappa_R(\mathcal{B})$ onto places of $\kappa_t(\mathcal{B})$. The reference configuration provides a way to label particles and equation (2.6) gives the place $\mathbf{x}$ at time t of the particle X that in the reference configuration is at $\mathbf{X}$. The choice of reference configuration is arbitrary, being the initial, or the undeformed, or a stress free configuration, usual choices to be taken as reference configurations.

Fields, either scalar, or vectorial, or tensorial, can be described with respect to any configuration of the body. A scalar valued field f describing a property of the body and its particles during a motion can be expressed either with respect to particles, places in the reference configuration, or places in the current configuration, i.e.

$$f = f(X,t) = \tilde{f}(\mathbf{X},t) = \bar{f}(\mathbf{X},t) , \tag{2.7}$$

where the relationship between the functions in equation (2.7) can be obtained with mappings (2.1), (2.4), and the corresponding inverses. Furthermore, (2.7) assigns a value of the property f to particle X at time t. The first description is called the material description, the second is called referential or Lagrangian description as it assigns the value at time t of the property f corresponding to the particle labeled as $\mathbf{X}$ in $\kappa_R(\mathcal{B})$, and the last is called spatial or Eulerian description as it assigns the value of f to the particle that is at $\mathbf{x}$ at time t.

2. *Measures of deformation*

The deformation gradient $\mathbf{F}_{\kappa_R}$, the linear approximation of the mapping χ_{κ_R}, is defined to be the referential gradient of the motion, i.e.

$$\mathbf{F}_{\kappa_R} = \mathrm{Grad}\, \chi_{\kappa_R} \equiv \frac{\partial \mathbf{x}}{\partial \mathbf{X}} . \tag{2.8}$$

The dependence on the choice of κ_R is stressed. An isochoric motion, i.e. volume preserving, is such that the Jacobian of the motion is

$$J \equiv \det \mathbf{F}_{\kappa_R} = 1 \tag{2.9}$$

for all time $t \in \mathcal{I}$.

Usually, the deformation gradient is represented with the aid of the polar decomposition theorem: for any non-singular 2$^{\text{nd}}$ order tensor $\mathbf{F}$, there exists a unique representation given by

$$\mathbf{F} = \mathbf{RU} = \mathbf{VR} \tag{2.10}$$

where $\mathbf{R}$ is an orthogonal tensor, and $\mathbf{U}$ and $\mathbf{V}$ are positive definite symmetric tensors.

The left and right Cauchy-Green stretch tensors, $\mathbf{B}_{\kappa_R}$ and $\mathbf{C}_{\kappa_R}$, are

$$\mathbf{B}_{\kappa_R} = \mathbf{V}_{\kappa_R}^2 = \mathbf{F}_{\kappa_R} \mathbf{F}_{\kappa_R}^{\text{T}}, \tag{2.11}$$

$$\mathbf{C}_{\kappa_R} = \mathbf{U}_{\kappa_R}^2 = \mathbf{F}_{\kappa_R}^{\text{T}} \mathbf{F}_{\kappa_R}. \tag{2.12}$$

The Green-St. Venant $\mathbf{E}_{\kappa_R}$, and the Almansi-Hamel $\mathbf{e}_{\kappa_R}$ strain tensors are

$$\mathbf{E}_{\kappa_R} = \frac{1}{2}(\mathbf{C}_{\kappa_R} - \mathbf{I}), \tag{2.13}$$

$$\mathbf{e}_{\kappa_R} = \frac{1}{2}(\mathbf{I} - \mathbf{B}_{\kappa_R}^{-1}). \tag{2.14}$$

The velocity gradient, $\mathbf{L}_{\kappa_R}$, is defined to be the spatial gradient of the velocity

$$\mathbf{L}_{\kappa_R} = \text{grad } \mathbf{v} = \frac{\partial \mathbf{v}}{\partial \mathbf{x}} = \dot{\mathbf{F}}_{\kappa_R}(\mathbf{F}_{\kappa_R})^{-1} \tag{2.15}$$

where dot signifies the material time derivative of the deformation gradient (cf. equations (2.2) and (2.3)).

The symmetric and skew parts of the velocity gradient are

$$\mathbf{D}_{\kappa_R} = \frac{1}{2}\left(\mathbf{L}_{\kappa_R} + \mathbf{L}_{\kappa_R}^{\text{T}}\right) \tag{2.16}$$

$$\mathbf{W}_{\kappa_R} = \frac{1}{2}\left(\mathbf{L}_{\kappa_R} - \mathbf{L}_{\kappa_R}^{\text{T}}\right) \tag{2.17}$$

3. Relative motions and histories

It is possible to refer motions and corresponding kinematical quantities to any other configuration instead of the arbitrarily chosen reference configuration. Consider two mappings of $\mathcal{B}$ at time t and τ, i.e. from (2.1)

$$\xi = \chi(X, \tau), \tag{2.18}$$

$$\mathbf{x} = \chi(X, t). \tag{2.19}$$

where ξ and $\mathbf{x}$ are the places of particle of particle X at time τ and t, respectively. Note that $\xi \in \kappa_\tau(\mathcal{B})$ and $\mathbf{x} \in \kappa_t(\mathcal{B})$. The relative motion is defined as

$$\xi = \chi(\chi^{-1}(\mathbf{x}, t), \tau) \equiv \chi_t(\mathbf{x}, \tau), \tag{2.20}$$

and at time τ, assigns a place ξ that is occupied by the particle that at time t is at $\mathbf{x}$. The relative deformation gradient $\mathbf{F}_t$ is defined as the gradient of the relative motion with respect to the configuration that the body occupies at time t, i.e.

$$\mathbf{F}_t(\mathbf{x}, \tau) \equiv \frac{\partial \xi}{\partial \mathbf{x}}. \tag{2.21}$$

With the aid of (2.8) and the chain rule, one obtains the relationship

$$\mathbf{F}(\mathbf{X}, \tau) = \mathbf{F}_t(\mathbf{x}, \tau)\mathbf{F}(\mathbf{X}, t). \tag{2.22}$$

which relates deformation gradients (with respect to $\kappa_R(\mathcal{B})$) with relative deformation gradients (with respect to $\kappa_t(\mathcal{B})$).

As hinted in the definition of the relative motion (2.20), it is possible not only to refer motions to any reference configuration but also to relate motions described with respect to different reference configurations. Let a motion (2.1) be described by two different reference configurations, $\kappa_1(\mathcal{B})$ and $\kappa_2(\mathcal{B})$, i.e.

$$\mathbf{x} = \chi_{\kappa_1}(\mathbf{X}_1, t) = \chi_{\kappa_2}(\mathbf{X}_2, t), \tag{2.23}$$

Note that $\mathbf{X}$ in the argument of each motion is the place of particle X in each reference configuration given by (2.4) for each reference configuration, i.e.

$$\mathbf{X}_1 = \kappa_1(X), \tag{2.24}$$

$$\mathbf{X}_2 = \kappa_2(X). \tag{2.25}$$

Hence, with (2.23) one can obtain a mapping, $\boldsymbol{\lambda}$, which maps labels from one reference configuration to the other, i.e.

$$\mathbf{X}_2 = \kappa_2(\kappa_1^{-1}(\mathbf{X}_1)) \equiv \boldsymbol{\lambda}(\mathbf{X}_1). \tag{2.26}$$

and the relationship between the motions with respect to each reference configuration becomes

$$\chi_{\kappa_1}(\mathbf{X}_1, t) \equiv \chi_{\kappa_2}(\boldsymbol{\lambda}(\mathbf{X}_1), t). \tag{2.27}$$

The deformation gradients $\mathbf{F}_1$ and $\mathbf{F}_2$ are the Lagrangian gradients of the motion, each taken with respect to each reference configuration, i.e.

$$\mathbf{F}_1 = \operatorname{Grad} \chi_{\kappa_1} \equiv \frac{\partial \mathbf{x}}{\partial \mathbf{X}_1} \tag{2.28}$$

$$\mathbf{F}_2 = \operatorname{Grad} \chi_{\kappa_2} \equiv \frac{\partial \mathbf{x}}{\partial \mathbf{X}_2} \tag{2.29}$$

where $\mathbf{X}_1$ and $\mathbf{X}_2$ are position vectors labeling places of particles in $\kappa_1(\mathcal{B})$ and $\kappa_2(\mathcal{B})$ respectively. They will generally be different as they depend on the choice taken as reference. With the chain rule can be related with each other, one obtains

$$\mathbf{F}_1 = \mathbf{F}_2 \mathbf{P} \tag{2.30}$$

where

$$\mathbf{P} \equiv \operatorname{Grad}_{\kappa_1} \boldsymbol{\lambda} = \frac{\partial \boldsymbol{\lambda}}{\partial \mathbf{X}_1}. \tag{2.31}$$

The history of any scalar, vector or tensor field ψ up to time t is defined by

$$\psi^{(t)}(s) = \psi(t-s) \tag{2.32}$$

when $s \geq 0$, yielding $\psi^{(t)}(0) = \psi(t)$ and $\psi^{(t)}(t) = \psi(0)$. Hence, the history of the motion up to time t $\chi^{(t)}$ is defined from (2.1) as

$$\mathbf{x} = \chi^{(t)}(X,s) = \chi(X,t-s). \tag{2.33}$$

The concept can be extended to the measures of strain defined in the previous section.

4. Kinematical linearization

Linearized theories often define the displacement field as

$$\mathbf{u} = \mathbf{x} - \mathbf{X}. \tag{2.34}$$

The deformation gradient (2.8) can be expressed as

$$\mathbf{F} = \mathbf{I} + \frac{\partial \mathbf{u}}{\partial \mathbf{X}}. \tag{2.35}$$

The dependence on the choice of the reference configuration still exist but it is not stressed. The displacement gradient

$$\nabla \mathbf{u} \equiv \operatorname{Grad} \mathbf{u} = \frac{\partial \mathbf{u}}{\partial \mathbf{X}} \tag{2.36}$$

is assumed to be infinitesimal small, i.e. there exists a norm and a positive scalar $\delta \ll 1$ such that

$$\max_{\substack{\mathbf{X} \in \kappa_R(\mathcal{B}) \\ t \in I}} \left\| \nabla \mathbf{u} \right\| = o(\delta). \tag{2.37}$$

A function $f(n)$ is said to be $o(\delta)$ if $f/\delta \to 0$. Under this assumption, the strain tensors (2.13) and (2.14) are approximated as

$$\mathbf{E} = \boldsymbol{\varepsilon} + o(\delta^2), \tag{2.38}$$

$$\mathbf{e} = \boldsymbol{\varepsilon} + o(\delta^2), \tag{2.39}$$

where $\boldsymbol{\varepsilon}$ is the linearized strain tensor, defined by

$$\boldsymbol{\varepsilon} = \frac{1}{2}\left[\nabla\mathbf{u} + (\nabla\mathbf{u})^{\mathrm{T}}\right]. \tag{2.40}$$

In simply connected bodies, the compatibility condition

$$\mathrm{curl}(\mathrm{curl}\,\boldsymbol{\varepsilon}) = \mathbf{0} \tag{2.41}$$

ensures the existence of a displacement $\mathbf{u}$, and consequently a motion χ that can be obtained from a linearized strain tensor (cf. [212], page 148). The curl of a vector $\mathbf{v}$ and of a 2nd order tensor $\mathbf{T}$ are defined by

$$(\mathrm{curl}\,\mathbf{v})\cdot\mathbf{a} = \mathrm{div}(\mathbf{v}\times\mathbf{a}) \tag{2.42}$$

$$(\mathrm{curl}\,\mathbf{T})\cdot\mathbf{a} = \mathrm{curl}(\mathbf{T}^{\mathrm{T}}\mathbf{a}) \tag{2.43}$$

where $\mathbf{a}$ is an arbitrary constant vector (cf. [212], page 70). The solution of equation (2.40) is non-unique and is obtained up to a rigid motion. A rigid motion is a motion that the distance between the points occupied by every pair of particles is invariant. Such motion is given by

$$\mathbf{x} = \mathbf{c}(t) + \mathbf{Q}(t)[\mathbf{X} - \mathbf{X}^0] \tag{2.44}$$

for all $\mathbf{X} \in \kappa_R(\mathcal{B})$ and $t \in \mathcal{I}$. $\mathbf{Q}(t)$ is a proper orthogonal tensor. Only translations ($\mathbf{c}(t)$ is the translation vector) and rotations about $\mathbf{X}^0$ are allowed as rigid body motions.

B. Balance laws

Balance laws describe axiomatic principles in mechanics. The law of conservation of mass was first clearly formulated by Lavoisier in 1789. The law of conservation of linear momentum is a generalization of Newton's second law obtained by Euler on his studies in fluid mechanics. Euler is also credited with the conservation of moment of momentum as an independent principle [213]. Not recorded here but used as common practice in mechanics, the balance of energy, also known as the first law of thermodynamics and the Clausius-Duhem inequality, the standard mechanical statement of the second law of thermodynamics.

1. Balance of mass

The concept of mass density ρ is associated with the body $\mathcal{B}$ and a placer κ, hence function of χ. The mass of body $\mathcal{B}$ and part $\mathcal{P}$ are given respectively by

$$M(\mathcal{B}) = \int_{\kappa_t(\mathcal{B})} \rho \; dv, \qquad\qquad (2.45)$$

$$M(\mathcal{P}) = \int_{\kappa_t(\mathcal{P})} \rho \; dv. \qquad\qquad (2.46)$$

Conservation of mass states that mass can be neither created nor destroyed. Considering ρ_R the density in the reference configuration $\kappa_R(\mathcal{B})$ and ρ the density in the current configuration $\kappa_t(\mathcal{B})$, the statement of balance of mass is

$$\int_{\kappa_R(\mathcal{P})} \rho_R \; dV = \int_{\kappa_t(\mathcal{P})} \rho \; dv. \qquad\qquad (2.47)$$

for any arbitrary part $\mathcal{P}$. It must be stressed that the body is assumed to be a closed system; hence its mass does not change from the reference configuration to any current configuration at any time *t*.

J is the Jacobian of the motion and given in (2.9). It can be shown from (2.8) that volumes in $\kappa_t(\mathcal{B})$ are mapped from volumes of $\kappa_R(\mathcal{B})$, hence the relationship

$$dv = J \; dV \qquad\qquad (2.48)$$

for infinitesimal volumes of $\kappa_t(\mathcal{B})$ and $\kappa_R(\mathcal{B})$. Equation (2.47) is valid for any arbitrary part $\mathcal{P}$, thus it can be inferred that

$$\rho_R = \rho J. \qquad\qquad (2.49)$$

Due to its connection with the reference configuration, equations (2.47) and (2.49) are called the integral and local forms of the Lagrangian balance of mass respectively. Balance of mass can also be stated in an Eulerian form, i.e. with respect to the current configuration, and is expressed as

$$\frac{d}{dt} \int_{\kappa_t(\mathcal{P})} \rho \; dv = 0 \qquad\qquad (2.50)$$

for any arbitrary part $\mathcal{P}$ and yields

$$\dot{\rho} + \rho \ \mathrm{div} \ \mathbf{v} = 0 . \tag{2.51}$$

The material time derivatives in both (2.50) and (2.51) must be stressed.

2. Forces and moments

Forces and torques are among the primitive elements of mechanics. Forces act on part $\mathcal{P}$ of a body $\mathcal{B}$ in a configuration $\kappa(\mathcal{B})$. Body forces and contact forces exist and are represented by $\mathbf{f}_b(\mathcal{P})$ and $\mathbf{f}_c(\mathcal{P})$, respectively. The resultant force $\mathbf{f}(\mathcal{P})$ acting on $\mathcal{P}$ is given by

$$\mathbf{f}(\mathcal{P}) = \mathbf{f}_b(\mathcal{P}) + \mathbf{f}_c(\mathcal{P}) , \tag{2.52}$$

where

$$\mathbf{f}_b(\mathcal{P}) = \int_{\kappa(\mathcal{P})} \rho \mathbf{b} \ \mathrm{dv} , \tag{2.53}$$

$$\mathbf{f}_c(\mathcal{P}) = \int_{\kappa(\partial \mathcal{P})} \mathbf{t} \ \mathrm{ds} . \tag{2.54}$$

$\mathbf{b}$ is the specific body force, defined on the entire configuration, and $\mathbf{t}$ the traction, defined on the surface $\kappa(\partial \mathcal{P})$ of the boundary $\partial \mathcal{P}$ of $\mathcal{P}$.

The resultant moment of force $\mathbf{L}(\mathcal{P}; \mathbf{x}_0)$ with respect to $\mathbf{x}_0$ is defined by

$$\mathbf{L}(\mathcal{P}; \mathbf{x}_0) = \int_{\kappa(\mathcal{P})} (\mathbf{x} - \mathbf{x}_0) \times \rho \mathbf{b} \ \mathrm{dv} + \int_{\kappa(\partial \mathcal{P})} (\mathbf{x} - \mathbf{x}_0) \times \mathbf{t} \ \mathrm{ds} . \tag{2.55}$$

3. Euler's laws of mechanics

The momentum $\mathbf{m}(\mathcal{P})$ and the moment of momentum $\mathbf{M}(\mathcal{P}; \mathbf{x}_0)$ of part $\mathcal{P}$ at time t are defined by

$$\mathbf{m}(\mathcal{P}) = \int_{\kappa_t(\mathcal{P})} \rho \dot{\mathbf{x}} \ \mathrm{dv} , \tag{2.56}$$

$$\mathbf{M}(\mathcal{P};\mathbf{x_0}) = \int_{\kappa_t(\mathcal{P})} (\mathbf{x} - \mathbf{x_0}) \times \rho\dot{\mathbf{x}} \, dv \, . \tag{2.57}$$

Euler's 1st law states the balance of momentum, i.e. the time rate of change of momentum (2.56) equals the resultant force $\mathbf{f}(\mathcal{P})$ (cf. (2.52)), and is

$$\mathbf{f}(\mathcal{P}) = \frac{d}{dt}\mathbf{m}(\mathcal{P}) \, . \tag{2.58}$$

for any arbitrary part $\mathcal{P}$. Similarly, Euler's 2nd law relates the resultant moment of force (cf. (2.55)) with the rate of change of moment of momentum $\mathbf{M}(\mathcal{P};\mathbf{x_0})$ and is

$$\mathbf{L}(\mathcal{P};\mathbf{x_0}) = \frac{d}{dt}\mathbf{M}(\mathcal{P};\mathbf{x_0}) \tag{2.59}$$

for any arbitrary part $\mathcal{P}$.

C. Cauchy's stress theory

Stress is an internal distribution of force per oriented areas inside a body as it reacts to external applied forces. While normal pressures were known in hydraulics by John Bernoulli and Euler, tensions in cables by Galileo and James Bernoulli, and internal shear stresses in loaded beams by Parent and Coulomb, Cauchy's general stress theory was obtained by adopting the common features and discarding the special aspects of the preceding theories [213].

1. Cauchy stress tensor and Cauchy's laws of motion

Tractions $\mathbf{t}$ defined on the boundary $\partial\mathcal{P}$ of part $\mathcal{P}$ (cf. (2.54)) are further simplified to be of the form

$$\mathbf{t} = \mathbf{t}(\mathbf{x}, t, \mathbf{n}) \tag{2.60}$$

and are called simple. It is assumed that $\mathbf{t}$ at place $\mathbf{x}$ and time t has a common value for all parts $\mathcal{P}$ with boundary $\partial\mathcal{P}$ that share a common tangent plane at $\mathbf{x}$ and lie upon the same side of it. $\mathbf{n}$ is the outward unit normal to $\partial\mathcal{P}$ in the configuration $\kappa_t(\mathcal{P})$.

Furthermore, Cauchy's lemma states that tractions acting upon opposite sides of the same surface at a given place are equal in magnitude and opposite in direction, i.e.

$$\mathbf{t}(\mathbf{x},t,\mathbf{n}) = -\mathbf{t}(\mathbf{x},t,-\mathbf{n}). \tag{2.61}$$

Cauchy's fundamental theorem asserts the existence and uniqueness of tensor $\mathbf{T}$, the Cauchy stress, of the form

$$\mathbf{t}(\mathbf{x},t,\mathbf{n}) = \mathbf{T}(\mathbf{x},t)\mathbf{n}. \tag{2.62}$$

2. Cauchy's laws of motion

Euler's 1st law (2.58) with (2.52) and (2.62) yields Cauchy's 1st law of continuum mechanics. Cauchy's 1st law, a sufficient and necessary condition for the balance of linear momentum to be satisfied, is

$$\operatorname{div}\mathbf{T} + \rho\mathbf{b} = \rho\ddot{\mathbf{x}}, \tag{2.63}$$

which holds at interior points of $\kappa_t(\mathcal{B})$. Similarly, Cauchy's 2nd law is obtained from (2.59) with (2.55) and (2.57). It is usually expressed as the requirement of symmetry of the Cauchy stress tensor, i.e.

$$\mathbf{T} = \mathbf{T}^{\mathrm{T}}. \tag{2.64}$$

More precisely, (2.64) is a necessary and sufficient condition for the balance of moment of momentum to be satisfied in a body where linear momentum is balanced (in the absence of body couples).

Lastly, due to the acceleration term in (2.63), it must be stressed that Cauchy's laws only hold in an inertial frame (and consequently in all).

3. Linearization

It is customary to restrict linearized theories to a linearized version of Cauchy's 1st law. Recall that the requirement of infinitesimal displacement gradients (cf. (2.37)), the deformation gradient is of the form

$$\mathbf{F} = \mathbf{I} + \mathbf{o}(\delta). \tag{2.65}$$

whereas the divergence of a vector is defined to be the trace of its gradient, the divergence of a 2nd order tensor $\mathbf{S}$ is defined to be the unique vector div $\mathbf{S}$ such that

$$(\text{div } \mathbf{S}) \cdot \mathbf{a} = \text{div } (\mathbf{S}^{\text{T}} \mathbf{a}) \tag{2.66}$$

holds for all constant vectors $\mathbf{a}$. Furthermore, the spatial divergence of a 2nd order tensor $\mathbf{S}$ is related to the corresponding referential divergence by (cf. [210], page 59)

$$\text{div } \mathbf{S} = J^{-1} \text{Div } (J\mathbf{F}^{-1}\mathbf{S}), \tag{2.67}$$

in which, if (2.65) holds, then

$$\text{div } \mathbf{S} = \text{Div } (\mathbf{S}) + \mathbf{o}(\delta^2). \tag{2.68}$$

Cauchy's 1st law (2.63) then becomes

$$\rho \ddot{\mathbf{u}} = \text{div } \boldsymbol{\sigma} + \rho \mathbf{b}, \tag{2.69}$$

where $\boldsymbol{\sigma}$ is called the linearized stress tensor and is related to the Cauchy stress by

$$\boldsymbol{\sigma} = \mathbf{T} + \mathbf{o}(\delta^2). \tag{2.70}$$

D. Constitutive equations

A constitutive equation is a relationship between the response of the body during a motion and the stress it is subjected to and correspondingly the forces that cause such motion. Several axiomatic restrictions are placed upon constitutive formulations, but still a certain level of generality is obtained and a wide variety of material behaviors are described with a few different classes of constitutive equations.

1. Restrictions on constitutive equations

The principles of determinism restricts the constitutive equation in a way that it is assumed that the Cauchy stress at particle X of the body $\mathcal{B}$ at time t is determined by the history of the motion of $\mathcal{B}$ up to time t, i.e.

$$\mathbf{T}(X,t) = \mathfrak{F}(\chi^{(t)}; X, t) \tag{2.71}$$

where $\mathfrak{F}$ is the constitutive functional of a material defined by $\mathfrak{F}$. In rough terms, the past and present configurations given by the motion of $\mathcal{B}$ determine the stress field over its present shape.

The principle of local action further restricts that the stress at a given particle X is not influenced by the motion of other particles outside an arbitrary neighborhood of X. Because of the smoothness required in motions, particles that are apart some finite distance will always be apart a finite distance.

Material frame indifference requires that material properties are indifferent to the choice of observer, hence $\mathfrak{F}$ must be such that the constitutive equation is invariant the transformation relating two equivalent dynamic processes. Two dynamical processes $\{\chi, \mathbf{T}\}$ and $\{\chi^*, \mathbf{T}^*\}$ are equivalent if they are related by

$$\chi^*(X, t^*) = \mathbf{c}(t) + \mathbf{Q}(t)[\chi(X, t) - \mathbf{x}_0] \tag{2.72}$$

$$t^* = t - a \tag{2.73}$$

$$\mathbf{T}^*(X, t^*) = \mathbf{Q}(t)\mathbf{T}(X, t)\mathbf{Q}(t)^{\mathrm{T}} \tag{2.74}$$

for every particle X. Hence, material frame indifference requires (2.71) to be such that

$$\mathbf{T}^* = \mathfrak{F}\left\{\chi^{*(t^*)}; X, t^*\right\} \tag{2.75}$$

for the two equivalent dynamical processes.

2. *Simple materials and internal constraints*

The principle of local action implies that the constitutive functional, i.e. the response of particle X at time t depends on $\chi^{(t)}$ only through its correspondent history of the deformation gradient up to time t with respect to some fixed choice of reference configuration,

$$\mathbf{T}(X, t) = \mathfrak{F}_{\kappa_R}\left\{\mathbf{F}_{\kappa_R}^{(t)}(X, s); X, t\right\}. \tag{2.76}$$

It must be stressed that the constitutive functional depends on the particular choice of reference configuration, indicated either in the subscript of the deformation gradient and of the response functional. For a cleaner notation, the dependence on the choice of reference will not be stressed anymore.

Furthermore, a simple material is a non-aging material, hence time no longer occurs as an independent variable and (2.76) becomes

$$\mathbf{T}(X,t) = \mathfrak{F}\left\{\mathbf{F}^{(t)}(X,s); X\right\},\tag{2.77}$$

where the same symbol was used for a less general constitutive functional $\mathfrak{F}$. Assuming the response of the material to be homogeneous, there will be no explicit dependence of $\mathfrak{F}$ on the particle, thus

$$\mathbf{T}(X,t) = \mathfrak{F}\left\{\mathbf{F}^{(t)}(X,s)\right\}.\tag{2.78}$$

A simple material is defined if and only if its response functional is of the form (2.78). Further restrictions of material frame indifference yield

$$\mathbf{T}(t) = \mathbf{R}(t)\mathfrak{G}\left\{\mathbf{U}^{(t)}(s)\right\}\mathbf{R}(t)^{\mathrm{T}},\tag{2.79}$$

where for brevity the dependence on the particle of either $\mathbf{T}$ or $\mathbf{U}^{(t)}$ is not shown but it is still in effect. $\mathbf{R}(t)$ and $\mathbf{U}^{(t)}$ are the rotation and obtained from the polar decomposition of $\mathbf{F}^{(t)}$ (cf. (2.10)). Reduced forms of constitutive equations can be obtained, i.e. similar forms of the stress representation but with the corresponding response functional dependent on other strain measures (cf. [207], sect. 29).

Simple materials can be constrained in such a way that only certain motions are possible. A simple constraint can be expressed as a requirement on kinematical quantities to satisfy certain equations, like for example

$$\gamma(\mathbf{F}) = 0.\tag{2.80}$$

If γ is a frame indifferent scalar function, then the constraint can be written in the form $\lambda(\mathbf{C}) = 0$. In a constrained simple material the stress is determined by the history

of the deformation gradient up to time t only within a stress $\mathbf{N}$ that does no work in any motion satisfying the constraint [207], i.e.

$$\mathbf{T} = \mathbf{N} + \mathfrak{F}_E(\mathbf{F}^{(t)}) \tag{2.81}$$

where $\mathfrak{F}_E$ is the extra stress, obtained from a response functional. An important example of a constrained material is an incompressible material. Incompressible materials are materials that only undergo isochoric motions (cf. (2.9)), hence the constraint is expressed as

$$\lambda(\mathbf{C}) = \det \mathbf{C} - 1 = 0 \tag{2.82}$$

for all times up to time t. Then (2.81) reduces to

$$\mathbf{T} = -p\mathbf{1} + \mathfrak{F}_E(\mathbf{F}^{(t)}), \tag{2.83}$$

where p is an arbitrary scalar and $\mathbf{1}$ the 2nd order identity tensor.

Classes of simple materials are obtained by prescribing the nature of the dependence of the constitutive functional $\mathfrak{F}$. Some special classes are recorded here (cf. [207], sect. 35, 36, and 37): (i) materials of the differential type, where $\mathfrak{F}$ is dependent on the time rates of change of the deformation gradient, i.e.

$$\mathbf{T} = \mathfrak{F}\left(\mathbf{F}, \dot{\mathbf{F}}, ..., \overset{(n-1)}{\mathbf{F}}, \overset{(n)}{\mathbf{F}} \right) \tag{2.84}$$

where n is called the grade of the material; (ii) materials of the rate type relating the pth convected stress rate with lower order rates and kinematical quantities, i.e.

$$\overset{(p)}{\mathbf{T}} = \mathfrak{F}\left(\mathbf{T}, \dot{\mathbf{T}}, ..., \overset{(p-1)}{\mathbf{T}}; \mathbf{F}, \dot{\mathbf{F}}, ..., \overset{(n-1)}{\mathbf{F}}, \overset{(n)}{\mathbf{F}} \right) \tag{2.85}$$

where the response functional is indeed a differential equation defining a class of materials; and (iii) materials of the integral type , which can be expressed as a sum of m iterated integrations with m the order of the material, the representation of the stress is given by

$$\mathbf{R}^{\mathrm{T}}\mathbf{T}\mathbf{R} = \mathfrak{f}(\mathbf{C}) + \int_0^\infty \mathbf{g}_1(s_1;\mathbf{C})[\mathbf{G}(s_1)]ds_1 + \int_0^\infty \int_0^\infty \mathbf{g}_2(s_1,s_2;\mathbf{C})[\mathbf{G}(s_1),\mathbf{G}(s_2)]ds_1 ds_2$$

$$+ \int_0^\infty ... \int_0^\infty \mathbf{g}_m(s_1,...,s_m;\mathbf{C})[\mathbf{G}(s_1),...,\mathbf{G}(s_m)]ds_1 ds_2 ... ds_m$$

(2.86)

where $\mathbf{g}_m(s_1,...,s_m;\mathbf{C})[\mathbf{G}(s_1),...,\mathbf{G}(s_m)]$ for any i from 1 to m is a multilinear tensor function of i tensor variables $\mathbf{G}(s_i)$, and its value $\mathbf{g}_m(s_1,...,s_m;\mathbf{C})$ can be regarded as tensors of order 2i. Furthermore, the function $\mathbf{G}$, given by

$$\mathbf{G}(s) = \mathbf{R}(t)^{\mathrm{T}}\mathbf{C}_t^{(t)}(s)\mathbf{R}(t) - \mathbf{1}$$

(2.87)

is used to describe the motion and $\mathfrak{f}(\mathbf{C})$ is an equilibrium term. Note that all integrands vanish when $\mathbf{G}(s) = \mathbf{0}$, i.e. a rest history.

3. Simple fluids and simple solids

An isotropic material requires that the response $\mathfrak{F}$, taken relative to an undistorted state considered as the reference configuration, is an isotropic tensor function of $\mathbf{F}^{(t)}$, i.e. it must satisfy the equation

$$\mathbf{Q}\mathfrak{F}(\mathbf{F}^{(t)})\mathbf{Q}^{\mathrm{T}} = \mathfrak{F}(\mathbf{Q}\mathbf{F}^{(t)}\mathbf{Q}^{\mathrm{T}})$$

(2.88)

for all $\mathbf{Q}$ orthogonal. Similar restrictions can be placed on $\mathfrak{G}(\mathbf{U}^{(t)})$ or other reduced constitutive equations (cf. (2.79)). A material that is not isotropic is called anisotropic.

An isotropic 2$^{\text{nd}}$ order tensor function $\mathbf{D} = \mathfrak{f}(\mathbf{A})$ has a representation of the form (cf. [207], sect. 12)

$$\mathbf{D} = \mathfrak{f}(\mathbf{A}) = \varphi_0 \mathbf{1} + \varphi_1 \mathbf{A} + ... + \varphi_{n-1}\mathbf{A}^{n-1}$$

(2.89)

where φ_k are invariants of $\mathbf{A}$ and hence can be expressed as functions $\varphi_k = \varphi_k(I_1,...,I_n)$ of the principal invariants of $\mathbf{A}$. For three-dimensional bodies, $n = 3$.

Fluids are unable to support shear stresses in equilibrium and are isotropic; hence the particularization of simple materials that yields the most general constitutive representation for simple fluids can be expressed by

$$\mathbf{T} = \mathfrak{R}(\mathbf{C}_t^{(t)}; \rho) \tag{2.90}$$

and $\mathfrak{R}$ must satisfy

$$\mathfrak{R}(\mathbf{Q}\mathbf{C}_t^{(t)}\mathbf{Q}^{\mathrm{T}}; \rho) = \mathbf{Q}\mathfrak{R}(\mathbf{C}_t^{(t)}; \rho)\mathbf{Q}^{\mathrm{T}}, \tag{2.91}$$

where $\mathbf{Q}$ is any orthogonal tensor, and

$$\mathfrak{R}(\mathbf{1}^{(t)}; \rho) = -p(\rho)\mathbf{1}. \tag{2.92}$$

Fluids have no preferred configuration. Their response functional should be invariant, i.e.

$$\mathfrak{F}(\mathbf{F}^{(t)}) = \mathfrak{F}(\mathbf{F}^{(t)}\mathbf{H}), \tag{2.93}$$

to all unimodular tensors $\mathbf{H}$ ($\mathbf{H}$ is unimodular if $\det \mathbf{H} = \pm 1$) for any of all reference configurations.

On the other hand, to keep a solid in a deformed state, a force must continue to be applied and to maintain its undeformed state no force is needed. A simple solid is defined by the existence of a particular reference configuration $\hat{\kappa}(\mathcal{B})$ with respect to which the constitutive functional is invariant to all unimodular tensors $\mathbf{H}$ that form a subgroup of the orthogonal group (cf. (2.93)). In an isotropic solid, the subgroup formed by all $\mathbf{H}$ that satisfy (2.93) is the orthogonal group. The particular reference configuration is called the undistorted state. Solids might have more than one preferred undistorted configuration. In a fluid, all states are undistorted states.

The definition of a simple solid is mutually exclusive with the definition of simple fluids. Note that simple solids and simple fluids are not defined by particular kinds of functional dependence but rather by properties of invariance of the response. On the other hand, there exist simple materials that are neither solids nor fluids, but show characteristics of both [207]. Elasticity is wrongly perceived as a characteristic of solids (e.g. Eulerian fluid) whereas viscosity as a characteristic of fluids (e.g. viscoelastic solid); the concepts are clearly separated at their inception.

4. Cauchy's elasticity, hyperelastic solids, and Eulerian fluids

Classical definitions of an homogeneous elastic material are: (i) the stress depends only on the deformation gradient (referred to as Cauchy elasticity), and (ii) there exists a stored energy function that depends on the deformation gradient from which the stress is derivable (referred to as Green elasticity) [214]. The latter is also usually referred as a hyperelastic material. Both are particular cases of simple materials.

Cauchy's elasticity states that the response functional (2.78) depends solely on the current value of the deformation gradient $\mathbf{F}$, i.e.

$$\mathbf{T} = \mathfrak{f}(\mathbf{F}). \tag{2.94}$$

Material frame indifference requirements and representation (2.89) for isotropic functions yield the representation of the stress for an isotropic elastic material, given obtained to be

$$\mathbf{T} = \beta_0 \mathbf{1} + \beta_1 \mathbf{B} + \beta_2 \mathbf{B}^2 \tag{2.95}$$

where β_0, β_1, and β_2 are the material properties, scalar functions of the invariants of the left Cauchy-Green stretch tensor $\mathbf{B}$, $\beta_k = \beta_k(I_{\mathbf{B}}, II_{\mathbf{B}}, III_{\mathbf{B}})$.

For hyperelastic materials the work assumption implies the existence of a scalar field, the stored energy function W, which is function of the deformation gradient from which a the Piola stress tensor $\mathbf{P}$ is derivable, i.e.

$$\mathbf{P} \equiv J\mathbf{F}^{-1}\mathbf{T} = \left(\frac{\partial W}{\partial \mathbf{F}}\right)^{\mathrm{T}}. \tag{2.96}$$

The stored energy function is required to be frame indifferent. The form of the stored energy function can be expressed as dependent of other strain measures. For a choice of $W = W(\mathbf{C})$, the Cauchy stress has the representation

$$\mathbf{T} = 2\rho \mathbf{F} \frac{\partial W}{\partial \mathbf{C}} \mathbf{F}^{\mathrm{T}}. \tag{2.97}$$

Isotropy of W requires that W must be a function of the principal invariants of $\mathbf{C}$, $W = W(I_{\mathbf{C}}, II_{\mathbf{C}}, III_{\mathbf{C}})$. The representation (2.97) can be cast in the same form as (2.95) but consequently, the material properties will be different.

Incompressible elastic materials follow from (2.83). The most general representation of an incompressible isotropic elastic solid is

$$\mathbf{T} = -p\mathbf{1} + \mu_1 \mathbf{B} + \mu_2 \mathbf{B}^2 = -p\mathbf{1} + 2\frac{\partial W}{\partial I_{\mathbf{C}}}\mathbf{B} - 2\frac{\partial W}{\partial II_{\mathbf{C}}}\mathbf{B}^{-1} \tag{2.98}$$

where $\mu_k = \mu_k\left(I_{\mathbf{B}}, II_{\mathbf{B}}\right)$ and $W = W(I_{\mathbf{C}}, II_{\mathbf{C}})$.

Further axiomatic restrictions on the response of elastic materials are required to be placed upon (2.94) because nothing regarding the direction of the response is said. It is expected that an elastic material should grow longer when pulled and must contract when subjected to pressure. For incompressible isotropic elastic materials the material properties must satisfy

$$\frac{\partial W}{\partial I_{\mathbf{C}}} > 0, \tag{2.99}$$

$$\frac{\partial W}{\partial II_{\mathbf{C}}} \geq 0. \tag{2.100}$$

As a record, several classical examples of elastic materials are shown: (i) the constitutive response of an Euler fluid (or ideal fluid or elastic fluid) is

$$\mathbf{T} = -p(\rho)\mathbf{I} \tag{2.101}$$

where p is the pressure field and is determined from the density field (if incompressible, p is indeterminate); (ii) the neo-Hookean incompressible hyperelastic solid is given by a stored energy function of the form

$$W = \frac{\mu}{2}(I_{\mathbf{C}} - 3) \tag{2.102}$$

where $\mu > 0$ is the material property, usually called the shear modulus; and (iii) an extension of this model is the Mooney-Rivlin incompressible hyperelastic solid, which stored energy function has the form

$$W = \frac{\mu_1}{2}(I_{\mathrm{C}} - 3) + \frac{\mu_2}{2}(II_{\mathrm{C}} - 3) \tag{2.103}$$

with two material properties, μ_1 and μ_2.

5. *Viscous fluids*

A class of fluids more general than the Euler fluid and that cannot be included under elastic materials is defined by the functional relation

$$\mathbf{T} = \mathfrak{h}(\rho, \mathbf{L}) = \mathfrak{h}(\rho, \mathbf{D}). \tag{2.104}$$

Material frame indifference implies that the dependence on the velocity gradient $\mathbf{L}$ can be reduced to a dependence on its symmetric part $\mathbf{D}$. If $\mathfrak{h}$ is isotropic (cf. (2.88)) and linear in $\mathbf{D}$, (2.104) yields the classical linearly viscous fluid and the stress representation is given by

$$\mathbf{T} = (-p + \lambda \operatorname{tr} \mathbf{D})\mathbf{1} + 2\mu\mathbf{D} \tag{2.105}$$

where p, λ, and μ are functions of ρ. Representation (2.105) yields the Navier-Stokes theory of fluids. The coefficients λ and μ are called the viscosities of the fluid. If considered incompressible, the constraint of isochoric motions (cf. (2.9)) implies that

$$\operatorname{tr} \mathbf{L} = \operatorname{tr} \mathbf{D} = 0 \tag{2.106}$$

and (2.105) becomes

$$\mathbf{T} = -p\mathbf{1} + 2\mu\mathbf{D} \tag{2.107}$$

where p is the indeterminate and μ a constant.

Nonlinear fluids are usually obtained with simple fluids of the differential type: note that Euler's fluid is of grade 0 and the Navier-Stokes fluid is of grade 1. Restricting the rate type response functional (2.84) with material frame indifference and invariance

of the response with respect to all reference configurations to all unimodular transformations (cf. the definition of a simple fluid) yields the Rivlin-Eriksen fluid of grade *n*.

6. Viscoelastic materials

Maxwell was among the first to discuss the viscoelasticity of matter. He observed that substances such as pitch or tar could be regarded neither as ideal elastic solids nor as viscous liquids, but seemed instead to share of the character of both [215]. For very rapidly applied stresses pitch behaves like an elastic body: increases in deformation promote increases in stress, and it shows a recovery upon rapid removal of stress. If stresses are applied slowly or for a long period of time, the pitch behaves like a very viscous liquid: continued deformation with time where the rate of deformation is related with the applied stress. Maxwell attempted to incorporate Hooke's law and Newton's law in the same equation. He proposed a one-dimensional constitutive equation for the shear response, which is called the Maxwell model

$$\frac{ds}{dt} = \frac{1}{G}\frac{df}{dt} + \frac{1}{\tau G}f \qquad (2.108)$$

where *s* is the shear strain, *f* the shear stress, *G* the shear modulus, and τ a relaxation time. The resemblance between (2.108) and a material of the rate type (2.85) must be remarked. The Maxwell model shows linear creep and stress relaxation to zero, indicating that the model represents fluid behavior.

The Kelvin-Voigt model incorporates elastic and viscous behavior in a slight different way. Its constitutive equation is

$$f = Gs + \tau G\frac{ds}{dt} \qquad (2.109)$$

The resemblance between (2.109) and a material of the differential type (2.84) must be remarked either. The Kelvin-Voigt model represents solid behavior that creeps and

shows instantaneous stress relaxation. Further generalizations of one-dimensional models can be obtained (cf. [215-217]).

A different approach towards the description of the response of viscoelastic materials is Boltzmann's accumulation theory. Boltzmann's superposition principle states: (i) that the creep (or stress relaxation) is a function of the entire loading (or deformation) history; (ii) each loading (or deformation) step makes an independent contribution to the current deformation (or loading); and (iii) the current deformation (or loading) can be obtained by addition of each contribution. The Boltzmann's accumulation theory was the driving factor for the nonlinear generalization of materials of the integral type (cf. (2.86)).

Nevertheless, the most general material that exhibits a viscoelastic response (as described above, but not necessarily linear) is the simple material. It comprises as particular cases the theories of elasticity, viscosity, and viscoelasticity.

Examples of particular nonlinear viscoelastic materials, that can be either solids of fluids in nature, are mostly integral representations of order $m = 1$, i.e. single integral constitutive equations. For incompressible isotropic nonlinear viscoelastic response of solids and fluids, the constitutive equation is

$$\mathbf{T} = -p\mathbf{I} + \mathfrak{h}(\mathbf{B}, t) + \int_0^t \mathfrak{g}(\mathbf{B}, \mathbf{C}_t(s), t-s) \, \mathrm{d}s \qquad (2.110)$$

where p is indeterminate due to the constraint of incompressibility and $\mathfrak{h}$ and $\mathfrak{g}$ are isotropic functions of $\mathbf{B}$ and of $\mathbf{B}$ and $\mathbf{C}_t$ [218].

A classical example of a single-integral nonlinear viscoelastic solid is the extension to three-dimensional bodies of the one-dimensional model developed by Pipkin and Rogers [219]. The stress has the following representation

$$\mathbf{T} = -p\mathbf{I} + \mathbf{F} \left[\mathbf{G}(\mathbf{C}(t), 0) + \int_0^t \frac{\partial}{\partial(t-s)} \mathbf{G}(\mathbf{C}(s), t-s) ds \right] \mathbf{F}^{\mathrm{T}} \qquad (2.111)$$

where p is indeterminate, $\mathbf{G}(\mathbf{C}, s)$ is a material property that represents a tensor-valued stress relaxation function that depends on the deformation, and is given by

$$\mathbf{G}(\mathbf{C},s) = \phi_0\mathbf{I} + \phi_1\mathbf{C} + \phi_2\mathbf{C}^2 \qquad (2.112)$$

where ϕ_0, ϕ_1, and ϕ_2 are scalar functions of the invariants of $\mathbf{C}$ and the variable s, $\phi_k = \phi_k(I_{\mathbf{C}}, II_{\mathbf{C}}, III_{\mathbf{C}}, s)$. Wineman [220] particularized this viscoelastic model with

$$\mathbf{G}(\mathbf{C}(s),\xi) = R(\xi)\{[1 + \mu \ \text{tr} \ \mathbf{C}(s)]\mathbf{1} - \mu\mathbf{C}(s)\} \qquad (2.113)$$

where

$$R(\xi) = C_\infty + (C_0 - C_\infty)e^{-\xi/\tau_R} \qquad (2.114)$$

where $R(\xi)$ is a relaxation function, C_0 and C_∞ denote the initial and the residual modulus. If time dependence is suppressed in (2.111) with (2.113) and (2.114), it reduces to a Mooney-Rivlin material in which $\mu = \mu_2/\mu_1$ (cf. (2.103)). Several solutions using this nonlinear viscoelastic material were obtained by Dai et al. [221-223].

Another nonlinear viscoelastic solid model was introduced by Fung [224], the quasi-linear viscoelastic model. The model was used extensively to describe the nonlinear viscoelastic response of biological tissues [225-227] and it is relevant due to its intuitiveness and simplicity. Fung introduced a hypothesis based on the observation that the stress developed after an imposed step in elongation (from $\lambda(0) = 1$ to λ_0) is a function of time as well as of the stretch λ_0. Furthermore, Fung observed that the stress response is insensitive to the rate of loading over a wide range. Hence, the history of the stress response, the stress relaxation function $K(\lambda,t)$, was assumed to be of the form

$$K(\lambda,t) = G(t)T^{(e)}(\lambda) \qquad (2.115)$$

where $G(t)$ is a normalized function of time, i.e. $G(0) = 1$, and is called the reduced relaxation response. $T^{(e)}(\lambda)$, a function of λ alone, is called the elastic response and is defined as the instantaneous stress response to applied stretch λ. Applying Boltzmann's superposition principle, the constitutive equation of the QLV model is

$$T(t) = \int_{-\infty}^{t} G(t-s) \frac{dT^{(e)}}{d\lambda} \frac{d\lambda}{ds} ds \tag{2.116}$$

Fung proposed a form for the reduced relaxation function formulated in terms of the relaxation spectrum, given by

$$G(t) = \frac{1 + C\left[E(t/\tau_2) - E(t/\tau_1)\right]}{1 + C \ln(\tau_2/\tau_1)} \tag{2.117}$$

with C a positive constant that determines the degree to which viscous effects are present, whereas the time constants τ_1 and τ_2 govern the fast and slow viscous phenomena, respectively [228]. $E(x)$ is the exponential integral function. The generalization to three dimensional bodies of Fung's one dimensional model follows naturally the generalization of the linearized theory of viscoelasticity, presented bellow.

Another example of a viscoelastic model, an incompressible isotropic viscoelastic material of the differential type of grade 1 and linear in **D** is characterized by the constitutive equation [229]

$$\mathbf{T} = -p\mathbf{1} + \alpha_1 \mathbf{B} + \alpha_2 \mathbf{B}^2 + \alpha_3 \mathbf{D} + \alpha_4 (\mathbf{DB} + \mathbf{BD}) + \alpha_5 (\mathbf{DB}^2 + \mathbf{B}^2 \mathbf{D}) \tag{2.118}$$

where α_i, the material properties, are scalar functions of the invariants of **B**, $\alpha_i = \alpha_i(I_{\mathbf{B}}, II_{\mathbf{B}})$. Note that if $\alpha_3 = \alpha_4 = \alpha_5 = 0$ yields the purely elastic case; if only $\alpha_3 \neq 0$, the incompressible linearly viscous fluid is obtained (cf. (2.98) and (2.107) respectively).

Zhou [230] obtained creep and stress relaxation in response to shearing of materials of the differential type obtained with simplifications of (2.118) (e.g. with $\alpha_4 = \alpha_5 = 0$, a generalization of the Kelvin Voigt solid). In a later work, Zhou [231] developed a viscoelastic material of the rate type given by

$$\dot{\mathbf{T}} + \mathbf{L}^{\mathrm{T}}\mathbf{T} + \mathbf{TL} = -\phi\left[\mathbf{T} - (-p\mathbf{1} + \alpha_1 \mathbf{B} + \alpha_2 \mathbf{B}^2 + \alpha_3 \mathbf{D})\right] \tag{2.119}$$

where ϕ is another material constant. If $\phi = 0$, the material is a particularization of a hypoelastic material (defined by the existence of a tensor function such that $\dot{\mathbf{T}} = \mathbf{g}(\mathbf{T}, \mathbf{L})$, cf. [207], sect. 99). If $\phi \to \infty$, the material of differential type is recovered.

7. Linearized theories of elasticity and viscoelasticity

Under the assumption of an infinitesimal displacement gradient (2.37), the linearization of the representation of the stress (2.95) yields

$$\mathbf{T} = \mathbb{C}\boldsymbol{\varepsilon} + \mathbf{o}(\delta^2) \tag{2.120}$$

where $\mathbb{C}$ is a 4$^{\text{th}}$ order tensor called the stiffness tensor. The linearized stress $\boldsymbol{\sigma}$ is defined as the 1$^{\text{st}}$ order approximation of stress (cf. (2.70)) and the constitutive equation is given by

$$\boldsymbol{\sigma} = \mathbb{C}\boldsymbol{\varepsilon} \tag{2.121}$$

where it is assumed that homogeneity and the stress-free state is chosen as the reference configuration. In order of the material to be isotropic, $\mathbb{C}$ must be an isotropic 4$^{\text{th}}$ order tensor. Hilbert's representation theorem with the restriction of symmetry of the linearized strain tensor implies that the response is given by

$$\boldsymbol{\sigma} = \lambda(\text{tr } \boldsymbol{\varepsilon})\mathbf{1} + 2\mu\boldsymbol{\varepsilon} \tag{2.122}$$

where λ and μ are two material properties that define the response of a linearized elastic solid, called the Lamé constants. μ is also called the shear modulus. Young's modulus and Poisson's ratio are related to the Lamé constants by

$$\lambda = \frac{E\nu}{(1+\nu)(1-2\nu)} \tag{2.123}$$

$$\mu = \frac{E}{2(1+\nu)} \tag{2.124}$$

Because the theory is linear, it is possible to find the inverse of the constitutive equation and obtain the strain in terms of the stress, i.e.

$$\boldsymbol{\varepsilon} = \frac{1}{E}\big[(1+\nu)\boldsymbol{\sigma} - \nu(\mathrm{tr}\,\boldsymbol{\sigma})\mathbf{1}\big] \tag{2.125}$$

Linearized viscoelasticity can be obtained as an extension of linearized elasticity. In a one-dimensional problem, the response functional $\mathfrak{A}$ for the linearized stress $\sigma(t)$ depends on the history up to time t of the linearized strain $\varepsilon^{(t)}(s)$ and is given by

$$\sigma(t) = \mathfrak{A}(\varepsilon^{(t)}) \tag{2.126}$$

where a non-aging and homogeneous body (no explicit dependence neither on time t nor particle X) with the stress-free state considered as reference configuration.

Constraining equation (2.126) with linear scaling and the principle of superposition [216], i.e.

$$\mathfrak{A}(\lambda_1\varepsilon_1^{(t)} + \lambda_2\varepsilon_2^{(t)}) = \lambda_1\mathfrak{A}(\varepsilon_1^{(t)}) + \lambda_2\mathfrak{A}(\varepsilon_2^{(t)}) \tag{2.127}$$

yields the representation of the stress for one-dimensional linear viscoelastic materials

$$\begin{aligned} \sigma(t) &= \varepsilon(0)\mathrm{G}(t) + \int_0^t \mathrm{G}(s)\mathrm{d}\varepsilon(s) \\ &= \int_{0^-}^t \mathrm{G}(s)\mathrm{d}\varepsilon(s) \\ &= \int_{0^-}^t \varepsilon^{(t)}(s)\mathrm{d}\mathrm{G}(s) \end{aligned} \tag{2.128}$$

where $\mathrm{d}\varepsilon(s) = \dot{\varepsilon}(s)\mathrm{d}s$. Similarly, creep forms can be obtained

$$\begin{aligned} \varepsilon(t) &= \int_{0^-}^t \sigma^{(t)}(s)\mathrm{d}\mathrm{J}(s) \\ &= \int_{0^-}^t \mathrm{J}(s)\mathrm{d}\sigma(s) \end{aligned} \tag{2.129}$$

Here $\mathrm{G}(t)$ and $\mathrm{J}(t)$ are the material properties of a one-dimensional linear viscoelastic material and are related to each other (cf. [216], sect. 4.1).

The one-dimensional model can be generalized to a three-dimensional linear viscoelastic material. For isotropic materials, four material properties, either in the stress relaxation form or in the creep form describe the response of such bodies: $E_R(t)$, $\mu_R(t)$,

$K_R(t)$ (or $E_C(t)$, $\mu_C(t)$, and $K_C(t)$), and $\nu(t)$. They correspond to responses in extension, shear, bulk deformations and the latter is the Poisson's ratio function. The representation of the stress for linearized viscoelastic materials is

$$
\begin{aligned}
\boldsymbol{\sigma}(t) &= \int_{0^-}^{t} \lambda_R^{(t)}(s)\,\mathrm{d}(\mathrm{tr}\,\boldsymbol{\varepsilon}(s))\mathbf{1} + 2\int_{0^-}^{t} \mu_R^{(t)}(s)\,\mathrm{d}\boldsymbol{\varepsilon}(s) \\
&= \int_{0^-}^{t} \mathrm{tr}\,\boldsymbol{\varepsilon}^{(t)}(s)\,\mathrm{d}\lambda_R(s)\mathbf{1} + 2\int_{0^-}^{t} \boldsymbol{\varepsilon}^{(t)}(s)\,\mathrm{d}\mu_R(s)
\end{aligned}
\tag{2.130}
$$

where $\lambda_R = K_R - \tfrac{2}{3}\mu_R$.

Inverse representations of the linearized strain $\boldsymbol{\varepsilon}(t)$ in terms of the stress history $\boldsymbol{\sigma}^{(t)}$ exist. Relationships between the material properties and creep forms of the response functional of a linearized viscoelastic material can also be found (cf. [216], page 167).

CHAPTER III

SEMICRYSTALLINE POLY(L–LACTIC ACID)

In this chapter, one particular biodegradable material, poly(L-lactic acid) (abbreviated as PLLA), is physicochemically and mechanically characterized. For more details on general characterization of polymeric materials, the reader is referred to the standard textbooks on the subject [215,217,232-234]. The first section of this chapter reports the general efforts done by others towards this difficult task. Then, results of experiments performed on fibers of non-degraded PLLA are shown and discussed. The objective of these experiments is the determination of a constitutive model that is able to describe the mechanical response of non-degraded PLLA.

On the other hand, PLLA is a biodegradable material: a spontaneous breakdown of backbone chain bonds occurs when in contact with water. This entropy producing process that the material inevitably undergoes will promote changes in the microstructure that eventually leads to a depreciation of its material properties. The remainder of this dissertation deals with constitutive models that reflect the effects of degradation on PLLA.

A. Poly(L-lactic acid)

Poly(lactic acid) (PLA) belongs to the family of aliphatic polyesters commonly made from α-hydroxy acids, which include poly(glycolic acid) or poly(mandelic acid), and are considered biodegradable and compostable [235]. PLA is a thermoplastic, high-strength, high-modulus polymer that can be made from annually renewable resources to yield articles for use in industrial packaging, in the agricultural field, or for the bioabsorbable medical device market. It is easily processed on standard plastics equipment to yield molded parts, films or fibers. It is one of the few polymers in which the stereochemical structure can be easily modified by polymerizing a controlled mixture of the L- and D-isomers to yield high molecular weight amorphous or crystalline polymers.
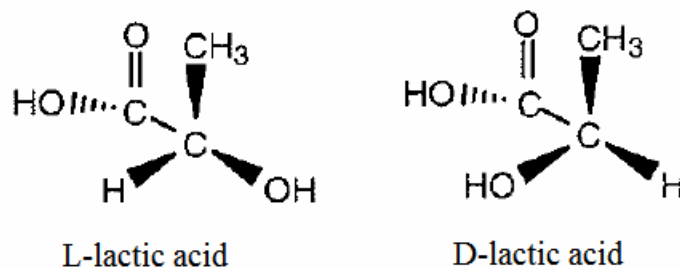
Fig. III.1. L- and D- enantiomers of lactic acid. Note the difference in location of the hydroxyl group in the chiral carbon.

PLA is degraded by simple hydrolysis of the ester bond. This reaction occurs spontaneously and does not require the presence of catalytic enzymes. When disposed of properly, PLA will hydrolyze to harmless, natural products in about six months (compared to 500 to 1000 years for conventional plastics such as polystyrene and polyethylene). It could be a technical and economic solution for the problem of the eventual disposal of the very large amount of plastic packaging used in the US [236].

1. Production, synthesis and processing of poly(lactic acid)

The basic building block for poly(lactic acid) is lactic acid, which was first isolated in 1780 from sour milk by the Swedish chemist Carl Wilhelm Scheele and first produced commercially in 1881 [237]. Food-related applications are the major use of lactic acid in the United States, and account for about 85% of the commercially produced product. It is used as a buffering agent, as an acidulant, and as a bacterial inhibitor in many processed foods [238]. Lactic acid can be manufactured either by carbohydrate fermentation or chemical synthesis from petrochemical feedstock, although fermentation predominates [239].

Lactic acid (2-hydroxy propionic acid) is the simplest hydroxyl acid with an asymmetric carbon atom and exists in two optically active configurations (cf. Fig. III.1). The L-isomer is produced in humans and other mammals, whereas both the D- and the

L-enantiomers are produced in bacterial systems. The majority of the world's commercially produced lactic acid is made by the bacterial fermentation of carbohydrates, using homolactic organisms such as modified and optimized strains Lactobacilli, which exclusively form lactic acid. The various types of carbohydrates that can be utilized in the fermentation depend on the particular strain. In general, most of the simple sugars obtained from agricultural byproducts can be used, including: (i) glucose, maltose, and dextrose from corn or potato starch; (ii) sucrose from cane or sugar beet; and (iii) lactose from cheese whey. Along with carbohydrates, the organisms require proteins and other complex nutrients. These requirements are very species-dependent, so it is typical to develop strains around the available nutrients, since these can add considerable cost to the process. High yield (up to 90% of weight of carbohydrate) commercial fermentation is usually conducted in a batch process, which takes three to six days to complete [237,238,240].

The synthesis of lactic acid into high molecular weight poly(lactic acid) can follow three different routes of polymerization. Lactic acid is condensation polymerized to yield low a molecular weight, brittle, glassy polymer, which for the most part is unusable unless external agents are used to increase its molecular weight. The second route is to collect, purify and ring-open polymerize the cyclic lactide dimer to yield high molecular weight PLA (>100,000). Ring opening polymerization was first demonstrated by Wallace Carothers in 1932 but significantly high molecular weights were obtained only with improved lactide purification techniques developed by DuPont in 1954. The third and most recent method yields higher molecular weights (>300,000) and is polymerization by azeotropic dehydration of lactic acid with a catalyst under high temperatures and reduced pressures. The residual catalysts can cause problems during further processing, such as unwanted degradation, or in the case of medical applications, catalyst toxicity [239].

In order for PLA to be processed in applications such as molding, forming, and extrusion, the polymer must possess adequate thermal stability to prevent degradation and maintain molecular weight properties [241]. With melt temperature of about 175 ºC

isotactic poly(lactic acid)
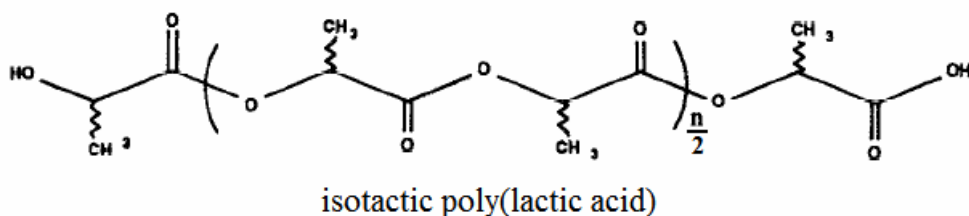
Fig. III.2. Isotactic poly(lactic acid). Either the L- or D- enantiomers yield stereoregular isotactic chains which are prone to stack in an ordered structure.

and processing temperatures in excess of 185-190 ºC, PLA has a very narrow processing window. At these temperatures, unzipping and chain scission reactions leading to loss of molecular weight, as well as thermal degradation, are known to occur [242]. The most widely used method for improving PLA processability is based on melting point depression by the random incorporation of small amounts of lactide enantiomers of opposite configuration into the polymer (i.e. adding a small amount of D-lactide to the L-lactide to obtain a copolymer, poly(DL-lactide), PDLLA). Unfortunately, the melting point depression is accompanied by a significant decrease in crystallinity and crystallization rates.

2. Morphological characterization

High molecular weigh poly(lactic acid) is a colorless, glossy, stiff thermoplastic with properties similar to polystyrene [243]. The amorphous PLA is soluble in most organic solvents such as tetrahydrofuran (THF), chlorinated solvents such as chloroform, benzene, and dioxane. Crystalline PLA is soluble in chlorinated solvents and benzene at elevated temperatures [237].

Due to the chirality of the central carbon and the methyl group, lactic acid has two enantiomers. Hence, when polymerized, poly(lactic acid) assumes two forms: poly(L-lactic) and poly(D-lactic acid) (cf. Fig. III.2). Both can coexist in the same chain, either in a random or in a block copolymer, poly(DL-lactic acid). Pure poly(L-lactic acid) or poly(D-lactic acid) are crystalline with an equilibrium crystalline melting

temperature of 207 ºC. Random or block poly(DL-lactic acid) is amorphous and the degree of crystallinity of the final polymer can be controlled with the racemization of the polymerizing mixture. Isotactic PLLA and PDLA have favorable mechanical properties over their atactic co-polymer relatives (PDLLA) largely due to their potential for high crystallinity within isotactic materials [244]. On the other hand, the maximum effect in temperature stability is achieved when a 1:1 mixture of PLLA and PDLA is crystallized, forming a racemic crystallite by stereocomplexation. The pure stereocomplex has a melting point of 230 ºC and mechanical properties greater than either pure polymer [237]. The addition of small amount of PDLA and the presence of stereocomplex crystallites that PDLA and PLLA form is effective to increase nucleation and consequently the number of spherulites and the overall crystallization rate [245].

De Santis and Kovacs [246] in 1968 concluded from x-ray scattering that the crystalline structure poly(L-lactic acid) consists of left handed helical chains whereas PDLA has a right handed helical crystalline structure. Both yield spherulitic crystalline morphologies. At least three different polymorphs of PLLA have been observed, the α, β, and γ forms [247], each with a different inherent anisotropy. Transformations from the α- to the β-form during tensile drawing and solid state extrusion have been observed [248,249]. Density changes slightly with crystallinity as well as with type of crystal: the density of an amorphous phase is reported to be 1.245 g/cm^3, a value that agrees with 1.25 g/cm^3 provided by Cargill Dow, a poly(lactic acid) manufacturer [241]. The densities of the α- and β- crystals is 1.285 g/cm^3 and 1.301 g/cm^3, respectively [250,251]. As the β form shows a helical chain that promotes an improved stacking and a closer packaging [251], its density is expected to be greater.

Macroscopic deformation of the bulk polymer promotes chain conformational changes at the microscopic level. The helical conformation of the PLLA chain reduces the stiffness along the chain axis and bond rotation is likely to play a significant role in the deformation mechanism of the polymer. Shear along the helixes is the easiest mode of deformation causing a disruption of the lamellar packaging of the chains and promoting the conversion between the phases [247]. Renouf-Glauser et al. [252] showed

that craze structures developed on deformation of the amorphous phase as series of striations in post-failure amorphous PLLA were observed and interpreted as cracks that formed when failed crazes continued to deform. Crystalline PLLA deformed through crystal-mediated deformation, with contributions from both cavitation and fibrillated shear, common deformation modes of lamellar systems. Moreover, Renouf-Glauser et al. [252] proposed that the mechanism by which craze developed changed significantly on hydration due to the plasticization effect of water. While for dry PLLA the dominating factor during deformation is the changing dimensions of crazes that formed soon after yield, the water content in hydrated PLLA allows better chain mobility so that new crazes with smaller and smaller fibril spacing are formed continually. Hydration also plasticized the movement of crystallites.

The glass transition temperature of poly(lactic acid), T_g, is located around 60 ºC, with small dependence on the molecular weigh, copolymerization and degree of crystallinity [253]. When implanted, the material will usually be at a temperature slightly lower than T_g. Therefore, the understanding of the glass transition dynamics is particular important as conformational dynamics will influence the behavior of the polymer at physiological temperatures, including structural relaxation that yields the inherent viscoelastic behavior. Perego et al. [244] and Jamshidi et al. [242] found that the glass transition temperature was not greatly affected by the stereochemical makeup or the range of molecular weights tested. Furthermore, Mano et al. [253] observed the presence of significant degrees of freedom that are not completely arrested in the glass forming process.

Final molecular weight and resultant crystallinity depends on the fabrication process, annealing, and thermal treatments. Miglaresi et al. [254] concluded that very high crystallization degrees can be attained by the combined effect of time and temperature of annealing. Nevertheless, the process is always associated with thermal cleavages that cause substantial reduction in molecular weight. Fambri et al. [255] reported that crystallinity depends on the fabrication process. Chains align as they deform, inducing an increase in crystallinity with strain. Fibers obtained by melt

spinning with a broad range of collection rates showed considerable differences in morphology: lower collection rates yielded mostly amorphous fibers while 30 to 40% crystalline as-spun fibers were produced at higher rates. Furuhashi et al. [256] showed that the higher-order structures that are obtained during the process of drawing strongly affects crystallinity obtained after with annealing.

3. Mechanical properties of poly(lactic acid)

The most common mechanical properties found in the literature for poly(lactic acid) are tensile strength at break, tensile yield strength, tensile modulus, and tensile elongation following ASTM methods D638 or D882 (tensile tests for dumbbell shapes and thin films respectively). As hinted above, the mechanical behavior is highly dependent not only on gross quantities of poly(lactic acid) such as molecular weight and degree of crystallinity, but also its microstructure seems to play an extremely important role in the mechanisms of deformation. This subsection reports general mechanical properties as well as common experimental methods obtained by other authors (an extensive amount of work is available, hence only the ones relevant to this dissertation are presented). Concerns should be raised on the typical methodology followed: although the viscoelastic nature of poly(lactic acid) is generally recognized among most of the studies, a shear majority of them seem to ignore it and present results based on linearized elasticity.

Cargill Dow LLC produces commercially available PLA as NatureWorks^{TM}. The various grades differ in stereochemical purity, molecular weight, and additive packages. Drumright et al. [241] reported the typical mechanical properties of NatureWorks PLA: 50 MPa of tensile strength at break, 60 MPa for tensile yield strength and 3.5 GPa for tensile modulus. The elongation at break differed in between grades, ranging from 2.5% to 6.0 %. When cast into fibers, the elongation decreased with draw ratio. No molecular weight data were provided to accompany these standard data.

Agrawal et al. [81] in 1992 studied the impact of draw ratios on the mechanical properties of extruded PLLA monofilaments of circular cross-section. The starting

polymer had values of 30,800 M_n and 59,300 M_w, no dramatic changes occurred during extrusion, drawing and annealing, but their molecular weight measurement showed great variance. Monofilaments were tested in tension at a constant displacement rate; with a torsional pendulum, the shear modulus was also obtained. For fibers with draw ratios of 4:1, an average Young's modulus of ≈ 3.5 GPa was obtained, while for 6:1 and 8:1 draw ratios, a considerable higher value was obtained, ≈ 6.0 GPa. The shear modulus did not change with draw ratio and its average was found to be ≈ 1.3 GPa. The ultimate tensile strength increased dramatically with draw ratio, from ≈ 140.0 MPa to ≈ 350.0 MPa. The percentage elongation before break decreased as the draw ratio increased. The effect of annealing of the fibers was also studied. Constrained and unconstrained annealing at 140 ºC was conducted for 15 minutes. Annealing in both conditions resulted in a partial reversal of the effects of drawing with an increase in the percentage of elongation before break.

Grabow et al. [108] reported the mechanical testing of laser cut PLLA micro-specimens of cross section of approximate dimension of 300 μm (related to the thickness of a laser cut PLLA stent strut). 35% crystalline PLLA had a M_w of 640,000 g/mol (a somewhat strangely high value) and a polydispersity index M_w/M_n of 1.7. Tensile tests were carried out in controlled force mode with a force ramping of 1 N/min until specimen failure. The elastic modulus of pure PLLA was found to be 2.58 GPa; a tensile strength and elongation at break of 44.9 MPa and 5.5% respectively were reported. The influence of rate of loading and the inherent viscoelasticity of the material were recognized: results on the stress vs. strain curve of a blend of PLLA/TEC (90/10) for 3 different loading rates, 10N/min, 1.0 N/min, and 0.1 N/min showed marked differences over the entire strain range. On the other hand, it can be concluded from their results (cf. [108], Figure 5) that loading rates above1.0 N/min do not show great differences in the small strain region ($< 5\%$).

Perego et al. [244] studied the effect of molecular weight and crystallinity on PLA mechanical properties of dumbbell specimens obtained by injection molding. The viscometric molecular weight in this study was determined through the inherent

viscosity in chloroform at 25 ºC and the Mark-Houwink equation. The mechanical characterization was performed on specimens maintained in anhydrous conditions. Tensile testing was performed at a constant displacement rate of 50 mm/min. Several molecular weights and copolymer composition were considered (PLLA and PDLLA), as well as annealing to dramatically increase crystallinity. Within the molecular weights studied (ranging from 20,000 to 60,000), their tensile results are not apart from the other studies above: Young's modulus in the range of 3.5-4.0 GPa, tensile strengths of about 50-60 MPa, and elongations at break increasing with molecular weight from 1.5% up to 7%. An overall increase in strength is obtained as the molecular weight increases, but seem to reach a plateau of property values at higher molecular weights (around $M_v = 55,000$). On the other hand, elongation at break is considerably decreased with annealing and increased crystallinity.

Renouf-Glauser et al. [252] investigated the failure of PLLA. Compression molded PLLA dumbbell samples with M_w and M_n of 320,000 and 130,000 g/mol respectively were subjected to a tensile test at a displacement rate of 0.12 mm/min. Amorphous PLLA showed an elastic modulus of 1.15 ± 0.01 GPa (a somewhat low value, taking to account the reported molecular weight), a yield stress of 62 ± 7 MPa and an elongation at break of 14.5% ± 2.2%. For samples annealed till complete crystallization, the elastic modulus had increased slightly and the strain at break decreased significantly in comparison to the amorphous material. Failure occurred in a ductile manner, with similar yield stress, either for crystalline or amorphous samples. Transition from ductile failure to brittle failure was reported to occur between samples annealed at 120 ºC and 150 ºC. Furthermore, Renouf-Glauser et al. observed that while hydration did not impart significant changes in elastic modulus or elongation at break, however tensile strength decreased upon hydration.

Takahashi et al. [249] reported a stress vs. strain plot of the tensile drawing of a highly oriented α-film at a constant draw temperature of 170 ºC (near the melting temperature, ≈ 180 ºC) at different crosshead speeds with strain rates ranging from 0.5 %/min to 100 %/min (cf. [249], Figure 2). While yield and ductility are observed to

be strain rate dependent (with achieved stress and strain increasing with increasing strain rate), the response of the film before the yield condition is quite independent of strain rate. Takahashi et al. provided another stress vs. strain plot (cf. [249], Figure 7) with a constant strain rate of 50 %/min with changing temperatures. Striking differences exist from the glass state, the transition region and the rubbery state.

Weir et al. [257] analyzed the influence of fabrication process in the mechanical properties of dumbbell shapes and did not found striking differences between compression molding and extrusion after annealing. As expected, the extruded material showed a slight increased crystallinity (before, 20% in the extruded to 10% in the compression molded, but after annealing, 40% on both,). Nevertheless, they reported elastic modulus of ≈ 0.65 GPa, a tensile strength at break of ≈ 67 MPa, and an extension at break $\approx 1.6\%$. The initial molecular weight (M_w) was 460,700, dropped to 415,100 after extrusion and to 58,000 after ethylene oxide sterilization, the reason for such low modulus.

Sarasua et al. [258] analyzed both PLLA and PDLA and did not observed striking differences between the behavior of both. Polymers with a molecular weight of $M_v = 320,000$ before processing were subjected to tensile tests at a single displacement rate of 5 mm/min. They observed a very long (up to 1.5% strain) linear response with elastic modulus of ≈ 3.5 GPa, yield at ≈ 65 MPa and a slightly lower tensile strength at break, which occurred at 3% extension.

B. Experiments towards a model for non-degraded poly(L-lactic acid)

A constitutive relation describes the gross behavior of a material, which results from its internal constitution, in response to applied loads. Furthermore, one should not expect any constitutive relation to describe accurately all behaviors exhibited by the material under all conditions. Rather, constitutive relations describe a material's behavior "under specific conditions of interest" [259]. This section deals with the formulation of constitutive relations for the description of the mechanical response of

non-degraded poly(L-lactic acid) over the range of room and body temperatures, i.e. in its glassy state, and

1. Initial experiments with PLLA fibers

Monofilament fibers obtained from PLLA pellets (Purasorb PL, Purac America, Lincolnshire, IL, USA) were supplied by TissueGen (Dallas, TX, USA) and were produced by a wet-spinning technique described elsewhere [260]. Only the intrinsic viscosity of the melt in chloroform at 25 ºC was provided by TissueGen, which has a value of 1.69 dl/g. From the Mark-Houwink equation,

$$\eta = 5.45 \times 10^{-4} M_v^{0.73},$$ (3.1)

here shown with constants for this particular solvent and temperature [244], the viscometric molecular weight is $M_v = 60,654$ g/mol. Melting point, glass transition and % crystallinity were not supplied and so were determined with a Differential Scanning Calorimeter Q-100 (TA Instruments, New Castle, DE, USA). Glass transition temperature was found to be T_g = 58 ºC, melting temperature T_m = 180 ºC, and the crystallization temperature range from 90 ºC to 110 ºC (cf. Fig. III.3). Integration of the peak corresponding to melting of the sample yields the enthalpy of fusion ΔH_m. The crystalline fraction x_c is obtained as the fraction

$$x_c = \frac{\Delta H_m}{\Delta H_m^0}$$ (3.2)

where ΔH_m^0 is the enthalpy of fusion of the 100% crystalline material (i.e. corresponding to an infinite thickness crystal). A value of $\Delta H_m^0 = 140$ J/g was used in the calculation [261,262]. Several samples were subjected to differential scanning calorimetry and the crystalline fraction of the non-degraded PLLA was found to be $x_c \approx 51\%$.

The fibers are approximately 5 cm long and have an approximate diameter of 1 mm. A more precise measurement of diameters was performed with a digital caliper
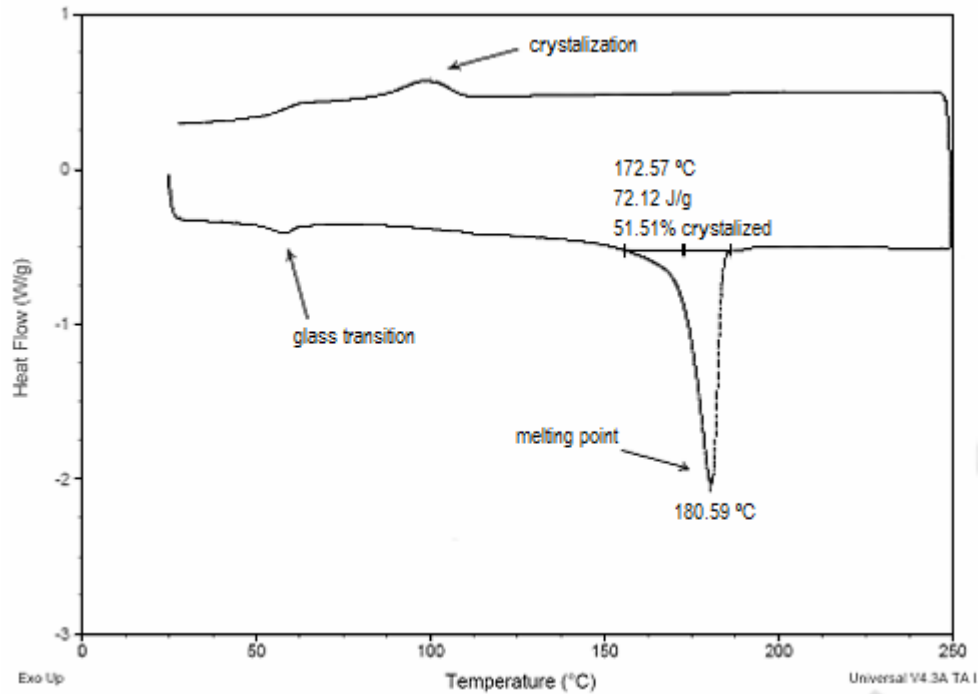
Fig. III.3. Differential scanning calorimetry of a typical non-degraded PLLA sample. The percentage crystallinity was found to be approximately 51%. Glass transition, melting point and crystallization on cooling are also identified in the DSC curve. The temperature was increased and decreased at a rate of 10 ºC/min up to 250 ºC. The bottom part corresponds to heating whereas the top part corresponds to cooling.

(Fischer Scientific, Pittsburgh, PA, USA) and the measurements yielded a variance in the diameters, ranging from 0.85 mm to 1.10 mm. Visual inspection also showed some kinks in portions of the fibers, most likely due to processing. In order to prevent these defects and the slight taper to have considerable impact in the tensile tests, 2 cm long samples were obtained from PLLA fibers. During the sample collection process, defects were avoided. Furthermore, the variance of the diameters of each sample due to the tapering of the fibers decreased significantly amongst the sample. When calculating stresses on each sample, the averaged initial cross sectional area of each sample was considered. Strains are computed as the ratio of the increase in length over the initial length.
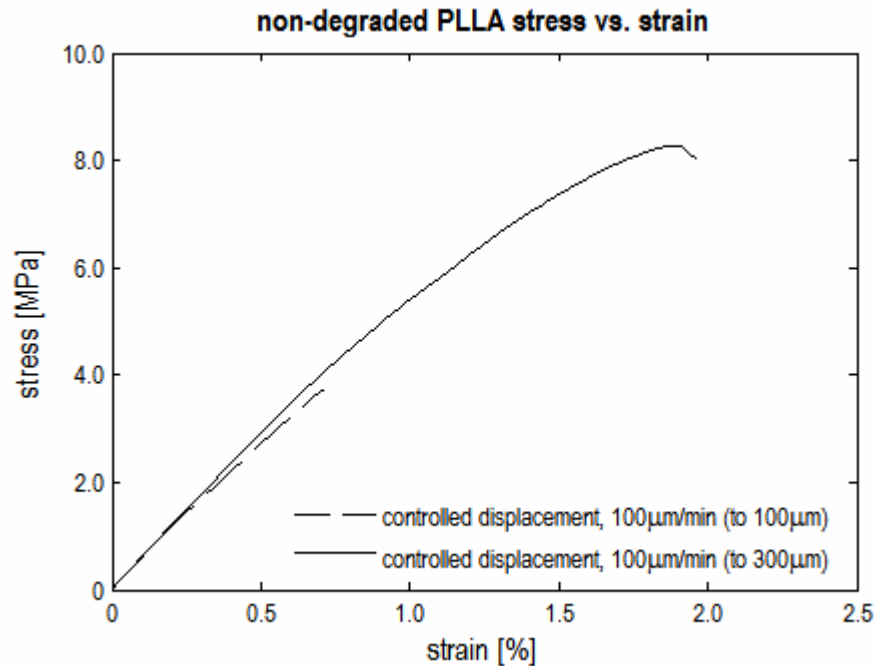
Fig. III.4. Stress vs. strain plot of the response of non-degraded PLLA to ramp displacements of 100 μm/min. The response is clearly nonlinear, with softening as strain increases. Furthermore, strain induced chain alignment might have been imparted to the sample during the 1st run (dashed line).

Mechanical testing was performed at air conditioned room temperature (≈ 25 °C) with samples that were moist free. Moist free samples were obtained through overnight desiccation in a vacuum oven (VWR 1400E, Sheldon Mfg. Inc., Cornelius, OR, USA) and storage with Drierite crystals (W.A. Hammond, Xenia, OH, USA). Mechanical testing comprised tension-elongation tests performed in a Dynamic Mechanical Analyzer Q-800 (TA Instruments, New Castle, DE, USA). Dynamic mechanical analysis can be performed under two modes: controlled force or controlled displacement.

The first set of mechanical tests performed was ramp increases in displacement of the clamp crossheads at a constant rate of 100 μm/min (Fig. III.4). Average strain rate is 0.71 %/min. The first test was conducted up to a maximum displacement of 100 μm (dashed line in Fig. III.4) and the stress vs. strain behavior shows an almost linear behavior, but in fact the slope decreases slightly as the strain increases. After the test was
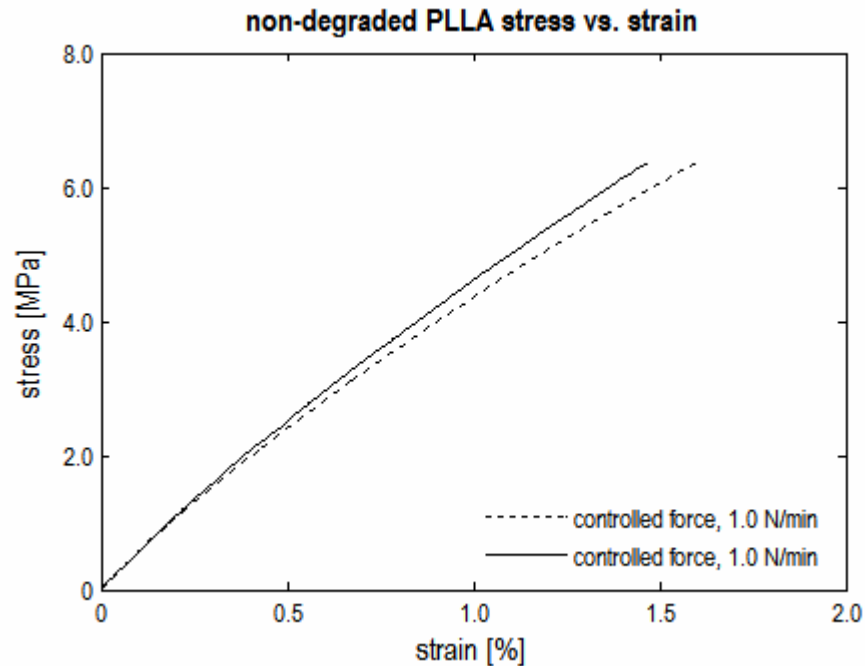
Fig. III.5. Stress vs. strain plot of the response of non-degraded PLLA to ramp in force of 1.0 N/min. The curves are bellow the previous ones due to the difference in rate of loading (slower in this test). Deformation might have induced hardening in the material (solid line shows the 2nd run).

performed, the displacement was released instantaneously and the sample did not recover its initial length immediately. After approximately 8 minutes, the initial and final lengths (measured accurately as length between crossheads) were considered to be similar: initially 14.0952 mm to 14.1034 mm after, yielding a discrepancy of 0.06%.

A second test under the same conditions was performed on the recovered sample, this time with a ramp displacement up to 300 μm (solid curve in Fig. III.4). Nonlinearities in the stress vs. strain curve became evident. Furthermore, the sample failed at 1.958% and a maximum followed by a decrease in stress observed is characteristic of ductile failure. Comparison between the two tests shows similar results under the same strain range: the measured stresses are just slightly apart. Nevertheless, at 0.70% strain, the second test yielded a greater stress by 7.5%. This can be attributed to the inherent scattering due to experimental error. On the other hand, the first deformation

non-degraded PLLA stress vs. strain for several averaged strain rates
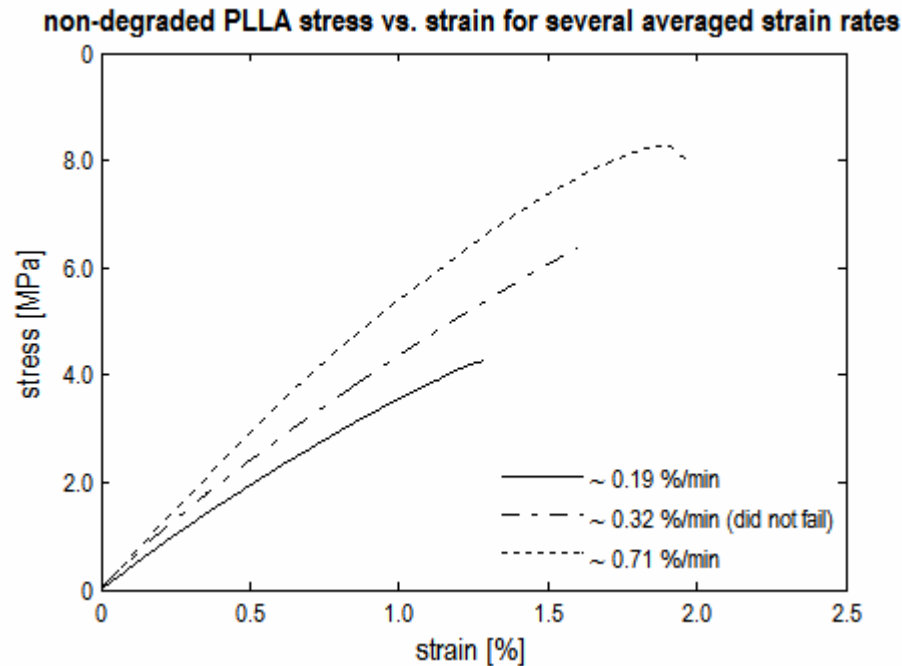
Fig. III.6. Stress vs. strain plot of the response of non-degraded PLLA to different strain rates. As strain rate decrease, so does the slope of the curves. Furthermore, extension at break is also reduced with decreasing strain rate.

might have promoted changes, i.e. strain induced chain alignment, which rendered the sample slightly stiffer for the second test.

The controlled force mode was investigated with a 2nd sample. Tests with prescribed ramps in force of 1.0 N/min were conducted consecutively, yielding an averaged strain rate of ≈ 0.32 %/min (Fig. III.5). The slope of the curves is considerably lower than the slopes obtained in the previous mode. Because the loading condition is considerably different, i.e. with a lower strain rate, it is expected the response to be different as well. The recovery was complete after 11 minutes: initially 7.4919 mm, 7.5017 mm after. A slight difference was observed from the 1st to the 2nd test (dotted and solid line in Fig. III.5, respectively), similar to the difference obtained with ramp displacements (cf. Fig. III.4). An approximate 7.5 % decrease in the achieved strain at the maximum force of 5.0 N was observed, which can be due to experimental error or changes promoted by the 1st run. Finally, the sample did not fail in any of the two runs.

Two major characteristics of these tensile experiments are: (i) a delayed recovery after the instantaneous release of either strain or stress, and (ii) a clear dependency of the response of the material on the rate at which it is loaded. Other strain rates were also considered (cf. Fig. III.6). As strain rate increases, the material becomes not only stiffer (meaning that greater forces are needed for a given deformation), but also stronger (meaning that failure only happens at greater loads and greater elongations), which is coherent with the rupture envelope for generic polymeric materials (cf. [233] Figure 12.32, page 370).

2. Non-degraded PLLA is not an elastic material

A general definition of elastic given in dictionaries is a material that is "capable of returning to its original length, shape, etc., after being stretched, deformed, compressed, or expanded". In more precise terms, the bulk response of an elastic material implies that (i) the loading and unloading paths coincide; (ii) the material responds instantaneously to an applied load and indeed its behavior is time-independent; and (iii) the material returns to its former unloaded configuration upon the removal of external loads [259]. The common trait of all this elastic behaviors is that the elastic response is a non-dissipative response, path independent (i.e. only the initial and final configuration determine the response), and no permanent set is imparted to the body.

It can be seen from Fig. III.4 through Fig. III.6 that the response of PLLA is not elastic as it violates the time independence requirement. The same deformation yield higher stresses if the material is deformed faster. Furthermore, the response is not instantaneous, as the fibers take around 10 minutes to recover their initial shape. Although no permanent set was induced to the body and this fact meets the rough definition found the dictionary, it is not a sufficient condition for a body to be treated as elastic, especially within the time scale involved. Also, changes within the material seem to occur during deformation as the response of a 2nd run does not follow the first.

The elastic behavior of non-degraded PLLA is further refuted as unloading curves show a lag form the loading curve (a cycle of ramp increase followed by a ramp
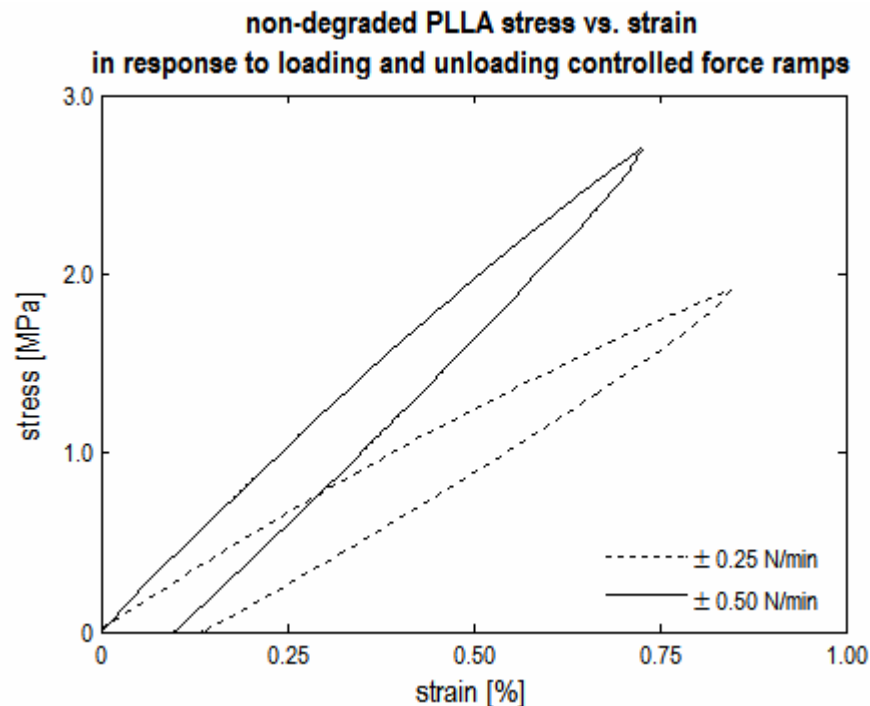
Fig. III.7. Stress vs. strain plot of the response of non-degraded PLLA to two different cycles in prescribed force. Slower deformations lead to lower slopes and the loading and unloading curves do not coincide. When force is returned to zero, an elongation still exists.

decrease in force is shown in Fig. III.7), phenomena commonly referred as mechanical hysteresis. Furthermore, when the load was returned to zero, a noticeable but recoverable elongation still existed: once again, the unloaded sample returned to its initial shape after some time. The work per unit volume can be calculated as the difference between areas of the loading and unloading curves. A characteristic of non-dissipative responses is that no work is done in a closed mechanical cycle (which implies that the loading and unloading should coincide). For non-degraded PLLA under a closed mechanical cycle, the unloading curve lies bellow the loading curve (cf. Fig. III.7) yielding a positive net work done. Hence, the response is dissipative and consequently not elastic.
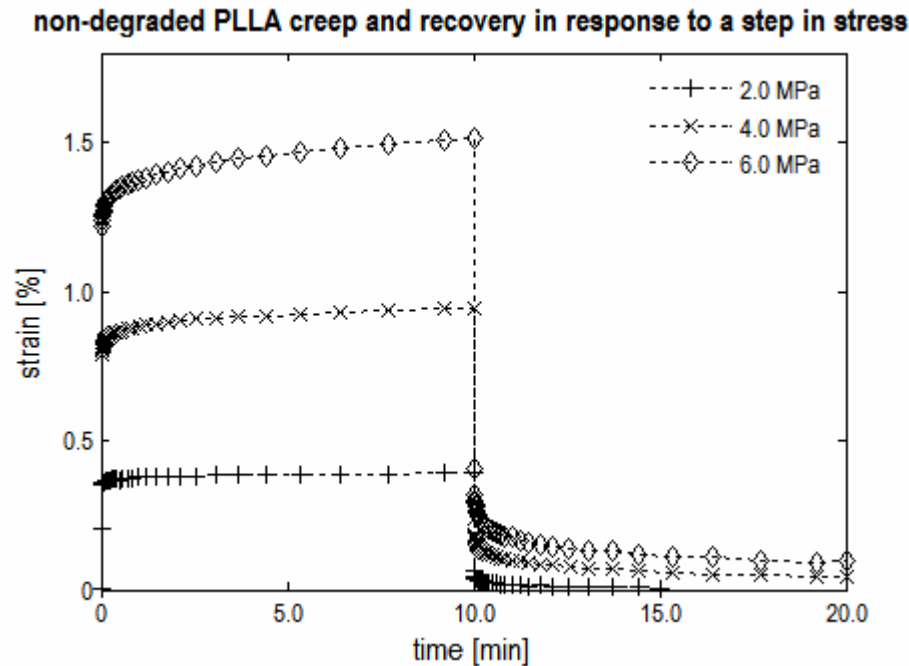
Fig. III.8. Creep and recovery of non-degraded PLLA samples in response to different steps in stress. After and instantaneous elastic response to the applied stress, the strain increases with time although a constant stress is applied. Upon removal, some part of the deformation is recovered instantaneously. Total recovery occurs but takes more time than the allowed 10 minutes.

3. Non-degraded PLLA is a viscoelastic material

When the behavior of a solid is not elastic, it is said to be inelastic. Inelastic response comprises viscoelastic and plastic responses. As seen above, no permanent set is induced to non-degraded PLLA, at least within the regimes tested, so plastic deformation is excluded. As the term suggests, viscoelastic behavior accounts for a combined viscous (or fluid-like) and elastic (or solid like) behavior, and it is observed in a broad class of polymers, due to common microstructural characteristics among them. As an external force is applied to a material, internal forces are produced by distortion of its physical structure. While the elastic response is mostly associated with metals on which large cohesive inter-atomic forces are brought into play by small deformations of
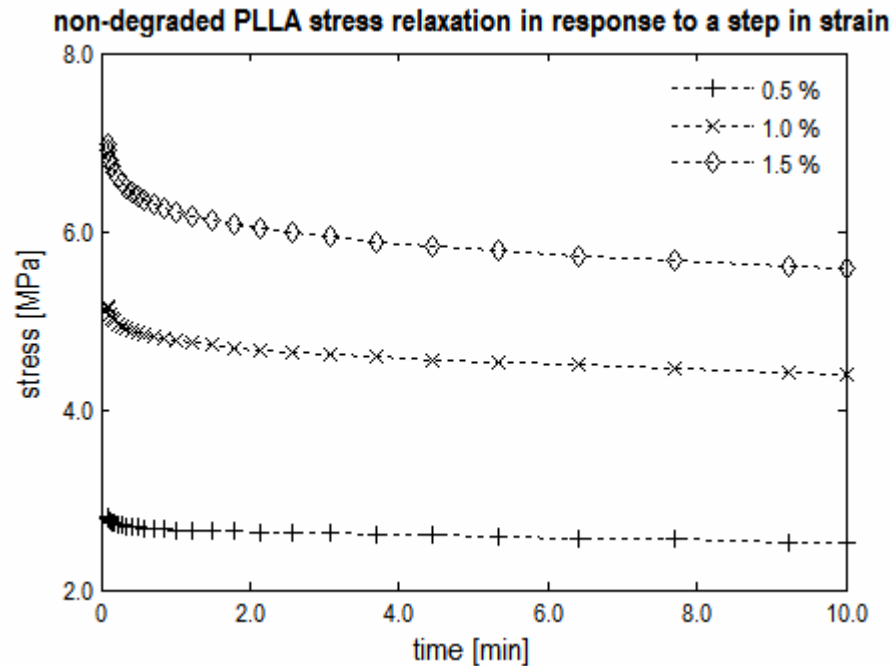
Fig. III.9. Stress relaxation response of non-degraded PLLA samples in response different steps in strain. Stress increases instantaneously in response to the increase in strain. Relaxation of stress occurs with time as less force is required to maintain the prescribed deformation.

the crystalline structure, viscoelastic phenomena in polymers is related to the movement of flexible thread-like long chain molecules. The conformational changes of these long molecules happen at different time and space scales, ranging from gross long-range contour rearrangement to the atomic level reorientation of bonds in the chains.

From a macroscopic standpoint, viscoelastic materials show three broad characteristics: (i) stress relaxation, which is a time dependent decrease in load for a constant deformation; (ii) creep, which is a time-dependent increase in deformation under the action of a constant load; and (iii) hysteresis, associated with dissipative systems, on which the work done by deformation is not fully recoverable but converted to heat energy.

It was seen above that non-degraded poly(L-lactic acid) shows hysteresis (cf. Fig. III.7). Non-degraded fibers of poly(L-lactic acid) were subjected to creep and stress relaxation tests (cf. Fig. III.8 and Fig. III.9, respectively).

On the creep test, the stress was instantaneously increased to an initial value σ_0 (2.0, 4.0, and 6.0 MPa) at time $t = 0$ and held fixed for 10 minutes (cf. Fig. III.8). Obviously, instantaneous loading is an idealized loading and can never be achieved in a practical sense either because of the inertia of the specimen or the testing device. Nevertheless, the DMA allows rapid and precise loading with a rise time of only 1.29 seconds, which compared with the entire 10 minutes of the creep test, is considered to be small and to impart negligible effects on the overall response of the sample.

The responses obtained share some typical features: an instantaneous increase in strain, and a continued straining in time at a non-constant rate. The instantaneous increase in strain is thought of as an instantaneous elastic response and the total creep curve is a combination of elastic and viscous effects. The strain seems to asymptotically reach a constant value ε_0, which implies that the material is solid-like [216]. Crystallites usually work as transient cross-links [215,232], conferring the network a "maximum" possible amount of deformation and causing the "return" to the original configuration. Obviously, due to the lack of permanent cross-linking, chains can always slip and slide over one another. After 10 minutes of creep, the stress was released to zero. The responses also share some typical features: some instantaneous strain recovery, followed by a delayed recovery. As expected from a solid-like material, all the strain seems to be recovered (although only 10 minutes of recovery were measured, this can be inferred from the asymptotic behavior shown as well as can be corroborated with the facts in the previous subsection).

The stress relaxation test is characterized by an instantaneous increase in strain to ε_0 (0.5%, 1.0%, and 1.5%) at $t = 0$ and then held fixed for 10 minutes (cf. Fig. III.9). Typical rise times for stress relaxation experiments are approximately 5 seconds. The typical features of the stress relaxation responses are: an instantaneous jump in stress followed by a gradual decrease of the stress required to maintain the constant strain ε_0 over time. The stress seems to decrease asymptotically to a non-zero residual value, which is a characteristic of solid-like materials. As reorientation of the molecular structure occurs in response to the applied strain, this reorientation allows the
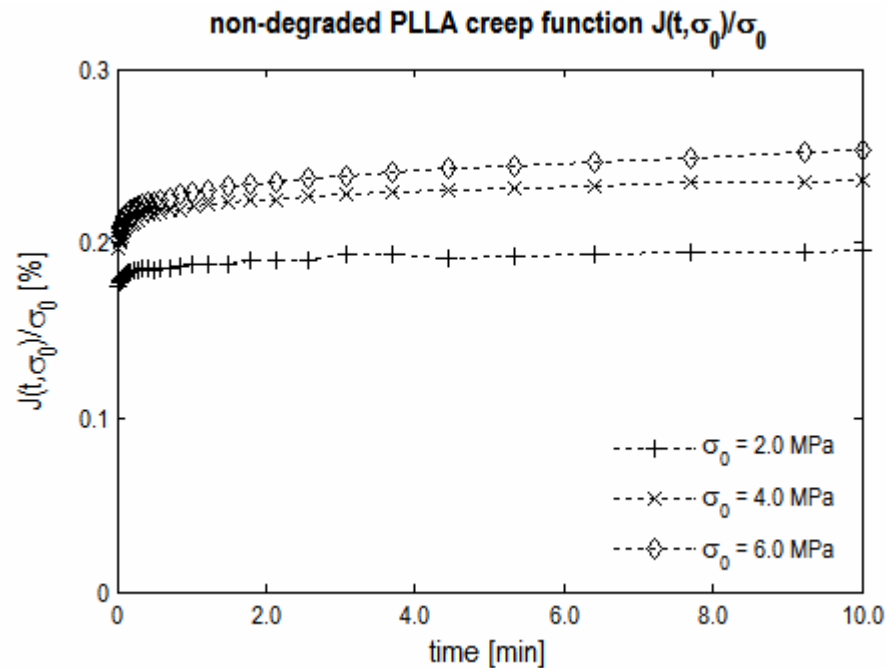
Fig. III.10. Creep modulus of non-degraded PLLA. Creep modulus was obtained for each of the stress levels of the creep experiment (cf. Fig. III.8). Because the material is viscoelastic, the modulus changes with time. Different stress levels yield different creep modulus, hence the response is not linear.

intermolecular forces to relax. Because of the transient crosslinks, this reorientation is limited, and the material will always require some force to maintain a distorted state.

4. Non-degraded PLLA is not a linear viscoelastic material

A linear viscoelastic material possesses a response that shows linear scaling and to which the principle of superposition applies. In other words, the time dependent viscoelastic response is independent of the deformation. Linear scaling and the superposition of separate responses are independent and both must be met in a linear viscoelastic material.

For non-degraded PLLA, the principle of superposition does not apply. For superposition to be valid, creep and recovery curves should be a "reflection" of each other. As the stress level increases the strains at the end of the recovery time are not zero
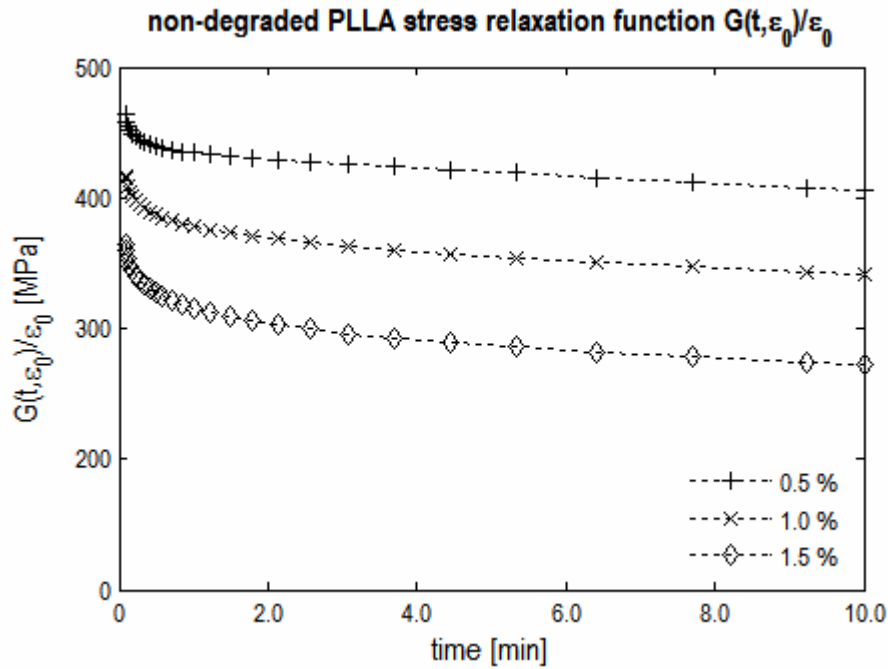
Fig. III.11. Stress relaxation modulus of non-degraded PLLA. Stress relaxation modulus was obtained for each of the strain levels of the stress relaxation experiment (cf. Fig. III.9). Stress relaxation modulus is found not only to depend on time (a viscoelastic material) but also on strain (a nonlinear viscoelastic material).

(cf. Fig. III.8). On the other hand, at the lowest stress level, the principle of superposition seems to be valid.

If $J(t,\sigma)$ and $G(t,\varepsilon)$ are the creep and stress relaxation responses of a material (shown in Fig. III.10 and Fig. III.11 respectively), linear scaling can be expressed mathematically in the form

$$J(t,\sigma) = \sigma \frac{J(t,\sigma_0)}{\sigma_0} = \sigma J(t) \qquad (3.3)$$

$$G(t,\varepsilon) = \varepsilon \frac{G(t,\varepsilon_0)}{\varepsilon_0} = \varepsilon G(t) \qquad (3.4)$$
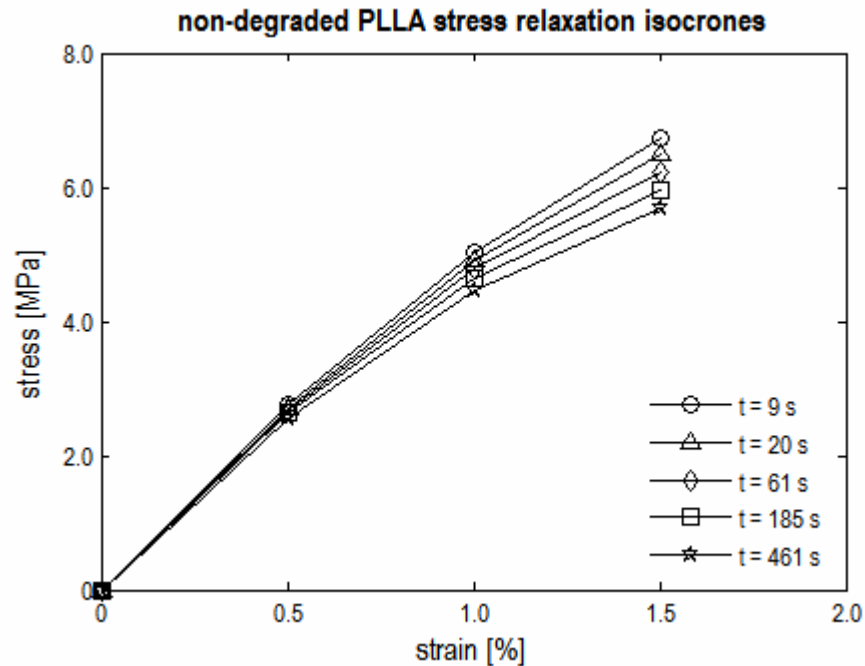
Fig. III.12. Isochrones of non-degraded PLLA. Isochrones were obtained from the stress relaxation experiment (cf. Fig. III.9). A linear viscoelastic material yields linear isochrones with constant slope.

i.e. there exist functions of time only, $J(t)$ and $G(t)$ called creep modulus and relaxation modulus respectively, that describe the creep and stress relaxation responses (cf. equations (2.128) and (2.129)). Moreover, the response is independent of stress or strain.

The creep modulus and relaxation modulus for non-degraded PLLA do not show linear scaling, i.e. a single curve to which all the creep or stress relaxation responses coincide when scaled by its corresponding stress or strain level does not exist (cf. Fig. III.10 and Fig. III.11). Hence non-degraded PLLA is not a linear viscoelastic material, at least under the range of strains/stresses tested.

Another method for determining whether linear scale is possible utilizes the notion of isochrones. An isochrone is obtained for a particular time t_0 and is the loci of $(\sigma(t_0), \varepsilon(t_0))$, each obtained at t_0 from different creep or stress relaxation tests. If the material is linear viscoelastic, the isochrones should be linear and have constant slope. Stress relaxation isochrones obtained with the three stress levels shown in Fig. III.12.
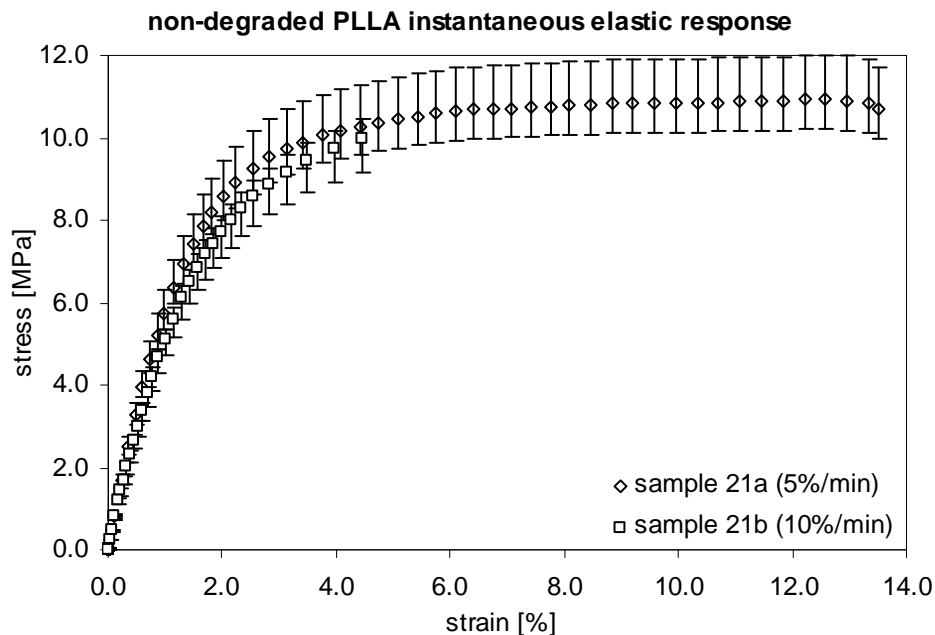
Fig. III.13. Experimental instantaneous elastic response of non-degraded PLLA at different high strain rates. Intense strain softening is observed after some deformation is achieved. Two regimens are clearly distinguished: an initial increase followed by deformation with little increase in stress. Sample 21b released from the clamp before this stage. The shape of the stress vs. strain curve can be roughly described as a fractional power, or as a logarithm, or as an exponential increase. Furthermore, there exists a strong linear relationship between $dP/d\lambda$ vs. P, where λ is the stretch.

Although only 3 different stress levels were used, the isochrones are clearly not linear, which corroborates with the conclusion that non-degraded PLLA is not a linear viscoelastic material.

C. The instantaneous elastic response of non-degraded PLLA

As the response of non-degraded PLLA at very high strain rates seems to be insensitive to strain rate of loading, a time independent "instantaneous" elastic response can be obtained from experimental testing. Two samples from the same fiber were tested at different strain rates: 5%/min and 10%/min (cf. Fig. III.13). Under these conditions,

the experiment becomes difficult to perform: sample 21b got released from the clamp before failure while sample 21a showed a failure point at considerably higher strains, which were achieved by a very small increase in stress. At this regime, the material was probably no longer behaving like an elastic material as it is extrapolated that most of these strains will not be recoverable, i.e. the material was almost like plastically flowing. On the other hand, the response before strain of 5%, which comprises both tests, seems to concord, and the validity of an instantaneous elastic response (abbreviated as IER) independent of strain rate seems to hold. Furthermore, the usual strain steps applied to the samples during stress relaxation tests are up to 3%, which are clearly inside this regime. Hence, for data reduction purposes, the range 0% to 5% will be chosen as a validity range for the constitutive equations employed to describe the IER of non-degraded PLLA.

Due to the nonlinear nature of the stress vs. strain plot of the IER (cf. Fig. III.13), the classical linear elastic model is clearly not valid in this case. Hence, a hyperelastic model will be used. The first natural choices for hyperelastic models are the neo-Hookean and the Mooney-Rivlin materials, with the corresponding stored energy functions given by equations (2.102) and (2.103) respectively.

The motion (cf. equation (2.1)) corresponding to uniaxial extension is given, in a Cartesian coordinate system, by,

$$x_1 = \frac{1}{\sqrt{\alpha}} X_1, \qquad x_2 = \frac{1}{\sqrt{\alpha}} X_2, \qquad x_3 = \alpha X_3 \qquad (3.5)$$

where (X_1, X_2, X_3) and (x_1, x_2, x_3) represent the coordinates of a typical material particle in the undeformed (or reference, κ_R) and deformed (or current κ_t at a particular time t) configurations, respectively. In equation (3.5), α is the axial stretch and is related to strain by

$$\alpha = 1 + \varepsilon \qquad (3.6)$$

The deformation gradient $\mathbf{F}_{\kappa_R}$ corresponding to the motion above is obtained from equation (2.8) and in a Cartesian coordinate system has a matrix representation:

$$\left(\mathbf{F}_{\kappa_R}\right) = \begin{pmatrix} 1/\sqrt{\alpha} & 0 & 0 \\ 0 & 1/\sqrt{\alpha} & 0 \\ 0 & 0 & \alpha \end{pmatrix} \qquad (3.7)$$

The above motion is isochoric as it satisfies equation (2.9). The left and right Cauchy-Green stretch tensor, given by equations (2.11) and (2.12) have the following same matrix representation with respect to the above defined coordinate system:

$$\left(\mathbf{B}_{\kappa_R}\right) = \left(\mathbf{C}_{\kappa_R}\right) = \begin{pmatrix} 1/\alpha & 0 & 0 \\ 0 & 1/\alpha & 0 \\ 0 & 0 & \alpha^2 \end{pmatrix}. \qquad (3.8)$$

The Cauchy stress in a neo-Hookean body undergoing this motion is obtained from representation (2.98) with the stored energy function (2.102) and has the following matrix representation

$$\left(\mathbf{T}_{\kappa_R}^{NH}\right) = \begin{pmatrix} -p + \mu/\alpha & 0 & 0 \\ 0 & -p + \mu/\alpha & 0 \\ 0 & 0 & -p + \mu\alpha^2 \end{pmatrix} \qquad (3.9)$$

Similarly, the Cauchy stress in a Mooney-Rivlin body undergoing uniaxial extension is obtained with the stored energy function (2.103) and has the following matrix representation:

$$\left(\mathbf{T}_{\kappa_R}^{MR}\right) = \begin{pmatrix} -p + \mu_1/\alpha - \mu_2\alpha & 0 & 0 \\ 0 & -p + \mu_1/\alpha - \mu_2\alpha & 0 \\ 0 & 0 & -p + \mu_1\alpha^2 - \mu_2/\alpha^2 \end{pmatrix}. \qquad (3.10)$$

As expected, when $\mu_2 = 0$, the Mooney-Rivlin model yields the neo-Hookean model.

The Lagrange multiplier for the enforcement of incompressibility and the entire stress field are easily obtained from the boundary conditions. The lateral surfaces of the rectangular block (or of the cylindrical fiber, if a cylindrical coordinate system is used in the first place, but due to this homogeneous deformation, both representations yield similar results in the axial direction; hence, the Cartesian coordinate system was chosen
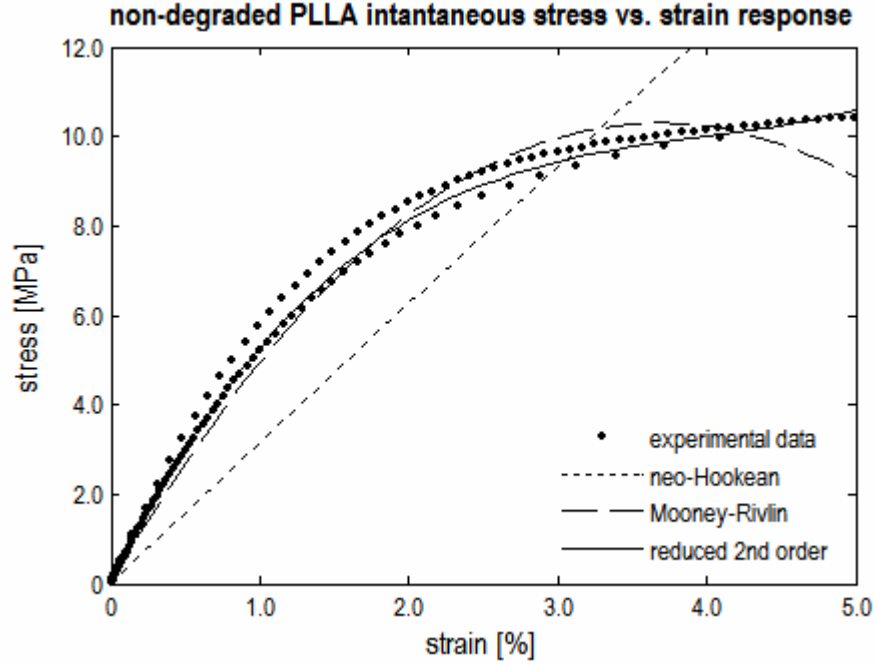
Fig. III.14. Experimental data, neo-Hookean, Mooney-Rivlin, and reduced 2nd order approximations for the instantaneous elastic response of non-degraded PLLA. The neo-Hookean model fails to describe the strain-softening behavior of the material. The Mooney-Rivlin material and the reduced 2nd order stored energy function are only able to do so with negative μ_1.

due to its inherent calculus simplicity) are traction free, and consequently, p will be independent of position and given by

$$p^{NH} = \mu/\alpha \tag{3.11}$$

$$p^{MR} = \mu_1/\alpha - \mu_2\alpha \tag{3.12}$$

The Cauchy stress tensor has only a single non-zero component, the axial direction T_{33}, that takes the form

$$T^{NH} \equiv T_{33}^{NH} = \mu\left(\alpha^2 - \frac{1}{\alpha}\right) \tag{3.13}$$

$$T^{MR} \equiv T_{33}^{MR} = \mu_1\left(\alpha^2 - \frac{1}{\alpha}\right) + \mu_2\left(\alpha - \frac{1}{\alpha^2}\right) \tag{3.14}$$

Table III.1. Material constants of classical hyperelastic models for the description of the instantaneous elastic response of non-degraded PLLA. Unconstrained curve fit of the stress vs. strain relationships obtained with the Mooney-Rivlin model and the reduced 2nd order stored energy function yield negative μ_1, a violation of the restrictions of the material functions of incompressible isotropic elastic materials. Constrained curve fits yield bad approximations similar to the one obtained with the neo-Hookean model.

Constitutive model	Material constants (MPa)		
neo-Hookean	$\mu = 106.64$		
Mooney-Rivlin	$\mu_1 = -2545.1$	$\mu_2 = 2739.0$	
Reduced 2nd order W	$\mu_1 = -5206.6$	$\mu_2 = 5433.6$	$\mu_3 = 22756$

The experimentally measured stress was defined as force over undeformed cross-sectional area, i.e. the Piola stress tensor (cf. (2.96)). Hence, (3.13) and (3.14) yield

$$P^{NH} \equiv P_{33}^{NH} = \mu \left(\alpha - \frac{1}{\alpha^2} \right) \tag{3.15}$$

$$P^{MR} \equiv P_{33}^{MR} = \mu_1 \left(\alpha - \frac{1}{\alpha^2} \right) + \mu_2 \left(1 - \frac{1}{\alpha^3} \right) \tag{3.16}$$

These relationships are nonlinear. For the neo-Hookean body, (3.15) yields generally three possible stretches for a given stress. α must be real and positive, greater than unity for positive values of stress and less than one if the body is under a state of compression.

Experimental data obtained for the IER of non-degraded PLLA in the range of validity chosen (strains up to 5%) was reduced with equations (3.15) and (3.16) using the Levenberg-Marquardt algorithm. It can be observed that the neo-Hookean fails to describe completely the stress vs. strain behavior of the IER of non-degraded PLLA (cf. Fig. III.14). On the other hand, the Mooney-Rivlin model is able to describe the initial development of the curve, but the later part is ill-approximated: the stress reaches a maximum and then decreases, which is not expected to happen. The constants obtained

for these classical hyperelastic models from experimental data reduction are shown in Table III.1.

With the purpose of better describe the experimental data, higher order stored energy functions were considered, such as the first natural extension of the Mooney-Rivlin material [265], i.e.

$$W^{2^{nd}red} = \frac{1}{2}\mu_1(I_C - 3) + \frac{1}{2}\mu_2(II_C - 3) + \frac{1}{6}\mu_3(I_C - 3)(II_C - 3) \qquad (3.17)$$

which is referred to as a reduced 2nd order stored energy function and includes a mixed term with both invariants of the right Cauchy-Green stretch tensor and an extra material constant, μ_3. When used in representation (2.98), terms with I_C and II_C will appear after the derivatives are taken due to the higher order of the stored energy function (3.17) and must be substituted. For this particular motion, the invariants of $\mathbf{C}$ are given by

$$I_C = \alpha^2 + \frac{2}{\alpha} \qquad (3.18)$$

$$II_C = \frac{1}{\alpha^2} + 2\alpha \qquad (3.19)$$

and consequently, the axial stress will be given by

$$P^{2^{nd}red} = (\mu_1 - \mu_3)\left(\alpha - \frac{1}{\alpha^2}\right) + (\mu_2 - \mu_3)\left(1 - \frac{1}{\alpha^3}\right) + \mu_3\left(\alpha^2 - \frac{1}{\alpha^4}\right) \qquad (3.20)$$

Note that with the reduced 2nd order, a quadratic term on α is introduced. As the polynomial expression of the stored energy function becomes richer (i.e. with higher order terms), so does the expression for the stress as a function of stretch and hence, it is expected to obtain a better fit of the experimental data. In fact, a better approximation is obtained with the reduced 2nd order stored energy function (cf. Fig. III.14). The significant improvement from the Mooney-Rivlin hyperelastic body to this higher order form is achieved only with the inclusion of an extra material constant (cf. equations (2.103) and (3.17)). The constants obtained in the data reduction with this particular form of stored energy function are summarized in Table III.1.
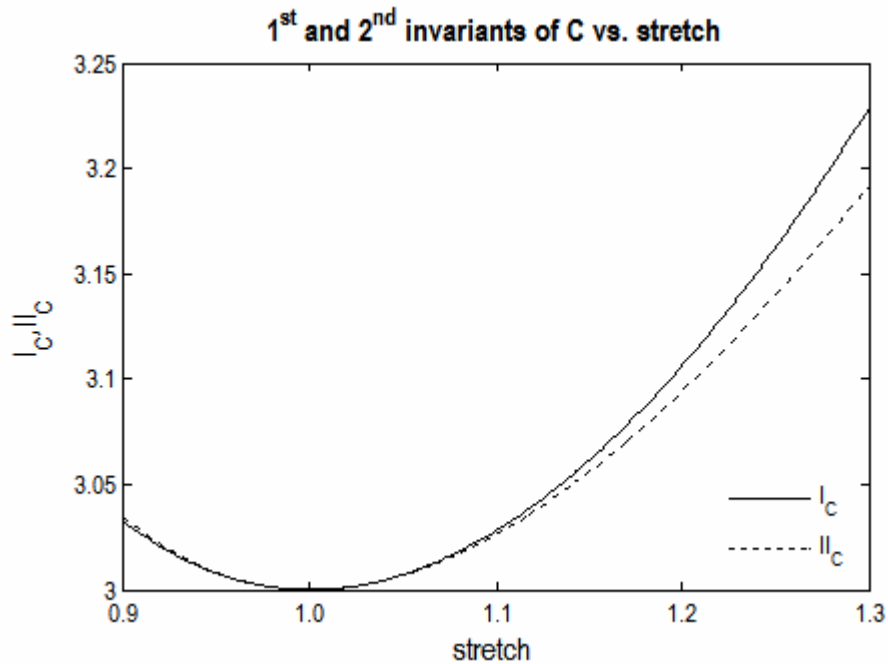
Fig. III.15. First and second invariants of **C** vs. stretch in uniaxial extension. As pointed out by Rivlin and Saunders [263] and Criscione [264], the two principal invariants of **C** or **B** show high co-linearity in this particular deformation. In simple shear or pure torsion, they are indeed equal.

Although the fit obtained with the reduced 2nd order stored energy function approximates quite well uniaxial extension data (cf. Fig. III.14), it is only able to do so if $\mu_1 < 0$. A similar event happens to the Mooney-Rivlin model. Both violate restriction (2.99) and hence the data reduction that yielded the constants listed in Table III.1 is not valid. Constrained curve fits with the proposed stored energy functions (either Mooney-Rivlin, the reduced 2nd order, or higher order stored energy functions as well) are not able to describe accurately the uniaxial extension response of non-degraded PLLA. Hence, other forms for stored energy must be considered.

Before proposing other possible forms for stored energy functions, it must be remarked that either the 1st or the 2nd invariants of the right Cauchy Green stretch tensor for this particular motion (cf. (3.18) and (3.19)) vary similarly with axial stretch (cf. Fig. III.15). As it was initially realized by Rivlin and Saunders [263] and followed by
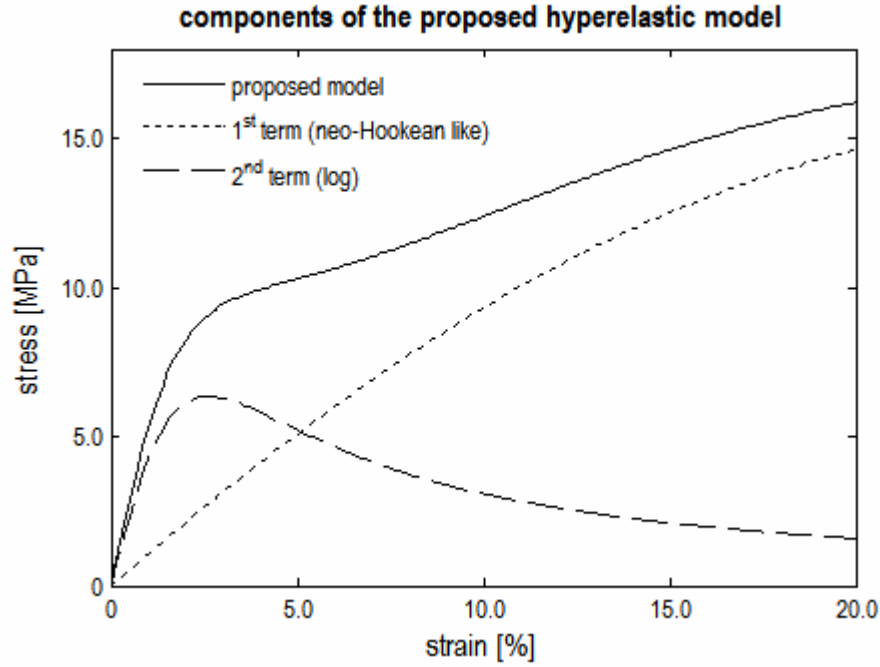
Fig. III.16. Components of the proposed stored energy function for the description of the instantaneous elastic response of PLLA. At lower strains, the stress is dominated by the logarithm term. As the strain increases, the neo-Hookean like term dominates the stress. Furthermore, due to the decreasing exponential of the first term, the "apparent" shear modulus decreases as strain increases.

Criscione [264], I_{C} and II_{C} are not well suited for experimental data reduction. Hence, a stored energy function that relies solely in the 1$^{\mathrm{st}}$ invariant was pursued. A particular form of stored energy function that is able to describe the uniaxial extension response of non-degraded PLLA within the stretch range required is

$$W^{PLLA} = \mu_1 e^{-(I_\mathrm{C}-3)}(I_\mathrm{C}-3) + \mu_2 \ln[1 + a(I_\mathrm{C}-3)] \qquad (3.21)$$

where μ_1, μ_2 and a are three positive material constants. This particular choice of stored energy function was obtained with an educated guess based on the shape of the stress vs. strain curve followed by an extensive exploration several possible forms. An additive separation was assumed. The first term is responsible for the general shape of the curve, as it follows a neo-Hookean model with decreasing apparent shear modulus (i.e.
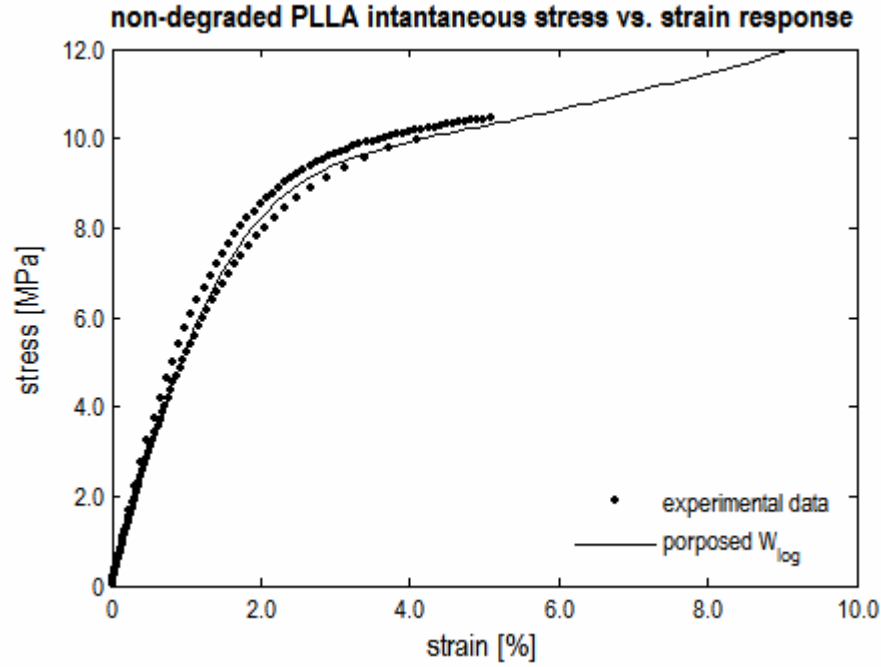
Fig. III.17. Experimental data and the proposed stored energy function for the instantaneous elastic response of non-degraded PLLA. The proposed model describes well the instantaneous elastic response of non-degraded PLLA in the required strain range. Furthermore, beyond 5% strain, the uniaxial stress vs. strain response of the proposed model also shows acceptable phenomenological characteristics.

$\mu_1 e^{-(I_C - 3)}$). The second term is mainly responsible for the shape of the curve in the small strain range (cf. Fig. III.16).

A lengthy analytical expression for the stress vs. stretch relation under uniaxial extension is obtained using (2.98) through a similar procedure as before,

$$P^{PLLA}(\alpha) = 2\left[\mu_1 e^{-(\alpha^2 + 2/\lambda - 3)}(4 - \alpha^2 - 2/\alpha) + \frac{a\mu_2}{1 + a(\alpha^2 + 2/\alpha - 3)} \right]\left(\alpha - \frac{1}{\alpha^2} \right) \quad (3.22)$$

which when used to reduce non-degraded PLLA uniaxial extension data yields a very good curve fit (cf. Fig. III.17 and Table III.2). In fact, not only the proposed stored energy function fits experimental data on the "required" range (0 to 5% strain), but also shows acceptable phenomenological characteristics beyond it.

Table III.2. Material constants of the proposed hyperelastic model for the description of the instantaneous elastic response of non-degraded PLLA. This particular set of constants renders inequality (2.99) valid for a large range of strains.

Constitutive model	Material constants		
proposed W_{PLLAg}	$\mu_1 = 17.999$	$\mu_2 = 0.17047$	$a = 477.28$

Linearization of (3.21) yields

$$W^{PLLA} = \mu_1 \left\{ 1 - (I_C - 3) + \frac{1}{2}(I_C - 3)^2 - ... \right\}(I_C - 3) +$$
$$+ \mu_2 \left\{ a(I_C - 3) - \frac{1}{2}a^2(I_C - 3)^2 + \frac{1}{3}a^3(I_C - 3)^3 - ... \right\} \qquad (3.23)$$
$$\approx (\mu_1 + a\mu_2)(I_C - 3)$$

which yields a Young's modulus (slope at the origin in Fig. III.17) of $E = 6(\mu_1 + a\mu_2)$.

This particular form of stored energy function with the obtained constants does not violate the restrictions (2.99) and (2.100). The latter follows immediately from the choice of stored energy function, i.e. no dependence on II_C, whereas the former is attained for a wide range of I_C (cf. Fig. III.18). As the state of deformation increases, the rate of change of stored energy decreases.

$$\partial W_{log}/\partial I_C \text{ vs. strain}$$
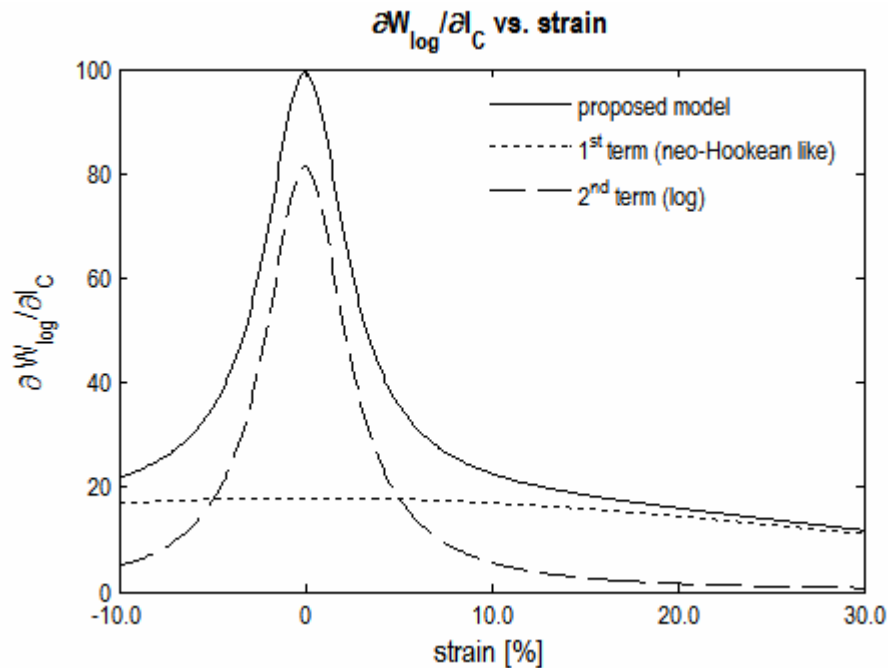
Fig. III.18. Derivative of the proposed stored energy function with respect to the first invariant of **C** vs. stretch in uniaxial extension. As extension increases, the contribution to the change in stored energy of the logarithm term tends to zero. The remainder term is responsible for a basal rate of change that decreases slightly as strain increases. The gist is that both and consequently their sum remain positive for the deformation of interest.

D. A quasi-linear viscoelastic model for non-degraded PLLA

The quasi-linear viscoelastic (abbreviated as QLV) model was introduced by Fung [224] and its concept is a multiplicative separation between the relaxation function and the elastic response. In this way the ability to have different relaxation behaviors at different strains is achieved with the introduction of an instantaneous elastic response and a reduced relaxation function (cf. equation (2.116)). The former was determined in the previous section, whereas the latter is the concern of this section.

Careful stress relaxation experiments were performed to several samples of non-degraded PLLA. A strain history of the form

experimentally prescribed strain history
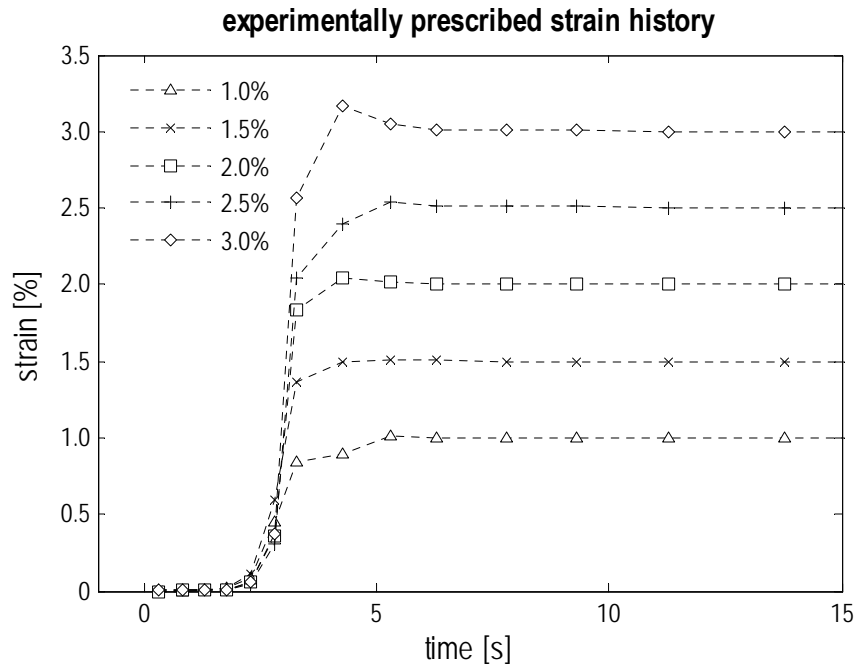
Fig. III.19. Experimentally prescribed strain history for stress relaxation experiments. Only the first 15 s are shown; after, the stretch is maintained constant for 10 min. An ideal loading would be an instantaneous change in stretch at 0^+; such stretch history is impossible to achieve experimentally, where the rise time is typically 4 s and small but noticeable overshoots are recorded occasionally.

$$\varepsilon(s) = \begin{cases} 0, & s < 0 \\ \dfrac{\varepsilon_0}{T_1} s, & s \in [0, T_1] \\ \varepsilon_0, & s > T_1 \end{cases} \qquad (3.24)$$

where ε_0 is the step in strain and T_1 the rise time. A constant rate increase to ε_0 occurs during the rise time interval and as $T_1 \to 0$, the ramp history (3.24) approaches the step strain history. This particular form of strain history is idealized and cannot actually be carried out experimentally because of inertial in the specimen and the testing device. The strain histories prescribed to non-degraded PLLA samples have an average rise time of 4 seconds and are shown in Fig. III.19 for the initial stages of the experiment (after the rise
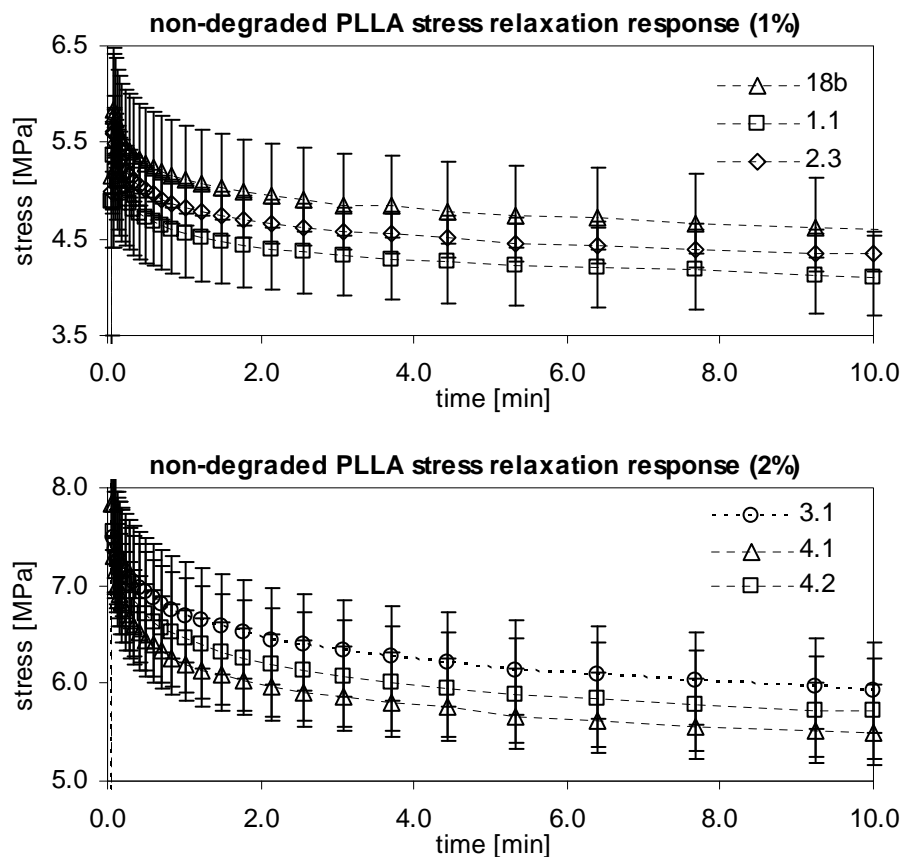
Fig. III.20. Stress relaxation responses ($\varepsilon_0 = 1.0\%$ and $\varepsilon_0 = 2.0\%$) of several non-degraded PLLA samples. Uncertainty in stress not only arises from the experimental measuring of areas but also due to inherently different. The overall range of possible locus of the stress relaxation curve is around 1.25 MPa.

interval, strain is held fixed during the 10 minutes of the stress relaxation experiment). When greater steps are prescribed, a slight overshoot in the prescribed strain is observed.

Stresses required to held the prescribed strain history were recorded. A variance on the response to similar conditions were observed for two reasons (Fig. III.20): (i) DMA records the force necessary to hold the deformation which in turn is averaged by the initial area to obtain the stress, and (ii) samples, although tested under the same conditions, are inherently different due to fabrication properties. Samples that do not show a significant taper will yield a more accurate measurement of the initial diameter
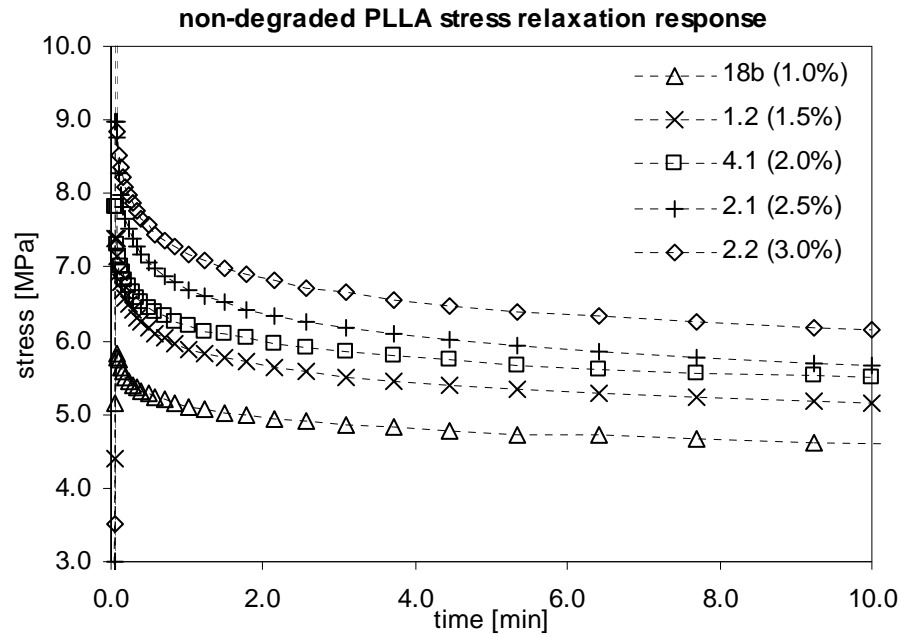
Fig. III.21 Experimentally determined non-degraded PLLA stress relaxation response. Samples 1.1 and 1.2 and samples 2.1 and 2.2 were collected from adjacent parts of the same fiber and a strong similarity is observed in the shapes of the curves of the corresponding pairs.

and hence the stress will be determined within a smaller interval (error bars in Fig. III.20). Samples collected from the same fiber expectedly have similar behaviors in response to similar stimuli. On the other hand, samples collected from different fibers behave somewhat differently, but still within a range that depicts the differences in between fibers. Those differences certainly arise from fabrication conditions.

An averaged stress relaxation response of non-degraded PLLA (cf. Fig. III.21) is obtained from the experiments performed with $\varepsilon_0 = 1.0\%$, 1.5%, 2.0%, 2.5%, and 3.0. Observation of the shape of the curves hints that two relaxations are occurring during the time of the experiment: (i) a short-term viscous relaxation that decreases the stress significantly during the first 60 seconds of relaxation, and (ii) a long-term viscous relaxation that is responsible for the slow decrease of stress during the entire time of the

Table III.3. Material constants of the QLV model for the description of the response of non-degraded PLLA. Each set of constants was obtained as the best constrained fit to the stress data of each experiment. The experimentally recorded stretch history was used. The constants are not that far apart from each other, hence the average was chosen to describe the stress relaxation response of non-degraded PLLA.

	k_1	τ_1 (s)	k_2	τ_2 (s)
sample 1.1 (1.0%)	0.12269	18.217	0.10604	253.97
sample 1.2 (1.5%)	0.14612	21.672	0.13415	276.19
sample 4.1 (2.0%)	0.18782	4.2762	0.13518	136.16
sample 2.1 (2.5%)	0.20601	9.1341	0.16201	177.29
sample 2.2 (3.0%)	0.22028	5.9618	0.15675	149.17
non-degraded PLLA	0.17659	11.852	0.13882	198.56

experiment. With this argument in view and simplicity in mind, a two term Prony series was chosen to represent the reduced relaxation function

$$G(t) = k_0 + k_1 e^{-t/\tau_1} + k_2 e^{-t/\tau_2}$$ (3.25)

where $k_0 = 1 - k_1 - k_2$ so that $G(0) = 1$. k_1, k_2, τ_1, and τ_2 are positive constants that describe the stress relaxation of non-degraded PLLA (moreover $0 < k_1, k_2 < 1$). As opposed to Fung's choice of a continuous relaxation spectrum between τ_1 and τ_2 (cf. (2.117) and [224]), this particular reduced relaxation function was chosen by later co-workers (cf. [227]), and is sufficient.

The stress response of the QLV model was obtained for each experimentally prescribed strain history (cf. Fig. III.21) with the instantaneous elastic response obtained previously (cf. (3.22), Fig. III.17, and Table III.2), and with the proposed form for reduced relaxation function (cf. (3.25)) through

$$P^{QLV}(t) = \int_{-\infty}^{t} G(t-s) \frac{dP^{PLLA}}{d\lambda} \frac{d\lambda}{ds} ds$$ (3.26)
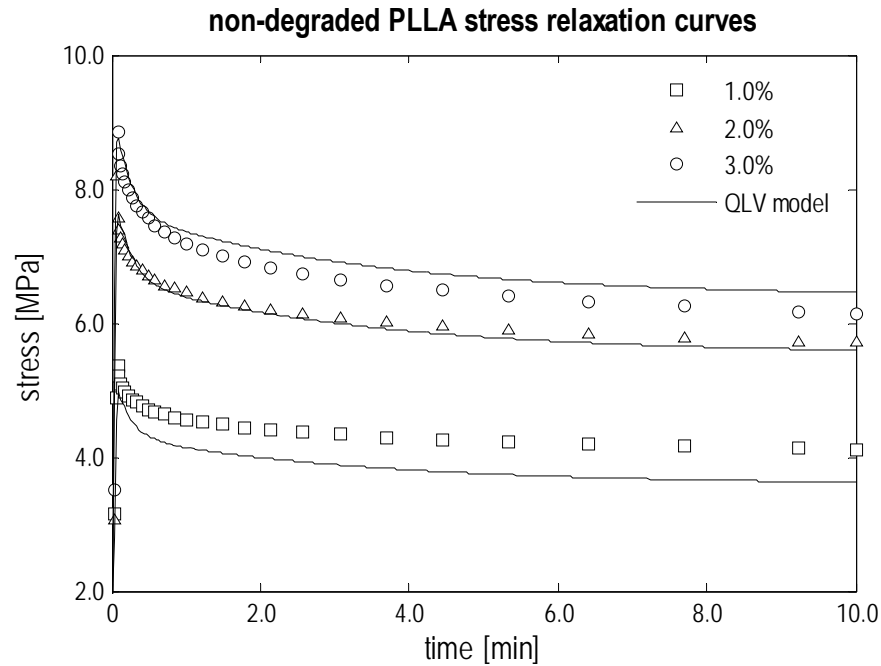
Fig. III.22. Non-degraded PLLA QLV model stress relaxation response. Taking into consideration the uncertainty range of the stress relaxation curves (cf. Fig. III.20), the QLV describes quantitatively the viscoelastic response of non-degraded PLLA in an acceptable manner.

i.e., the Piola stress counterpart of (2.116) and $\lambda = \lambda(t)$ the uniaxial stretch history. Experimental data was reduced to equation (3.26) so that the constants in (3.25) are found. Constrained data reduction was performed individually for each stress relaxation test and the constants obtained are shown in Table III.3.

Due to the inherent uncertainty of using different samples for different tests, the constants obtained for each are different. A quick inspection of Fig. III.21 shows that samples 1.1 and 1.2 (tested at $\varepsilon_0 = 1.0\%$ and $\varepsilon_0 = 1.5\%$ respectively) possess a quicker and less significant long-term viscous relaxation when compared to samples 2.1 and 2.2 and that is reflected in the difference observed in the obtained constants. Nevertheless, all the obtained constants show coherency and are within a small range. Hence an average response was obtained simply with averaging the constants obtained in each

non-degraded PLLA stress relaxation curves
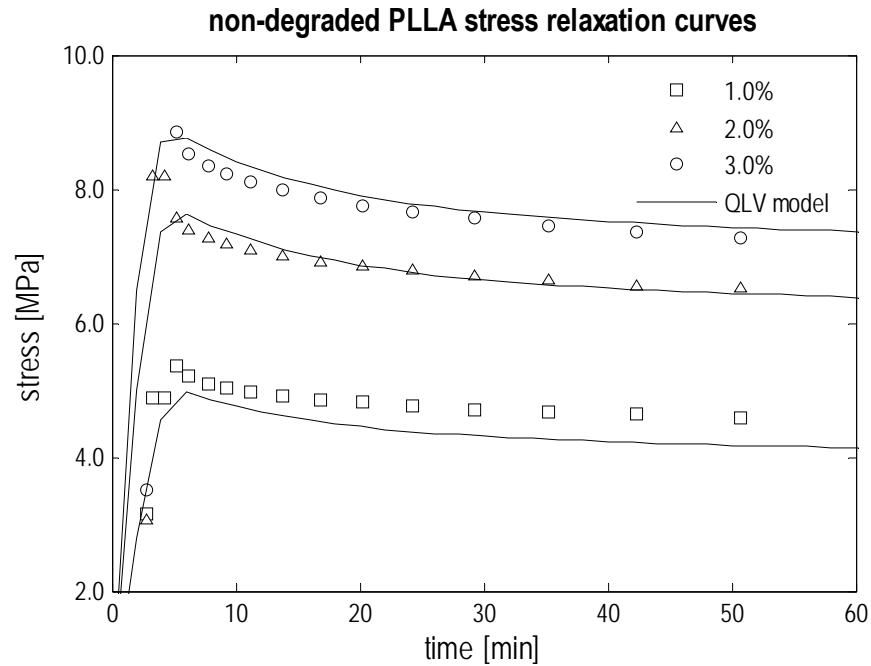
Fig. III.23 Non-degraded PLLA QLV model stress relaxation response (first minute). A somewhat good agreement is observed either at 2 and 3%. The 1% curve is slightly underestimated.

individual data reduction. They portrait the stress relaxation response of non-degraded PLLA and are shown in Table III.3.

The analysis of this averaged QLV model was further inspected with ideal strain histories of the form (3.24) with $T_1 = 4$ s (cf. Fig. III.19). The comparison between the QLV model and experimental data is somewhat acceptable (shown in Fig. III.22 and in Fig. III.23): (i) it must be remarked that the ideal and experimental strain histories are different; (ii) the averaged model is certainly most apart of the models describing the $\varepsilon_0 = 1.0\%$ and $\varepsilon_0 = 3.0\%$ step responses (cf. Table III.3), and (iii) the inherent uncertainty of each experimental stress determination in conjunction with variability between samples yields a somewhat large allowable interval for the stress (cf. Fig. III.20). Hence, although not perfect, the QLV describes within certain accuracy the viscoelastic response of non-degraded PLLA.

E. A Pipkin & Rogers viscoelastic model for non-degraded PLLA

A single integral representation of the nonlinear viscoelastic model by Pipkin and Rogers was investigated under uniaxial extension. The Cauchy stress is given by

$$\mathbf{T} = -p\mathbf{I} + \mathbf{F}\left[\mathbf{G}(\mathbf{C}(t),0) + \int_0^t \frac{\partial}{\partial(t-s)}\mathbf{G}(\mathbf{C}(s),t-s)ds\right]\mathbf{F}^{\mathrm{T}} \qquad (2.111)$$

Following Wineman [220], the choice of $\mathbf{G}(\mathbf{C},s)$ was made such that if time dependence was suppressed, the hyperelastic model for the instantaneous elastic response of non-degraded PLLA (cf. Section III.C) is recovered. This particular case of the Pipkin & Rogers viscoelastic model is characterized by

$$\mathbf{G}(\mathbf{C}(s),\xi) = R(\xi)\left\{\frac{\partial W^{PLLA}}{\partial \mathbf{C}}\right\} = R(\xi)\left\{\frac{\partial W^{PLLA}}{\partial I_{\mathbf{C}}}\frac{\partial I_{\mathbf{C}}}{\partial \mathbf{C}}\right\} \qquad (3.27)$$

where $R(\xi)$ is a scalar relaxation function. Using the chain rule with $W^{\log} = W^{\log}(I_{\mathbf{C}})$ given by (3.21), $\mathbf{G}(\mathbf{C},s)$ for is given by

$$\mathbf{G}(\mathbf{C}(s),\xi) = R(\xi)\left[\mu_1 e^{-(I_{\mathbf{C}}-3)} - \mu_1 e^{-(I_{\mathbf{C}}-3)}(I_{\mathbf{C}}-3) + \frac{a\mu_2}{1+(I_{\mathbf{C}}-3)}\right]\mathbf{1} \qquad (3.28)$$

With a similar reasoning as for the QLV model, a two term relaxation function was chosen, i.e.

$$\begin{aligned}R(\xi) &= A_0 + A_1 e^{-\xi/\tau_1} + A_2 e^{-\xi/\tau_2} \\ &= 2C_\infty + (C_1 - C_\infty)e^{-\xi/\tau_1} + (C_2 - C_\infty)e^{-\xi/\tau_2}\end{aligned} \qquad (3.29)$$

It can be easily seen from (3.29) that $R(0) = C_1 + C_2$ and as $\xi \to \infty$, $R(\xi) = 2C_\infty$, i.e. the initial and the residual modulus. Hence, the constants A_0, A_1, A_2, τ_1, and τ_2 in (3.29) are restricted to be positive.

The kinematical tensors are obtained similarly as in (3.7) and (3.8) considering the uniaxial stretch history $\lambda(t)$ and hence become time dependent, i.e.

$$\left(\mathbf{F}(t) \right) = \begin{pmatrix} 1/\sqrt{\lambda(t)} & 0 & 0 \\ 0 & 1/\sqrt{\lambda(t)} & 0 \\ 0 & 0 & \lambda(t) \end{pmatrix} \tag{3.30}$$

$$\left(\mathbf{B}(t) \right) = \left(\mathbf{C}(t) \right) = \begin{pmatrix} 1/\lambda(t) & 0 & 0 \\ 0 & 1/\lambda(t) & 0 \\ 0 & 0 & \lambda(t)^2 \end{pmatrix}. \tag{3.31}$$

For algebraic manipulation the response (2.111) is separated in two components

$$\begin{aligned} \mathbf{T} &= -p\mathbf{1} + \mathbf{F} \left\{ R(0) \frac{\partial W^{PLLA}}{\partial \mathbf{C}} \right\} \mathbf{F}^{\mathrm{T}} + \mathbf{F} \left\{ \int_0^t \frac{\partial}{\partial m} \mathbf{G}(\mathbf{C}^{(t)}(m), m) \Big|_{m=t-s} ds \right\} \mathbf{F}^{\mathrm{T}} \\ &= -p\mathbf{1} + \mathbf{F}\mathbf{G}^{IER}\mathbf{F}^{\mathrm{T}} + \mathbf{F}\mathbf{G}^{VE}\mathbf{F}^{\mathrm{T}} \end{aligned} \tag{3.32}$$

i.e., an instantaneous elastic response and a viscoelastic decay. $\mathbf{C}^{(t)}$ is the history of the right Cauchy-Green stretch tensor obtained with (2.32). Similarly as before, boundary conditions imply that the state of stress is uniaxial

$$\begin{aligned} T_{11}(t) &= T_{22}(t) = -p + \frac{1}{\lambda(t)}(G_{11}^{IER} + G_{11}^{VE}) \quad ; \\ T_{33}(t) &= -p + \lambda(t)^2 (G_{33}^{IER} + G_{33}^{VE}) \end{aligned} \tag{3.33}$$

and the Lagrange multiplier is obtained from boundary conditions, i.e.

$$p = \frac{1}{\lambda}(G_{11}^{IER} + G_{11}^{VE}) \tag{3.34}$$

hence $T_{11} = T_{22} = 0$ and

$$T_{33}(t) = \lambda(t)^2 (G_{33}^{IER} + G_{33}^{VE}) - \frac{1}{\lambda(t)}(G_{11}^{IER} + G_{11}^{VE}). \tag{3.35}$$

Because stresses are computed with respect to the undeformed area, one is concerned with the Piola stress (related to the Cauchy stress by (2.96)) is given by

$$P_{33} = \lambda(G_{33}^{IER} + G_{33}^{VE}) - \frac{1}{\lambda^2}(G_{11}^{IER} + G_{11}^{VE}) \tag{3.36}$$

Note that the instantaneous elastic response $\mathbf{G}^{IER}$ in (3.32) is a spherical 2nd order tensor and hence

$$G^{IER} = G_{11}^{IER} = G_{11}^{IER} = G_{22}^{IER} =$$
$$= R(0)\left[\mu_1 e^{-(I_C-3)}[1-(I_C-3)]+\frac{a\mu_2}{1+(I_C-3)}\right] \tag{3.37}$$

The integrand of the viscoelastic decay $\mathbf{G}^{VE}$ in (3.32) is also obtained with the aid of the chain rule, i.e.

$$\frac{\partial}{\partial m}\mathbf{G}(\mathbf{C}^{(t)}(m),m)=\left[\frac{\partial\mathbf{G}(\mathbf{C}^{(t)},m)}{\partial\mathbf{C}^{(t)}}\right]\frac{\partial\mathbf{C}^{(t)}(m)}{\partial m}+\frac{\partial\mathbf{G}(\mathbf{C}^{(t)},m)}{\partial m} \tag{3.38}$$

where the first term is the application of a 4th order tensor to a 2nd order tensor. Because of the simplicity of this motion (that yields diagonal stretch tensors) and the isotropy of the material (that yields a spherical $\mathbf{G}(\mathbf{C}(s),\xi)$), thus the second term of (3.32) results in a simple expression that is computed numerically

$$G^{VE}(t) = G_{11}^{VE}(t) = G_{22}^{VE}(t) = G_{33}^{VE}(t) =$$
$$= \int_0^t\left[2\frac{\partial G}{\partial C_{11}^{(t)}}\frac{\partial C_{11}^{(t)}}{\partial m}+\frac{\partial G}{\partial C_{33}^{(t)}}\frac{\partial C_{33}^{(t)}}{\partial m}+\frac{\partial G}{\partial m}\right]_{m=t-s}ds \tag{3.39}$$

where

$$G(\mathbf{C},\xi) = R(\xi)\left[\mu_1 e^{-(I_C-3)}[1-(I_C-3)]+\frac{a\mu_2}{1+(I_C-3)}\right] \tag{3.40}$$

is the spherical component of the response function. Finally, the uniaxial Piola stress is given by

$$P_{33}(t) = 2(G^{IER}+G^{VE}(t))\left(\lambda(t)-\frac{1}{\lambda(t)^2}\right) \tag{3.41}$$

Stress relaxation data (Fig. III.21) was reduced to equation (3.41) to obtain constants A_0, A_1, A_2, τ_1, and τ_2 in (3.29). The relaxation function $R(\xi)$ appears in (3.41) through (3.37) and (3.39). Constrained data reduction of the nonlinear viscoelastic

Table III.4. Material constants of the relaxation function for the nonlinear viscoelastic model (P&R) describing the response of non-degraded PLLA. Data reduction was performed with three stress relaxation curves either individually or simultaneously (1%, 2%, and 3% strain). The last set of constants is the one that bestly describes the considered experimental data as a whole.

	A_0	A_1	τ_1 (s)	A_2	τ_2 (s)
1.0 % (sample 11)	1.6836	0.4444	18.091	0.0277	386.08
2.0 % (sample 41)	1.3035	0.5557	8.7415	0.3069	350.59
3.0 % (sample 22)	1.2935	0.2575	29.741	0.3469	388.59
simultaneous curve fit	1.3469	0.3158	12.859	0.3265	380.06

model presented fits perfectly all stress relaxation curves when considered individually (cf. Table III.4). Unfortunately, the constants obtained for each one are different when compared with other fibers. Thus, when using the set of constants obtained for one sample with other stress relaxation steps, the results deviate (cf. Fig. III.24 , where the constants obtained for the 2% step are used to generate data for different strain steps). This is a clear indication of different material properties in between samples.

Because of this disparity, a different strategy was employed: instead of the averaging process used in the QLV data reduction, the three stress relaxation curves (correspondingly to responses in steps in strain of 1%, 2% and 3%) were reduced at the same time yielding a set of constants that best fit the three experiments (cf. Table III.4). The nonlinear viscoelastic model shows a slightly improved agreement when compared with the previously investigated QLV model (cf. Fig. III.25).

non-degraded PLLA stress relaxatio curves
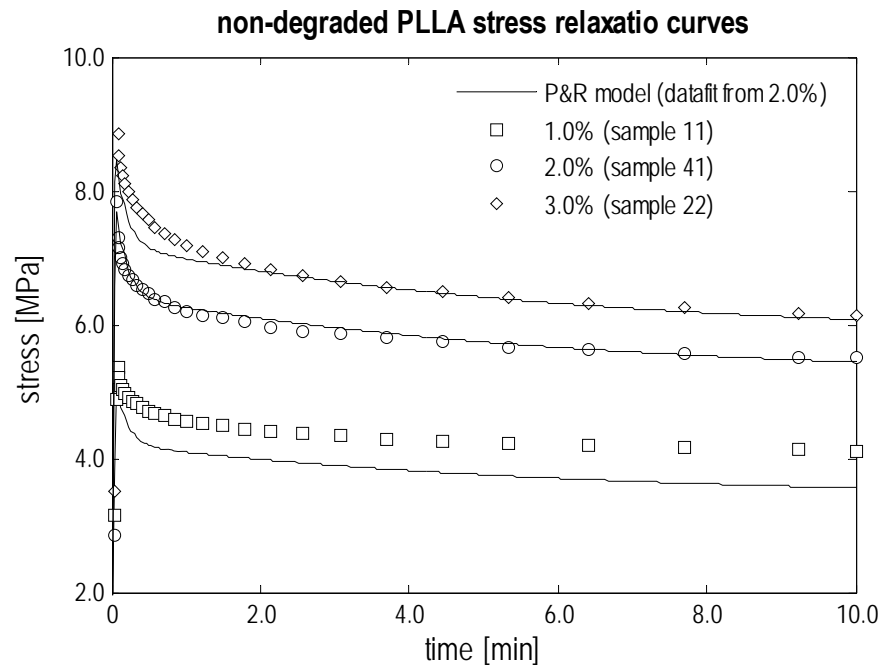
Fig. III.24 Non-degraded PLLA non-linear viscoelastic model (P&R) stress relaxation response (with data reduced from the 2.0% strain step). The obtained curve fit describes almost perfectly the 2.0% step in strain response. On the other hand, it clearly underestimates the 1.0% curve (similarly as the QLV model, cf. Fig. III.22), and approximates to a certain degree the curve corresponding to the 3.0% step in strain.
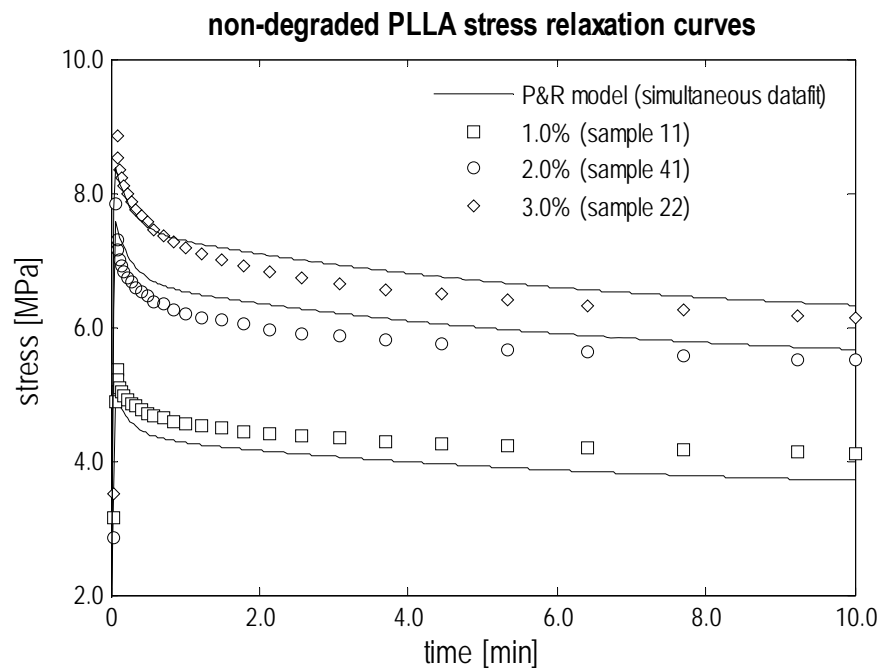
non-degraded PLLA stress relaxation curves

Fig. III.25. Non-degraded PLLA non-linear viscoelastic model (P&R) stress relaxation response (with simultaneous data reduction). With the inclusion of the data from the stress relaxation experiment at 1% strain, the curve fit the approximation becomes worse. Taking into consideration the error produced by the measurement of the sample diameters (cf. Fig. III.20, it can be concluded that the P&R nonlinear viscoelastic model describes the stress relaxation response of non-degraded PLLA up to a certain extent. Finally, note that if data from the 1% experiment were not curve fitted simultaneously, the approximation would be quite good for the remaining two samples (cf. Fig. III.24).

CHAPTER IV

CONSTITUTIVE MODEL FOR BIODEGRADABLE POLYMERIC MATERIALS

Based within a general framework that describes the response of dissipative systems, Rajagopal et al. [266] developed a model for polymeric solids undergoing strain-induced degradation. The thermodynamic based model was obtained through the incorporation of an appropriate form for the rate of dissipation ξ associated with the degradation process in the reduced energy dissipation equation

$$\xi := \mathbf{T} \cdot \mathbf{D} - \rho \dot{\psi} \geq 0, \tag{4.1}$$

where $\mathbf{T} \cdot \mathbf{D}$ is the stress power and $\dot{\psi}$ the rate of increase of the Helmholtz potential. Following the framework of Rajagopal and coworkers (cf. [267,268] and references therein), the specification of constitutive forms for the Helmholtz potential and for the rate of entropy production with the maximization of the latter with (4.1) as a restriction on allowable processes, yields a constitutive model, i.e. a representation for the stress as well as a differential equation governing the evolution of the natural configuration due to the dissipative process.

As pointed in Rajagopal et al. [266] "it is common practice in developing constitutive theories of this sort to stipulate the constitutive equation for the stress in terms of the derivatives of ψ as well as for the reaction rate and choose coefficients such that the inequality (4.1) is met, thus satisfying the second law of thermodynamics". The development of models for degradable polymeric solids following such phenomenological approach is the main concern of this section. Section A contains general consideration about the behavior of the material that the model is intended for and Section B presents the development of the model. Section C deals with materials that respond elastically if degradation is fixed whereas Section D deals with materials that follow a viscoelastic response at fixed levels of degradation. Lastly, a discussion of existing theories that are connected to the one developed here is presented in Section E.

A. Polymer networks, scission and mechanical properties

Before proceeding with the development of a constitutive model for degradable polymeric solids, it is necessary to consider briefly the structure of a polymeric network. The basic structure of polymer molecules consists of flexible chains that can adopt a very large number of conformations. These chains ordinarily are connected to one another by cross-linkages, but the preponderance of the structure consists of the intervening polymer chains each comprising a sufficiently high number of bonds between crosslinks. Upon application of external stimuli, the long chains are able to rearrange to other conformations, in particular to more extended ones that allow sufficiently large deformations. Uncoiling takes place and chains tend to become aligned parallel to the axis of elongation. The ability to recover large deformations is related to the ability of the chains to return to their initial configurations. For ideal rubbery behavior, two more requirements are needed: (i) chains must also be mobile such that conformational changes can occur (hence, neither crystalline to an appreciable degree nor in the glassy state), and (ii) a permanence of structure is required. A permanent structure is achieved through the insertion of crosslinks restricting free movement of the chains. A similar effect is achieved with "transient" cross-links associated with crystallites [232].

The well established statistical theory for rubber elasticity based on these assumptions made at the molecular level yields

$$W = \frac{\rho RT}{2M_c}(\lambda_1^2 + \lambda_2^2 + \lambda_3^2 - 3),$$ (4.2)

where W is the work of deformation or the stored energy, λ_i, $i = 1,2,3$ are the principal stretches, ρ the density, R the universal gas constant, T the absolute temperature, and M_c is the molecular weight of the portion of a molecule lying between successive junction points [148]. After its inception, refinements that account for a more detailed structure of the network were developed [215,232].

Equation (4.2) and the stored energy of a neo-Hookean hyperelastic material (cf. (2.102)) are similar but were obtained from different reasonings. Hence, there is an obvious relationship between the properties of the polymeric network (through M_c) and its macroscopic shear modulus μ, i.e. as the size of the segments between crosslinks decreases the network becomes stiffer and the modulus increases. As an example, natural rubber increases significantly its stiffness upon vulcanization (as M_c decreases dramatically), and a further increase in stiffness follows increases in the crosslink density.

Since the connection between hyperelastic materials and the simplest statistical model for molecular networks, the statistical theory of rubber elasticity and non-linear elasticity became closely related, providing possible molecular interpretations for higher order moduli. But more important than all, experiments with rubber validated nonlinear elasticity models (e.g. classical experiments of Rivlin and coworkers [263,265]).

Tobolsky [215] showed that in competition to the changes in chain conformation, another molecular mechanism can occur during the response of networks which causes a change in microstructure. This mechanism consists of scission and subsequent crosslinking and leads to substantial softening and permanent set on removal of the load. Wineman, Rajagopal and coworkers explored the implications of this constitutive theory (cf. [267], [269] and references therein). The theory initiated with a discrete conversion in a two-network model and later was extended to continuous scission and healing into new networks. Within the context of the Rajagopal and Wineman scission and crosslinking multi-network theory, polymer degradation occurs when scission is not followed by healing.

The thermodynamic framework that accounts changes in microstructure leading to multiple natural states has lead to the development of constitutive theories that incorporate the microstructural details within a continuum perspective and has been extensively and successfully used in a large class of material behaviors by Rajagopal and co-workers such as: traditional plastic and viscoelastic response [270-272], twinning and solid to solid phase transition [273,274], shape memory alloys [275], polymer

crystallization [276,277], growth and adaptation of biological tissues [278], and the response of asphalt mixtures [279], among others.

On the other hand, such effects can be incorporate into constitutive theories in a ad hoc fashion with phenomenological reasoning. The events that occur to the polymer bulk upon scission follow the stages: (i) a reduction in molecular weight resulting directly from the chemical reaction, (ii) a loss of mechanical properties directly related with the decrease amount of effective crosslinked segments, and (iii) a loss in mass that is perceived as dissolution and erosion of oligomers and monomers [139,141]. Erosion occurs rather quickly in late stages of degradation and is a distinct but consequent process to scission. Hence, mass loss will not be in the scope of the proposed model. The proposed model tries to describe scission and loss of mechanical properties that occur during the short- and medium-term period of degradation when mechanical integrity still exists but is being continuously depreciated by scission.

B. Constitutive framework for biodegradable polymeric materials

This section proposes the constitutive framework within which biodegradable polymeric materials are to be described. The concept was developed initially within the scope of the theory of linearized elasticity [280], and further expanded to account nonlinear responses under finite deformations [281]. The framework presented here yields materials that are not simple in the sense of Truesdell & Noll (cf. [207]).

1. Measures of degradation

The introduction of a scalar parameter that reflects the degradation is the central assumption to this constitutive theory. Microstructural changes take place due to scission as the body is deformed. The cause of these modifications may be the hydrolytic cleavage of the backbone chains that constitute the degradable polymer. These changes result in reduction in the molecular weight that translates into a reduction of the number of effective crosslinked segments and consequent depreciation of bulk mechanical properties.

The properties of the body are made to depend on the extent of scission and consequent molecular weight reduction (more precisely, reduction in number of effective crosslinked segments). Such dependence is captured by introducing a degradation parameter. We assume the existence of a positive finite measure of scission which is a measure of the number of broken bonds that may be assigned to a representative volume element at time t and location $\mathbf{x}$. Moreover, there exists a scalar field d with values between zero and unity, which henceforth should be called the degradation parameter or simply the degradation, that expresses the fraction of broken bonds and quantifies the degree of local degradation of a given particle at place $\mathbf{x}$ at time t

$$d = d(\mathbf{x}, t).$$ (4.3)

The degradation parameter will always be non-negative with the upper bound being unity; $1-d$ is a measure of the fraction of intact crosslinks in a representative volume element of the body. The value $d = 0$ will represent a virgin specimen and $d = 1$ corresponds to the state of maximum possible degradation, i.e. a network without any remaining crosslinked segments.

2. *Processes of degradation*

Mechanical energy transferred to a polymeric system can be dissipated via two harmless (i.e. not inducing chemical changes) relaxation processes: the slippage of chains relative to surrounding molecules, and changes in chain conformation [150]. In addition, scission of chemical bonds can occur. Bond rupture occurs when sufficient energy is concentrated in a certain segment of a macromolecule as a consequence of non-uniform distribution of internal stresses. Strain is a pre-requisite and the probability of scission should increase as relaxation is impeded [145]. Besides mechanical loads promoting bond rupture per se, microstructural changes can occur due to high temperature (thermal degradation), ultraviolet radiation (photo-degradation), or the presence of a small molecular weight reactant such as oxygen (oxidation) or water (hydrolysis).

The major mechanism for the degradation of aliphatic polyesters is by random attack by water molecules in a chemical reaction denoted as hydrolysis. The rate of swelling of these polymers is usually higher than the rate of hydrolysis, hence the reaction occurs extensively through the polymer bulk and the common mode of erosion observed in this class of polymers is bulk or homogeneous erosion.

Hydrolytic scission occurs spontaneously in the presence of the readily available water and its rate may be influenced by the properties of the molecular network: (i) dramatic changes in network morphology occur as a consequence of chain alignment in response to uniaxial tensile strain such as in strain-induced crystallization [276], (ii) the crystalline phase is more resistant to degradation than the amorphous phase, possibly due to differences in bond availability and steric hindrance [143], (iii) Baek and Srinivasa developed a model that describes changes in swelling of a polymer network due to deformation [282], and finally, (iv) experimental evidence shows that deformation and degradation are a coupled process [163,164,168]. Hence, the properties of the molecular network and consequently the rate of hydrolysis are dependent on the state of deformation.

While thermal and radiation-induced degradation are assumed not to occur (in common isothermal biomedical applications) and the major mechanism of degradation is scission by available water, the effects of stresses on bond scission might influence the rate of the reaction. A rate equation governing the degradation process is assumed, where the rate of change of degradation is

$$\frac{\partial d}{\partial t} = \mathfrak{D}(d, \mathbf{F}, \mathbf{T});$$ (4.4)

that is, the rate of change of degradation is assumed to be dependent on the state of deformation, stress, the extent of degradation, and implicitly on both spatial location and time. An activation criterion may be placed such that degradation is active under only certain conditions and takes the general form

$$A(\mathbf{F}, \mathbf{T}) = 0.$$ (4.5)

It is possible that A defined in (4.5) can take on a complicated form in that it is a functional that depends on the histories of the deformation gradient rather than just its current value.

Rajagopal et al. [266] following a constitutive framework that maximizes the rate of dissipation obtained for strain-induced degradation a governing equation of the form

$$\frac{\partial d}{\partial t} = (1-d)\mathfrak{G}(D),\tag{4.6}$$

where $\mathfrak{G}$ is a function of the "driving forces D" which in turn depend on the deformation gradient $\mathbf{F}$ through the invariants of $\mathbf{B}$. The activation criterion was defined as a threshold on the driving force, and the rate of dissipation was assumed to be a convex function of $\partial d/\partial t$ and to vanish when $\partial d/\partial t = 0$, i.e. when degradation is fixed. Equation (4.6) governs the rate of increase of degradation in a material that undergoes strain-induced scission and that at fixed levels of degradation behaves elastically (hence, $\xi = 0$ when $\partial d/\partial t = 0$). Equation (4.4) was obtained through phenomenological reasoning and allows cases where stress might induce degradation per se as well as cases where the rate of increase of degradation is not necessarily proportional to $1-d$.

3. Forms of degradation

The degradation at a given particle and its consequent molecular weight reduction leads to depreciation in the mechanical properties of the corresponding particle. The Cauchy stress $\mathbf{T}$ in a simple material (non-aging, homogeneous) is given by

$$\mathbf{T} = \mathfrak{F}(\mathbf{F}^{(t)}),\tag{4.7}$$

where $\mathbf{F}^{(t)}$ is the history of the deformation gradient up to time t (Truesdell & Noll's definition is being used, cf. [207]).

The constitutive models of interest for the description of degradable polymers are such that their response functional is made to depend on the degradation parameter and assumes the general form

$$\mathbf{T} = \mathfrak{F}(\mathbf{F}^{(t)}, d), \tag{4.8}$$

i.e. a one parameter family of materials described by (4.7).

Consider the case when d is fixed, i.e. the response of a "d degraded" material, and denote it by $\mathfrak{F}_d(\mathbf{F}^{(t)}) = \mathfrak{F}(\mathbf{F}^{(t)}, d)$. This response functional implies that there exists a stress representation and a reference configuration (usually chosen to be stress free, but not necessarily) from which the stress is represented.

The stress representation of a particular material involves a set of constants $C = \{\mu_i\}$, $i = 1, ..., k$ where k is the number of material properties involved in that representation. Each representation usually describes one particular class of material behavior: for example, the response of an isotropic incompressible Mooney-Rivlin material admits the representation $\mathbf{T} = -p\mathbf{1} + \mu_1 \mathbf{B} + \mu_2 \mathbf{B}^2$ with two material properties, $C = \{\mu_1, \mu_2\}$. The material properties are dependent not only in the representation chosen for such material but also on the particular choice of reference configuration.

One subclass of the response functional for degradable materials (4.8) is one characterized by degradable models on which degradation is felt only as a reduction in material properties. The material properties become functions of d, i.e. C is no longer a set of material constants, but instead, a set of material functions, $C = \{\mu_i(d)\}$. This subclass will henceforth be generally referred as degradable materials, and are the models concerned by this research.

Consider now the case when $d = 0$, i.e. the response of the non-degraded material, and denote it by $\mathfrak{F}_0(\mathbf{F}^{(t)}) = \mathfrak{F}(\mathbf{F}^{(t)}, 0)$, with associated constants $C_0 = \{\mu_i(0)\}$. Note that as degradation only promotes changes in the material properties, no changes will be imparted in the reference configuration from which the stress is represented. In a degradable material, not only does the reference configuration not change with degradation but also the class of stress representations at given d, $\mathfrak{F}_d(\mathbf{F}^{(t)})$, is shared by all stages of degradation starting at $\mathfrak{F}_0(\mathbf{F}^{(t)})$.

C. A degradable material that at fixed degradation is hyperelastic

We assume that the bodies under consideration when non-degraded (i.e. the virgin material) are incompressible, isotropic hyperelastic solids. The most general representation for the Cauchy stress $\mathbf{T}$ for this class of elastic solids is given by

$$\mathbf{T} = -p\mathbf{1} + 2\frac{\partial W}{\partial I_{\mathbf{C}}}\mathbf{B} - 2\frac{\partial W}{\partial II_{\mathbf{C}}}\mathbf{B}^{-1}. \tag{2.98}$$

Hyperelastic materials are characterized by a stored energy function $W = W(\mathbf{F})$ from which the stress can be derived (cf. (2.96)). In order to have a body that is an incompressible, isotropic hyperelastic solid that is allowed to degrade, the stored energy function will depend on the degradation parameter and assumes the general form

$$W = W(\mathbf{F}, d), \tag{4.9}$$

i.e. a one parameter family of hyperelastic materials. It must be stressed that the form of the stored energy given above does not correspond to a hyperelastic body. One expects that as the material degrades, its ability to store energy will change, albeit at a fixed value of the degradation, the model does correspond to a hyperelastic body. The virgin state is hyperelastic, characterized by a stored energy function $W_0 = W(\mathbf{F}, 0)$.

Material frame indifference and isotropy imply that (4.9) becomes

$$W = W(I_{\mathbf{C}}, II_{\mathbf{C}}, d). \tag{4.10}$$

Restricting the equation governing degradation (4.4) to account only for strain-induced degradation, i.e. no explicit dependence on stress, similar requirements of material frame indifference and restrictions by isotropy yield

$$\frac{\partial d}{\partial t} = \mathfrak{D}(d, \mathbf{F}) = \mathfrak{D}(d, I_{\mathbf{C}}, II_{\mathbf{C}}). \tag{4.11}$$

One expects that greater deformations to lead to greater degradation, and also, the same deformation, when acting during longer periods of time, leads to greater

degradation. A measure of deformation s can be defined as the radius in (I_C, II_C) plane through

$$s = [(I_C - 3)^2 + (II_C - 3)^2]^{1/2}. \tag{4.12}$$

Thus, when a material is in undeformed state, $I_C = II_C = 3$ and $s = 0$. The activation criterion (4.5) is defined to be

$$A(I_C, II_C) = [(I_C - 3)^2 + (II_C - 3)^2]^{1/2} - s_a = 0, \tag{4.13}$$

where s_a is a threshold of activation. Activation takes place when the pair (I_C, II_C) lies outside the envelope defined by (4.13).

The rate of the reaction should increase as the state of deformation departs from the activation curve. Also, as degradation proceeds, less bonds will be available for degradation and consequently the rate of degradation should decrease as $d \to 1$. This desired behavior in strain-induced degradation particularizes (4.11) into the following form

$$\frac{\partial d}{\partial t} = \mathcal{K}(s - s_a)(1 - d), \tag{4.14}$$

where $\mathcal{K}$ can be thought as a deformation dependent reaction rate. The solution of (4.14) with a constant rate yields an exponential decay on the number of remaining crosslinks. One plausible choice for $\mathcal{K}(s)$ can be, for example, linear in $s - s_a$.

1. Classical hyperelastic models that degrade

The above framework describes the response of degradable bodies that at a fixed value of degradation d are incompressible isotropic homogeneous hyperelastic (cf. equation (4.10)) undergoing strain-induced degradation following reaction kinetics described by (4.14). The equation governing degradation (4.14) with balance of linear and angular moment (cf. equations (2.63) and (2.64)) yield the fully description of the degradable material undergoing deformation and degradation. To illustrate the idea,
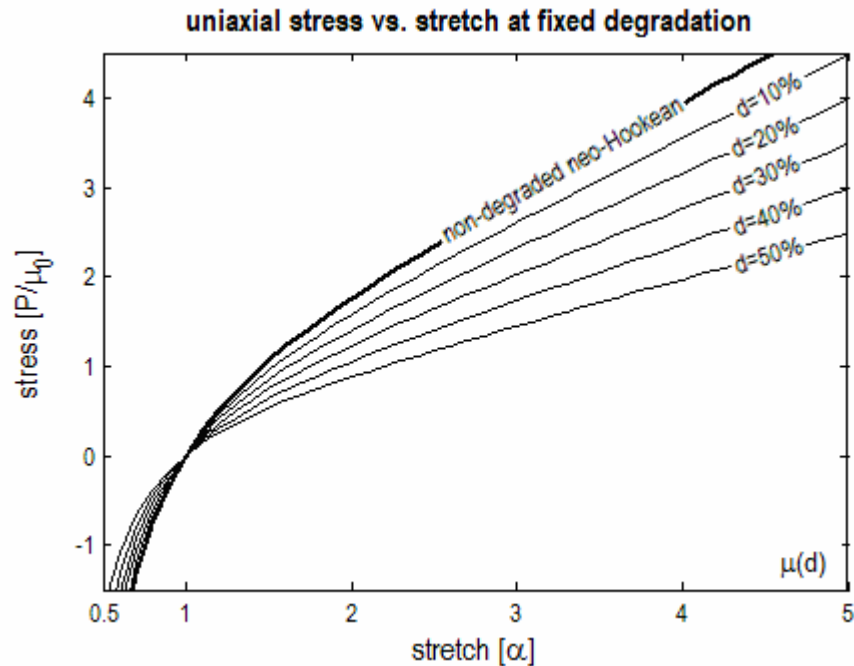
Fig. IV.1 Uniaxial stress vs. stretch at different levels of degradation of a degradable material that in the virgin state responds as a neo-Hookean material. Note that the stress free configuration is similar to all degradation levels, i.e. each response corresponding to a given level of degradation share this natural configuration.

classical hyperelastic material models such the neo-Hookean and the Mooney-Rivlin models will be subjected to degradation.

The stored energy function of a neo-Hookean material is given by (2.102). A degradable material of the form (4.10) that at fixed degradation responds like a neo-Hookean material is given by

$$W(I_{\mathrm{c}},d) = \frac{\mu(d)}{2}(I_{\mathrm{c}} - 3),$$

(4.15)

where the material property, the shear modulus $\mu = \mu(d)$, is no longer a material constant but instead a material function of degradation. The form of material property reduction with the amount of degradation will be chosen to be the simplest possible, i.e. a linear decrease in d, and takes the following form

$$\mu(d) = \mu_0(1 - \beta d), \tag{4.16}$$

where μ_0 is the shear modulus of the virgin specimen (when $d = 0$) and $\beta < 1$ is a constant related with the maximum state of degradation. Note that the modulus of the material when the maximum degradation is achieved (when $d \to 1$) is given by $\mu_0(1 - \beta)$. Failure by complete degradation is possible if $\beta = 1$ and (4.16) becomes

$$\mu(d) = \mu_0(1 - d). \tag{4.17}$$

In this case, when the material is completely degraded, its shear modulus goes to zero as $d \to 1$, hence it loses its load carrying capacity.

Under uniaxial extension, a neo-Hookean material shows the following stress vs. stretch response

$$P = \mu\left(\alpha - \frac{1}{\alpha^2}\right), \tag{3.13}$$

where P is the uniaxial Piola stress and α is the uniaxial stretch (cf. Section III.C). The stress vs. stretch response of the family of neo-Hookean materials following (4.15) with (4.17) is shown in Fig. IV.1 at different levels of degradation. Note that there is no permanent change in shape upon loading and unloading. The body has only one natural configuration but a variety of elastic responses from this natural configuration, each one characterized by a value of d.

A similar procedure can be applied to the Mooney-Rivlin material (whose stored energy function is given in (2.103)). Note that two material functions, $\mu_1(d)$ and $\mu_2(d)$, define the response of the degradable material that at fixed degradation responds like a Mooney-Rivlin material. Either one or both of the mechanical properties can be chosen to change with increasing d. Similarly as in (4.16), the material functions are given by

$$\mu_1(d) = \mu_1^0(1 - \beta_1 d), \tag{4.18}$$

$$\mu_2(d) = \mu_2^0(1 - \beta_2 d), \tag{4.19}$$
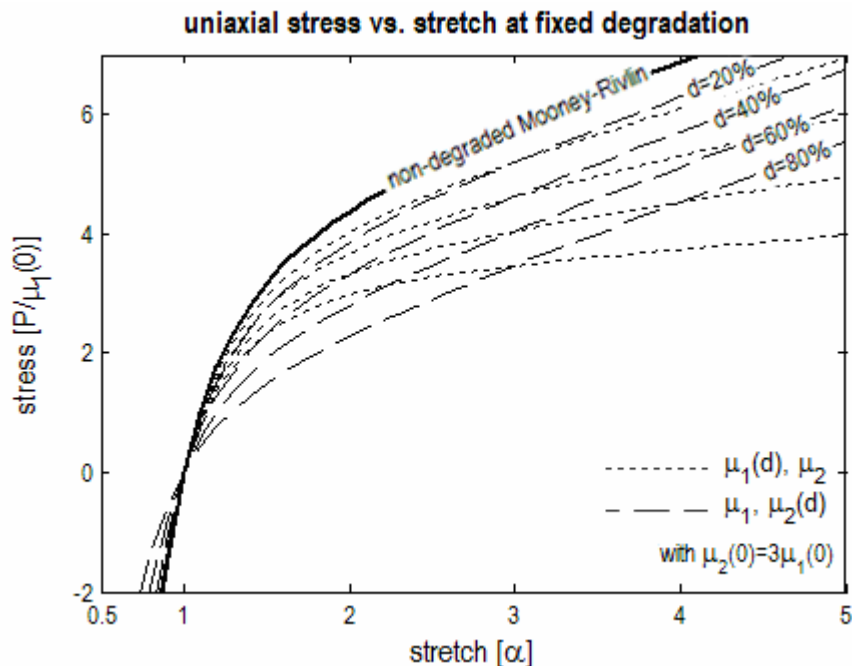
Fig. IV.2 Uniaxial stress vs. stretch at different levels of degradation of μ_1 or μ_2 of a degradable material that in the virgin state responds as a Mooney-Rivlin material (with $\mu_2(0)=3\,\mu_1(0)$). Because the Mooney-Rivlin model involves two constants, two different modes of degradation can be achieved from a virgin state. As expected, degradation in μ_1 shows similar characteristics as the previous example with a single constant, whereas a new form of downwards shift of the stress vs. strain curve is achieved with degradation of μ_2.

where μ_1^0 and μ_2^0 are the respective non-degraded material constants (at $d=0$), and β_1 and β_2 are related with the maximum degradable modulus at $d \to 1$. Similar to the situation presented for the degradable material based on the neo-Hookean response presented above, the moduli are allowed to decrease to zero, i.e. $\beta_1 = \beta_2 = 1$. Still, a three-fold variety of elastic responses can be obtained with different combinations of (4.18) and (4.19): (i) $\mu_1(d)$ is allowed to degrade while μ_2 is held constant at μ_2^0 (dashed lines in Fig. IV.2), (ii) μ_1 held constant at μ_1^0 while $\mu_2(d)$ degrades (dotted lines in Fig. IV.2), and (iii) both $\mu_1(d)$ and $\mu_2(d)$ are allowed to degrade, which yields
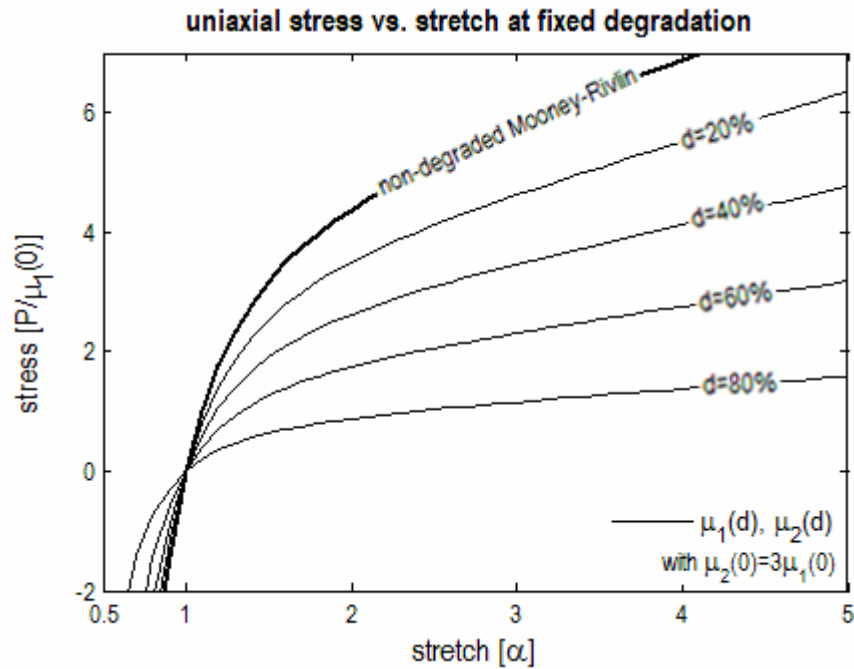
Fig. IV.3 Uniaxial stress vs. stretch at different levels of degradation of a degradable material that in the virgin state responds as a Mooney-Rivlin material (with $\mu_2(0)=3\,\mu_1(0)$). The response is the composite of the two modes of degradation, i.e. reduction in each of the material properties (μ_1 or μ_2), shown in Fig. IV.2.

a composite response of (i) and (ii) (in Fig. IV.3). Note that $\mu_2 = 0$ yields the previous case based on the neo-Hookean response.

2. *The instantaneous elastic response of PLLA that degrades*

The instantaneous elastic response (IER) of non-degraded PLLA is described by a stored energy function of the form

$$W^{PLLA} = \mu_1 e^{-(I_C-3)}(I_C - 3) + \mu_2 \ln[1+a(I_C - 3)],\qquad(3.21)$$

with the constants given on Table III.2 and stress vs. strain curve shown in Fig. III.17. A degradable material that describes the degradable instantaneous elastic response of PLLA is given by
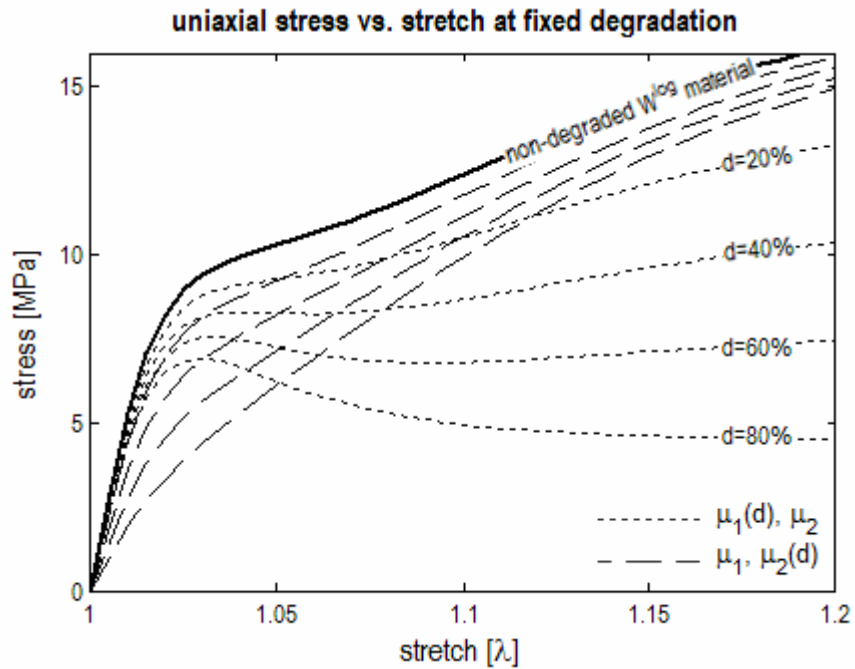
Fig. IV.4. Uniaxial stress vs. stretch at different levels of degradation of μ_1 or μ_2 of a degradable material that in the virgin state responds as a hyperelastic material characterized by the proposed stored energy function. Degradation of one of the modes gives preponderance to the other.

$$W^{PLLA}(d) = \mu_1(d)e^{-(I_C-3)}(I_C-3)+\mu_2(d)\ln[1+a(I_C-3)], \qquad (4.20)$$

where the two material properties, μ_1 and μ_2 (each determine the contribution of the respective term in the instantaneous elastic response of the material, cf. Fig. III.16) are allowed to degrade. Similarly, the material properties where chosen to decrease linearly from the non-degraded constants (in Table III.2) to zero, i.e.

$$\mu_1(d) = \mu_1^0(1-d), \qquad (4.21)$$

$$\mu_2(d) = \mu_2^0(1-d), \qquad (4.22)$$

a was set to be constant as its reduction with others fixed (not shown) is closely related to the mode of degradation $\mu_2(d)$. The two modes of degradation for each material
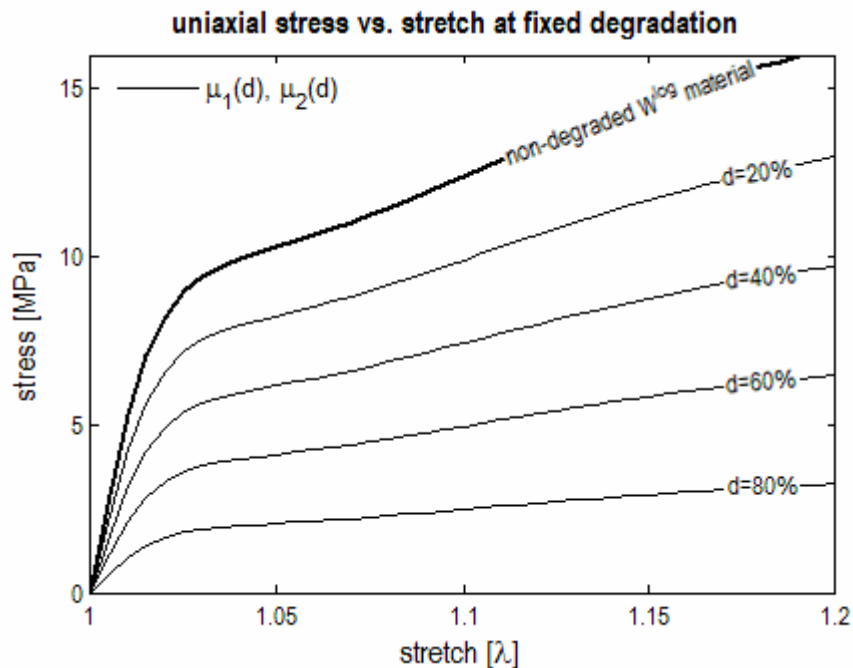
Fig. IV.5. Uniaxial stress vs. stretch at different levels of degradation of a degradable material that in the virgin state responds as a hyperelastic material characterized by the proposed stored energy function. Each material property is allowed to degrade equally till zero. The shape similarity between each response is remarkable. As the material degrades, not only the slope at the origin decreases but also less stress is necessary to achieve similar stretches.

function (defined as allowing one to degrade while maintaining the other fixed) are shown in Fig. IV.4.

The composite response is shown in Fig. IV.5. The instantaneous elastic response of degradable PLLA is characterized by a steep increase in stress in the low strain region followed by a mild increase in stress with strain. As degradation increases, the slope at the origin decreases substantially due to the decrease of $\mu_1(d)$ (cf. dashed lines in Fig. IV.4), whereas $\mu_2(d)$ is mostly responsible for the reduction in the latter part of the IER curve. Finally, note the similarity of the curves at each level of degradation.

3. *Time dependent homogeneous extension of a degradable neo-Hookean-like body*

In order to illustrate the response obtained with models of this kind, the simplest degradable model, the degradable neo-Hookean-like material model presented previously, is subjected to the simplest deformation, uniaxial extension. Henceforth, the suffix –like should be thought as an abbreviation with meaning of a degradable material that responds following the model (to which the suffix is attached and degradable will always be found previously) at fixed levels of degradation. The motion is given by (3.5) with a time dependent homogeneous stretch $\lambda(t)$, i.e.

$$x_1 = \frac{1}{\sqrt{\lambda(t)}} X_1, \qquad x_2 = \frac{1}{\sqrt{\lambda(t)}} X_2, \qquad x_3 = \lambda(t) X_3. \tag{4.23}$$

The deformation gradient **F** and the left and right Cauchy-Green stretch tensors **B** and **C** are given by (3.30) and (3.31) respectively. Due to the properties of this particular motion, degradation is occurs homogeneously, i.e. d is independent of position

$$d = d(t), \tag{4.24}$$

The stored energy function of a degradable neo-Hookean-like material is given in (4.15), where the shear modulus is given by (4.17), i.e. a linear decrease from μ_0 (the shear modulus of the non-degraded material) to zero as $d \to 1$.

The equation governing degradation is given by (4.14) where the rate of hydrolysis was chosen to be linearly dependent with the deformation radius as given in (4.12). Setting a threshold of activation equal to zero, i.e. $s_a = 0$, the equation governing degradation reduces to

$$\frac{\mathrm{d}}{\mathrm{dt}} d(t) = C\left(1 - d(t)\right)\left[\left(I_{\mathbf{C}} - 3\right)^2 + \left(II_{\mathbf{C}} - 3\right)^2\right]^{1/2}, \tag{4.25}$$

where C is a constant that describes this particular mode of strain-induced degradation. Usage of

$$I_{\mathbf{C}} = \lambda(t)^2 + \frac{2}{\lambda(t)}, \tag{4.26}$$

and

$$II_{\mathbf{C}} = 2\lambda(t) + \frac{1}{\lambda(t)^2},$$

(4.27)

in (4.25) yields

$$\frac{\mathrm{d}}{\mathrm{dt}}d(t) = C\left(1-d(t)\right)\frac{\left(\lambda(t)-1\right)^2}{\lambda(t)^2}\left(\lambda(t)^4 + 4\lambda(t)^3 + 8\lambda(t)^2 + 4\lambda(t) + 1\right)^{1/2}.$$

(4.28)

Constant C is related with the process strain-induced degradation. It can be expressed as

$$C = \frac{1}{\tau_D},$$

(4.29)

where τ_D can be thought of as a half time of degradation per unit deformation.

Finally, balance of linear momentum (cf. (2.63)) neglecting body forces yields

$$\mathrm{div}\left[-p\mathbf{1} + \mu_0\left(1-d\right)\mathbf{B}\right] = \rho\frac{\partial^2\boldsymbol{\chi}}{\partial t^2}.$$

(4.30)

Note that the balance of angular momentum (cf. (2.64)) is automatically satisfied for this material under this motion due to the form of the stress representation and **B**.

If the motion is restricted to be quasi-static, the inertial contribution on the linear momentum balance through the right hand side of (4.30) becomes negligible and yields

$$\frac{\partial p}{\partial X_1} = \frac{\partial p}{\partial X_2} = \frac{\partial p}{\partial X_3} = 0,$$

(4.31)

which implies that the Lagrange multiplier is independent of position and at most a function of time, i.e.

$$p = p(t).$$

(4.32)

The divergence in (4.30) was computed in a referential sense with the aid of relationship (2.67) and the deformation gradient (3.30).

The Lagrange multiplier (4.32) is easily computed from boundary conditions. Assuming a finite body with traction free lateral surfaces, one obtains

$$p = \mu_0(1 - d(t))\frac{1}{\lambda(t)}. \tag{4.33}$$

Finally, the Cauchy stress field **T** is completely determined and has only one non-zero component given by

$$T(t) \equiv T_{33}(t) = \mu_0(1 - d(t))\left(\lambda(t)^2 - \frac{1}{\lambda(t)}\right), \tag{4.34}$$

i.e. a state of uniaxial tension exists. This relationship is nonlinear, yielding generally three possible solutions for a given stress. $\lambda(t)$ must be real and positive, greater than unity for positive values of stress and less than one if the body is under a state of compression. As by definition $0 \le d < 1$, these phenomenological restrictions are automatically satisfied if $\mu_0 > 0$ (cf. (2.99)).

Equation (4.28) and (4.30) (or if attention is restricted to quasi-static motions, equation (4.34) instead) are the governing for homogeneous extension of an initially neo-Hookean material that degrades. They can be solved for any two of the following three quantities, $\lambda(t)$, $T(t)$, or $d(t)$. For the situation in which a controlled stretch is applied over time, the amount of degradation is obtained by integration of (4.28) and the necessary stress to maintain that stretch as the material degrades is given by (4.34). On the other hand, for the case in which a stress $T(t)$ is imposed, the stretch $\lambda(t)$ is obtained as one solution of (4.34), and from it, the corresponding increase of degradation is obtained with (4.28). The response of the degradable material to steps in stress and steps in stretch are presented in the following subsection.

4. Response to steps in stretch, stress, and to a cycle in stretch with constant rate

With time, the stress necessary to maintain a given constant stretch decreases, i.e. stress relaxation is observed (Fig. IV.6). Moreover, the decay is exponential, with half time dependent on the applied stretch. For larger stretches, the initial required stress is larger, but it relaxes faster. Degradation due to a constant stretch increases steeply during the initial stage of degradation. This rate is directly related to the amount of stretch, i.e.

Cauchy stress *T* in reponse toclose a step in stretch
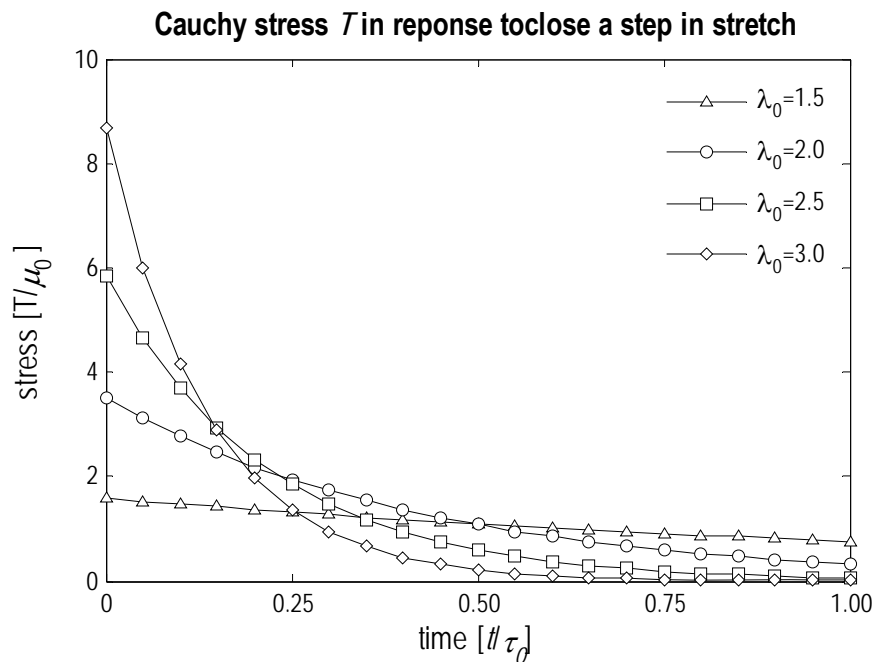
Fig. IV.6. Non-dimensional Cauchy stress required to maintain a constant stretch. The material softens as it degrades and consequently less force is necessary to maintain a given deformation, i.e. stress relaxation occurs. When the material is fully degraded, the shear modulus and the required stress decay to zero. Higher initial stretching leads to greater rate of degradation, and thus a shorter time to effective material breakdown.

more stretch will lead to a faster degradation. The degradation tends asymptotically to its maximum value of unity as time tends to infinity (Fig. IV.7).

Under the influence of constant loads, the stretch consistently increases over time (Fig. IV.8). The extent of this creep-like behavior is dependent on the amount of degradation and consequent softening of the material. The amount of degradation increases progressively (not shown, but easily inferred through the reduction in shear modulus shown in Fig. IV.9) where the effects of greater softening lead to greater stretches and the final steep increase in degradation. Two of the cases considered reach the point of maximum allowable amount of degradation in the time interval considered. Close to this point, the modulus of the material approaches zero and the stretch increases dramatically.

degradation *d* in reponse to a step in stretch
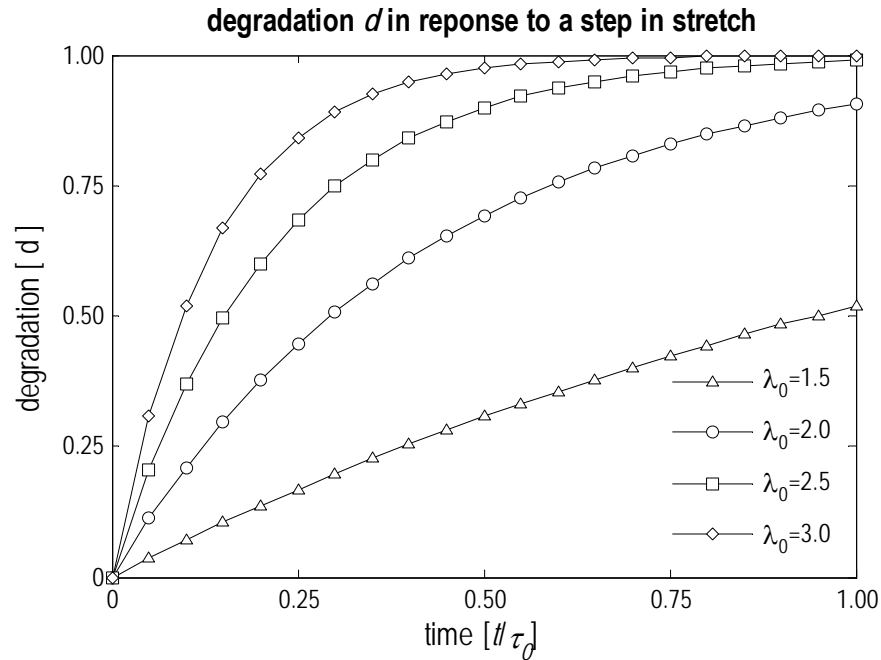
Fig. IV.7. Degradation for several constant stretches. The deformation on the right hand side of equation (4.28) will be constant, and hence, due to the $1-d$ term, the degradation asymptotically tends to its maximum allowable value. For greater stretches, the material degrades at a greater rate.

Hysteresis loops are observed in the non-dimensional Cauchy stress $T(t)/\mu_0$ vs. stretch $\lambda(t)$ diagram when the stretch is cycled between 1.00 and 1.25 (Fig. IV.10). Hysteresis is dependent on the stretching rate, with the area spanned by the hysteresis loop increasing as the rate of stretch decreases. The effects of degradation are indistinguishable during the initial stages of stretching for the four stretch rates considered, but as degradation proceeds the curves deviate from each other. Lastly, no permanent set is induced due to degradation: when the body is back to the original configuration, it is stress free (Fig. IV.11).

stretch λ in response to a step in stress
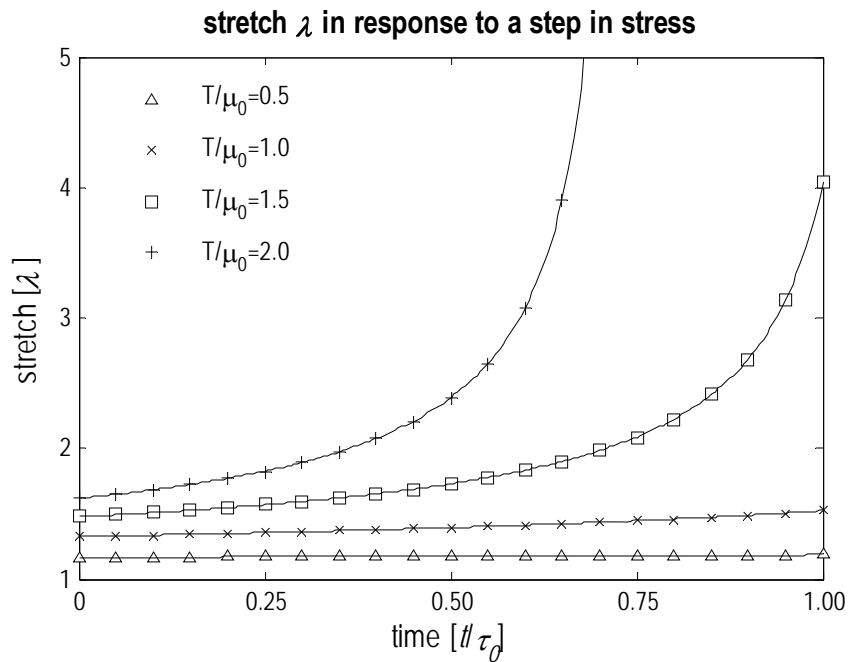
Fig. IV.8. Stretch for several constant applied stresses. As the stress increases, the impact of degradation is greater. Although the applied stress remains constant in each case, the stretch increases over time, i.e. the body exhibits creep-like behavior.

nondimensional shear modulus μ/μ_0 in response to a step in stress
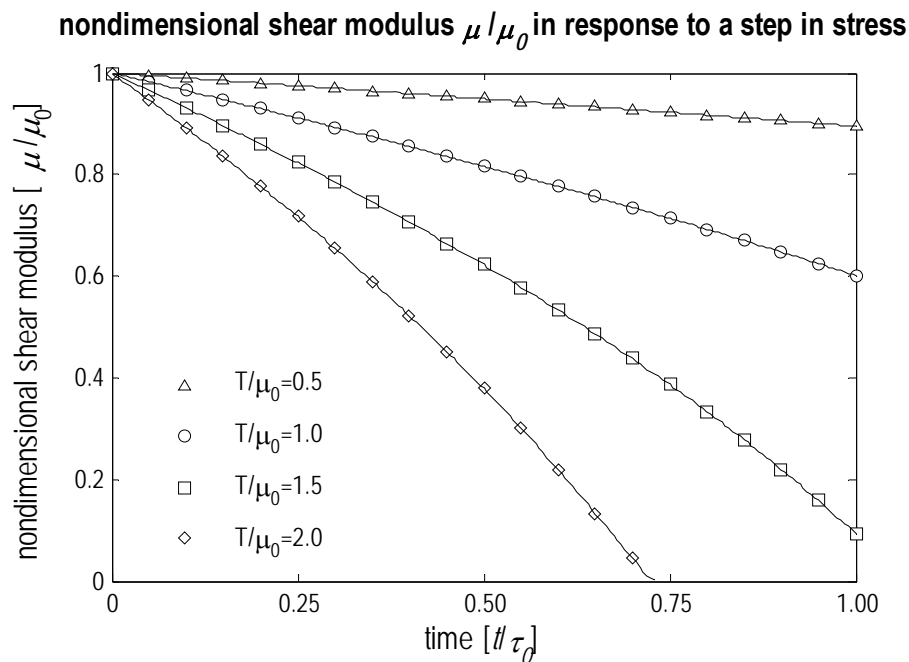
Fig. IV.9. Shear modulus of the material under several applied constant stresses. The decrease in shear modulus is directly related with the amount of degradation. As the material degrades and softens, the applied stresses (although remaining constant) lead to greater deformations (cf. Fig. IV.8) that consequently lead to greater increases in degradation, i.e. the degradation increases asymptotically and reaches its maximum allowable value. Greater stresses induce greater deformations that lead to different rates of increase of degradation.
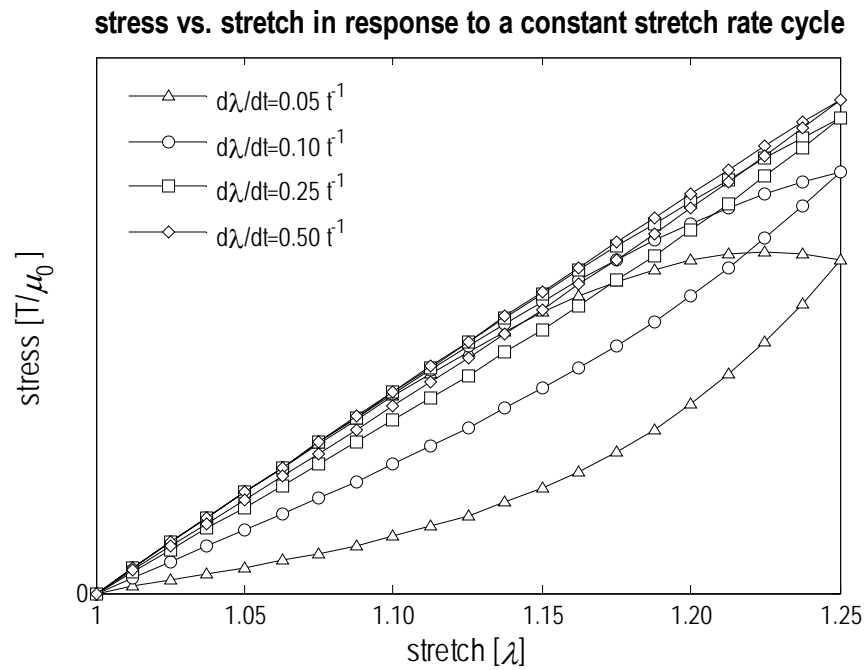
Fig. IV.10. Non-dimensional Cauchy stress vs. stretch for several stretching rates. The stretch cycles between 1.00 and 1.25 with constant stretching rates. Hysteresis can be observed.
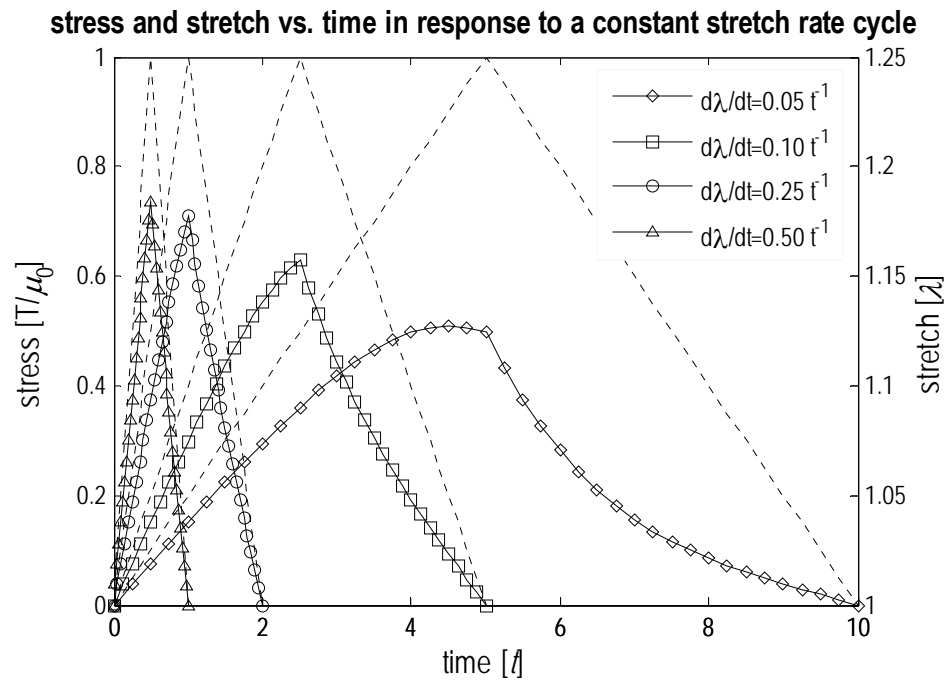
Fig. IV.11. Non-dimensional Cauchy stress vs. time for cycles in stretch with constant stretching rate. Stress is shown with lines with markers, whereas the prescribed cycle in stretch follows the dashed lines. As the rate of stretch decreases, the degradation mechanism is effective for a longer period of time and is responsible for greater softening.

5. *Stress relaxation, creep, and hysteresis*

The ability to model the behavior of biodegradable polymers subjected to mechanical loads would enhance the predictive nature of biodegradable stent design. Several particularizations of the proposed model were considered in the previous sections and provide, qualitatively, phenomenological support. Degradation is quantified by a parameter that describes locally the amount of degradation and changes the mechanical properties through a constitutive equation that is dependent on the aforementioned degradation parameter. The body starts out in a virgin state and due to the imposed stretch or due to the imposed loads, it degrades. The results indicate an increase in degradation (Fig. IV.7) and a consequent decrease in the shear modulus (Fig. IV.9).

One particular feature of the response of such models is stress relaxation in response to a constant stretch history (observed in Fig. IV.6). Stress decreases as the material degrades: as the shear modulus decreases, less force is required to maintain a constant deformation. The decay in stress results from the exponential increase in degradation (Fig. IV.7). In fact, when $\lambda(t)$ is the step history given by

$$\lambda(t) = \begin{cases} 0, & t < 0 \\ \lambda_0, & t \geq 0 \end{cases},$$

(4.35)

the increase of degradation is directly obtained from (4.28) and with initial condition $d(0) = 0$ yields

$$d(t) = 1 - e^{-\int_{0^-}^{t} \mathcal{K}(s)\, ds},$$

(4.36)

where $\mathcal{K}$ is the deformation dependent rate of increase of degradation. With stretch history given by (4.35), $\mathcal{K}$ is constant and given by

$$\mathcal{K}(\lambda_0) = \frac{1}{\tau_D} \frac{(\lambda_0 - 1)^2}{\lambda_0^2} (\lambda_0^4 + 4\lambda_0^3 + 8\lambda_0^2 + 4\lambda_0 + 1)^{1/2},$$

(4.37)

relative stress T/T_0 **in reponse to a step in stretch**
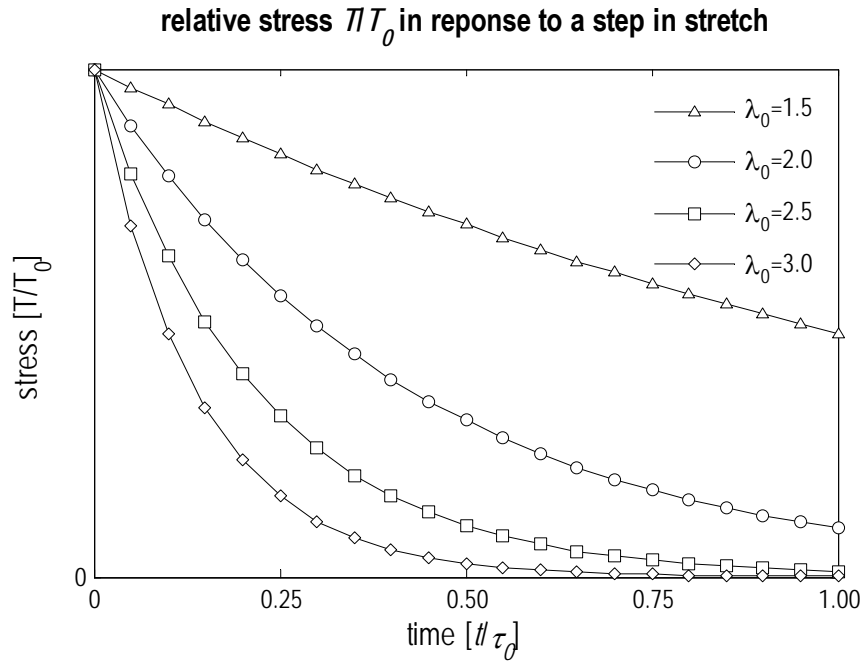
Fig. IV.12. Relative Cauchy stress required to maintain a constant stretch. Relative stresses are obtained with normalization with the instantaneously obtained stress for each stretch level. While this figure and Fig. IV.6 bear the same information, it is the converse of Fig. IV.7. Degradation follows an exponential increase to 1 (cf. equation (4.36) with constant $\mathcal{K}$), whereas relative relaxation follows an exponential decrease (cf. equation (4.39)).

where τ_D is a characteristic time of degradation per unit deformation. Using (4.34) to compute the stresses, one obtains

$$T(t) = \mu_0 e^{-\mathcal{K}(\lambda_0)t} \left(\lambda(t)^2 - \frac{1}{\lambda(t)} \right). \tag{4.38}$$

Considering T_0 to be the necessary stress to stretch the non-degraded material λ_0 and stretch history (4.35), then

$$T(t)/T_0 = e^{-\mathcal{K}(\lambda_0)t}. \tag{4.39}$$

The evolution of the relative stresses is shown in Fig. IV.12. Stress relaxation in response to a step in stretch follows form (4.39) with $\mathcal{K}(\lambda_0)$ given by (4.37).

On the other hand, when the force is maintained constant, an increase in stretch occurs due to degradation, i.e. the body creeps as it degrades under a constant load (Fig. IV.8). Increases in stretch promote greater changes in degradation and this cycle is repeated until the material reaches a point where the maximum degradation and a zero modulus are achieved, allowing infinitely large deformations. Of course, structural failure probably occurs much sooner.

The material exhibits behavior similar to mechanical hysteresis when the stretch is cycled. The extent of hysteresis is dependent on degradation, as the four cases (shown in Fig. IV.10 and Fig. IV.11) demonstrate. For a quick rate of stretching/unstretching (the two most on the left in Fig. IV.11), degradation acts during a smaller period of time and the stress almost follows the corresponding stretch. As the rate of stretching decreases, the effects of degradation are more pronounced due to the fact that the deformation is occurring over a time period on which significant degradation occurs.

The rate of dissipation in this material can be obtained with (4.1). The symmetric part of the velocity gradient can be obtained with (2.15) and (2.16) with the material time derivative of the deformation gradient (3.30) and is given by

$$(\mathbf{D}) = \begin{pmatrix} -\dot{\lambda}/2\lambda & 0 & 0 \\ 0 & -\dot{\lambda}/2\lambda & 0 \\ 0 & 0 & \dot{\lambda}/\lambda \end{pmatrix}, \tag{4.40}$$

and with the material time derivative of the degradable material obtained with (4.15) and the stress field (4.34), (4.1) becomes

$$\xi = -\mu_0(1-d)\left(\lambda^2 - \frac{1}{\lambda}\right)\frac{\dot{\lambda}}{\lambda} + \mu_0(I_C - 3)\dot{d}. \tag{4.41}$$

Under constant stretch λ_0, the rate of dissipation is

$$\xi = \mu_0(I_C - 3)\mathcal{K}(\lambda_0)e^{-\mathcal{K}(\lambda_0)t}, \tag{4.42}$$

where $\mathcal{K}(\lambda_0)$ is given by (4.37).

To conclude, it is worth remarking that equation (4.9) is a reasonably general constitutive equation for a degradable material. Nevertheless, note that: (i) uniaxial extension is a homogeneous deformation, and only homogeneous degradation will result from it, (ii) the specific forms of equations (4.11) or (4.14) with activation criterion (4.13) were chosen on the basis of the simplicity that they accord, and (iii) biodegradable polymers, like PLLA, are not linear elastic materials and in this context should perhaps be modeled as fully nonlinear viscoelastic materials.

D. Degradable materials that at fixed degradation are viscoelastic

Theoretical models to predict degradation and erosion of biodegradable materials under load would seem to be important design tools for a vast number of applications. Besides understanding the processes of degradation and erosion, the mechanical response and its influence on degradation and erosion are equally relevant. A theoretical framework for such phenomena was introduced above and used to model degradable materials that at fixed levels of degradation are elastic. Degradation is quantified by a scalar field, the degradation parameter, that changes the properties of the material. A rate equation that governs the change of degradation is coupled with the balance of linear momentum. The degradable material presented in Section C, which is hyperelastic if degradation is fixed, shows stress relaxation, creep and hysteresis as it degrades. These phenomena, although superficially similar to viscoelastic behavior, arise from different mechanisms, i.e. irreversible chain scission instead of conformational relaxations.

Poly(lactic acid) is not a simple material. Besides being able to degrade, several factors influence its mechanical properties and response, such as molecular weight, degree of crystallinity, or hydration [244]. The most common mechanical properties found in the literature for PLA are tensile strength at break, tensile yield strength, tensile modulus at infinitesimal deformation and tensile elongation following ASTM methods D638 or D882 [81,108,241,244,252,257]. Unfortunately, PLA is not an elastic material (cf. Chapter III, Section B.2): (i) the loading and unloading paths do not coincide; (ii) the

material does not respond instantaneously to an applied load and its behavior is time dependent, and (iii) the material does not return instantaneously to its former unloaded configuration upon the removal of the load. Consequently, the response of the material is affected by the rate at which it is loaded.

On the other hand, non-degraded PLLA shows stress relaxation, creep, and hysteresis, phenomena that are characteristic of most polymers and arises directly from the inherent microstructure and conformational changes of the polymeric network. The response of PLA is clearly one of a viscoelastic material (cf. Chapter III, Section B.3), hence viscoelastic models should be used to describe its response.

1. A degradable material that at fixed degradation is QLV

One of the simplest viscoelastic solid models, the quasilinear viscoelastic model (cf. equation (2.116)) is determined by two material properties, the instantaneous elastic response (IER) and the reduced relaxation function (RRF). The simplest choices for these material properties are a neo-Hookean elastic solid for the former (cf. stored energy function (2.102) and uniaxial stress vs. stretch relationship (3.13)) and a one term Prony's series for the latter, i.e.

$$G(\xi) = k_0 + k_1 e^{-\xi/\tau_1}. \tag{4.43}$$

The reduced relaxation function is restricted by $G(0) = 1$, hence $k_0 = 1 - k_1$. This simplest viscoelastic material is characterized by an instantaneous elastic response with shear modulus μ and a stress decay normalized by k_1/k_0 occurring with a single relaxation time, τ_1. In other words, this particular QLV model is characterized by three materials constants, hence three distinct modes of degradation are possible.

The first mode of degradation, the decrease of the shear modulus of the instantaneous elastic response, follows the same rationale as the presented above, i.e. $\mu(d)$ is characterized by equation (4.17) and the uniform extension of the degradable instantaneous elastic response is characterized by Fig. IV.1 at different levels of fixed

Fig. IV.13. Stress relaxation response to steps in strain (1% and 4%) of the degradable QLV-like material with degradable IER and constant RRF. As expected, the instantaneous elastic response is mostly responsible for the vertical location of the curves, i.e. the magnitude of the stress.

degradation. The response to steps in strain at fixed levels of degradation of the degradable QLV-like material is shown in Fig. IV.13. The viscoelastic characteristics of the material remain unchanged as the reduced relaxation function is unchanged. Only the stress levels achieved with the same steps in strain (shown for step histories of 1% and 4%) are different.

The reduced relaxation function is also a material function of degradation, i.e.

$$G(\xi, d) = k_0(d) + k_1(d)e^{-\xi/\tau_1(d)} , \qquad (4.44)$$

and allows two distinct modes of degradation (cf. Fig. IV.14 and Fig. IV.15). As a viscoelastic material degrades, it is expected that its relaxation occurs not only faster, i.e. the relaxation time decreases with degradation

$$\tau_1(d) = \tau_1^0(1 - \beta_1 d) , \qquad (4.45)$$
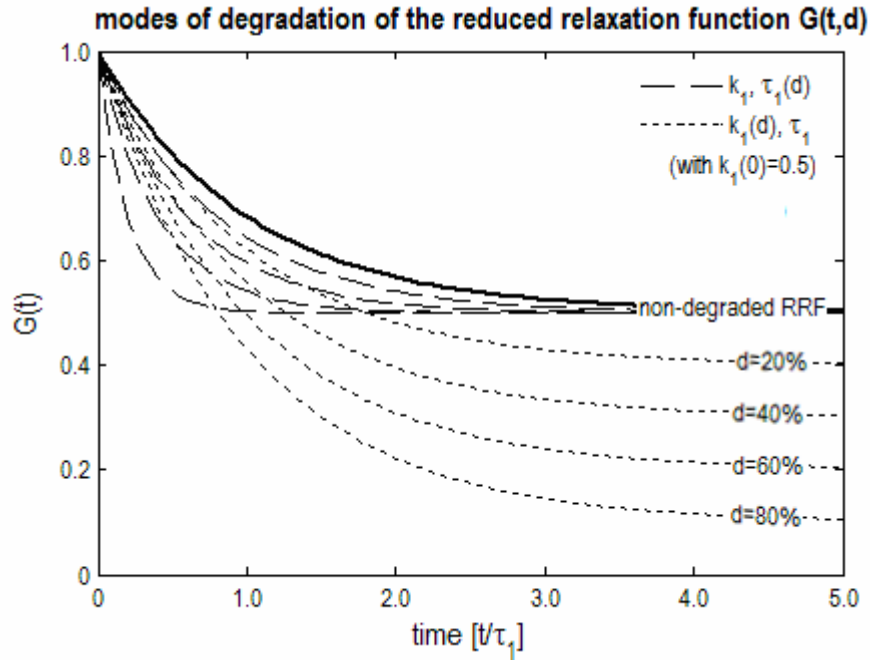
Fig. IV.14. Modes of degradation of the reduced relaxation function $G(t,d)$ at fixed levels of degradation. Two modes of degradation are considered for the RRF: (i) a reduction in the characteristic relaxation time, and (ii) a decrease in the residual modulus. As the material degrades, it is expected that the material not only relaxes faster but also loses its ability to withstand the same levels of stress. Note that the instantaneous elastic response is independent of the reduced relaxation function.

but also its residual modulus might be hampered, i.e.

$$k_0(d) = 1 - k_1(d) = 1 - k_1^0(1 - \gamma_1 d),$$ (4.46)

where τ_1^0 and k_1^0 are material constants that characterized the reduced relaxation function of the virgin material and $\tau_1(d)$ and $k_1(d)$ material functions that characterize the degradable material. β_1 and γ_1 are constants that define the values of the material functions at the stage of maximum degradation. For simplicity, they are considered to be $\beta_1 = \gamma_1 = 1$, and hence, the viscoelastic properties approach zero as $d \to 1$.
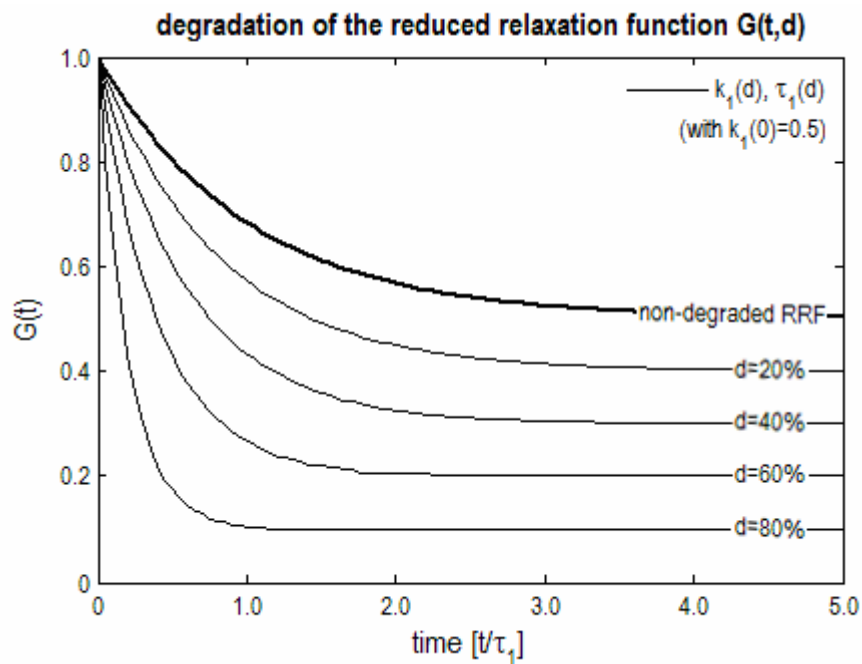
Fig. IV.15. Degradable reduced relaxation function $G(t,d)$ at fixed levels of degradation. A composite effect of the reduction of the two material constants that characterize the reduced relaxation function (the relaxation time and the residual modulus) is obtained. Note the similarity between each curve. One degradable material that at fixed level of degradation responds as a QLV model is defined by this particular choice of degradable RRF with degradable IER shown in Fig. IV.1.

The stress relaxation response to steps in strain for these modes of degradation is shown in Fig. IV.16 and Fig. IV.17. Together with the degradation of IER (cf. Fig. IV.13), they form a basis from which different degradable materials that at fixed relaxation respond like a QLV material can be constructed. As an example, considering full degradation of each material property (i.e. $\mu(d)$, $k_0(d)$, and $\tau_1(d)$ tend to zero as $d \rightarrow 1$), yields a degradable material which exhibits the stress relaxation response to steps in strain shown in Fig. IV.18.

The family of QLV models that compose the degradable material shows the following characteristics: (i) as the material degrades, the stress levels achieved with similar strain histories decrease, (ii) the amount of stress decay increases with
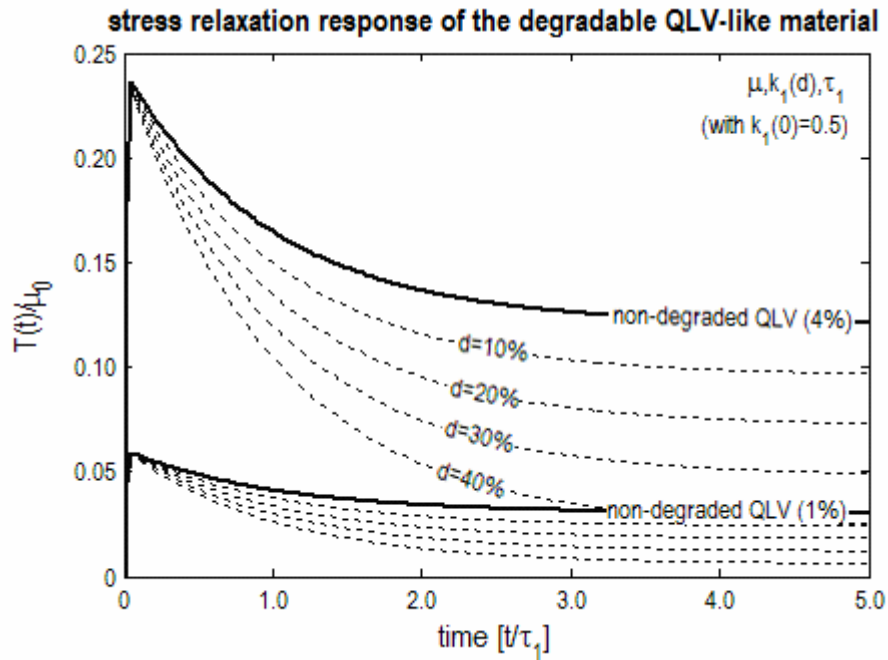
Fig. IV.16. Stress relaxation response to steps in strain (1% and 4%) of the degradable QLV-like material with constant IER and degradable residual modulus. While the instantaneous value of stress obtained with the step history does not change with level of degradation (due to this particular mode), the residual modulus decreases with degradation. The relaxation time is also remaining constant. The viscoelastic properties are directly related with the reduced relaxation function.

degradation, and (iii) the material relaxes faster. This expected behavior shows acceptable phenomenological characteristics: as the number of effective crosslinks is reduced with increasing degradation, the ability for the network to withstand load is decreased, and that is characterized by either a decrease in the initial and in the residual moduli. Furthermore, smaller and less constrained chains allow faster conformational relaxations and hence a faster relaxation towards the residual modulus.
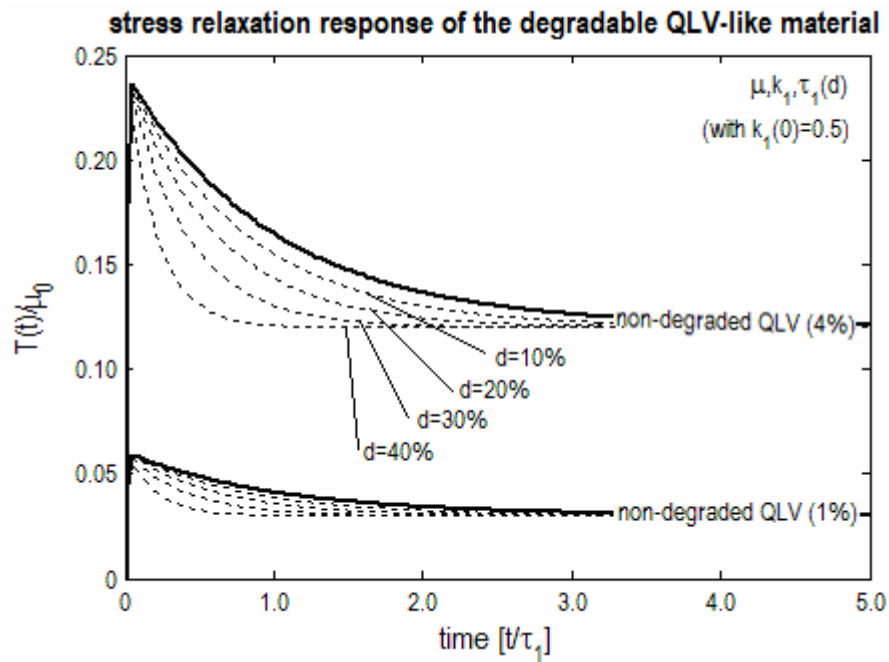
Fig. IV.17. Stress relaxation response to steps in strain (1% and 4%) of the degradable QLV-like material with constant IER and degradable relaxation time. Here, only the relaxation time is made to change with degradation level. Note that either the instantaneously achieved stress or the residual stress is the same for materials with different levels of degradation.
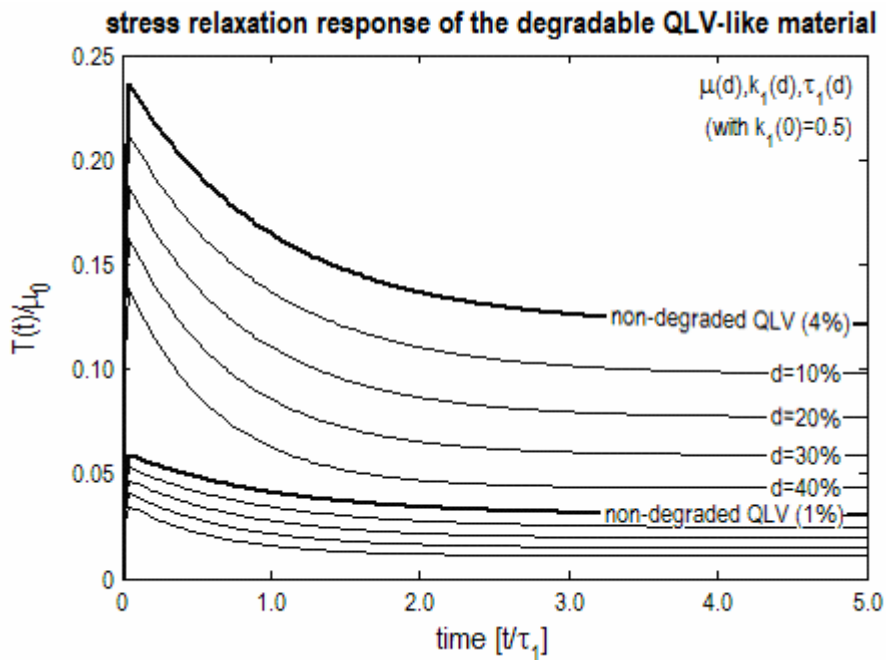
Fig. IV.18. Stress relaxation response to steps in strain (1% and 4%) of the degradable QLV-like material. A composite effect of the three modes shown in Fig. IV.13, Fig. IV.16, and Fig. IV.17 is achieved with simultaneous reduction of each material property. As opposed to the variation of each individual mode, this particular variety of responses is much more phenomenological acceptable. Still, an infinite amount of different varieties exist and can be obtained with the inclusion of maximum degradation levels or different combinations of each degradation mode.

2. A degradable material that at fixed degradation is nonlinearly viscoelastic

The nonlinear viscoelastic model introduced by Pipkin & Rogers [219] and particularized by Wineman [220] to yield a Mooney-Rivlin elastic solid if time dependence is neglected was extended within current degradable framework. The stress representation of such materials is given by equation (2.111). The response is characterized by

$$\mathbf{G}(\mathbf{C}(s),\xi) = R(\xi)\{[1 + \mu \ \mathrm{tr} \ \mathbf{C}(s)]\mathbf{1} - \mu\mathbf{C}(s)\} , \qquad (2.113)$$
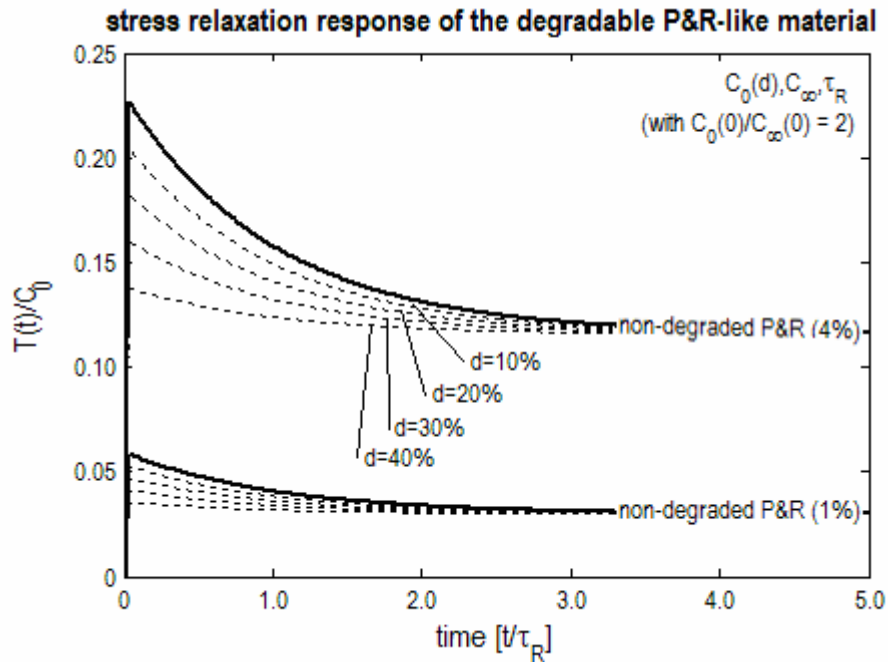
Fig. IV.19. Stress relaxation response to steps in strain (1% and 4%) of the degradable P&R-like degradable material with degradable initial modulus. All other material properties remain constant. The initial modulus is mostly responsible by the initial level attained by the step in strain. Note that in a viscoelastic material, phenomenological reasoning implies that the initial modulus is greater than the residual modulus. Note that when the initial is allowed to degrade, it can attain lower values than the residual modulus.

where

$$R(\xi) = C_\infty + (C_0 - C_\infty)e^{-\xi/\tau_R}. \qquad (2.114)$$

The model is characterized by four material properties, the initial and residual moduli, C_0 and C_∞ respectively, a viscoelastic relaxation time τ_R, and $\mu = \mu_2/\mu_1$ (the ratio of the material properties of the corresponding Mooney-Rivlin elastic material, cf. (2.103)).

Similarly, each material property can be allowed to be a function of degradation. A variety of material responses is obtained for each individual variation of one of the mechanical properties. At fixed levels of degradation, each response follows the single integral nonlinear viscoelastic with (2.113) and (2.114). Similarly, stress relaxation
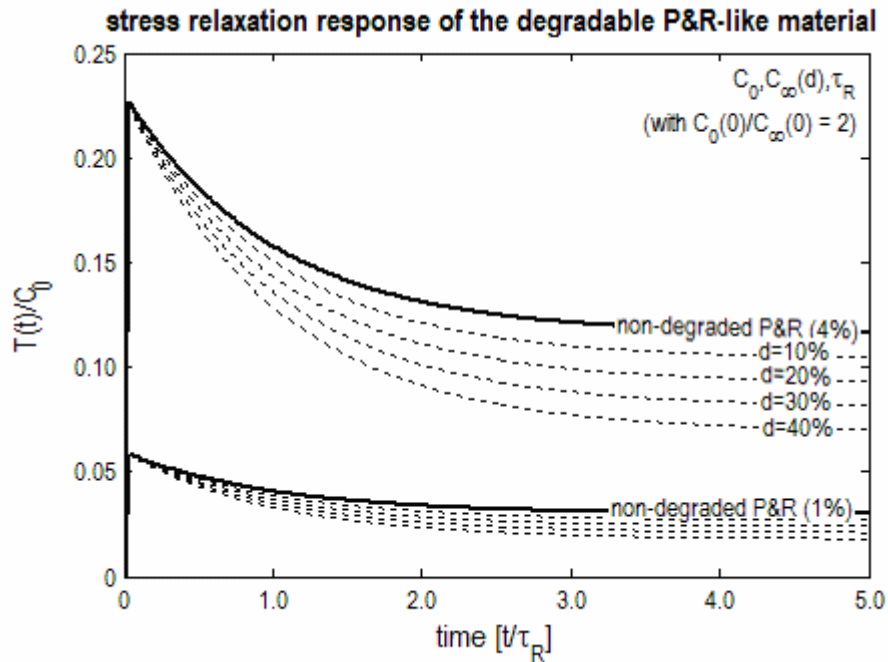
Fig. IV.20. Stress relaxation response to steps in strain (1% and 4%) of the degradable P&R-like material with degradable residual modulus. Similarly to the QLV model, the decrease of the residual modulus changes the properties of stress relaxation of a viscoelastic material.

curves in response to steps in stretch are used to investigate the response of this degradable material. In order to be possible to draw comparisons between both viscoelastic models (the quasilinear and the nonlinear), μ was set to zero, such that (2.113) yields a viscoelastic material that if time dependence is neglected responds as a neo-Hookean material.

Three distinct modes of degradation are possible: (i) variations in initial modulus $C_0(d)$ (that is related with the modulus of the neo-Hookean material), (ii) variations in residual modulus $C_\infty(d)$ (which initially was considered to be half of the initial modulus, similar as k_1 in the QLV model presented above), and (iii) variations in viscoelastic relaxation time $\tau_R(d)$. Each variety is shown in Fig. IV.19, Fig. IV.20, and Fig. IV.21, respectively. The composite response when all material properties degrade equally to zero is shown in Fig. IV.22.
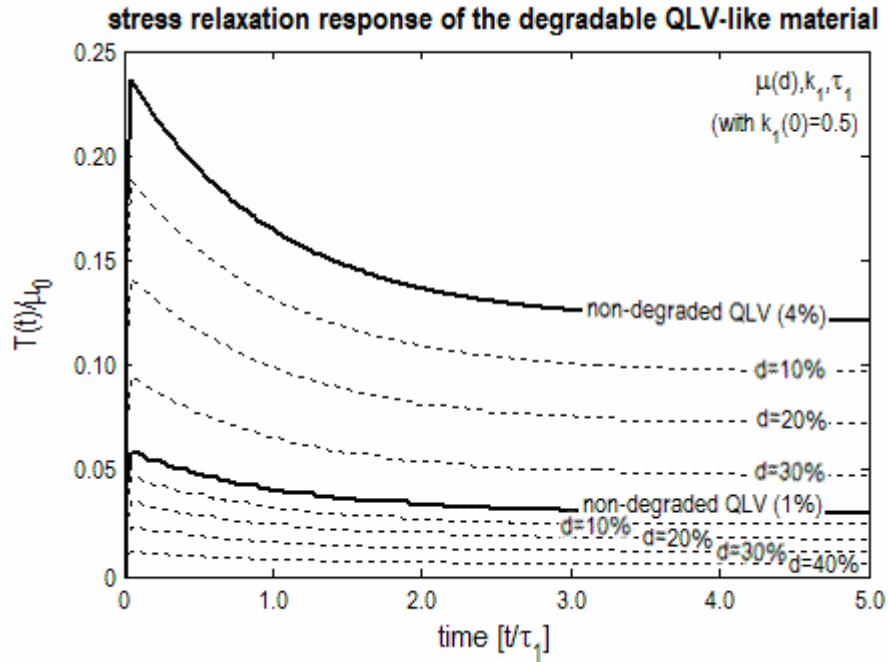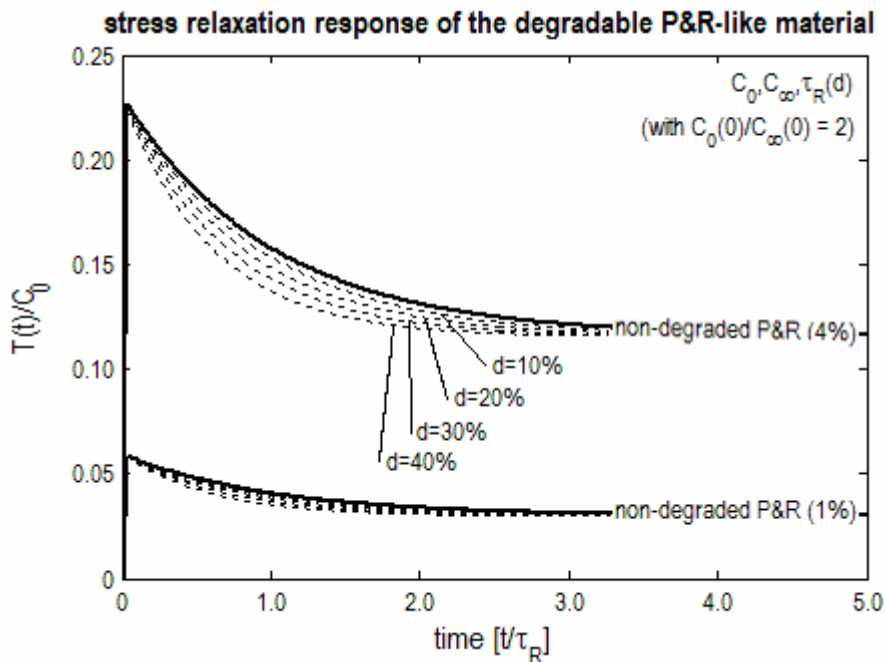
Fig. IV.21. Stress relaxation response to steps in strain (1% and 4%) of the degradable P&R-like material with degradable relaxation time. The relaxation time is the only property allowed to change. All responses within this variety have similar initial and residual moduli.

The major conclusion that can be drawn from the varieties of responses of degradable viscoelastic materials shown here is their phenomenological acceptance. As the material degrades, its ability to withstand stress is reduced: more precisely, less stress is required to maintain the prescribed stretch on a degraded material (not only the instantaneous response to changes in deformation but also its residual value after relaxation). Furthermore, as degradation increases, the material relaxes faster.

Once again, note that only stress relaxation in response to steps in strain of 1% and 4% were shown. Creep in response to constant stretches or responses to arbitrary histories could also be obtained. The response of a viscoelastic material is hard to characterize (as opposed to one of an elastic material, which one single stress vs. strain curve is sufficient) due to the history-dependence of the stress. Hence, it should be remarked that the stress relaxation response shown here is just one among the multitude
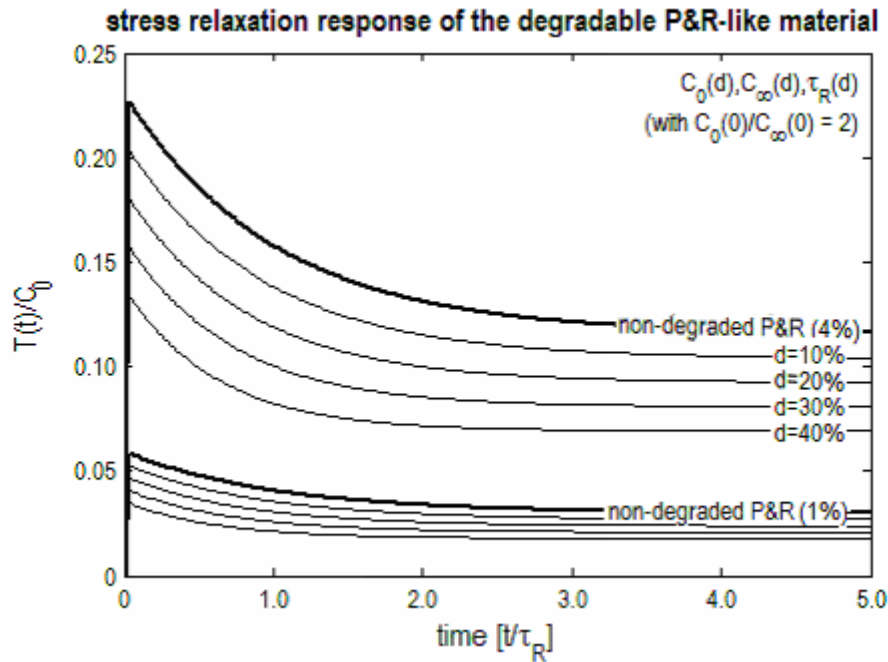
Fig. IV.22. Stress relaxation response to steps in strain (1% and 4%) of the degradable P&R-like material. A composite effect of the three modes shown in Fig. IV.19, Fig. IV.20, and Fig. IV.21 is achieved with simultaneous reduction of each material property. As opposed to the variation of each individual mode, this particular variety of responses is much more phenomenological acceptable. Note the similarity of the stress relaxation response of the QLV model and the P&R viscoelastic model.

of responses to different stretch that can be achieved for each variety of responses of this particular degradable material.

Still, the material is fully characterized by (2.113) and (2.114) with degradation dependent material properties, i.e. $C_0(d)$, $C_\infty(d)$, and $\tau_R(d)$. Similarly as before, the material is not a viscoelastic material per se: the degradable material responds as a viscoelastic material following the single integral representation by Pipkin & Rogers and the particularization by Wineman if and only if degradation is fixed. The degradable material possesses a variety of responses, each one corresponding to a value of d between 0 and 1.

3. *Time dependent homogeneous extension of a degradable P&R-like body*

In order to illustrate the response of models of this kind, time-dependent homogeneous extension of a degradable material developed above was computed. The rate of increase of degradation was chosen to vary linearly with the amount of deformation measured in (I_C, II_C) space, i.e. (cf. (4.4) or (4.11))

$$\frac{\mathrm{d}}{\mathrm{dt}} d(t) = \frac{(1 - d(t))}{\tau_D} \left[(I_C - 3)^2 + (II_C - 3)^2 \right]^{1/2}. \tag{4.47}$$

The threshold of activation was chosen to be $s_a = 0$ (cf. (4.13)), i.e. any deformation departing from the reference state causes degradation to occur. Further, constant C was replaced by a characteristic time of degradation, τ_D. Note that the characteristic time of degradation is connected to the amount of deformation, i.e. τ_D should be seen as a half-time of degradation per unit deformation (which is measured through s).

Time dependent homogeneous extension is characterized by a motion of the form (4.23). The deformation gradient $\mathbf{F}$ and the left and right Cauchy-Green stretch tensors $\mathbf{B}$ and $\mathbf{C}$ are given by (3.30) and (3.31) respectively. The stress has the following representation

$$\mathbf{T} = -p\mathbf{I} + \mathbf{F} \left[\mathbf{G}(\mathbf{C}(t), 0) + \int_0^t \frac{\partial}{\partial(t-s)} \mathbf{G}(\mathbf{C}(s), t - s) ds \right] \mathbf{F}^{\mathrm{T}}, \tag{2.111}$$

where p is the Lagrange multiplier for the enforcement of incompressibility. Because $\mu = 0$, $\mathbf{G}$ is independent of $\mathbf{C}$ (cf. equation (2.113)) but because the material is degradable, dependent on d through the material properties, i.e.

$$\mathbf{G}(\xi, d) = \left[C_0(d) - C_\infty(d)(1 - e^{-\xi/\tau_R(d)}) \right] \mathbf{1}. \tag{4.48}$$

Initially, the material is non-degraded, i.e. at $t = 0$, $d = 0$. The material constants that characterize the viscoelastic response of the virgin state are

$$\overline{C}_0 = C_0(0), \qquad \overline{C}_\infty = C_\infty(0), \qquad \overline{\tau}_R = \tau_R(0), \tag{4.49}$$

and the time independent response of the virgin material is characterized by

$$\bar{\mathbf{G}} = \mathbf{G}(0) = \bar{C}_0 \mathbf{1} . \tag{4.50}$$

The history dependent term of the stress is of more complex computation. Note that the material properties depend on d which in turn depends on t, i.e.

$$C_0(d) = \bar{C}_0(1-d) , \tag{4.51}$$

$$C_\infty(d) = \bar{C}_\infty(1-d) , \tag{4.52}$$

$$\tau_R(d) = \bar{\tau}_R(1-d) . \tag{4.53}$$

Nevertheless, due to the independence of $\mathbf{G}$ on the deformation (achieved by setting $\mu = 0$), the integral is easily computed and yields

$$\int_0^t \frac{\partial}{\partial m} \mathbf{G}(m) \bigg|_{m=t-s} ds = -C_\infty(d)(1-e^{-t/\tau_R(d)})\mathbf{1} . \tag{4.54}$$

Substituting (3.30), (4.48) through (4.50) and (4.54) in (2.111), the stress field is given by

$$\begin{aligned}
T_{11} = T_{22} &= -p + \frac{1}{\lambda}\left[\bar{C}_0 - C_\infty(d)(1-e^{-t/\tau_R(d)})\right] \\
T_{33} &= -p + \lambda^2\left[\bar{C}_0 - C_\infty(d)(1-e^{-t/\tau_R(d)})\right]
\end{aligned} , \tag{4.55}$$

with all other components null. Applying boundary conditions (traction free side surfaces) with the assumption of quasi-static motions yields

$$p = \frac{1}{\lambda}\left[\bar{C}_0 - C_\infty(d)(1-e^{-t/\tau_R(d)})\right] , \tag{4.56}$$

and finally

$$T(t) \equiv T_{33} = \left[\bar{C}_0 - C_\infty(d)(1-e^{-t/\tau_R(d)})\right]\left(\lambda^2 - \frac{1}{\lambda}\right) . \tag{4.57}$$

Equation (4.57) yields the axial stress as a function of time and degradation in response to a step history $\lambda = \lambda(t)$. The stress depends not only on the deformation but

degradation in response to steps in stretch
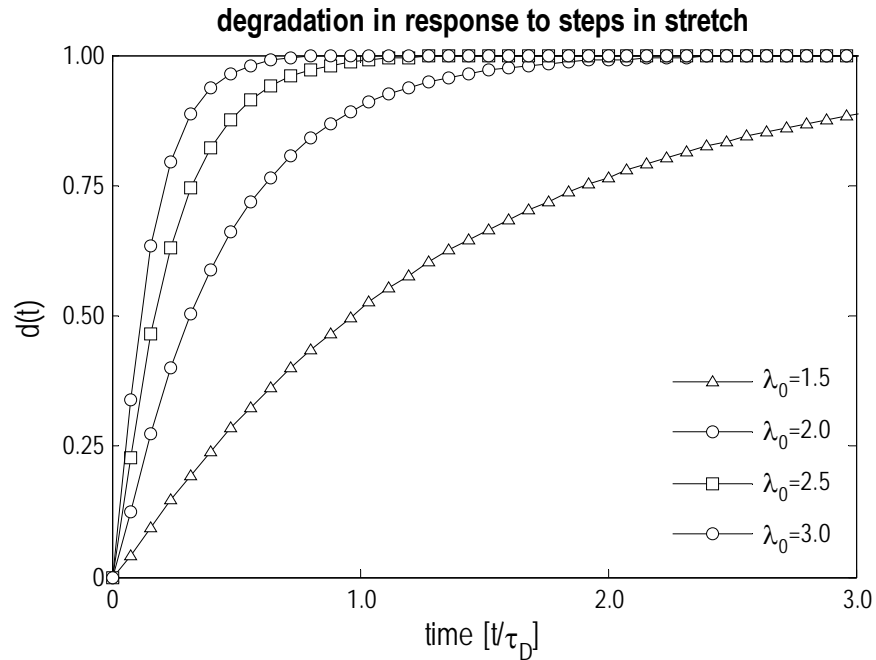
Fig. IV.23. Degradation in response to several step stretch histories. The values of degradation are directly related with the amount of stretch imposed on the material and constant τ_D. Note that as degradation is induced solely by deformation, hence similar stretch histories provoke the same amount of degradation, independently of the class of degradable materials (here shown for viscoelastic degradable P&R-like material, cf. Fig. IV.7 for hyperelastic-like degradable material).

also on the current degradation. Once the stretch history is prescribed (step in strain of the form (3.24)), the degradation that is obtained due to such deformation is directly obtained upon integration of (4.47) (which for uniaxial extension yields (4.28)). That was the procedure followed before in Section IV.C.

Note that because degradation is induced solely by deformation, the amount of degradation due to similar stretch histories is similar. Hence, the amount of degradation obtained here for the degradable P&R-like material (shown in Fig. IV.23) is similar to the amount of degradation obtained for the degradable neo-Hookean-like material (cf. Fig. IV.7). The only difference between them is that for the neo-Hookean material, the stretch of λ_0 was instantaneously applied at $t = 0$, while for the nonlinear viscoelastic

stress relaxation of the degradable P&R-like material
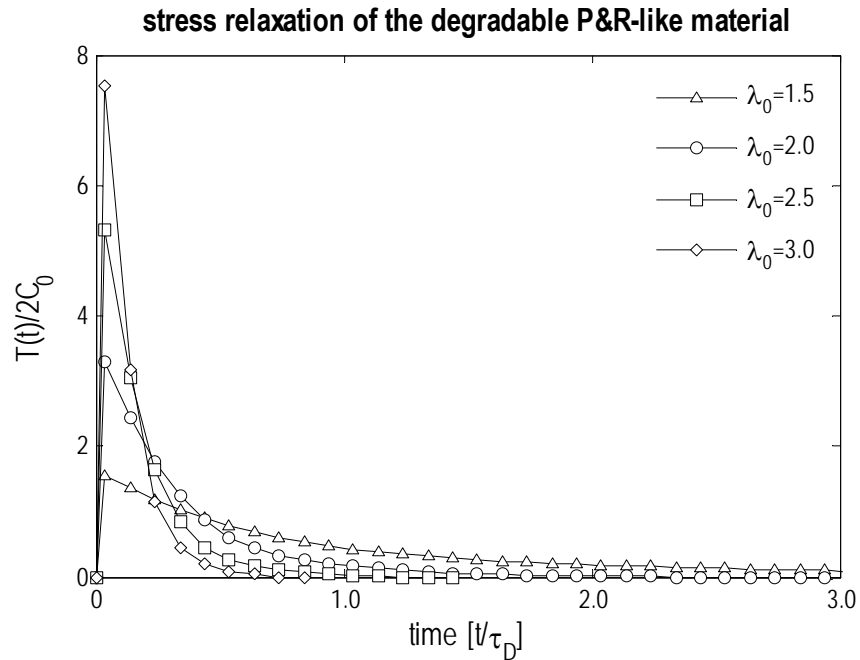
Fig. IV.24. Non-dimensional Cauchy stress required to maintain the prescribed stretch history. As opposed to Fig. IV.6 where the stress response was instantaneous in response to an instantaneous change in stretch, the stress here follows the finite rise time of the prescribed stretch history. Also, notice that relaxation is more intense in this degradable material: stress relaxation is not only due to degradation but also due to inherent relaxation mechanisms associated with viscoelasticity.

counterpart analyzed here, a step history with rise time of $t_0 = \tau_D/50$ was considered (cf. (3.24)). The difference between the degradation that both stretch histories yield (instantaneously applied or with a small rise time) is negligible as can be concluded by inspection of both plots (Fig. IV.7 and Fig. IV.23, respectively).

Similarly as for the degradable neo-Hookean-like material, stress relaxation is observed in the uniaxial extension of the degradable nonlinear viscoelastic solid (shown in Fig. IV.24). The stress relaxation is more pronounced than the stress relaxation observed in the hyperelastic-like degradable material (analyzed in Section IV.C, shown in Fig. IV.6).
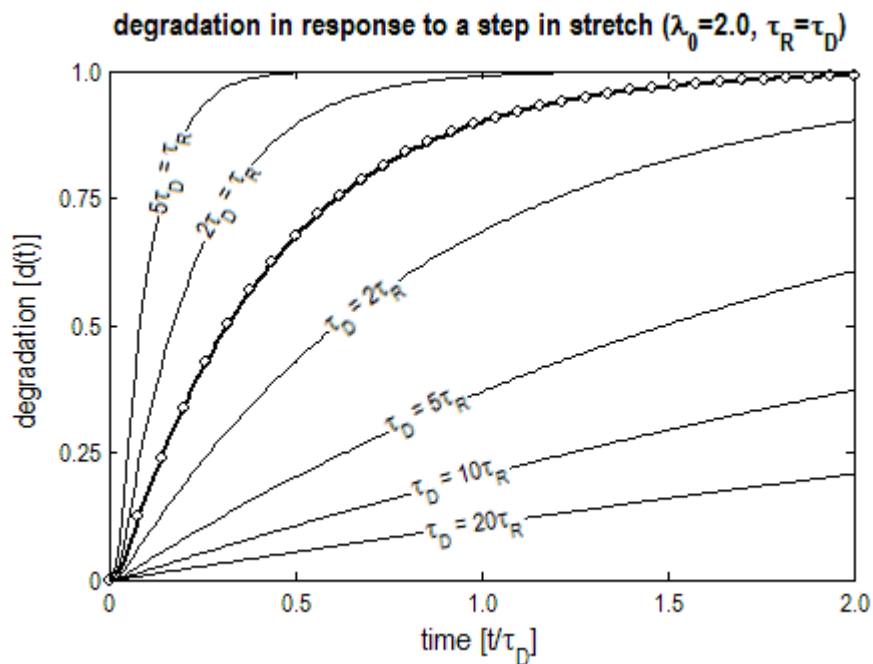
Fig. IV.25. Degradation in response to a step in stretch for several τ_D. The marked curve corresponds to the case shown in Fig. IV.23. The characteristic time of degradation dictates the effect of the deformation in the rate of increase of degradation. As τ_D decreases, degradation occurs faster.

In the case of a degradable material that at fixed levels of degradation responds like a hyperelastic material, stress relaxation occurred solely due to degradation. The stress relaxation occurring in the uniaxial extension of the degradable viscoelastic solid has two contributions: (i) relaxation occurring due to degradation, and (ii) relaxation occurring due to the inherent viscoelastic response of the degradable material at fixed levels of degradation. The latter is characteristic of the constitutive model that the degradable material follows at fixed levels of degradation (single integral P&R nonlinear viscoelastic solid that if time independent is neo-Hookean) whereas the former happens through the decrease of the material properties of such model due to degradation.

Viscoelastic stress relaxation (characterized by equation (2.114)) occurs from the initial modulus C_0 to the infinitesimal modulus C_∞ with a characteristic time τ_R. Stress

relaxation due to degradation is the directly related with characteristic time τ_D and the amount of deformation and yields a decrease in mechanical properties of the degradable material towards zero (characterized by equations (4.51), (4.52), and (4.53)). Finally, Fig. IV.24 was obtained with $\tau_D = \tau_R$.

Constant τ_D is a constant related with the degradation process and governs the increase of degradation. It can be seen as the half time of degradation per unit deformation, measured in s, the radius in $(I_\mathbf{C}, II_\mathbf{C})$ plane (cf. (4.12)) . Notice that as stretch increases, the increase of degradation is more accentuated, i.e. $d \rightarrow 1$ occurs faster (cf. Fig. IV.23). Naturally, changes in the characteristic time of degradation imparts changes in the degradation process, i.e. if τ_D increases, degradation takes more time to occur; whereas if τ_D decreases, degradation occurs quickly when subjected to the same deformation (cf. Fig. IV.25, for the response to a step in stretch of $\lambda_0 = 2.0$, where the marked line corresponds to Fig. IV.23).

Degradation decreases the material properties and hence changes the response of the material under the same deformation. Note that if $\tau_D \rightarrow \infty$, the model yields a non-degradable material with constant material properties (and similar as the virgin material). As τ_D decreases, degradation is more pronounced and the mechanical properties decrease faster and vice versa. With degradation, the material that in the virgin state is neo-Hookean shows stress relaxation (cf. Fig. IV.26) due to degradation, and the material that in the virgin state is nonlinear viscoelastic shows an augmented stress relaxation due to degradation and viscoelasticity (cf. Fig. IV.27).
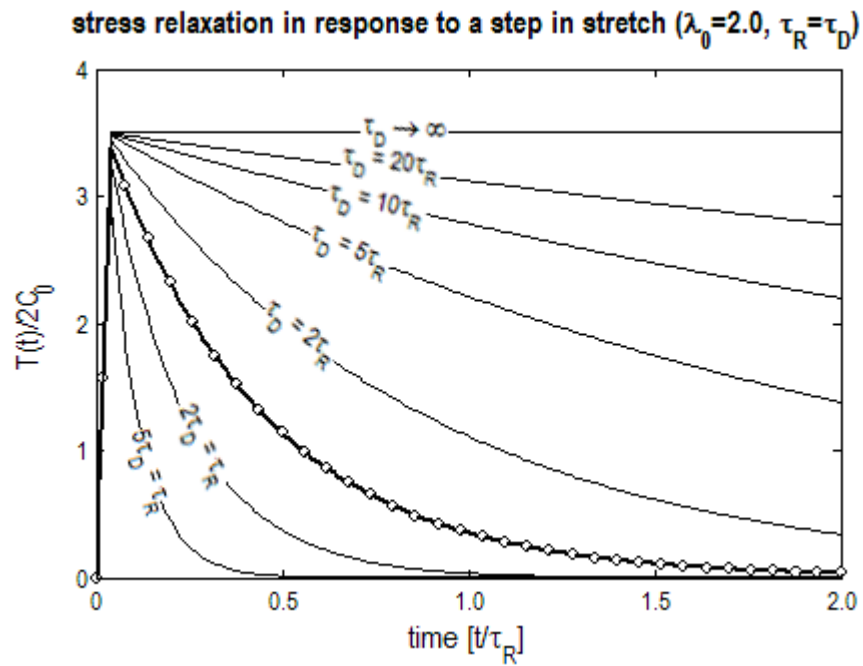
Fig. IV.26. Stress relaxation in response to a step in stretch for several τ_D in a degradable neo-Hookean-like material. When τ_D approaches infinity, the neo-Hookean model is recovered and the stress to maintain a constant stretch is constant. If the material degrades, the stress relaxes due to the decrease of the shear modulus.
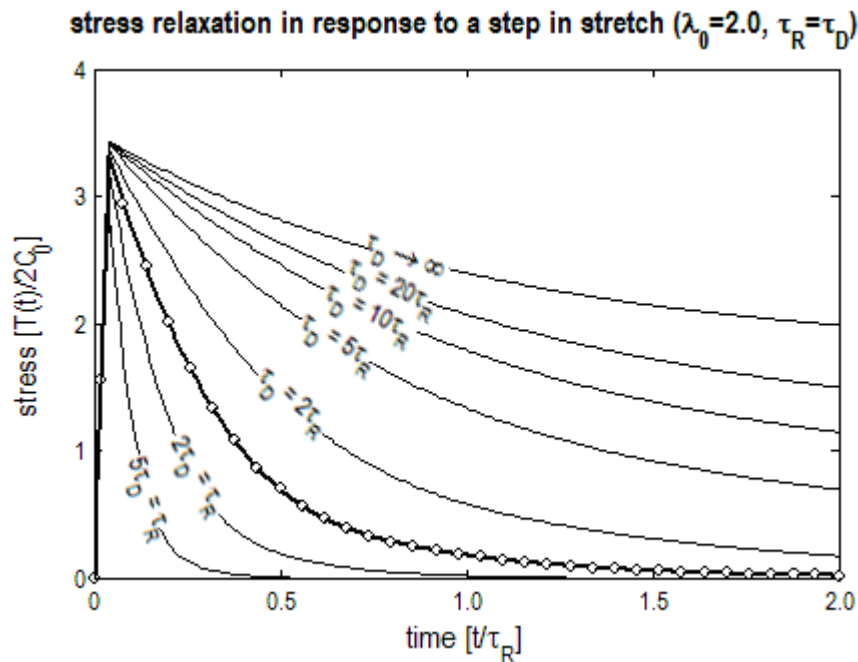
Fig. IV.27. Stress relaxation in response to a step in stretch for several τ_D in a degradable P&R-like material. The marked curve corresponds to the case shown in Fig. IV.24. The material shows stress relaxation both by itself and due to degradation. The P&R viscoelastic model is recovered if degradation does not occur, i.e. $\tau_D \rightarrow \infty$. τ_R is the relaxation time of the P&R viscoelastic solid.

4. Viscoelasticity and degradation

It is possible to separate the contribution of both relaxation mechanisms: (i) stress relaxation occurring due to the viscoelasticity of the material and characterized by τ_R, and (ii) stress relaxation occurring due to scission and consequent mechanical properties reduction characterized by τ_D.

The case shown in Fig. IV.24 corresponds to the case when $\tau_D = \tau_R$. The response of the material is significantly different for different ratios of the two characteristic times. Firstly, if $\tau_D \rightarrow \infty$, the material responds like a non-degradable material (cf. Fig. IV.27 and Fig. IV.28). Degradation does not increase from the initial

stress relaxation in response to step in stretch (λ_0 = 2.0)
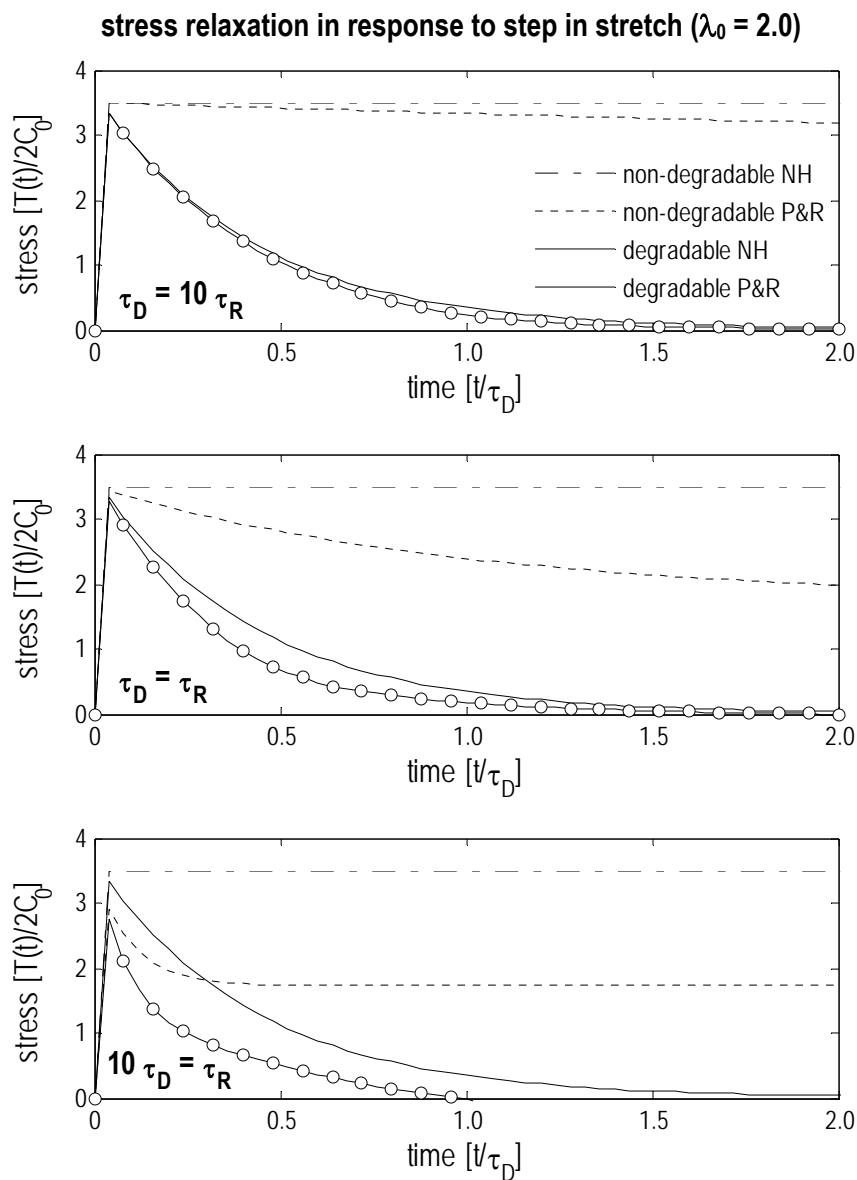
Fig. IV.28. Stress relaxation in response to step in stretch ($\lambda_0 = 2.0$). The response of the neo-Hookean model follows the deformation is independent of time because is elastic and does not degrade. The stress relaxation seen in the P&R model is due to viscoelasticity. Degradation is held constant while τ_R varies. When viscoelasticity is mild, stress relaxation is dominated by the effects due to degradation (top figure); on the other hand, the effect of viscoelasticity in the response of a degradable material is clearly noticeable as it augments the amount of relaxation (bottom figure).

value (chosen to be $d = 0$ at $t = 0$), i.e. the response of the material remains the virgin response. On the other hand, if $\tau_R \to \infty$, the material loses its viscoelasticity yielding the corresponding time independent model. This can be seen in the top plot of Fig. IV.28: τ_R is significantly greater than the characteristic time of degradation and loading, hence relaxation due to degradation is dominant as the response of the elastic and viscoelastic counterparts, either degradable or non-degradable, are very similar. The other two plots (middle and bottom of Fig. IV.28) shows the opposite cases: as τ_R decreases, viscoelastic relaxation is gains dominance over the degradation relaxation. The relaxation curve is a blend between both curves (as $\tau_R \to \infty$ and as $\tau_D \to \infty$, the solid and dashed lines respectively). Finally, note that the response of a degradable viscoelastic material cannot be obtained with an addition of the two curves of the degradable neo-Hookean and non-degradable P&R (hence the terminology blend above). In other words, degradation can be perceived as a variation from the non-degraded model with material properties decreasing functions of d over $0 < d < 1$ (cf. Fig. IV.26 and Fig. IV.27).

On the other hand, viscoelasticity (of the current viscoelastic material, cf. (2.114)) is a decrease from the initial modulus to the residual moduli as $t \to \infty$, and also yields a variety of responses when τ_R, the intensity of viscoelasticity, is varied. The viscoelastic effect on the stress relaxation of the corresponding non-degradable body is shown in dashed lines in Fig. IV.29: when $\tau_R \to \infty$, the neo-Hookean model is recovered and all other curves are viscoelastic P&R with different characteristic times.

The viscoelastic effect on a degradable body is shown in solid lines in Fig. IV.29: viscoelasticity can also be perceived as a relaxation from a response that is relaxing per se due to degradation. The viscoelastic variety obtained with changing τ_R is still a relaxation from an initial modulus to a residual modulus, but now both degradation dependent, and shows a departure from the curve of the time independent but degradable model (degradable neo-Hookean-like).
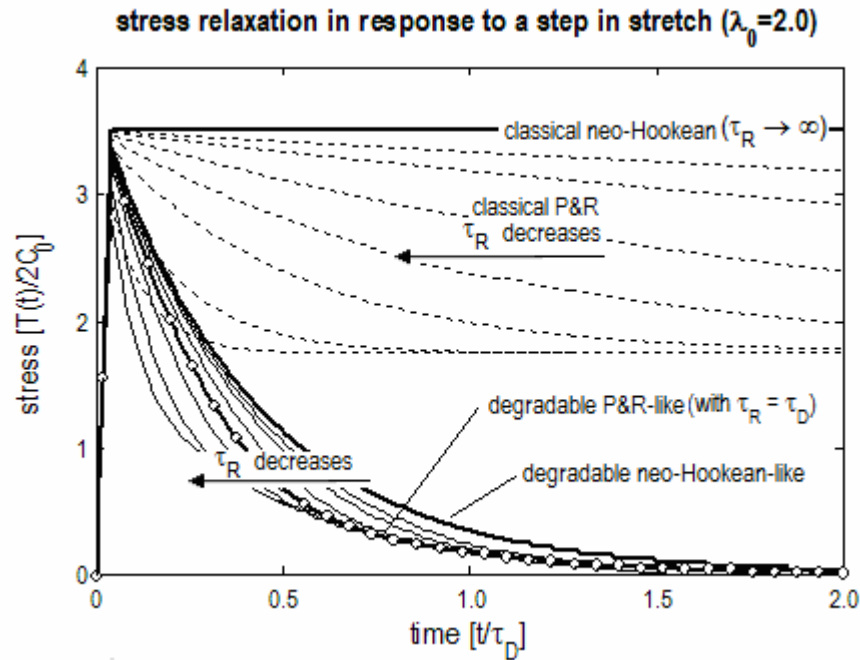
Fig. IV.29. Stress relaxation in response to a step in stretch for several τ_R in degradable materials. The marked curve corresponds to the case shown in Fig. IV.24. The response of neo-Hookean material and the degradable neo-Hookean-like material are thickened. The effect of viscoelasticity in either material is characterized by a departure from both curves obtained with $\tau_R \to \infty$.

5. *Multi-step histories and constant stretching cycles in a degradable QLV-like body*

The body that at fixed degradation responds like a QLV material introduced above (cf. reduced relaxation function (4.44) and instantaneous elastic response (4.34)) was subjected to a multi-step stretch history (shown in the top figure of Fig. IV.30): increasing steps of 1% strain during $4\ \tau_1$ each (where τ_1 is the viscoelastic characteristic time). Degradation increases due to the deformation at different rates, faster for greater strains. τ_D is the characteristic time of increase of degradation. A tenfold enhancement of the degradation mechanism through τ_D (though as occurring faster) provokes approximately a tenfold increase in the amounts of degradation (middle figure of Fig.

IV.30). Nevertheless, note that here small amounts of degradation are being considered and it must be remarked that as $d \to 1$ this scaling property will be lost.

The stress required to maintain the stretch history of the degradable material relaxes (bottom figure of Fig. IV.30). The first step provokes negligible amounts of degradation; both bodies (with $\tau_1 = \tau_D$ and $\tau_1 = 10\ \tau_D$) and the non-degradable model with the corresponding virgin properties are very similar during the first step. On the second and third steps, the differences become noticeable: (i) the body under enhanced degradation shows greater relaxation during the second step and at $t/\tau_1 = 8$ is in a stage of degradation such that the instantaneous response to the increase in strain clearly falls short of the virgin counterpart, and (ii) the body with $\tau_1 = \tau_D$ shows only a negligible difference from the virgin properties, i.e. the body does not degrade appreciably enough to cause a significant departure from the non-degraded state.

Another stretch history of interest is the constant stretching rate cycle. The following cycle in stretch was applied to a degradable QLV-like material with $\tau_1 = \tau_D$

$$\lambda(s) = \begin{cases} 1 + \frac{\lambda_{1/2}-1}{t_{1/2}}s, & 0 < s \le t_{1/2} \\ \lambda_{1/2} - \frac{\lambda_{1/2}-1}{t_{1/2}}s, & t_{1/2} < s \le 2\ t_{1/2} \end{cases}, \tag{4.58}$$

where $\lambda_{1/2}$ is the maximum stretch a the middle of the cycle occurring at $t_{1/2}$ (shown in the top figure of Fig. IV.31 for $t_{1/2} = 4\ \tau_1$ with $\lambda_{1/2}$ of 1.10, 1.25, and 1.50, which lead to stretch rates of $d\lambda/dt = 0.025\ \tau_1^{-1}$, $0.0625\ \tau_1^{-1}$, and $0.125\ \tau_1^{-1}$, respectively).

The increase of degradation, at a rate proportional to the amount of deformation (considering the same τ_D), follows a progressive increase during the first branch of the stretch history as the stretch increases, and is then followed by an increase with decreasing rate as the stretch decreases back to zero (shown in the middle figure of Fig. IV.31). At low levels of stretch, either initially or during the end of the cycle, the increase of degradation is small; oppositely, the rate of increase of degradation achieves a maximum at $t_{1/2}$ when the stretch reaches its maximum $\lambda_{1/2}$.

response of degradable QLV-like material to multi-step history
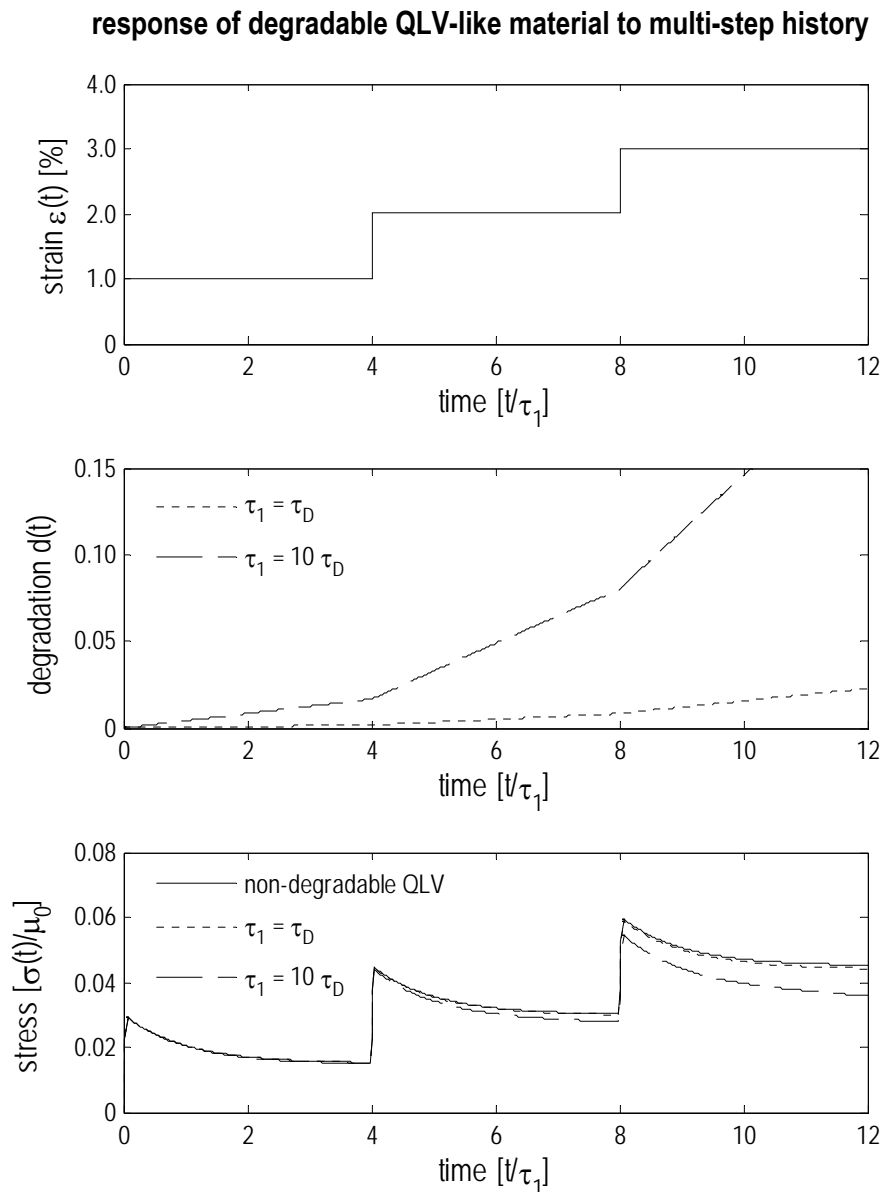
Fig. IV.30. Response of degradable QLV-like material to multi-step stretch history. A degradable QLV-like material was subjected to a three step strain history (shown in the top figure), under two distinct modes of degradation: $\tau_1 = \tau_D$, and enhanced degradation with $\tau_1 = 10\,\tau_D$. Degradation increases during the period under interest are small for both cases (< 5% and < 20%, respectively). Hence the asymptotic behavior of degradation increase in not observed (middle figure), where increases in degradation are approximately linear with slope proportional to applied strain. Nevertheless, enhanced degradation provokes a sufficiently significant departure from the non-degradable response, not only on the relaxation characteristics but also on the instantaneous response.

response of degradable QLV-like material to constant stretching cycle
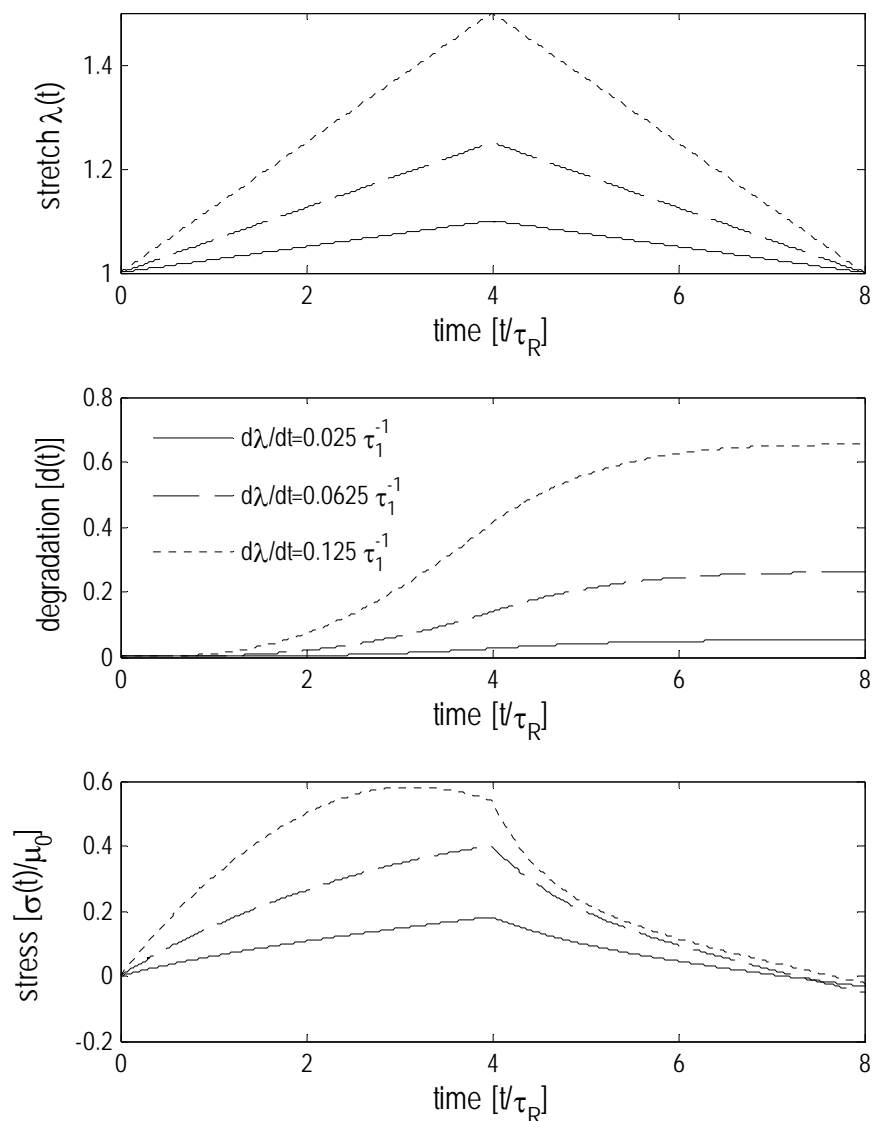
Fig. IV.31. Response of degradable QLV-like material to constant stretching cycles of different magnitudes. Under similar degradation schemes ($\tau_1 = \tau_D$), the effect of stretch on degradation is directly proportional to its magnitude, i.e. the smaller stretches of the beginning and end of the cycles promote smaller increases, whereas the maximum increase of degradation occurs at the middle of the cycle (top and middle figure). Note that the greater stretch promotes sufficient degradation ($\approx$ 80%) to impart a significant departure from the non-degraded QLV response (bottom figure). Immediately prior the maximum, degradation is occurring a rate that decreases stress more than the increase of stretch increases it; thus, a stress decrease with an increase in stretch is observed.

The stress response to the constant stretching cycle is composed of the two relaxation mechanisms: the general viscoelastic behavior and the stress relaxation that is occurring due degradation (cf. bottom figure of Fig. IV.31). As the cycle magnitude increases, the body degrades more and the stress response clearly deviates from the general response of a viscoelastic material. The deviation is cumulative, hence the initial parts of the cycle follows the flattened stress increase characteristic of viscoelastic behavior. At the two lower levels of stretch, degradation is less intense, thus the stress response resembles general viscoelastic behavior. More precisely, small degradations induced by small deformations promote small departures from the response of the virgin (QLV) material. Similarly as previously done with the nonlinear viscoelastic that degrades, a comparison between viscoelastic and degradation induced effects on the response of the degradable material to constant stretching cycles can be analyzed. Note that the limit $\tau_1 \to \infty$ yields negligible viscoelastic effects and characterizes bodies that do not show viscoelastic relaxation whereas $\tau_D \to \infty$ characterizes negligible degradation increase representing non-degradable constitutive equations.

Two constant stretching cycles up to $\lambda_{1/2} = 1.50$ were conducted with two different deformation rates, $d\lambda/dt = \tau_1^{-1}$ and $0.25 \ \tau_1^{-1}$. If the rate of stretching is fast (top figure of Fig. IV.32), neither the viscoelastic effects nor the effects due to degradation have time to become appreciable in the response. The departure from either the elastic response or the non-degraded response is small. For slower deformations, degradation occurs during a greater period of time (bottom figure of Fig. IV.32) and hence greater variations from the non-degraded responses occur due to degradation and viscoelasticity. Here, $\tau_1 = \tau_D$ was considered.

Finally, one important feature that must be remarked is that degradation does not induce changes in the natural configuration. The degradable neo-Hookean-like response is similar to the one obtained in Fig. IV.11 and no permanent set is induced by degradation. Interestingly, the stress free configuration of both degradable QLV-like and

stress vs. stretch of degradable QLV-like material for several stretching rates
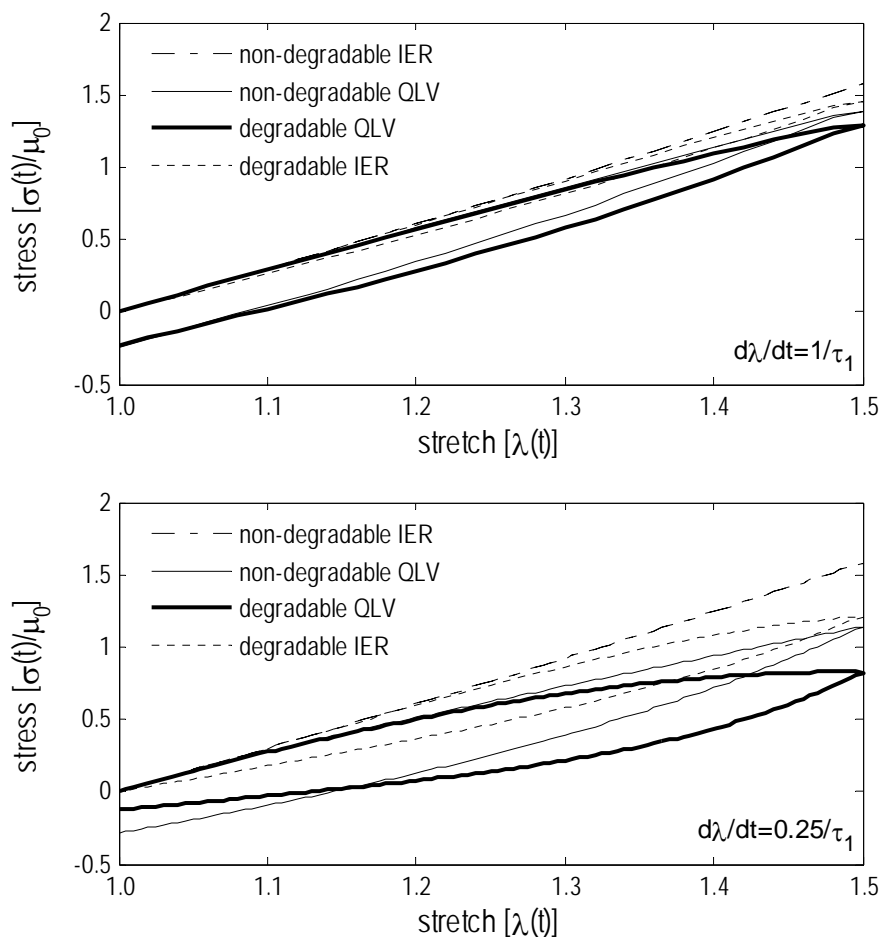
Fig. IV.32. Stress vs. stretch of degradable QLV-like material for several stretching rates. Cycles of maximum stretch $\lambda = 1.5$ were subjected with two distinct stretching/unstretching rates with $\tau_1 = \tau_D$ (fast and slow, top and bottom figure respectively). A quicker loading does not allow neither viscoelastic nor degradation relaxation to occur to an appreciably extent, whereas both effects are clearly noticeable with a slower stretching. Note that degradation does not impart changes in the stress free configuration, whereas viscoelasticity does.

non-degradable QLV is the same (cf. both figures of Fig. IV.32), where the strain remaining at the end of each cycle is solely due to viscoelasticity.

E. Encompassment within existing theories

As already referred to, Rajagopal and Wineman developed a model of a nonlinear elastic material which describes a network that is able to undergo scission and healing, forming new networks in new natural states [267,269]. The framework was further developed by allowing for the effect of temperature [283,284], and the solution of several boundary value problems have been carried out by Wineman and coworkers to account for different situations and describing several particular scission materials [285]. The conversion of networks in Rajagopal and Wineman scission model is dependent on a state variable that quantifies the extent of deformation. It was recognized that inhomogeneity of the material after some scission would result from an inhomogeneous scission mechanism [286]. Stress relaxation due to softening and permanent set associated with the new natural state at which new networks are formed was also recognized in the response of such materials [287-289]. The model presented here is a related case, but where no new networks are formed and the degree of scission is quantified by the degradation parameter. The evolution of the degradation parameter is governend by the equation governing degradation describing the kinetics of degradation, which in turn are dependent on the deformation.

The theory of materials that allow multiple natural states was further developed by Rajagopal and co-workers (cf. [268,273]). A much more general theory was constructed, wherein the stress is determined by a functional that depends on the history of the deformation gradient computed from a one parameter family of preferred natural configurations. It is necessary to know a priori how the one-parameter family of configurations depend on the parameter, an information that provides closure to such theories. Usually, an evolution equation, a differential equation in which the parameter is the independent variable, is assumed.

A connection between the present model and the theory of multiple natural configurations can be established. Note that, in the sense of Noll (cf. equation (2.76)), a constitutive response is defined by a representation of the stress with respect to a reference configuration that should be regarded locally. The representation of the stress

also features the material properties that characterize the response of the material with respect to such reference configuration.

It was observed that the present model of degradation does not promote changes in the stress free state (cf. bottom figure of Fig. IV.32, where each degradable response and its non-degradable counterpart share the same stress free state). Instead, degradation changes the material properties of the material. As mentioned before, the response of degradable materials can be regarded as a one-parameter family of responses. Each member of such familiy represents the response of the material at some fixed level of degradation and all share the same reference configuration. This setting is similar to but the converse of the theory of multiple configurations: here, all responses share the same natural configuration and are characterized by one-parameter families of material properties, whereas Rajagopal et al. consider responses characterized by a representation with constant materials properties with respect to a one-parameter family of natural states. In both, evolution equations are prescribed to govern the evolution of the microstructure of the material.

Lastly, one relevant example of multiple natural states occurs in a classical viscoelastic material where changes in natural configuration result from the characteristic dissipative behavior and are determined by a rate of dissipation function. Using a maximum rate of dissipation criterion, Rajagopal and Srinivasa obtained a whole plethora of rate type fluid models for different choices of stored energy and rate of dissipation functions [272]; a similar procedure can be applied to the Pipkin & Rogers single integral nonlinear viscoelastic solid model. Thus, the degradable P&R-like material presented in this work is not only material a whose reference configuration changes due to classical viscoelastic effects (and its evolution is associated to a particular form of rate of dissipation function and can be determined with the maximum rate of dissipation criterion), but also whose response with respect to the current natural configuration is a one-parameter family of different responses characterizing the respone of the material at the current level of degradation and share the same current natural configuration.

On the other hand, a direct connection between the presented degradation model and damage mechanics can be immediately established [290]. In a more general sense, a degradable material can be regarded as a material with one internal variable, the degradation parameter (cf. [291] for the general theory). The amount of published work on such theories is large and often reoccurring: only relevant references that are directly related or influenced to some extent the current degradation model will be referred in this section.

Stouffer and Wineman [292] expansion of linear thermo-viscoelasticity by allowing the stress relaxation function (the material property) to be depedent on environment parameters, such as humidity, temperature, concentration, etc, yielding families of relaxation responses was of extreme importance. Aging viscoelastic materials were simply achieved within the same framework by introducing an explicit time dependence on the stress relatation function [293] and the Stouffer and coworkers successfully studied degradation through stress-corrosion with such model [294]. After these initial ideas, Stouffer and Strauss established the theory of material divagation. Material divagation was defined as the process where the mechanical properties of a material change in time or wander from the values that characterize the material in a reference configuration [295]. A direct connection with damage mechanics was clearly stated in their theory, but it was extensively remarked that divagation could also be perceived as enhancement of mechanical properties.

The idea that originated the current degradation model is present in Rajagopal and Wineman note on viscoelastic materials that can age [296,297]. Relaxation in an aging viscoelastic material was observed to be constituted by two distinct components: one that is characteristic of viscoelasticity and other distinctly different and arising from aging. The connections are evident: Rajagopal and Wineman defined an aging measure (simply increasing linearly with time), material properties that are dependent on such measure, and an activation criterion that states conditions beyond which aging is initiated. In the current degradation case, the measure quantifying decrease in mechanical properties (degradation) arises naturally as a measure of bond scission (or

molecular weight reduction) and is governed by a coupled differential equation describing the process.

On a lighter note, softening can be achieved in a variety of ways. Ogden and Roxburgth considered a body whose stored energy function depends on a damage parameter due to softening and were able to describe Mullins effect, mechanical properties reduction, and hysteresis [298]. Horgan and Sacomandi, based on phenomenological reasoning, developed the theory of chain inextenbility and obtained strain-softening or strain-hardening by allowing the material properties to be dependent on some measure of strain [299,300]. Beatty and coworkers described Mullins effect and strain softening in elastomers with a strain intensity parameter and a softening function on which the material properties depend on [301-303]. Conversely to the aforementioned cases, instead of the parameter on which the response of the material depends being completely determined by kineamtics, degradation is governed by a coupled partial differential equation describing the entropy producing mechanism responsible for softening of the material.

As a final note, the usage of the governing equation of degradation establishes an interesting connection between softening and viscoelasticity. The integration of the governing equation for degradation (cf. (4.4)) yields

$$d(\mathbf{x},t) = d(\mathbf{x},0) + \int_0^t \mathfrak{D}(d,\mathbf{F}) \, ds \qquad (4.59)$$

where the integrand can be seen as an intrinsic material clock function. This concept was originally proposed by Bernstein and Shokooh [304] as a stress clock function for viscoelastic fluids and was further extended by Wineman and coworkers with a strain clock for viscoelastic solids [305,306]. In the particular case of deformation-induced degradation (cf. (4.11)), due to the sole dependence on kinematical quantitites yields a strain clock. The clock introduces a degradation scale, describing locally the evolution of degradation and providing a form to measure and relate different amounts of degradation.

CHAPTER V

INFLATION, EXTENSION, TORSION, AND SHEARING OF AN

INCOMPRESSIBLE DEGRADABLE CYLINDRICAL ANNULUS

The combined inflation, extension, torsion and shearing of an isotropic incompressible degradable annular right cylinder is studied. A semi-analytical solution scheme that can be used for a large choice of stored energy functions is employed. The arrangement of this chapter is as follows. Section A introduces the type of degradable constitutive models considered in this study, Section B introduces the specific motions that are allowed and boundary value problems that they yield, followed by the solution methods employed to solve this class of problems in Section C. Section D introduces examples of how such methodology can be used for classic hyperelastic materials and Section E discusses several results obtained for degradable hyperelastic-like bodies undergoing such motions.

A. Constitutive relations

This study is restricted to degradable hyperelastic-like bodies whose stored energy function is such that

$$W = W(I_{\mathrm{C}}, II_{\mathrm{C}}, d). \tag{4.10}$$

i.e., bodies that at fixed levels of degradation behave as incompressible, isotropic hyperelastic solids. Then, the Cauchy stress is given by

$$\mathbf{T} = -p\mathbf{1} + 2\frac{\partial W}{\partial I_{\mathrm{C}}}\mathbf{B} - 2\frac{\partial W}{\partial II_{\mathrm{C}}}\mathbf{B}^{-1}. \tag{2.98}$$

The stored energy function must satisfy (2.99) and (2.100) (cf. [207]). The Cauchy stress can be expressed as

$$\mathbf{T} = -p\mathbf{1} + \mathbf{T}^{e}, \tag{5.1}$$

where $\mathbf{T}^e$ is the extra stress and is given by

$$\mathbf{T}^e = 2\frac{\partial W}{\partial I_{\mathbf{C}}}\mathbf{B} - 2\frac{\partial W}{\partial II_{\mathbf{C}}}\mathbf{B}^{-1}. \tag{5.2}$$

This decomposition is convenient for this analysis. The stored energy function under consideration will be of the form

$$W(I_{\mathbf{C}},d) = \frac{\mu(d)}{2}(I_{\mathbf{C}} - 3), \tag{4.15}$$

i.e. a one parameter family of constitutive relationships following a neo-Hookean solid where the material property, the shear modulus $\mu = \mu(d)$, is a material function of degradation. The form of material property reduction with degradation is chosen to be a linear decrease in d towards zero as $d \to 1$, and takes the following form

$$\mu(d) = \mu_0(1-d), \tag{4.17}$$

where μ_0 is the shear modulus of the virgin material. Then, the extra stress in the degradable material is given by

$$\mathbf{T}^e = \mu_0(1-d)\mathbf{B}. \tag{5.3}$$

If the processes under consideration are restricted to be quasi-static and if body forces are neglected, the balance of linear momentum reduces to

$$\text{div }\mathbf{T} = \mathbf{0}. \tag{5.4}$$

Degradation increases only due to deformation, i.e. the equation governing the degradation process is of the form (cf. (4.4))

$$\frac{\partial d}{\partial t} = \mathfrak{D}(d, I_{\mathbf{C}}, II_{\mathbf{C}},). \tag{4.11}$$

Furthermore, a similar form as previously considered is chosen, i.e.

$$\frac{\partial d}{\partial t} = \mathcal{K}(s - s_a)(1-d), \tag{4.14}$$

where s is given by (4.12). An analogous activation criterion is chosen (cf. (4.13)) where the threshold of activation was chosen to be zero, i.e. $s_a = 0$. The deformation dependent hydrolysis rate $\mathcal{K}$ is linear in s. Hence, equation (4.14) reduces to

$$\frac{\partial d}{\partial t} = \frac{1}{\tau_D}(1-d)\left[\left(I_\mathbf{C}-3\right)^2 + \left(II_\mathbf{C}-3\right)^2\right]^{1/2}. \tag{5.5}$$

Note that equation (5.5) is the counterpart of equation (4.25) for this class of problems. The degradation field is assumed to be position and time dependent (cf. (4.3)), i.e.

$$d = \hat{d}(\mathbf{X},t) = \tilde{d}(\mathbf{x},t). \tag{5.6}$$

The Lagrangian form is also shown here and it will be seen that it is the most convenient form of expressing the degradation field. Nevertheless, changes to the Eulerian form can be achieved once the motion of the body is defined. Furthermore, the circumflex and the tilde distinguishing in between both forms will be suppressed as the description is usually implicit in the context. Finally, it must be noted that an inhomogeneous degradation field (defined as particle dependent) will impart a similar dependence (implicitly through d) on the stored energy function (4.10) hence making the body inhomogeneous.

B. Kinematics

The analysis is confined to a body $\mathcal{B}$ that is the annular region between two co-axial right circular cylinders characterized by inner and outer radii R_i and R_o:

$$\mathcal{B} = \left\{(R,\Theta,Z) \mid R_i \leq R \leq R_o, 0 \leq \Theta \leq 2\pi\right\}, \tag{5.7}$$

where (R,Θ,Z) represent the coordinates of a typical material point before deformation (chosen to be the reference configuration) in cylindrical polar coordinates.

A reasonably large class of inhomogeneous motions that have been studied in great detail for isotropic elastic solids is considered. A semi-inverse solution of the following form, for the motion in cylindrical polar coordinates, is sought

$$
\begin{aligned}
r &= r(R,t) \\
\theta &= \phi(R,t)+\beta(t)\Theta+\Omega(t)Z, \\
z &= w(R,t)+\kappa(t)\Theta+\lambda(t)Z
\end{aligned}
\tag{5.8}
$$

where (r,θ,z) represent the coordinates of a typical material point at time t. $\beta(t)$, $\Omega(t)$, $\kappa(t)$, and $\lambda(t)$ are functions of time. The function $r(R,t)$ describes the inflation or deflation of the annular region, $\phi(R,t)$ denotes the circumferential shear while $w(R,t)$ denotes the transverse or anti-plane shear. $\Omega(t)$ is the angle of twist per unit length of the undeformed cylinder, $\kappa(t)$ is the azimuthal shear, $\lambda(t)$ the extension along the direction of the axis of the cylinder, and $\beta(t)$ is related to the angular displacements undergone by radial filaments.

As with all semi-inverse methods, the traction that is necessary to engender such motion can be calculated once the functions that appear in (5.8) are determined. The functions are determined such that they satisfy the linear momentum balance (5.4) and the boundary conditions (yet to be specified) for all time t. It is of course possible that these equations cannot be satisfied as well as there can exist a multitude of possible solutions satisfying the boundary value problem that do not follow structure of the semi-inverse solution that is sought.

The deformation gradient $\mathbf{F}$ is obtained through (2.8) and in a cylindrical coordinate system has the matrix representation given by

$$
(\mathbf{F}) = \begin{pmatrix}
r_{,R} & 0 & 0 \\
r\phi_{,R} & \beta\frac{r}{R} & r\Omega \\
w_{,R} & \frac{\kappa}{R} & \lambda
\end{pmatrix},
\tag{5.9}
$$

where $(\cdot)_{,R}$ denotes $\partial(\cdot)/\partial R$, a notation used throughout this Chapter. Note that for algebraic simplicity, the independent variables (R and t or solely t, e.g. $\phi \equiv \phi(R,t)$ or $\lambda \equiv \lambda(t)$) were omitted. The left Cauchy green stretch tensor $\mathbf{B}$ and its inverse $\mathbf{B}^{-1}$ have the following matrix representation

$$(\mathbf{B}) = \begin{pmatrix} r_{,R}^2 & r\phi_{,R}r_{,R} & w_{,R}r_{,R} \\ r\phi_{,R}r_{,R} & (r\phi_{,R})^2 + (\beta\frac{r}{R})^2 + (r\Omega)^2 & r\Omega\lambda + rw_{,R}\phi_{,R} + \beta\kappa\frac{r}{R^2} \\ w_{,R}r_{,R} & r\Omega\lambda + rw_{,R}\phi_{,R} + \beta\kappa\frac{r}{R^2} & \lambda^2 + w_{,R}^2 + (\frac{\kappa}{R})^2 \end{pmatrix}, \qquad (5.10)$$

$$\left(\mathbf{B}^{-1}\right) = \frac{1}{\varphi^2} \begin{pmatrix} \frac{1}{r_{,R}^2}[\varphi^2 + (\xi_1 R)^2 + \xi_2^2] & -\frac{1}{rr_{,R}}[\lambda\xi_1 R^2 + \kappa\xi_2] & -\frac{1}{r_{,R}}[\Omega\xi_1 R^2 + \beta\xi_2] \\ -\frac{1}{rr_{,R}}[\lambda\xi_1 R^2 + \kappa\xi_2] & \frac{1}{r^2}[\kappa^2 + (R\lambda)^2] & -\frac{1}{r}[\beta\kappa + \Omega\lambda R^2] \\ -\frac{1}{r_{,R}}[\Omega\xi_1 R^2 + \beta\xi_2] & -\frac{1}{r}[\beta\kappa + \Omega\lambda R^2] & [\beta^2 + (R\Omega)^2] \end{pmatrix}, (5.11)$$

where

$$\varphi \equiv \varphi(t) = \beta\lambda - \Omega\kappa, \qquad (5.12)$$

$$\xi_1 = w_{,R}\Omega - \phi_{,R}\lambda, \qquad (5.13)$$

$$\xi_2 = w_{,R}\beta - \phi_{,R}\kappa, \qquad (5.14)$$

For this deformation,

$$I_{\mathbf{B}} = r_{,R}^2 + (r\phi_{,R})^2 + \left(\beta\frac{r}{R}\right)^2 + (r\Omega)^2 + \lambda^2 + w_{,R}^2 + \left(\frac{\kappa}{R}\right)^2, \qquad (5.15)$$

$$II_{\mathbf{B}} = \frac{1}{\varphi^2}\left[\frac{\varphi^2 + (\xi_1 R)^2 + \xi_2^2}{r_{,R}^2} + \frac{\kappa^2 + (R\lambda)^2}{r^2} + \beta^2 + (R\Omega)^2\right], \qquad (5.16)$$

$$III_{\mathbf{B}} = \left(\varphi\frac{r}{R}r_{,R}\right)^2. \qquad (5.17)$$

Because $III_{\mathbf{B}} > 0$ and if inversion of the cylinder is not allowed, i.e. $\varphi > 0$, it immediately follows that $r_{,R} > 0$. Hence, $\beta\lambda > \Omega\kappa$ is a restriction enforced in this study.

The bodies of interest are incompressible, hence (5.9) yields a condition that the motion must satisfy for all t, i.e.

$$J = \det \mathbf{F} = 1. \qquad (5.18)$$

Constraint (5.18) can be integrated directly to yield the radial relationship between the reference and the current configurations, i.e.

$$r(R,t)^2 - r(R_i,t)^2 = \frac{R^2 - R_i^2}{\varphi}, \tag{5.19}$$

and the form of $r(R,t)$ is now defined up to a function of time $C_r(t)$ resulting from integration and can be expressed as

$$r(R,t) = \frac{\sqrt{\varphi R^2 + C_r(t)\varphi^2}}{\varphi}, \tag{5.20}$$

where $C_r(t)$ can be chosen to be related with the time dependent current inner radius $r_i(t) = r(R_i,t)$, i.e.

$$C_r(t) = r_i(t)^2 - \frac{R_i^2}{\varphi}. \tag{5.21}$$

C. Linear momentum balance and solution methods

For the special form of the assumed motion, the deformation gradient is only a function of one spatial coordinate, R, and time t. Hence, the linear momentum balance (5.4) simplifies to

$$\frac{\partial T_{rr}}{\partial r} + \frac{1}{r}(T_{rr} - T_{\theta\theta}) = 0, \tag{5.22}$$

$$\frac{\partial T_{r\theta}}{\partial r} + \frac{2}{r}T_{r\theta} = 0, \tag{5.23}$$

$$\frac{\partial T_{rz}}{\partial r} + \frac{1}{r}T_{rz} = 0. \tag{5.24}$$

Equations (5.23) and (5.24) can be integrated to yield

$$T_{r\theta}(r,t) = \frac{C_\theta(t)}{r^2}, \tag{5.25}$$

$$T_{rz}(r,t) = \frac{C_z(t)}{r^2}, \tag{5.26}$$

where $C_\theta(t)$ and $C_z(t)$ are functions of time only. If the traction at the inner surface $\mathbf{t}|_{r=r_i}$ is assumed to be known, the stresses at the inner surface are obtained with (2.62):

$$\mathbf{t}|_{r=r_i} = \mathbf{T}|_{r=r_i} (-\mathbf{e_r}) = \begin{pmatrix} T_{rr}^i(t) \\ T_{r\theta}^i(t) \\ T_{rz}^i(t) \end{pmatrix}, \tag{5.27}$$

where $T_{rr}^i(t) = T_{rr}(r_i,t)$, $T_{r\theta}^i(t) = T_{r\theta}(r_i,t)$, and $T_{rz}^i(t) = T_{rr}(r_i,t)$ are the known radial, circumferential, and axial components of the traction at the inner surface $\mathbf{t}|_{r=r_i}$ for all time t. $C_\theta(t)$ and $C_z(t)$ obtained during the integration process are

$$C_\theta(t) = \frac{r_i(t)^2}{T_{r\theta}(r_i,t)}, \tag{5.28}$$

$$C_z(t) = \frac{r_i(t)}{T_{rz}(r_i,t)}, \tag{5.29}$$

and finally, (5.25) and (5.26) become

$$T_{r\theta}(r,t) = \frac{r_i(t)^2}{r^2} T_{r\theta}^i(t), \tag{5.30}$$

$$T_{rz}(r,t) = \frac{r_i(t)}{r} T_{rz}^i(t). \tag{5.31}$$

A solution method for a similar class of problems was employed by Saravanan and Rajagopal for inhomogeneous compressible bodies undergoing static deformations [307,308]. The stress field is obtained through constitutive equation (2.98) with (5.10) and (5.11). Substituting for $T_{r\theta}(r,t)$ and $T_{rz}(r,t)$ in (5.30) and (5.31), one gets two equations in terms of $\phi_{,R}$ and $w_{,R}$. Note that for incompressible bodies, because of constraint (5.18), the form of $r(R,t)$ is known up to a function of time $C_r(t)$; hence $r_{,R}$ is obtained from (5.20) and $C_r(t)$ is still an unknown. The equation that closes the system is the radial component of the linear momentum balance (5.22).

Change of differentiation from the current configuration to the reference configuration is achieved with the aid of relationship (2.67) or the chain rule and yields

$$\frac{T_{rr,R}}{r_{,R}} + \frac{1}{r}(T_{rr}^e - T_{\theta\theta}^e) = 0, \tag{5.32}$$

where decomposition (5.1) was used to eliminate p on the term inside parenthesis. Substituting the stress (2.98) with (5.10) and (5.11), one obtains a partial differential equation of the form

$$p_{,R} - f(\phi_{,R}, w_{,R}, C_r(t), R, t) = 0, \tag{5.33}$$

from which

$$p = p(R,t) = \int_{R_i}^{R} f(S,t)dS + C_p(t) \tag{5.34}$$

can be obtained. Once p is known, functions of time only $C_p(t)$ and $C_r(t)$ can be found such that boundary conditions (either displacement, traction, or mixed) are met.

D. Preliminary results with non-degradable hyperelastic bodies

This section exemplifies the solution method applied to a neo-Hookean body. It will be seen that this choice of stored energy function confines enough simplicity to the scheme such that it is feasibly to handle it algebraically. Nevertheless, a numerical integration scheme will be is used such that the method can be naturally extended to more complicated cases. Furthermore, in this preliminary result, the body is assumed to be non-degradable and homogeneous. Lastly, inflation and extension with a numerical example will be analyzed.

1. Solution scheme using non-degradable neo-Hookean bodies

When **T** is given by

$$\mathbf{T} = -p\mathbf{1} + \mu\mathbf{B}, \tag{5.35}$$

the components of the stress field are simply

$$T_{rr} = -p + \mu r_{,R}^2 , \tag{5.36}$$

$$T_{\theta\theta} = -p + \mu[(r\phi_{,R})^2 + (\beta \tfrac{r}{R})^2 + (r\Omega)^2], \tag{5.37}$$

$$T_{zz} = -p + \mu[\lambda^2 + w_{,R}^2 + (\tfrac{\kappa}{R})^2], \tag{5.38}$$

$$T_{r\theta} = \mu r\phi_{,R} r_{,R} , \tag{5.39}$$

$$T_{rz} = \mu w_{,R} r_{,R} , \tag{5.40}$$

$$T_{\theta z} = \mu[r\Omega\lambda + r w_{,R}\phi_{,R} + \beta\kappa \tfrac{r}{R^2}]. \tag{5.41}$$

Substituting in (5.30) and (5.31), and considering (5.20), the two equations obtained are

$$a_1(R,t)\phi_{,R} = b_1(R,t), \tag{5.42}$$

$$a_2(R,t)w_{,R} = b_2(R,t), \tag{5.43}$$

where

$$a_1(R,t) = \mu\frac{\sqrt{\varphi R^2 + \varphi^2 C_r(t)}}{\varphi}, \qquad b_1(R,t) = \frac{\varphi^2}{\varphi R^2 + \varphi^2 C_r(t)} r_i^2 T_{r\theta}(r_i,t), \quad (5.44)$$

$$a_2(R,t) = \mu\frac{R}{\sqrt{\varphi R^2 + \varphi^2 C_r(t)}}, \qquad b_2(R,t) = \frac{\varphi}{\sqrt{\varphi R^2 + \varphi^2 C_r(t)}} r_i T_{rz}(r_i,t), \quad (5.45)$$

and hence

$$\phi(R,t) = r_i^2 T_{r\theta}^i(t)\frac{\varphi}{\mu C_r(t)}\ln\frac{R}{\sqrt{R^2 + \varphi C_r(t)}} + f(t), \tag{5.46}$$

$$w(R,t) = r_i T_{rz}^i(t)\frac{\varphi}{\mu}\ln R + g(t), \tag{5.47}$$

where $f(t)$ and $g(t)$ are unknown functions of time only that will be determined by boundary conditions. Note that in (5.46) and (5.47), the stresses at the inner surface, $T_{r\theta}(r_i,t)$ and $T_{rz}(r_i,t)$, are known functions of time only (cf. (5.27)) but the position of the inner surface is related to $C_r(t)$ (still an unknown) through (5.21).

The radial component of the balance of linear momentum (5.32) with (5.36) and (5.37) yields

$$a_3(R,t)p_{,R} = b_3(R,t),$$
(5.48)

where $\phi_{,R}$ in (5.37) was replaced by $\phi_{,R} = b_1/a_1$ (cf. equation (5.42)) yielding

$$a_3(R,t) = \frac{\sqrt{\varphi R^2 + \varphi^2 C_r(t)}}{R},$$
(5.49)

$$b_3(R,t) = \frac{2\mu}{\sqrt{\varphi R^2 + \varphi^2 C_r(t)}} + \frac{\mu R}{\varphi R^2 + \varphi^2 C_r(t)}\left(\frac{2R\varphi}{\sqrt{\varphi R^2 + \varphi^2 C_r(t)}} - 1\right)$$
$$-\frac{\mu}{R}\left(\frac{\varphi^4 r_i^4 T_{r\theta}(r_i,t)^2}{\mu^2 R^2(\varphi R^2 + \varphi^2 C_r(t))} + \frac{\varphi R^2 + \varphi^2 C_r(t)}{\varphi^2}\left(\frac{\beta^2}{R^2} + \Omega^2\right)\right)$$
(5.50)

Equation (5.48) does not have a closed-form solution but yields a solution of the form (5.34), which needs to be evaluated numerically.

2. *Inflation and extension of a non-degradable homogeneous neo-Hookean body*

If one considers the case when

$$r(R,t) = r(R,t), \qquad \lambda(t) = \lambda, \qquad \beta = 1$$
(5.51)

and $\phi(R,t) = w(R,t) = \kappa = \Omega = 0$, the following matrix representation for the deformation gradient **F** is obtained

$$(\mathbf{F}) = \begin{pmatrix} \frac{R}{\sqrt{\lambda R^2 + \lambda^2 C_r}} & 0 & 0 \\ 0 & \frac{\sqrt{\lambda R^2 + \lambda^2 C_r}}{\lambda R} & 0 \\ 0 & 0 & \lambda \end{pmatrix},$$
(5.52)

and with the incompressibility constraint, one obtains,

$$r(R,t) = \frac{\sqrt{\lambda R^2 + C_r(t)\lambda^2}}{\lambda},$$
(5.53)

i.e. to solve the problem, $C_r(t)$ must be found.

The stress field is for a neo-Hookean body obtained from (5.36)-(5.41) and is

$$T_{rr} = -p + \mu \frac{R^2}{\lambda R^2 + \lambda^2 C_r(t)}, \tag{5.54}$$

$$T_{\theta\theta} = -p + \mu \left(\frac{1}{\lambda} + \frac{C_r(t)}{R^2} \right), \tag{5.55}$$

$$T_{zz} = -p + \mu \lambda^2, \tag{5.56}$$

$$T_{r\theta} = T_{rz} = T_{\theta z} = 0. \tag{5.57}$$

Only the radial component of the balance of linear momentum does not vanish and one finds convenient to consider equation (5.32) upon integration as

$$T_{rr}(R,t) = T_{rr}(R_i,t) + \int_{R_i}^{R} \frac{r_{,R}(s,t)}{r(s,t)} [T_{\theta\theta}^e(s,t) - T_{rr}^e(s,t)] ds, \tag{5.58}$$

where the extra stresses are

$$T_{rr}^e(R,t) = \mu \frac{R^2}{\lambda R^2 + \lambda^2 C_r(t)}, \tag{5.59}$$

$$T_{\theta\theta}^e(R,t) = \mu \left(\frac{1}{\lambda} + \frac{C_r(t)}{R^2} \right). \tag{5.60}$$

Note that with knowledge of the radial stress at the inner surface $T_{rr}(R_i,t)$, the radial stress is completely determined with (5.58) if $C_r(t)$ is found. The Lagrange multiplier p can be obtained and then all other components of the stress field. For such task, boundary conditions at the outer surface must be provided.

The boundary conditions considered here to obtain a solution for this problem are of the type

$$\mathbf{t}\big|_{R=R_i} = P_i(t)\mathbf{e_r} \Rightarrow -T_{rr}(R_i,t) = P_i(t), \tag{5.61}$$

$$\mathbf{t}\big|_{R=R_o} = -P_o(t)\mathbf{e_r} \Rightarrow T_{rr}(R_o,t) = -P_o(t), \tag{5.62}$$

i.e. known normal pressures are applied to the inner and outer part of the cylinder. Hence, considering the case when $R = R_o$, equation (5.58) becomes

$$\Delta P(t) = P_i(t) - P_o(t) = \int_{R_i}^{R_o} \frac{r_{,R}(s,t)}{r(s,t)} [T_{\theta\theta}^e(s,t) - T_{rr}^e(s,t)] ds, \qquad (5.63)$$

which holds for all time t and $C_r(t)$ can be obtained if the pressure differential $\Delta P(t)$ is known. Note that λ is a constant known a priori (cf. (5.51)) but a time dependent axial stretch $\lambda(t)$ can also be considered. Obviously, the radial deformation achieved with a pressure differential will be dependent on the amount of axial stretch applied to the cylinder. Equation (5.63) is solved numerically for each time t. Finally, once $C_r(t)$ is found, the Lagrange multiplier can be obtained through

$$p(R,t) = P_i(t) + T_{rr}^e(R,t) - \int_{R_i}^{R} \frac{r_{,R}(s,t)}{r(s,t)} [T_{\theta\theta}^e(s,t) - T_{rr}^e(s,t)] ds, \qquad (5.64)$$

and then, the entire stress field follows from (5.54)-(5.57).

3. Numerical example with a neo-Hookean body

Consider a constant shear modulus of $\mu = 1\,\text{GPa}$, inner and outer radii of $R_i = 2.4\,\text{mm}$ and $R_o = 2.5\,\text{mm}$ respectively. Once $\Delta P(t)$ and $\lambda(t)$ are prescribed, $C_r(t)$ can be obtained from (5.63). Once $C_r(t)$ is known, the current radial position and the Lagrange multiplier can be obtained from (5.53) and (5.64) respectively. Finally, the stress field is obtained with equations (5.54)-(5.57).

Equations (5.63) and (5.64) were solved numerically. At each time step t^n, the integral in (5.63) was evaluated with a composite trapezoid rule with a discretization of the domain of integration from R_i to R_o with $m = 20$ subintervals of length δs, i.e.

$$\delta s = \frac{R_o - R_i}{m+1}, \qquad (5.65)$$

transmural Cauchy stress distribution
(λ=1.0, changing ΔP)

transmural Cauchy stress distribution
(ΔP=600 kPa, changing λ)

Fig. V.1. Transmural distribution of Cauchy stress in a neo-Hookean cylindrical annulus at multiple pressures and constant axial stretch. A case of pure inflation (λ=1.0) is considered. Note the thinning of the wall and the increased gradients that occur for pressures that cause greater inflations.

Fig. V.2. Transmural distribution of Cauchy stress in a neo-Hookean cylindrical annulus at multiple axial stretches and constant transmural pressure. As stretch increases, the deformed radius decreases. Further, the axial stretch dominates the axial stress, while has minor effects on the other stresses.

such that $C_r^n \equiv C_r(t^n)$ is determined with the knowledge of $\Delta P^n \equiv \Delta P(t^n)$ and $\lambda^n \equiv \lambda(t^n)$.

Equation (5.63) is a nonlinear equation and its solution was found iteratively using an iterative Newton-Raphson method. The domain of the body was discretized in k subintervals ΔR (with $k = 50$), yielding

$$\Delta R = \frac{R_o - R_i}{k+1}, \tag{5.66}$$

and the current radius corresponding to each location R_j at time step t^n was obtained with equation (5.53), i.e.

$$r_j^n \equiv r(R_j, t^n) = \frac{\sqrt{\lambda^n R_j^2 + C_r^n (\lambda^n)^2}}{\lambda^n}, \qquad j = 1, \ldots, k+1. \tag{5.67}$$

The Lagrange multiplier was obtained at each R_j at t^n with (5.64) where the integral was evaluated similarly, but now the limit of integration is from R_i to R_j, i.e.

$$\delta s = \frac{R_j - R_i}{m+1}, \qquad R_i < R_j \leq R_o, \tag{5.68}$$

yielding

$$p_j^n \equiv p(R_j, t^n), \qquad j = 1, \ldots, k+1, \tag{5.69}$$

where the extra radial stress $T_{rr}^e(R, t)$ was evaluated in a similar fashion with (5.59), i.e.

$$(T_{rr}^e)_j^n \equiv T_{rr}^e(R_j, t^n) = \mu \frac{R_j^2}{\lambda^n R_j^2 + (\lambda^n)^2 C_r^n}, \qquad j = 1, \ldots, k+1. \tag{5.70}$$

Finally, the stress field at t^n can be fully evaluated at all R_j with (5.54)-(5.57) substituting C_r^n and p_j^n, i.e.

$$(T_{rr})^n_j = -p^n_j + \mu \frac{R_j^2}{\lambda^n R_j^2 + (\lambda^n)^2 C_r^n}, \qquad j = 1,...,k+1 \tag{5.71}$$

$$(T_{\theta\theta})^n_j = -p^n_j + \mu \left(\frac{1}{\lambda^n} + \frac{C_r^n}{R_j^2} \right), \qquad j = 1,...,k+1 \tag{5.72}$$

$$(T_{zz})^n_j = -p^n_j + \mu(\lambda^n)^2, \qquad j = 1,...,k+1 \tag{5.73}$$

Under pure inflation ($\lambda = 1$) the annulus deforms increasingly with increases of transmural pressure (shown in the horizontal axis of Fig. V.1 for applied transmural pressures ΔP of 100 kPa, 200 kPa, 400 kPa, 600 kPa, and 1000 kPa). Furthermore, due to incompressibility, the thickness of the deformed annulus decreases slightly upon inflation (cf. Fig. V.1, where the dashed vertical lines show the initial inner and outer surfaces at R_i and R_o respectively).

Note that an instantaneously applied pressure differential will promote an oscillation that is not being depicted due to the quasi-static assumption in the linear momentum balance (5.4). An instantaneous change in deformation is not a quasi-static motion. Temporal changes in deformation (which influence the stress field due to the right hand side of the linear momentum balance, cf. (2.63) and quasi-static counterpart (5.4)) are not being accounted, hence the solutions obtained correspond to static solutions.

The radial stress component T_{rr} (cf. top figure of Fig. V.1) is dominated by the boundary conditions. The outer pressure P_o is set to zero while the inner pressure P_i is allowed to change in order to obtain the transmural pressure ΔP. Hence, the radial component of the stress matches $-P_i = \Delta P$ at the inner surface and $P_o = 0$ at the outer surface. The circumferential and axial stress components $T_{\theta\theta}$ and T_{zz} (shown in the middle and bottom figures of Fig. V.1 respectively) increase with transmural pressure. Because the thickness of the annulus is small, the deformation is approximately homogeneous, which yields a negligible gradient between the inner and the outer surface, i.e. its variation is small and indeed its average value is dictated by the amount

of transmural pressure applied and the corresponding achieved inflation. Nevertheless, a small increase in the intensity of this transmural gradient of the stress components is observed with the increasing inflation pressure.

When radial inflation and axial extension are considered together (shown in Fig. V.2 for a transmural pressure of $\Delta P = 600$ kPa and several axial stretches λ of 1.00, 1.05, 1.10, 1.15, and 1.20), the deformation exhibits two competing effects: (i) axial extension promotes a inwards contraction in the radial direction due to incompressibility, and (ii) radial inflation promotes an outwards deformation due to the transmural pressure. Pure inflation yields one of the solutions shown in Fig. V.1. As axial stretch dominates the deformation, the annulus deforms inwards increasingly with greater axial stretches (once again, the vertical dashed lines show the undeformed position of the inner and outer surface).

Similarly as in the previous case, the radial stress component (cf. top figure of Fig. V.2) is dictated by the transmural pressure ΔP, i.e. $T(r_i) = -600$ kPa and $T(r_0) = 0$. The circumferential stress is now dominated by the axial deformation with the corresponding compressive state in the circumferential direction (cf. first term inside the parenthesis in equation (5.55)) which counteracts the effect of the inflation and decreases the values of the circumferential stress significantly when compared with the previous case of pure inflation. Beforehand, inflation would promote an extension in the circumferential direction and an increase in circumferential stress whereas the addition of positive axial stretching promotes a state of compression that significantly decreases $T_{\theta\theta}$. The opposite effect occurs in the axial stress T_{zz} (cf. bottom figure of Fig. V.2). Pure inflation promotes a state of tension in this direction which is amplified by the introduction of a positive axial stretch through the 2nd term of (5.56).

4. Numerical example with the instantaneous elastic response of non-degraded PLLA

As previously stated, the current method to obtain solutions for the inflation and extension of a cylindrical annulus can be employed to any hyperelastic material. The instantaneous elastic response of non-degraded PLLA (cf. Chapter III.C), described by

transmural Cauchy stress distribution
(λ=1.0, changing ΔP)

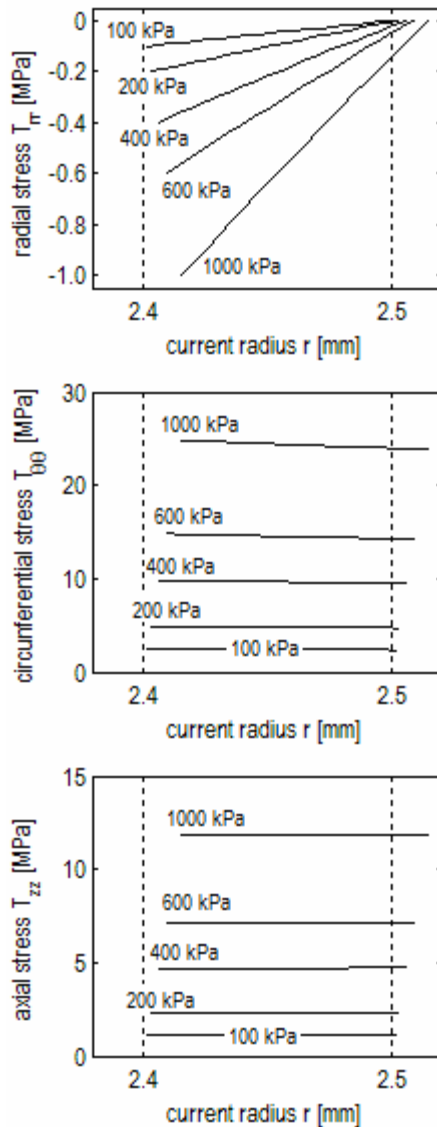**transmural Cauchy stress distribution**
(ΔP=300 kPa, changing λ)
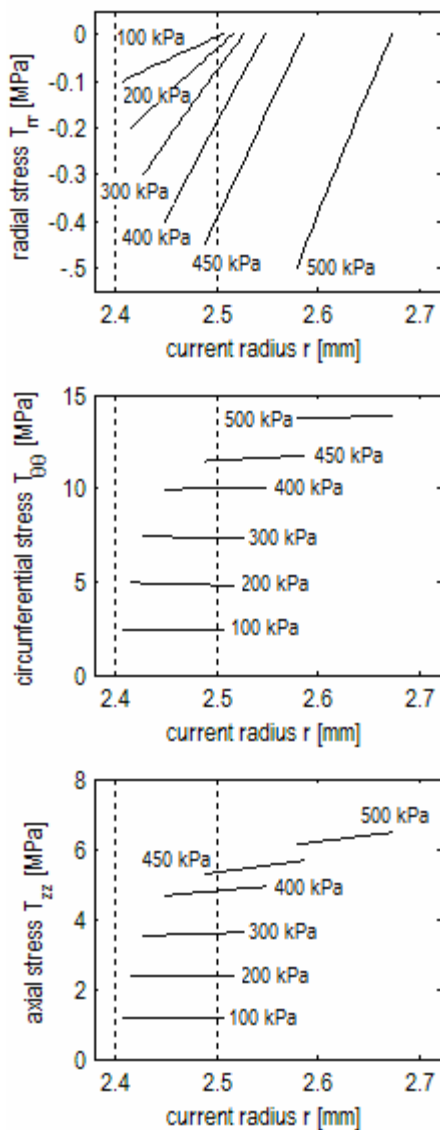
Fig. V.3. Transmural distribution of Cauchy stress in a non-degraded PLLA cylindrical annulus at multiple pressures and constant axial stretch. Significant differences (cf. Fig. V.2) exist due to the nonlinearity of the material. Beyond 400 kPa, large radii are achieved with small increases of pressure due to strain-softening (cf. Fig. III.17).
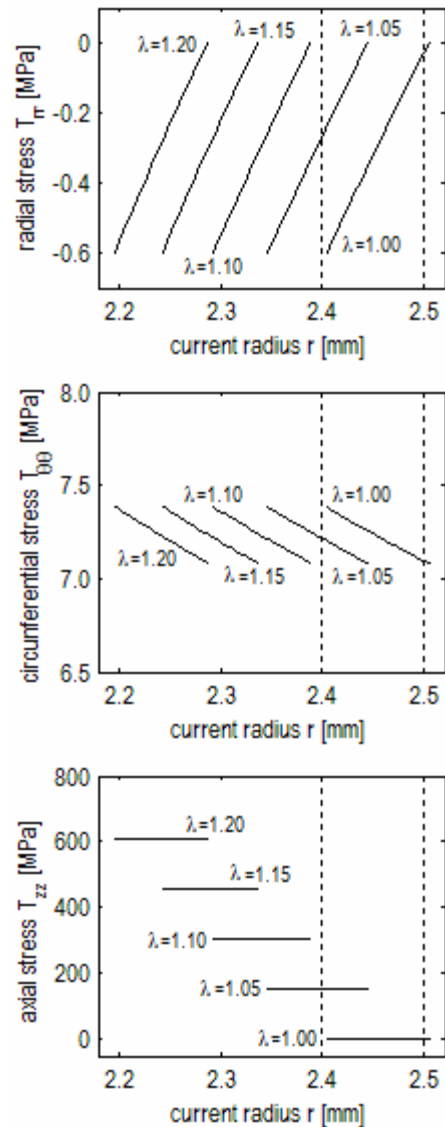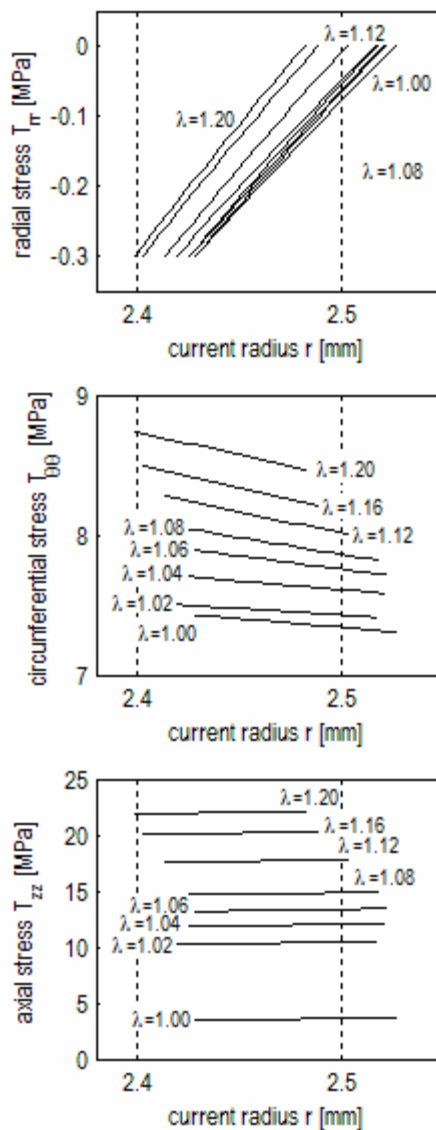
Fig. V.4. Transmural distribution of Cauchy stress in a non-degraded PLLA cylindrical annulus at multiple axial stretches and constant transmural pressure. Only the cases of pure inflation and λ=1.02 are within small strain behavior (with a greater modulus). Note the competing effect of stretching and inflation exists as λ increases.

$$W^{\log} = \mu_1 e^{-(I_{\mathbf{C}}-3)}(I_{\mathbf{C}}-3) + \mu_2 \ln[1+a(I_{\mathbf{C}}-3)], \tag{3.21}$$

with parameters listed in Table III.2, was considered as the material that a similar cylindrical annulus ($R_i = 2.4$ mm and $R_o = 2.5$ mm) is constituted. The same method was employed for the solution of equations (5.63) and (5.64). The only difference between the two procedures is in the constitutive equation (beforehand a neo-Hookean body, now a hyperelastic material characterized by (3.21)). The extra stress field is now given by

$$T_{rr} = -p + 2\mathcal{M}\frac{R^2}{\lambda(R^2 + C_r \lambda)}, \tag{5.74}$$

$$T_{\theta\theta} = -p + 2\mathcal{M}\frac{(R^2 + C_r \lambda)}{\lambda R^2}, \tag{5.75}$$

$$T_{zz} = -p + 2\mathcal{M}\lambda^2, \tag{5.76}$$

where

$$\mathcal{M} = \frac{\partial W^{\log}}{\partial I_{\mathbf{B}}} = \left(\mu_1 e^{-(I_{\mathbf{B}}-3)}(4-I_{\mathbf{B}}) + \frac{\mu_2 a}{1+a(I_{\mathbf{B}}-3)} \right), \tag{5.77}$$

and $I_{\mathbf{B}}$ is obtained from (5.15) for incompressible inflation and extension, i.e.

$$I_{\mathbf{B}} = \frac{R^2}{\lambda(R^2 + C_r \lambda)} + \frac{(R^2 + C_r \lambda)}{\lambda R^2} + \lambda^2. \tag{5.78}$$

The solutions obtained for pure inflation for several transmural pressures clearly show the nonlinearity of the material (cf. Fig. V.3). The response of non-degraded PLLA under uniaxial extension was shown before (cf. Fig. III.17), and as discussed previously, two different regimes can be identified: a somewhat steep increase under small strains followed by strain-softening occurring beyond that point. The achieved deformation in the pure inflation of a non-degraded PLLA cylindrical annulus (cf. horizontal axis of Fig. V.3) clearly shows the two different patterns: under $\Delta P = 400$ kPa , the achieved deformation is proportional to the amount of transmural pressure, whereas beyond this

point, the achieved deformation increases dramatically with small increases of pressure (cf. lines corresponding to $\Delta P = 450$ kPa and 500 kPa in Fig. V.3). Note that the non-deformed inner and outer surfaces are marked with vertical dashed lines.

The transmural stress field follows the same trend as for the pure inflation of the neo-Hookean annulus reported earlier (cf. Fig. V.1). The radial stress is prescribed by boundary conditions, whereas the circumferential increases due to the extension in the circumferential direction that accompanies radial inflation. Similarly, the axial stress increases with the amount of inflation. The transmural stress gradients achieved due to inflation are somewhat more significant than in the previous case as well as after the onset of softening, the necessary pressure to obtain a certain deformation is considerably less than in the previous case.

When axial stretching is applied to the annulus, significant differences exist (the stress distribution is shown in Fig. V.4 for a fixed transmural pressure $\Delta P = 300$ kPa and several stretches ranging from $\lambda = 1.00$ to 1.20). Firstly, it must be remarked that only the case of $\lambda = 1.02$ is within the initial regime of the material characterized by a stiffer modulus. Indeed, the deformation achieved by the transmural pressure is the least at this stretch. Pure inflation with $\Delta P = 300$ kPa produces enough strain in the material such that its modulus has softened. A similar effect is obtained with the combined effects of a stretch of $\lambda = 1.04$ with the same transmural pressure. Both deformations promote greater inflations than the aforementioned case.

This interesting situation arising from the nonlinearity of the material is well portrayed with a pressure vs. radius plot for several axial stretches (cf. Fig. V.5). Note that the two regimes of the material (cf. Fig. III.17) are clearly observed in the case of pure inflation (corresponding to the curve $\lambda = 1$). As transmural pressure increases, the material behaves with a greater modulus up to a certain point, where strain softening begins to occur. On the other hand, as stretching increases the pressure at which this transition occurs decreases due to the amount of deformation promoted by the axial stretch. For $\lambda > 1.02$, the material is beyond this transition point and hence the initial stiffer regime is not depicted, i.e. inflation occurs solely in soft (lower modulus) region.

transmural pressure ΔP vs. inner radius r_i for several axial stretches λ
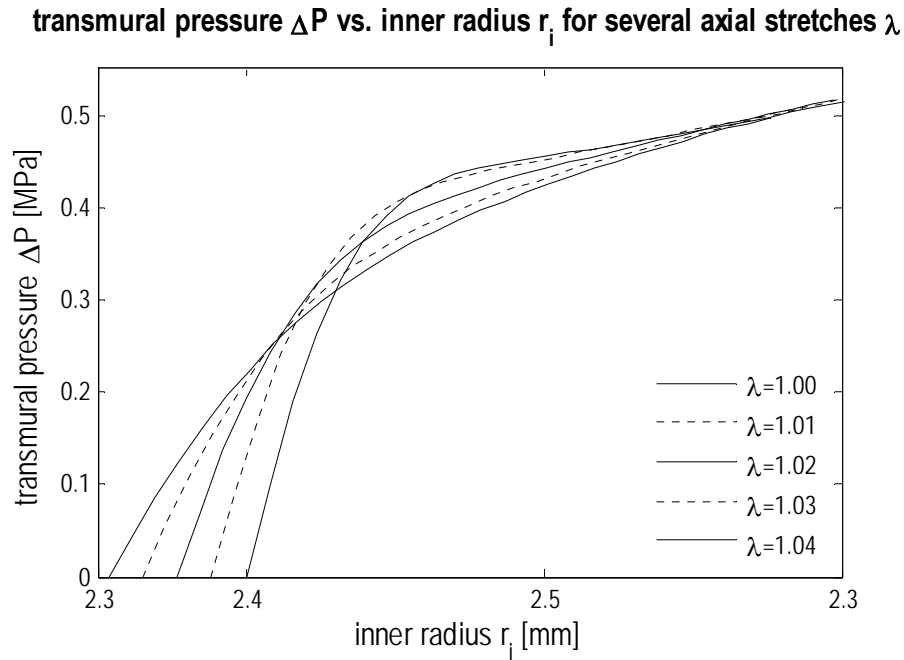
Fig. V.5. Transmural pressure vs. inner radius for several axial stretches in a non-degraded PLLA cylindrical annulus. The uniaxial stress vs. strain response of non-degraded PLLA is shown in Fig. III.17. For axial stretches greater than 1.02, deformations are such that the greater slope that characterizes the small strain regime is not seen in the pressure vs. radius plot, i.e. inflation occurs within the soft region. On the other hand, for pure inflation, the curve is somewhat related to Fig. III.17.

Indeed, the same amount of transmural pressure (e.g. $\Delta P = 400$ kPa) promotes greater inflations for a stretched annulus (e.g. with $\lambda = 1.05$) rather than for pure inflation.

E. Results with degradable hyperelastic-like bodies

The same procedure is now applied to degradable bodies. The equation governing degradation is coupled to the balance of linear momentum and degradation is the extra unknown that needs to be found.

1. Solution scheme for degradable neo-Hookean-like bodies

The solution of the inflation and extension of a degradable cylindrical annulus follows as an extension of the previous non-degradable case. Linear momentum balance (5.4) is coupled with the equation governing the degradation process (5.5) to yield the description of the motion and degradation of the body. The constitutive equation of the degradable hyperelastic-like material is characterized by stored energy function (4.10), and the stress field is obtained through (2.98).

The linear momentum balance (5.4) and the equation governing the degradation process (5.5) must be solved simultaneously, starting from initial conditions. Assuming that the body starts out uniformly non-degraded, i.e.

$$d(\mathbf{X}, 0) = 0, \tag{5.79}$$

the corresponding deformation can be obtained for the uniformly non-degraded material defined by stored energy function W_0 that characterizes the virgin state (not necessarily position independent; inhomogeneous bodies can be considered as a starting point, as well as bodies that are inhomogeneously degraded).

The deformation will promote an increase in degradation following (5.5). Note that deformations are generally inhomogeneous and hence the increase of degradation will follow in the same fashion, i.e. there will be particles of the body that suffer greater degradation because their deformation is also greater (measured as s, cf. (4.12)). Hence, the particles of degradable material will not be characterized by a common stored energy function, but instead, each particle will respond accordingly to its current amount of degradation. More precisely, the stored energy function of the degradable material and hence its response will depend on the position and time implicitly through d (cf. (5.6)).

If the constitutive equation of the degradable hyperelastic-like material is further particularized to a material that at fixed levels of degradation responds like a neo-Hookean material, i.e. characterized by stored energy function (4.15), where the shear modulus decreases linearly from a virgin value μ_0 to zero (cf. (4.17)), the stress field in the incompressible annulus undergoing motion (5.8) will be given by (5.36)-(5.41) with

$$\mu \equiv \mu(d) = \mu_0 (1-d) .$$ (5.80)

Note that degradation d is the extra unknown to be found. The resulting system will have four equations and four unknowns: (i) equations (5.42) and (5.43), now with coefficients a_1, a_2, b_1, and b_2 dependent on R, t, and degradation d, still decouple due to incompressibility and allow $\phi(R,t)$ and $w(R,t)$ to be found up to functions of time only; (ii) the equation governing degradation (5.5) is the extra equation that is added to the system and is of the form

$$\tau_D \frac{\partial d}{\partial t} + \mathcal{K}(I_{\mathbf{C}}, II_{\mathbf{C}})d = \mathcal{K}(I_{\mathbf{C}}, II_{\mathbf{C}}) ,$$ (5.81)

where $\mathcal{K}(I_{\mathbf{C}}, II_{\mathbf{C}}) = [(I_{\mathbf{C}}-3)^2 + (II_{\mathbf{C}}-3)^2]^{1/2}$ is dependent on R and t through $I_{\mathbf{C}}$ and $II_{\mathbf{C}}$ which in turn are obtained similarly as (5.15) and (5.16) for this particular class of motions; and finally, (iii) the radial component of the linear momentum balance

$$\frac{T_{rr,R}}{r_{,R}} + \frac{1}{r}(T_{rr}^e - T_{\theta\theta}^e) = 0 ,$$ (5.32)

which now not only will contain a spatial derivative of the Lagrange multiplier (as previously, cf. (5.48)) but also a spatial derivative of d, responsible for the coupling of deformation and degradation, i.e.

$$a_3(R,t)p_{,R} + c_3(R,t)d_{,R} = b_3(R,t,d) .$$ (5.82)

System of partial differential equations (5.42), (5.43), (5.81), and (5.82) do not have known closed form non-trivial solutions. When supplied with suitable initial and boundary conditions, the evaluation of the solution must be performed numerically.

2. Example with a degradable neo-Hookean-like body

The inflation and axial extension of a degradable neo-Hookean-like cylindrical annulus is characterized by a motion of the form (5.53) and a stress field given by (5.54)-(5.57), but now with degradation dependent shear modulus given by (5.80). When

crept displacement vs. reference radius at several times (λ=1,ΔP=2 MPa)
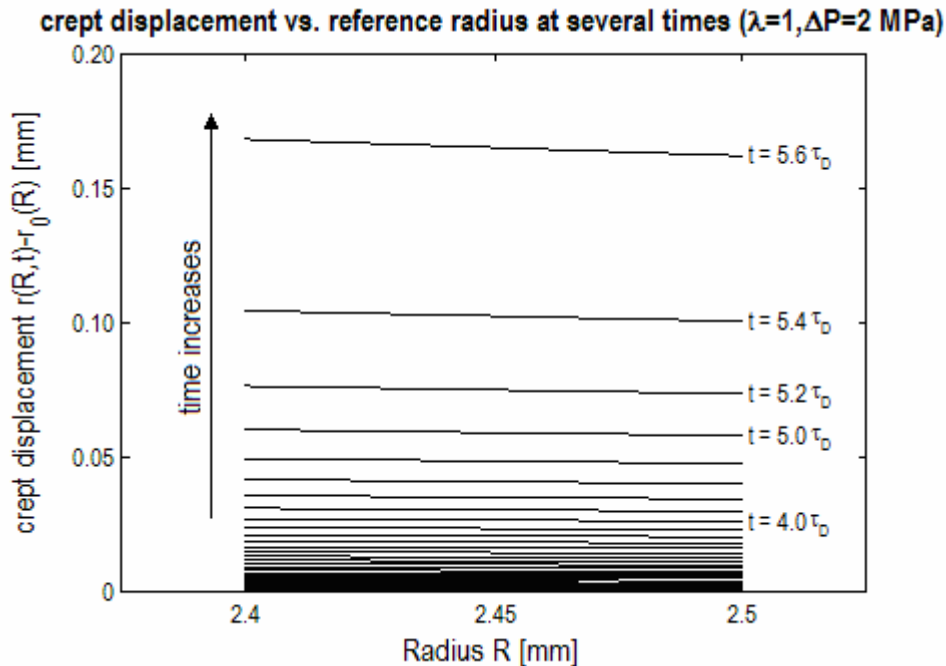
Fig. V.6. Crept displacement vs. reference radius at several times for a degradable neo-Hookean-like annulus undergoing pure inflation. As time increases and the body degrades, the crept displacement (defined as the difference between the current radius and the deformed radius of the non-degradable counterpart) increases with a progressive rate. Degradation will then be even more intense due to the amplification of the deformation, which in turn will lead to greater shear modulus reductions and allow the same load to produce greater deformations.

traction boundary conditions are applied to the inner and outer surfaces (cf. (5.61) and (5.62)), the radial equation (the only non-trivial equation from (5.4)) can be integrated directly yielding (5.63). Given inputs $\Delta P(t)$ and $\lambda(t)$, the solution of the problem consists in finding $C_r(t)$ and $d(R,t)$ such that (5.63) and (5.81) are met. This task will be performed numerically. Once solved, the Lagrange multiplied $p(R,t)$ can be determined with equation (5.64), and then the entire stress field follows from equations (5.54)-(5.57).

Equation (5.81) is solved with a 4th order Runge-Kutta method. Space and time are discretized using the same scheme as in the previous non-degraded example. A set of

$k+1$ ordinary differential equations at each R_j is obtained from the spatial discretization of equation (5.81). Degradation at each location R_j at time step t^n

$$d_j^n \equiv d(R_j, t^n), \qquad j = 1, ..., k+1 \tag{5.83}$$

is obtained from conditions in the previous time step t^{n-1}, d_j^{n-1}, starting from initial conditions d_j^0. $\mathcal{K}$ is evaluated numerically at each location in the previous time step, i.e. $\mathcal{K}_j^{n-1} \equiv \mathcal{K}(R_j, t^{n-1})$.

Once d_j^n is known, the shear modulus at R_j at t^n, $\mu_j^n \equiv \mu_0(1-d_j^n)$ follows directly from (5.80) and equation (5.63) can be solved at the current time step yielding C_r^n. The difference between the current degradable case and the previous non-degradable case is the fact that the shear modulus (that appears inside the integral (5.63) through the extra stresses) depends now on d, which in turn depends on R and t. Once C_r^n is known, r_j^n and p_j^n can be found with (5.67) and (5.64) respectively. Finally, the stress field is determined by

$$(T_{rr})_j^n = -p_j^n + \mu_0(1-d_j^n)\frac{R_j^2}{\lambda^n R_j^2 + (\lambda^n)^2 C_r^n}, \qquad j = 1, ..., k+1 \tag{5.84}$$

$$(T_{\theta\theta})_j^n = -p_j^n + \mu_0(1-d_j^n)\left(\frac{1}{\lambda^n} + \frac{C_r^n}{R_j^2}\right), \qquad j = 1, ..., k+1 \tag{5.85}$$

$$(T_{zz})_j^n = -p_j^n + \mu_0(1-d_j^n)(\lambda^n)^2, \qquad j = 1, ..., k+1 \tag{5.86}$$

3. Pure inflation of a degradable neo-Hookean-like body

As time increases and degradation proceeds, the overall value of the radial deformation of the cylindrical annulus increases at a progressive rate, that is, the annulus creeps outwards when subjected to the same transmural pressure (cf. Fig. V.6)

Due to the geometry of the body considered, slightly inhomogeneous deformations are achieved upon inflation. Hence, the deformation can only induce
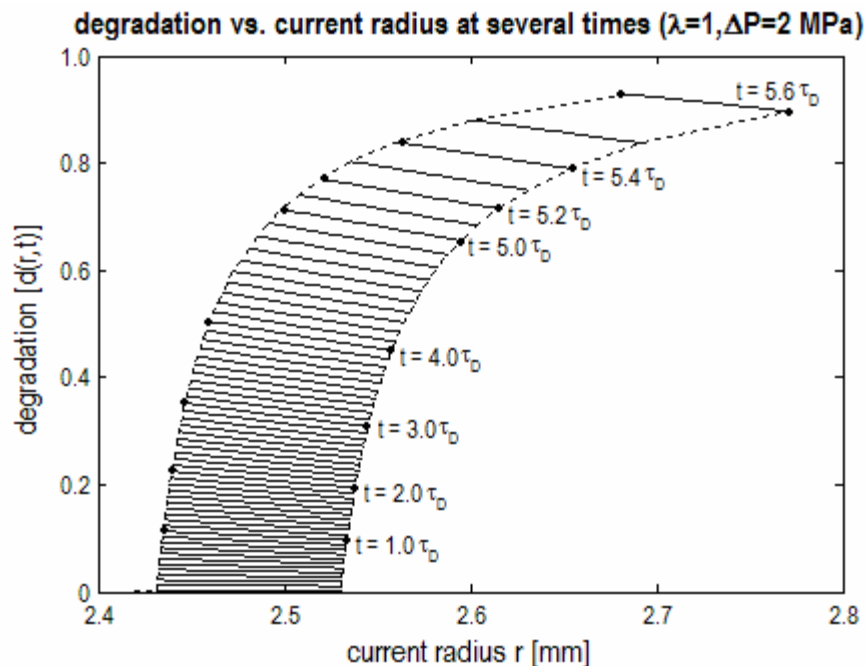
Fig. V.7. Degradation vs. current radius at several times for a degradable neo-Hookean-like annulus undergoing pure inflation. As time increases, the degradation increases. Degradation is slightly more aggressive near the inner wall where deformation is more intense. Initially, degradation is nearly homogeneous but as the thickness decreases upon large inflations, degradation gradients become more intense.

slightly inhomogeneous increases in degradation as well (cf. Fig. V.7). The inner part of the annulus is subjected to greater deformations and therefore it feels a stronger degradation. This degradation has consequences in the material properties, and the shear modulus decreases steadily through the thickness as degradation and time increases (cf. Fig. V.8). At the inner surface, where the degradation is more intense, the reduction in shear modulus is consequently greater than at the rest of the annulus.

Stress relaxation at the inner half of the annulus and an increase in the overall value of stress in the outer part is observed (middle and bottom figures of Fig. V.9). As degradation proceeds the circumferential stress $T_{\theta\theta}$ and the axial stress T_{zz} show considerable differences from the non-degraded solution (shown in Fig. V.1), both departing from an approximately constant distribution along the thickness to solutions

shear modulus vs. reference radius at several times (λ=1,ΔP=2 MPa)

Fig. V.8. Shear modulus vs. reference radius at several times for a degradable neo-Hookean-like material undergoing pure inflation. The shear modulus, initially constant throughout the thickness of the annulus, shows radial dependence after the onset of degradation.

that are characterized by more intense stress gradients. However, the radial stress T_{rr} is prescribed by boundary conditions, hence no change occurs at the inner and outer surface (cf. top figure of Fig. V.9). Nevertheless, radial stress augmentation inside the cylindrical annulus occurs due to degradation.

One particular case of the model for strain induced degradation is the representative case presented in Fig. V.6 through Fig. V.9. The cylindrical annulus is subjected to pure inflation as it is allowed to degrade. Its solution provides phenomenological support for the model. The annulus starts out non-degraded and the imposed loads at the inner and outer surfaces are responsible for a deformation. Simultaneously, degradation dependent on the deformation given by the equation governing the degradation process comes into play. Both are coupled by the constitutive equation of the degradable neo-Hookean-like material.

relative stress components vs. reference radius at several times (λ=1,ΔP=2 MPa)
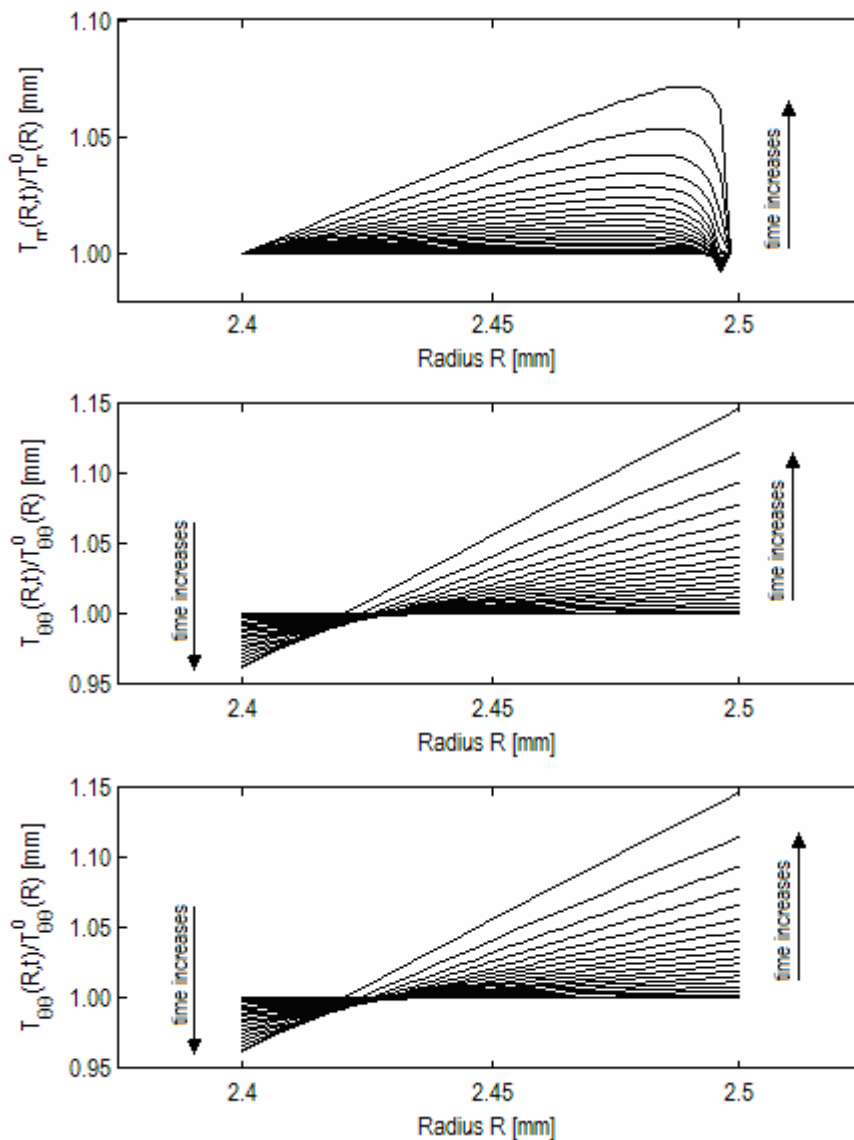
Fig. V.9 Relative transmural stress components vs. reference radius at several times for a degradable neo-Hookean-like material undergoing pure inflation. Relative stresses are defined as the ratio between the current stress and the stress achieved by the same transmural pressure applied to a similar non-degraded annulus. Due to boundary conditions, the axial stress (top figure) is prescribed at the inner and outer wall, but nevertheless stress augmentation occurs inside the annulus. The circumferential and the axial components (middle and bottom figures) show stress relaxation in the inner part of the annulus. On the outer half, stress increases in order to satisfy the linear momentum balance. Dramatic departures from the non-degraded solution (cf. Fig. V.1) occur due to degradation.

The overall features of the solution obtained clearly show an increase in the degradation field and a reduction in the mechanical properties (Fig. V.7 and Fig. V.8 respectively). A decrease to approximately zero is seen over the time march considered. However, it must be remarked that such levels of degradation under the time scale considered is a consequence of the choice of (4.17) and the value of τ_D. In order to obtain a realistic model for describing a particular deformation-induced degradable material, these parameters must be obtained from designed experiments.

The non-zero components of the Cauchy stress (cf. Fig. V.9) have distinct characteristics when compared with the non-degraded case (shown in Fig. V.1). The axial component is prescribed by boundary conditions at the inner and outer surface, hence no changes with degradation occur at both these locations. Stress relaxation of the circumferential and axial components is observed at the inner half of the annulus and that is caused by localized shear modulus reduction. The deformation is greater over the inner half and therefore degradation is increases more intensely over this region. Because the degraded cylinder still has to withstand the same loading conditions, the stresses at the outer half increase in magnitude in order to compensate for the decrease in modulus and relaxation occurring at the inner part. The radial component shows a similar amplification behavior for the same reasons.

Due to degradation, the cylinder creeps outwards under a constant transmural pressure. The crept displacement (defined as the difference between the radial deformation achieved in the degradable body at each time and the constant radial deformation in the non-degradable counterpart) increases progressively with time (cf. Fig. V.6). Under the same inflation pressure, the displacement of the inner surface increases due to degradation. Thus the cylinder inflates over time, inducing a progressively higher deformation and consequent further degradation. Furthermore, when the levels of degradation approach the maximum level and the shear modulus approaches zero, the transmural pressure is responsible for such a great deformation in such a low modulus material that the deformed thickness becomes infinitesimally small and the numerical scheme breaks down.

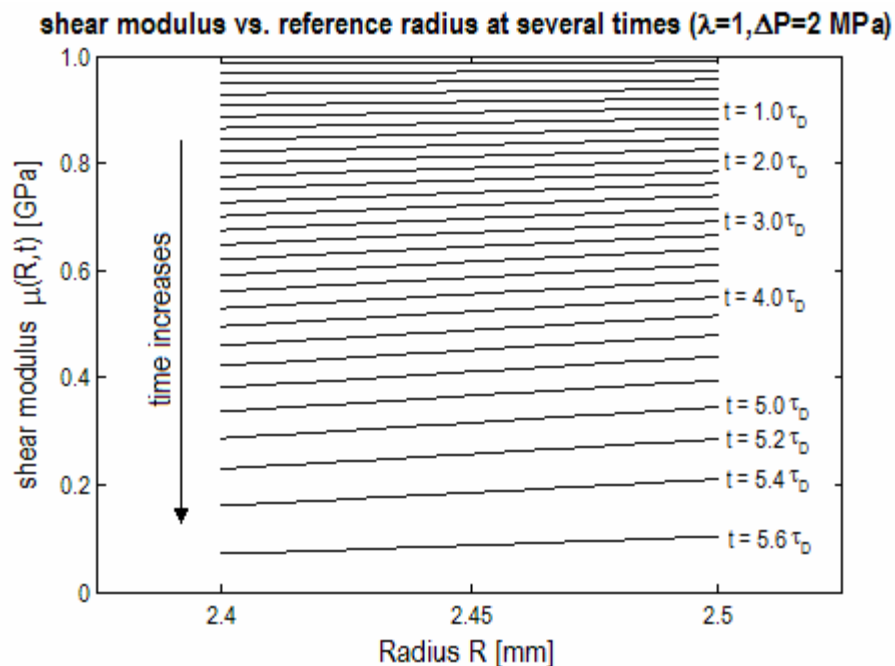Fig. V.10. Influence of wall thickness on the crept displacement, degradation, and shear modulus reduction *vs.* reference radius at several times for a degradable neo-Hookean-like material undergoing pure inflation. For a thin walled annulus (first row) degradation is almost homogeneous throughout the thickness. For the other two geometries, the inhomogeneity of the deformation is more intense and consequently different parts of the annulus degrade to different extents.

Stress relaxation and creep under a constant load are inherent characteristics of a viscoelastic material. However, deformation-induced degradation of the degradable neo-Hookean-like material subjected to pure inflation shows similar characteristics but arising from completely different mechanisms. The annulus responds like a neo-Hookean material if no degradation occurs; and an inhomogeneous neo-Hookean material if any degradation and shear modulus decrease occurred already, due to the inhomogeneity of pure inflation.

Another remarkable consequence of this degradation mechanism is its inherent inhomogeneity. The equation governing degradation (5.5) states that degradation increases proportionally with the amount of degradation left (i.e. $1-d$) and the amount of deformation (measured through s, cf. (4.12)). Both terms are local quantifiers, hence if two particles are subjected to different deformations, consequently they will degrade to different extents. Similarly, if one particle is degraded to a greater extent, it will degrade less when compared with a less-degraded particle undergoing the same deformation. The shear modulus, once constant through the annulus in the virgin state, will become position dependent after the onset of degradation. It is interesting how an initially homogeneous body becomes inhomogeneous after the occurrence of any degradation induced by an inhomogeneous deformation.

Fig. V.10 shows the differences among several inhomogeneous motions. The most significant difference obtained when considering different thickness to outer radius ratios is the decrease of homogeneity of the motion. A motion is said to be homogeneous if straight lines are mapped through the motion into straight lines (or, if in a Cartesian coordinate system, which is not the case here, the components of the deformation gradient $\mathbf{F}$ are constants in space). In the case of a thin-walled annulus (first row of Fig. V.10), deformation is almost homogeneous. Consequently, degradation will proceed in an almost homogeneous fashion, as each particle in the entire cross section is subjected to almost identical deformations at the same time and therefore the corresponding degradation rates are similar inducing all to degrade approximately by the same amount. Thus, the differences throughout the thickness are small.

On the other hand, when the thickness of the annulus is increased, the deformation becomes more inhomogeneous, leading to different amounts of deformation at each location (first column of Fig. V.10). The degradation behavior of the body is completely different: the annulus is subjected to considerably greater deformations near the inner surface, and consequently, the degradation rate and the achieved degradation are greater in this region, and eventually lead to greater shear modulus reductions (second and third columns of Fig. V.10, respectively).

The main feature of Fig. V.10 is the qualitative change in the nature of the solutions. Degradation clearly proceeds in the outward direction, as can be observed from the significant differences between the inner and outer surfaces of the thick-walled annulus (second and third columns and second and third rows of Fig. V.10 respectively). Finally, the differences in shear modulus for each particle are enormous and the degree of inhomogeneity of the cylinder after some degradation is vast.

4. Inflation and extension of a degradable neo-Hookean-like body

When inflation is accompanied with a constant extension, two competing effects on the increase of degradation occur. Extension to a stretch λ is obtained with a certain axial load that promotes an axial stretch. If the transmural pressure is set to zero, then the annulus is uniaxially extended in the axial direction and the results are similar to the one-dimensional case analyzed in the Chapter IV.C (cf. Fig. IV.7).

Under pure extension, the degradation increases exponentially from the initial value $d = 0$ to $d \to 1$ (shown in Fig. V.11 at the inner radius for several constant axial stretches) The deformation is constant, hence the only change occurring in the equation governing the degradation process arises from the $1 - d$ term. Moreover, the motion is homogeneous, hence increases of degradation are of the same amount throughout the thickness. Finally, greater deformations promote more intense and quicker increases of degradation and relaxation occurs, i.e. less axial load is necessary to maintain such fixed deformation (cf. Fig. IV.6 for the corresponding one-dimensional counterpart).

degradation at inner radius vs. time for pure extension (ΔP=0)

Fig. V.11. Degradation at inner and outer radii vs. time for several axial stretches in a degradable neo-Hookean-like cylindrical annulus undergoing pure extension. An axial stress with no transmural pressure promotes an homogeneous degradation, hence no difference is observed between the inner and the outer radii. Degradation increases due to a constant stretch applied to the material with a decreasing rate as it reaches the point of maximum degradation. This is analogous as the case presented in chapter IV.C when the one-dimensional model is subjected to a fixed constant stretch (cf. Fig. IV.7). The force necessary to impose such stretch decreases as the shear modulus decreases (not shown).

As shown in Chapter IV.C, a completely different pattern of increase of degradation is obtained if a constant load is applied to a degradable body. The load promotes deformation that then promotes degradation of the material. When subjected to the same load, the material will then deform to a greater extent, i.e. it creeps. Such deformations will then promote steeper increases in degradation (cf. Fig. IV.8 and Fig. IV.9 for the corresponding one-dimensional counterparts).

This case happens similarly under pure inflation (cf. Fig. V.12 showing degradation at the inner surface for several transmural pressures): no departure from the reference configuration is due to stretching (as $\lambda = 1$) and the load promotes a
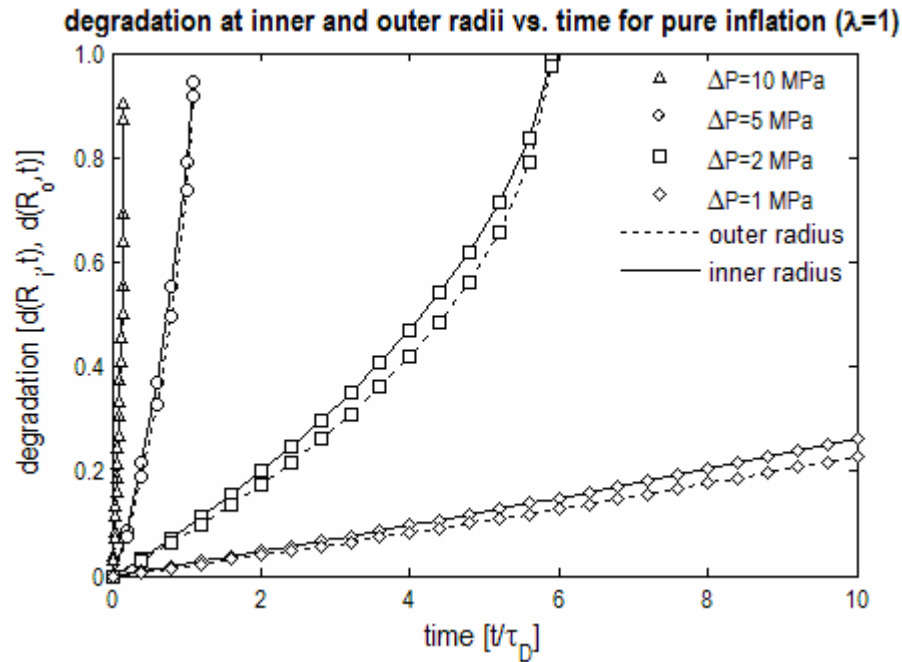
Fig. V.12. Degradation at inner and outer radii vs. time for several transmural pressures in a degradable neo-Hookean-like cylindrical annulus undergoing pure inflation. Degradation is more aggressive at the inner wall. Degradation increases steadily due to a fixed transmural pressure. As the shear modulus decreases, the material undergoes greater deformations that are then responsible to greater degradation rates. This is analogous to the case presented in chapter IV.C when the one-dimensional model is subjected to a fixed constant stress (cf. Fig. IV.9).

deformation that will increase progressively as the annulus degrades and its modulus decreases (cf. Fig. V.13). Indeed, when degradation approaches its maximum value and the shear modulus tends to zero, the inner and the outer radii increase to such an extent that the thickness of the annulus becomes very small.

When stretching and inflation occur at the same time, both effects occur synergistically and it is possible to depict the shift from the creep-like mode of degradation (due to a constant transmural pressure) to the exponential increase of degradation characteristic of a fixed deformation as the amount of stretch is increased (cf. Fig. V.14). Nevertheless, as the shear modulus of the material approaches zero due
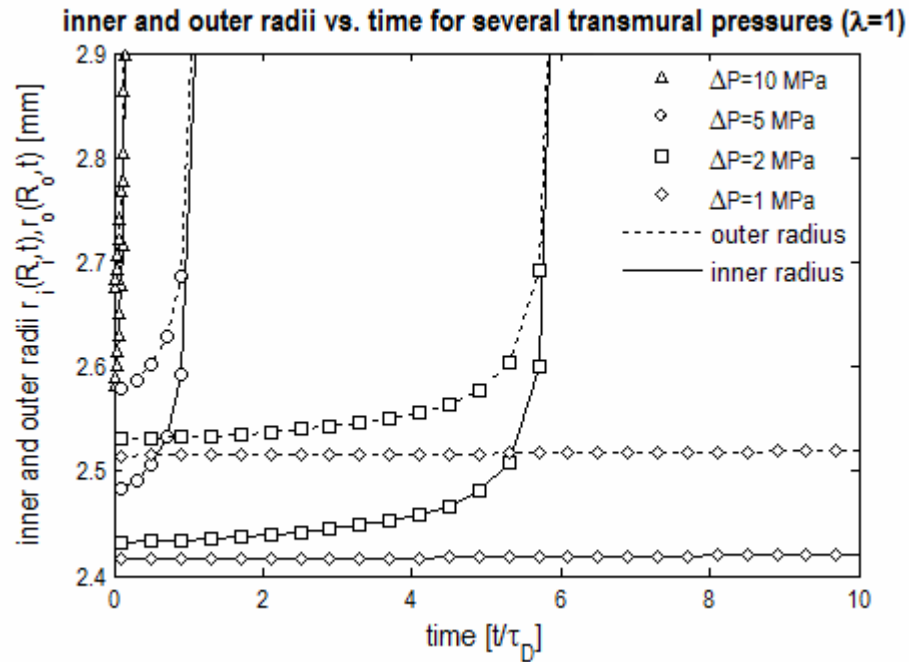
Fig. V.13. Current inner and outer radii vs. time for several transmural pressures in a degradable neo-Hookean-like cylindrical annulus undergoing pure inflation. The initial inner and outer radii are 2.4 and 2.5 mm respectively. Upon initial inflation, the annulus deforms to a certain extent determined by the initial material properties. With degradation, the deformation achieved with the same fixed pressure increases steadily, i.e. the annulus creeps. When the shear modulus approaches zero, the thickness becomes infinitesimally small due to inflation, and at this point the numerical scheme breaks down. This is analogous to the case presented in chapter IV.C when the one-dimensional model is subjected to a fixed constant stress (cf. Fig. IV.8).

to degradation, any transmural pressure, even if infinitesimally small, will promote dramatic inflations (cf. Fig. V.15) and the failure of the numerical scheme.

degradation at inner radius vs. time for several λ (ΔP=2 MPa)
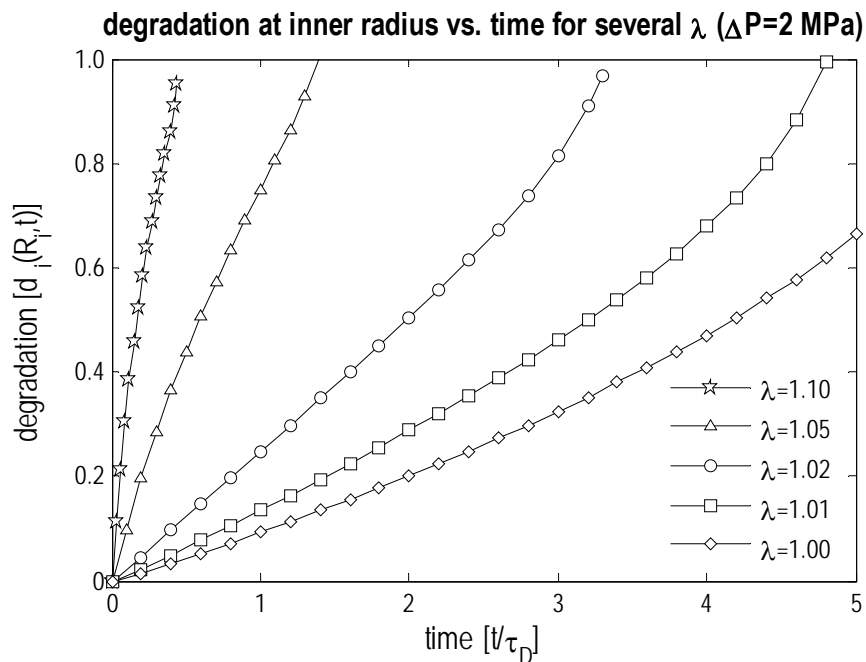
Fig. V.14. Degradation at inner radius vs. time for a degradable neo-Hookean-like material subjected to inflation and extension (for fixed transmural pressure and several axial stretches). If a material is subjected to a fixed deformation, degradation increases in an inverse exponential manner towards its maximum (cf. Fig. V.11). When a constant force is applied to the material, its deformation increases and promotes an abrupt increase of degradation (cf. Fig. V.12). When the axial stretch becomes more relevant, the shape of the curve resembles initially the inverse exponential up to a point when the load becomes responsible for the majority of the deformation that drives degradation.

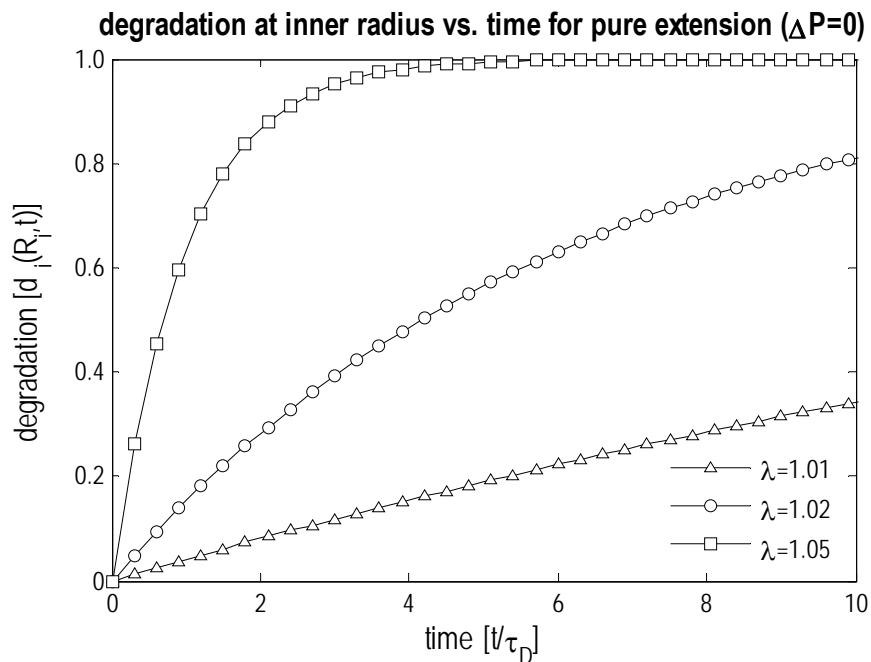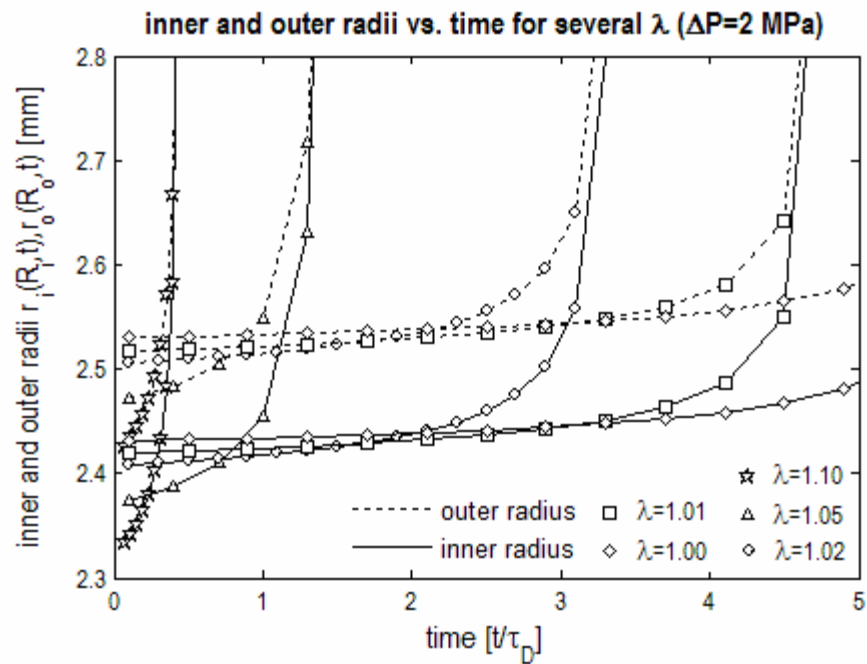Fig. V.15. Current inner and outer radii vs. time for several transmural pressures in a degradable neo-Hookean-like cylindrical annulus undergoing inflation and extension. Upon initial inflation and extension, the annulus deforms to a certain extent determined by the amount of each. Both components of the deformation promote degradation; note the time range shown is half of the corresponding in Fig. V.13.

CHAPTER VI

A NOTE ON THE EQUATION GOVERNING DEGRADATION

Polymer degradation resultant from chain scission can be modeled within the scope of the presented theory using the non-linear field theories of mechanics as a baseline and a body which material properties depend on a scalar field, the degradation field. The degradation field describes the extent of degradation that had occurred locally and its evolution is governed by a reaction equation that depicts the mechanisms of bond scission. Bond scission (degradation) in aliphatic polyesters occurs through random hydrolysis [123]. The rate at which degradation occurs is certainly driven by many factors such as simply the presence of water, temperature, to effects due to the particularity of each bond. States of stress or strain have been shown to influence the rate of degradation either in vivo and in vitro [163,164,167]. A study on how stress or strain could influence the rate of degradation and its impact on the mechanical properties is the primary objective of the current chapter.

The solution of the partial differential equations that result from the linear momentum balance in a degradable material, even when simple material behaviors and semi-inverse methods assuming simplistic motions are employed. Hence, their approximate solution must be obtained numerically. The secondary objective of the current chapter is to develop a numerical formalism to solve the full dynamic problem such that can be implemented to a wide range of response types.

Due to the simplicity it confers to the linear momentum balance, classical linearized theories were employed (in fact, this setting was the starting point of this entire research [280]). The degradable body was considered to be a finite cylinder under pure inflation and it was chosen to respond as a linearized elastic solid with degradation dependent Young's modulus, i.e. a one-parameter family of linear elastic responses. Degradation evolution is described by the aforementioned equation governing degradation.

A. Constitutive relations

The constitutive model of interest is based upon the three assumptions presented before (cf. Chapter IV.B): (i) the existence of the degradation field as an homogenization that describes locally at each time the ratio of broken bonds over breakable bonds varying from zero to unity, zero meaning a non-degraded material, and 1 the maximum amount of possible degradation, i.e.

$$d = d(\mathbf{x},t): \mathbf{x} \in \kappa_t(\mathcal{B}) \mapsto [0,1), \tag{6.1}$$

where d is the amount of degradation of particle X at time t (although not important due to the kinematical linearization, its Eulerian description is employed, i.e. d is associated with location $\mathbf{x}$ in the configuration $\kappa_t(\mathcal{B})$ that the body $\mathcal{B}$ occupies at time t); (ii) a constitutive equation that represents the response of the body at fixed levels of degradation, that was chosen to follow the classical linear elastic isotropic solid (cf. equation (2.122))

$$\boldsymbol{\sigma} = \frac{E\nu}{(1+\nu)(1-2\nu)}(\mathrm{tr}\,\boldsymbol{\varepsilon})\mathbf{1} + \frac{E}{(1+\nu)}\boldsymbol{\varepsilon}, \tag{6.2}$$

where $\boldsymbol{\varepsilon}$ is the linearized strain tensor and the degradable behavior is conferred by a Young's modulus that decreases with degradation

$$E \equiv E(d) = E_0(1-\beta d), \tag{6.3}$$

with β associated with the Young's modulus of the material at maximum possible degradation (not required, but set to $\beta = 0$); and finally, (iii) a reaction equation governing the degradation process

$$\frac{\partial d}{\partial t} = \mathfrak{D}(d,\boldsymbol{\varepsilon},\boldsymbol{\sigma}), \tag{6.4}$$

which is the counterpart of (4.4) for linearized theories. An envelope in the $(\boldsymbol{\sigma},\boldsymbol{\varepsilon})$ plane defining necessary conditions towards the activity of degradation could be associated with (6.4) as an activation criterion, but it is chosen that the increase of degradation will

always be active under any strain or stress different from zero (i.e., the body is not in its natural stress free configuration). The choice of the particular form for the equation governing the degradation process is done bellow.

B. Kinematics

The analysis is confined to a body $\mathcal{B}$ that is the region confined between two co-axial right circular cylinders characterized by inner and outer radii r_i and r_o and two planes normal to the axis of the cylinders:

$$\mathcal{B} = \left\{ (r,\theta,z) \mid r_i \leq r \leq r_o, 0 \leq \theta \leq 2\pi, 0 \leq z \leq L \right\}, \tag{6.5}$$

where (r,θ,z) represent the coordinates of a typical material point in cylindrical polar coordinates and L is distance between the two planes and defines half of the height of the cylinder.

A semi-inverse method is employed, i.e. the displacement field is assumed to have the following form

$$\mathbf{u} = \mathbf{u}(r,z,t) = u_r(r,z,t)\mathbf{e_r} + u_z(r,z,t)\mathbf{e_z}, \tag{6.6}$$

which in matrix form (with respect to the chosen coordinate system) is given by

$$(\mathbf{u}) = \begin{pmatrix} u_r(r,z,t) \\ 0 \\ u_z(r,z,t) \end{pmatrix}. \tag{6.7}$$

Due to the axisymmetry of the problem, degradation is assumed to be an independent function of the circumferential position, i.e.

$$d = d(r,z,t). \tag{6.8}$$

The matrix form of the displacement gradient tensor is given by

$$(\text{grad } \mathbf{u}) = \begin{pmatrix} \dfrac{\partial u_r}{\partial r} & 0 & \dfrac{\partial u_r}{\partial z} \\[3mm] 0 & \dfrac{u_r}{r} & 0 \\[3mm] \dfrac{\partial u_z}{\partial r} & 0 & \dfrac{\partial u_z}{\partial z} \end{pmatrix}, \tag{6.9}$$

and the linearized strain $\boldsymbol{\varepsilon}$ is computed with (2.40) and yields

$$(\boldsymbol{\varepsilon}) = \begin{pmatrix} \dfrac{\partial u_r}{\partial r} & 0 & \dfrac{1}{2}\left(\dfrac{\partial u_r}{\partial z}+\dfrac{\partial u_z}{\partial r}\right) \\[3mm] 0 & \dfrac{u_r}{r} & 0 \\[3mm] \dfrac{1}{2}\left(\dfrac{\partial u_r}{\partial z}+\dfrac{\partial u_z}{\partial r}\right) & 0 & \dfrac{\partial u_z}{\partial z} \end{pmatrix}. \tag{6.10}$$

C. Linear momentum balance and initial and boundary conditions

The linearized stress $\boldsymbol{\sigma}$ is obtained from constitutive equation (6.2) and its components (with respect to the aforementioned cylindrical coordinate system) are

$$\sigma_{rr} = \frac{E(d)}{(1+v)(1-2v)}\left[(1-v)\frac{\partial u_r}{\partial r}+v\left(\frac{u_r}{r}+\frac{\partial u_z}{\partial z}\right)\right], \tag{6.11}$$

$$\sigma_{\theta\theta} = \frac{E(d)}{(1+v)(1-2v)}\left[(1-v)\frac{u_r}{r}+v\left(\frac{\partial u_r}{\partial r}+\frac{\partial u_z}{\partial z}\right)\right], \tag{6.12}$$

$$\sigma_{zz} = \frac{E(d)}{(1+v)(1-2v)}\left[(1-v)\frac{\partial u_z}{\partial z}+v\left(\frac{\partial u_r}{\partial r}+\frac{u_r}{r}\right)\right], \tag{6.13}$$

$$\sigma_{rz} = \frac{E(d)}{2(1+v)}\left(\frac{\partial u_r}{\partial z}+\frac{\partial u_z}{\partial r}\right), \tag{6.14}$$

where the dependence of the Young's modulus on degradation was stressed.

The linearization of the balance of linear momentum (2.63) considering no body forces ($\mathbf{b} = \mathbf{0}$) yields

$$\operatorname{div} \boldsymbol{\sigma}^{\mathrm{T}} = \rho \frac{\partial^2 \mathbf{u}}{\partial t^2}, \tag{6.15}$$

which with respect to this coordinate system yields

$$\frac{\partial \sigma_{rr}}{\partial r} + \frac{\partial \sigma_{rz}}{\partial z} + \frac{\sigma_{rr} - \sigma_{\theta\theta}}{r} = \rho \frac{\partial^2 u_r}{\partial t^2}, \tag{6.16}$$

$$\frac{\partial \sigma_{rz}}{\partial r} + \frac{\partial \sigma_{zz}}{\partial z} + \frac{\sigma_{rz}}{r} = \rho \frac{\partial^2 u_z}{\partial t^2}, \tag{6.17}$$

and the trivial equality for the circumferential component. Note that the dynamic problem is being considered here. Furthermore, it must be remarked that the spatial derivatives of the stress field must take into account the dependence on degradation which in turn is a function of position (cf. (6.8)).

Equations (6.16), (6.17), and (6.4) are the partial differential equations describing the deformation and degradation of a finite cylinder. r, z, and t are the independent variables. The equations arising from the linear momentum balance are hyperbolic in space and time, whereas the equation governing degradation is parabolic. The system of equation is non linear due to the dependence of the Young's modulus on the degradation field, one of the solutions pursued. The system of partial differential equation is defined in the domain $\Omega \times \mathcal{I}$, where

$$\Omega = \{(r,z) \mid r_i < r < r_o, 0 < z < L\}, \tag{6.18}$$

$$\mathcal{I} = (0, \infty). \tag{6.19}$$

The inner and outer surfaces of the cylinder are defined through

$$\Gamma_i = \{(r,z) \mid r = r_i, 0 < z < L\}, \tag{6.20}$$

$$\Gamma_o = \{(r,z) \mid r = r_o, 0 < z < L\}, \tag{6.21}$$

respectively, and the top and bottom boundaries of Ω are

$$\Gamma_t = \{(r,z) \mid r_i < r < r_o, z = L\}, \tag{6.22}$$

$$\Gamma_b = \{(r,z) \mid r_i < r < r_o, z = 0\}. \tag{6.23}$$

Equations (6.16), (6.17) and (6.4) must be solved for the three dependent variables, $u_r(r,z,t)$, $u_z(r,z,t)$, and $d(r,z,t)$. For that, initial and boundary conditions must be supplied.

Traction boundary conditions are supplied at the inner and outer surfaces

$$\mathbf{t} = P_i(t)\mathbf{e_r} \Leftrightarrow \begin{cases} \sigma_{rr}(r_i,z,t) = -P_i(t) \\ \sigma_{zz}(r_i,z,t) = 0 \end{cases} \quad \text{on } \Gamma_i, \quad (6.24)$$

$$\mathbf{t} = -P_o(t)\mathbf{e_r} \Leftrightarrow \begin{cases} \sigma_{rr}(r_o,z,t) = -P_o(t) \\ \sigma_{zz}(r_o,z,t) = 0 \end{cases} \quad \text{on } \Gamma_o, \quad (6.25)$$

and the top of the cylinder is assumed to have a prescribed known displacement

$$\mathbf{u} = \mathbf{u}^L \Leftrightarrow \begin{cases} u_r(r,L,t) = u_r^L(r,t) \\ u_z(r,L,t) = u_z^L(r,t) \end{cases} \quad \text{on } \Gamma_t. \quad (6.26)$$

At the bottom boundary, symmetry with respect to the plane $z = 0$ is assumed, i.e.

$$\begin{cases} \dfrac{\partial u_r}{\partial z} = 0 \\ u_z = 0 \end{cases} \quad \text{on } \Gamma_b. \quad (6.27)$$

Finally, initial conditions on the displacement and the degradation must be prescribed. They are

$$\mathbf{u}\big|_{t=0} = \mathbf{0} \Leftrightarrow \begin{cases} u_r(r,z,0) = 0 \\ u_z(r,z,0) = 0 \end{cases} \quad \text{on } \Omega, \quad (6.28)$$

$$\frac{\partial \mathbf{u}}{\partial t}\bigg|_{t=0} = \mathbf{0} \Leftrightarrow \begin{cases} \dfrac{\partial u_r(r,z,t)}{\partial t}\bigg|_{t=0} = 0 \\ \dfrac{\partial u_z(r,z,t)}{\partial t}\bigg|_{t=0} = 0 \end{cases} \quad \text{on } \Omega, \quad (6.29)$$

$$d\big|_{t=0} = 0 \quad \text{on } \Omega, \quad (6.30)$$

with the understanding that the cylinder is initially at rest and non-degraded.

D. Computational setting

The development of a finite element scheme to solve (6.15) and (6.4) is formally developed in this section. A weak form of the linear momentum balance is used and an approximate solution is obtained with the spatial discretization of the domain (6.18). Time is also discretized in order to obtain solutions through a time marching technique. Because the resulting system of equations is nonlinear, an Picard iteration method is employed. The contents shown in this section draws heavily from [309]. The results are recorded within a general scope, but details can be found in [310-313]. For generic computational techniques, the reader is referred to [314].

1. Variational formulation

The variational formulation of the initial and boundary value problem follows the usual procedure: (i) the system of differential equations is multiplied by test functions $v(r,z) \in H^1(\Omega)$, the Hilbert space $H^1(\Omega)$ given by

$$H^1(\Omega) = \left\{ v : \begin{array}{l} v(r,z) \text{ is continuous on } \Omega \\ \dfrac{\partial v}{\partial r} \text{ and } \dfrac{\partial v}{\partial z} \text{ exist in a generalized sense} \end{array} \right\}, \qquad (6.31)$$

and integrated to yield

$$\int_{\Omega} (\text{div } \boldsymbol{\sigma}) \cdot \mathbf{v} - \rho \frac{\partial^2 \mathbf{u}}{\partial t^2} \cdot \mathbf{v} \, d\Omega = 0 ; \qquad (6.32)$$

(ii) integration by parts of (6.32) employs the equality

$$\text{div } (\mathbf{Tv}) = (\text{div } \mathbf{T}) \cdot \mathbf{v} + \mathbf{T} \cdot \text{grad } \mathbf{v} , \qquad (6.33)$$

where the inner product between 2nd order tensors is defined as $\mathbf{T} \cdot \mathbf{S} = \text{tr } (\mathbf{T}^{\text{T}}\mathbf{S})$, and yields

$$\int_{\Omega} \boldsymbol{\sigma} \cdot \text{grad } \mathbf{v} + \rho \frac{\partial^2 \mathbf{u}}{\partial t^2} \cdot \mathbf{v} \, d\Omega = \int_{\Omega} \text{div } (\boldsymbol{\sigma}\mathbf{v}) \, d\Omega ; \qquad (6.34)$$

and, (iii) Stoke's theorem is used on the right hand side of (6.34) to yield

$$\int_{\Omega} \boldsymbol{\sigma} \cdot \text{grad } \mathbf{v} + \rho \frac{\partial^2 \mathbf{u}}{\partial t^2} \cdot \mathbf{v} \ d\Omega = \int_{\Gamma} \boldsymbol{\sigma} \mathbf{v} \cdot \mathbf{n} \ d\Gamma \,, \tag{6.35}$$

where $\mathbf{n}$ is the outward unit normal of the boundary Γ of the domain Ω. With the definition of the transpose, $\mathbf{u} \cdot \mathbf{S} \mathbf{v} = \mathbf{S}^T \mathbf{u} \cdot \mathbf{v}$, and the traction $\mathbf{t} = t_r \mathbf{e}_r + t_z \mathbf{e}_z = \boldsymbol{\sigma}^T \mathbf{n}$, (6.35) is further simplified to

$$\int_{\Omega} \boldsymbol{\sigma} \cdot \text{grad } \mathbf{v} \ d\Omega + \int_{\Omega} \rho \frac{\partial^2 \mathbf{u}}{\partial t^2} \cdot \mathbf{v} \ d\Omega = \int_{\Gamma} \mathbf{v} \cdot \mathbf{t} \ d\Gamma \,. \tag{6.36}$$

With the employment of constitutive equation (6.2), (6.36) becomes

$$a_1(\mathbf{u}, \mathbf{v}, d) = L_1(\mathbf{v}, d) \,, \tag{6.37}$$

where

$$\begin{aligned} a_1(\mathbf{u}, \mathbf{v}, d) = &\int_{\Omega} \frac{E\nu}{(1+\nu)(1-2\nu)} (\text{div } \mathbf{u})(\text{div } \mathbf{v}) \ d\Omega \\ &+ \int_{\Omega} \frac{E}{(1+\nu)} \left[\text{grad } \mathbf{u} + (\text{grad } \mathbf{u})^T \right] \cdot \text{grad } \mathbf{v} \ d\Omega \,, \\ &+ \int_{\Omega} \rho \frac{\partial^2 \mathbf{u}}{\partial t^2} \cdot \mathbf{v} \ d\Omega \end{aligned} \tag{6.38}$$

$$L_1(\mathbf{v}, d) = \int_{\Gamma} \mathbf{v} \cdot \mathbf{t} \ d\Gamma \,, \tag{6.39}$$

Note that both $a_1(\mathbf{u}, \mathbf{v}, d)$ and $L_1(\mathbf{v}, d)$ depend on the degradation through the Young's modulus $E \equiv E(d)$.

Information on parts of the boundary Γ where Dirichelet boundary conditions have been specified is usually used to reduce the domain of integration of the boundary integral on (6.39) (requiring at the same time that test function $\mathbf{v}$ vanishes at these locations and hence restricting the space $H^1(\Omega)$ to some $H_0^1(\Omega)$). In order to avoid loss of generality, this methodology is not considered at this point.

Similarly, the weak form of the equation governing degradation is

$$a_2(d,v) = L_2(v,\mathbf{u},d),\tag{6.40}$$

where

$$a_2(d,v) = \int_\Omega \frac{\partial d}{\partial t} v \, d\Omega,\tag{6.41}$$

$$L_2(d,v,\mathbf{u}) = \int_\Omega \mathfrak{D}(d,\boldsymbol{\varepsilon},\boldsymbol{\sigma})v \, d\Omega.\tag{6.42}$$

Note that $L_2(d,v,\mathbf{u})$ with its dependence on $\mathbf{u}$ and d and the dependence of $a_1(\mathbf{u},\mathbf{v},d)$ and $L_1(\mathbf{v},d)$ on d introduce the nonlinearity of the problem.

Formally, the variational formulation of the problem is: find $\mathbf{u} \in H^1(\Omega) \times \mathcal{I}$ and $d \in H^1(\Omega) \times \mathcal{I}$ such that (6.36) and (6.40) hold for all $v \in H^1(\Omega)$. The solution space V is approximated with a finite dimensional space $V_h \subset H^1(\Omega)$ and the solution $\mathbf{u} \in H^1(\Omega) \times \mathcal{I}$ will be approximated with an approximate solution $\mathbf{u}_h \in V_h \times \mathcal{I}$

2. Finite element partition

Ω was partitioned into triangles τ, such that: (i) they are disjoint, and (ii) their intersection is either a vertex, an edge, or empty. Together with the set of linear polynomials on each independent variable $\mathcal{P}_1 = \{C_1 + C_2 r + C_3 z, \; C_i \text{ real constants}\}$, the approximating space V_h can now be defined

$$V_h = \left\{ v(r,z) : \begin{array}{l} v \text{ is continuous on } \Omega \\ v \in \mathcal{P}_1 \text{ in each } \tau \end{array} \right\}.\tag{6.43}$$

The values at the vertexes, $P_j, j = 1,...,N$, where N is the number of vertexes, was naturally chosen as the set of linearly independent functionals Σ that is $\mathcal{P}_1$-unisolvent; hence a nodal basis $\phi_j(r,z), j = 1,...,N$ is constructed with piecewise linear functions

$$\phi_j(x,y) = \begin{cases} 1 \text{ if } (x,y) = P_j \\ 0 \text{ if } (x,y) = P_k, k \neq j \\ \phi_j \in \mathscr{P}_1 \text{ over each } \tau \end{cases} \tag{6.44}$$

$(\tau, \mathscr{P}_1, \Sigma)$ defines the finite element, the linear triangle.

3. *Approximating space*

At this point, it is important to remark that $\mathbf{u}(r,z,t) = u_r \mathbf{e_r} + u_z \mathbf{e_z}$, i.e. composed of two dependent variables, the radial displacement u_r and the axial displacement u_z. Hence, $\mathbf{u}_h(r,z,t)$, the approximate solution of the displacement is given by

$$\mathbf{u}_h(r,z,t) = \bar{u}_r(r,z,t)\mathbf{e_r} + \bar{u}_z(r,z,t)\mathbf{e_z}. \tag{6.45}$$

The bar means that one is dealing with the approximate solution of the corresponding component of the displacement, each belonging to V_h. It was used in order to avoid the usage of two subscripts (r or z to determine the component, and h the approximation.

Elements of V_h can be represented as linear combinations of $\phi_j(r,z)$, i.e.

$$\bar{u}_r(r,z,t) = \sum_{j=1}^{N} U_j(t)\phi_j(r,z), \text{ where } U_j(t) = \bar{u}_r(P_j,t), \tag{6.46}$$

$$\bar{u}_z(r,z,t) = \sum_{j=1}^{N} W_j(t)\phi_j(r,z), \text{ where } W_j(t) = \bar{u}_z(P_j,t), \tag{6.47}$$

$$d_h(r,z,t) = \sum_{j=1}^{N} D_j(t)\phi_j(r,z), \text{ where } D_j(t) = d_h(P_j,t). \tag{6.48}$$

$U_j(t)$, $W_j(t)$, and $D_j(t)$ are the time dependent radial displacement, axial displacement, and degradation at vertex $P_j = (r_j, z_j)$, respectively. It is convenient to consider the vectorial form of the nodal displacements $\mathbf{U}_j(t), j = 1,...,N$, i.e.

$$\mathbf{U}_j(t) = \begin{Bmatrix} U_j(t) \\ W_j(t) \end{Bmatrix}, \tag{6.49}$$

as well as

$$\mathbf{\Phi}_j(r,z) = \phi_j(r,z)\mathbf{e}_r + \phi_j(r,z)\mathbf{e}_z, \tag{6.50}$$

such that the approximate solution $\mathbf{u}_h$ and test function $\mathbf{v}$ appearing in (6.37) are

$$\mathbf{u}_h(r,z,t) = \sum_{j=1}^{N} \mathbf{U}_j(t) \cdot \mathbf{\Phi}_j(r,z), \tag{6.51}$$

$$\mathbf{v}(r,z) = \sum_{j=1}^{N} \mathbf{V}_j \cdot \mathbf{\Phi}_j(r,z), \tag{6.52}$$

with $\mathbf{V}_j = \{V_j^1 \quad V_j^2\}$ arbitrary.

When replacing (6.52) and (6.51) in (6.37) and setting only one entry of the arbitrary test function $\mathbf{v}$ to 1 with all others zero, (6.37) reduces to a system of $2N$ equations for the unknown nodal values U_j and $W_j, j = 1,..., N$. As an example, the last term of (6.38) yields

$$\int_{\Omega} \rho \frac{\partial^2 \mathbf{u}}{\partial t^2} \cdot \mathbf{v} \, d\Omega = \int_{\Omega} \rho \left(\sum_{i=1}^{N} \mathbf{V}_i \cdot \mathbf{\Phi}_i \right) \cdot \left(\sum_{j=1}^{N} \ddot{\mathbf{U}}_j \cdot \mathbf{\Phi}_j \right) d\Omega$$

$$= \sum_{i=1}^{N} \sum_{j=1}^{N} \int_{\Omega} \rho \left(\mathbf{V}_i \cdot \mathbf{\Phi}_i \right) \cdot \left(\mathbf{\Phi}_j \cdot \ddot{\mathbf{U}}_j \right) d\Omega, \tag{6.53}$$

$$= \sum_{i=1}^{N} \sum_{j=1}^{N} \mathbf{V}_i \cdot \left(\int_{\Omega} \rho \mathbf{\Phi}_i \otimes \mathbf{\Phi}_j d\Omega \right) \ddot{\mathbf{U}}_j$$

Then, the entire variational problem reduces to two systems of equation for the unknown nodal values $\mathbf{U}_j(t), j = 1,..., N$ and $D_j, j = 1,..., N$

$$\sum_{j=1}^{N} a_1(\mathbf{\Phi}_i, \mathbf{\Phi}_j, d_h)\mathbf{U}_j(t) = L_1(\mathbf{\Phi}_i), \ i = 1,..., N, \tag{6.54}$$

$$\sum_{j=1}^{N} a_2(\phi_i, \phi_j)D_j(t) = L_2(\phi_i, \bar{u}_r, \bar{u}_z, d_h), \ i = 1,..., N, \tag{6.55}$$

or

$$\mathbf{M\ddot{U}} + \mathbf{AU} = \mathbf{b},\tag{6.56}$$

$$\mathbf{M}_d\dot{\mathbf{d}} = \mathbf{b}_d.\tag{6.57}$$

The mass stiffness matrix in (6.56), $\mathbf{M}$ and $\mathbf{A}$ respectively, are given by

$$(\mathbf{M})_{ij} = \int_\Omega \rho \mathbf{\Phi}_i \otimes \mathbf{\Phi}_j \ d\Omega = \begin{pmatrix} \int_\Omega \rho\phi_i\phi_j \ d\Omega & 0 \\ 0 & \int_\Omega \rho\phi_i\phi_j \ d\Omega \end{pmatrix},\tag{6.58}$$

$$(\mathbf{A})_{ij} = a_1(\mathbf{\Phi}_i,\mathbf{\Phi}_j,d) = \begin{pmatrix} A_{ij}^{rr} & A_{ij}^{rz} \\ A_{ij}^{zr} & A_{ij}^{zz} \end{pmatrix},\tag{6.59}$$

with

$$A_{ij}^{rr} = (\lambda+2\mu)\frac{\partial\phi_i}{\partial r}\frac{\partial\phi_j}{\partial r} + \mu\frac{\partial\phi_i}{\partial z}\frac{\partial\phi_j}{\partial z} + \frac{2\lambda}{r}\frac{\partial\phi_i}{\partial r}\phi_j + \frac{(\lambda+2\mu)}{r^2}\phi_i\phi_j$$

$$A_{ij}^{zz} = (\lambda+2\mu)\frac{\partial\phi_i}{\partial z}\frac{\partial\phi_j}{\partial z} + \mu\frac{\partial\phi_i}{\partial r}\frac{\partial\phi_j}{\partial r}\tag{6.60}$$

$$A_{ij}^{rz} = A^{zr} = (\lambda+2\mu)\frac{\partial\phi_i}{\partial r}\frac{\partial\phi_j}{\partial z} + \frac{\lambda}{r}\frac{\partial\phi_i}{\partial z}\phi_j$$

where λ and μ related to $E(d)$ and ν through (2.123) and (2.124). Load vector $\mathbf{b}$ given by

$$(\mathbf{b})_i = L_1(\mathbf{\Phi}_i,d) = \begin{pmatrix} \int_\Gamma \phi_i t_r \ d\Gamma \\ \int_\Gamma \phi_i t_z \ d\Gamma \end{pmatrix}.\tag{6.61}$$

The vectors with the dependent variable in (6.56) are

$$(\mathbf{U})_j = \begin{pmatrix} U_j(t) \\ W_j(t) \end{pmatrix}, \qquad (\mathbf{\ddot{U}})_j = \begin{pmatrix} \ddot{U}_j(t) \\ \ddot{W}_j(t) \end{pmatrix}.\tag{6.62}$$

Finally, system of equations (6.57) is composed by a mass matrix $\mathbf{M}_d$ and a load vector $\mathbf{b}_d$ given by

$$(\mathbf{M}_d)_{ij} = \int_\Omega \phi_i\phi_j \ d\Omega,\tag{6.63}$$

$$(\mathbf{b}_d)_i = L_1(\phi_i, \mathbf{u}, d) = \int_\Omega \mathfrak{D}(d, \boldsymbol{\varepsilon}, \boldsymbol{\sigma})\phi_i \ d\Omega, \tag{6.64}$$

while the solution vector is

$$(\dot{\mathbf{d}})_j = \dot{D}_j. \tag{6.65}$$

4. Element-wise calculations

Consider triangle τ_{ijk} with vertices P_i, P_j, and P_k, and the restriction over τ of (6.44). The element matrixes and load vectors are obtained with (6.58), (6.59), (6.61), (6.63), and (6.64). System of equations (6.56) yields 6 by 6 mass and stiffness element matrixes, which components are given by

$$\left(\mathbf{M}^{\tau_{ijk}}\right) = \begin{pmatrix} \left(\mathbf{M}\right)_{ii} & \left(\mathbf{M}\right)_{ij} & \left(\mathbf{M}\right)_{ik} \\ & \left(\mathbf{M}\right)_{jj} & \left(\mathbf{M}\right)_{jk} \\ sym & & \left(\mathbf{M}\right)_{kk} \end{pmatrix}, \tag{6.66}$$

$$\left(\mathbf{A}^{\tau_{ijk}}\right) = \begin{pmatrix} \begin{pmatrix} A_{ii}^{rr} & A_{ii}^{rz} \\ A_{ii}^{zr} & A_{ii}^{zz} \end{pmatrix} & \begin{pmatrix} A_{ij}^{rr} & A_{ij}^{rz} \\ A_{ij}^{zr} & A_{ij}^{zz} \end{pmatrix} & \begin{pmatrix} A_{ik}^{rr} & A_{ik}^{rz} \\ A_{ik}^{zr} & A_{ik}^{zz} \end{pmatrix} \\ & \begin{pmatrix} A_{jj}^{rr} & A_{jj}^{rz} \\ A_{jj}^{zr} & A_{jj}^{zz} \end{pmatrix} & \begin{pmatrix} A_{jk}^{rr} & A_{jk}^{rz} \\ A_{jk}^{zr} & A_{jk}^{zz} \end{pmatrix} \\ sym & & \begin{pmatrix} A_{kk}^{rr} & A_{kk}^{rz} \\ A_{kk}^{zr} & A_{kk}^{zz} \end{pmatrix} \end{pmatrix}, \tag{6.67}$$

where $\mathbf{M}$ and $\mathbf{A}$ correspond to the 2 by 2 nodal matrix given by (6.58) and (6.59) respectively. The element vector is generally null, but it will have entries following (6.61) if the corresponding nodes belong to portions of the boundary to which traction is being applied (cf. (6.24)-(6.25)). The dependent variable vectors are

$$(\mathbf{U}^{\tau_{ijk}}) = \begin{pmatrix} \begin{pmatrix} U_i(t) \\ W_i(t) \end{pmatrix} \\ \begin{pmatrix} U_j(t) \\ W_j(t) \end{pmatrix} \\ \begin{pmatrix} U_k(t) \\ W_k(t) \end{pmatrix} \end{pmatrix}, \qquad (\ddot{\mathbf{U}}^{\tau_{ijk}}) = \begin{pmatrix} \begin{pmatrix} \ddot{U}_i(t) \\ \ddot{W}_i(t) \end{pmatrix} \\ \begin{pmatrix} \ddot{U}_j(t) \\ \ddot{W}_j(t) \end{pmatrix} \\ \begin{pmatrix} \ddot{U}_k(t) \\ \ddot{W}_k(t) \end{pmatrix} \end{pmatrix}. \tag{6.68}$$

Similarly, for the system corresponding to the equation governing degradation, the element equations are obtained with (6.63)-(6.65):

$$\begin{pmatrix} \int_\Omega \phi_i\phi_i \ d\Omega & \int_\Omega \phi_i\phi_j \ d\Omega & \int_\Omega \phi_i\phi_k \ d\Omega \\ & \int_\Omega \phi_j\phi_j \ d\Omega & \int_\Omega \phi_j\phi_k \ d\Omega \\ sym & & \int_\Omega \phi_k\phi_k \ d\Omega \end{pmatrix} \begin{pmatrix} \dot{D}_i \\ \dot{D}_j \\ \dot{D}_k \end{pmatrix} = \begin{pmatrix} \int_\Omega \mathfrak{D}(d,\boldsymbol{\varepsilon},\boldsymbol{\sigma})\phi_i \ d\Omega \\ \int_\Omega \mathfrak{D}(d,\boldsymbol{\varepsilon},\boldsymbol{\sigma})\phi_j \ d\Omega \\ \int_\Omega \mathfrak{D}(d,\boldsymbol{\varepsilon},\boldsymbol{\sigma})\phi_k \ d\Omega \end{pmatrix}. \tag{6.69}$$

5. *Homogeneous coordinates*

A nodal basis for V_h can be easily constructed with homogeneous coordinates. Consider the triangle τ_{ijk} with vertices $P_i = (r_i, z_i)$, $P_j = (r_j, z_j)$, and $P_k = (r_k, z_k)$. The area of the triangle is given by

$$\left|\tau_{ijk}\right| = \frac{1}{2}\left[r_i\left(z_j - z_k\right) + z_i\left(r_k - r_j\right) + r_j z_k - r_k z_j \right] = \frac{\Delta}{2}. \tag{6.70}$$

Given a point $P = (r,z) \in \tau_{ijk}$, one can define three distinct triangles and introduce the following functions based on their areas

$$\lambda_i(r,z) = \frac{\left|\tau_{Pjk}\right|}{\left|\tau_{ijk}\right|}, \quad \lambda_j(r,z) = \frac{\left|\tau_{Pik}\right|}{\left|\tau_{ijk}\right|}, \quad \lambda_k(r,z) = \frac{\left|\tau_{Pij}\right|}{\left|\tau_{ijk}\right|}, \tag{6.71}$$

where

$$\left|\tau_{Pjk}\right| = \frac{1}{2}\left[x\left(y_j - y_k\right) + y\left(x_k - x_j\right) + x_j y_k - x_k y_j \right], \tag{6.72}$$

which simplify to

$$\lambda_p(r,z) = \left(a_p + b_p r + c_p z\right)\big/\Delta, \quad p \in \{i,j,k\}, \tag{6.73}$$

where

$$a_p = x_q y_r - x_r y_q, \quad b_p = y_a - y_r, \quad c_p = x_r - x_q, \quad (p,q,r) \equiv (i,j,k), \tag{6.74}$$

and the triple (p,q,r) is used in a cyclic way. Finally, note that

$$\lambda_p(x_q, y_q) = \begin{cases} 1 & \text{if } p = q \\ 0 & \text{if } p \neq q \end{cases} \quad p,q \in \{i,j,k\}, \tag{6.75}$$

hence λ_i, λ_j, λ_k are the restrictions over τ_{ijk} of the corresponding functions of the nodal basis ϕ_i, ϕ_j, ϕ_k.

6. The reference element

The reference element $\hat{\tau}$ defined by the three vertices $\hat{P}_1 = (0,0)$, $\hat{P}_2 = (1,0)$, and $\hat{P}_3 = (0,1)$ is a right triangle with the vertex corresponding to the right angle at the origin of the (ξ, η)-plane and unit length catheti in the directions of the coordinate axis ξ and η. One can define the homogeneous coordinates in the reference element in a similar way. Note that (6.70) yields

$$\left|\hat{\tau}\right| = \frac{\Delta}{2} = \frac{1}{2}, \tag{6.76}$$

and the corresponding nodal basis functions of the reference element will be obtained from (6.73) and (6.74) and are given by

$$\hat{\lambda}_1(\xi,\eta) = 1 - \xi - \eta, \quad \hat{\lambda}_2(\xi,\eta) = \eta, \quad \hat{\lambda}_3(\xi,\eta) = \xi. \tag{6.77}$$

They are linear functions which value is unity at the corresponding vertex and vanish at the other two.

7. Element transformation

Each triangle τ_{ijk} is mapped onto the reference triangle $\hat{\tau}$ through an one-to-one mapping

$$T_\tau : (\xi,\eta) \in \hat{\tau} \mapsto (r,z) \in \tau_{ijk} \ ,$$ (6.78)

where the subscript τ on the mapping stresses its dependence on the element τ_{ijk}. The transformation is given by

$$\begin{aligned} r &= r(\xi,\eta) \\ z &= z(\xi,\eta) \end{aligned}.$$ (6.79)

Further, with nodal basis functions (6.77), the transformation (6.79) is easily obtained. Note that

$$r(\xi,\eta) = \sum_{m=1}^{3} r_m \hat{\lambda}_m(\xi,\eta),$$ (6.80)

$$z(\xi,\eta) = \sum_{m=1}^{3} z_m \hat{\lambda}_m(\xi,\eta),$$ (6.81)

where (r_m, z_m) are the coordinates of the vertex of triangle τ_{ijk}, P_m with $m \in \{i,j,k\}$, that is being mapped onto the vertex of triangle $\hat{\tau}$, $\hat{P}_{\hat{m}}$ with $\hat{m} \in \{1,2,3\}$.

Note that

$$d\tau = J \ d\hat{\tau},$$ (6.82)

where J is the Jacobian of the transformation and is given by

$$J = \frac{\partial r}{\partial \xi} \frac{\partial z}{\partial \eta} - \frac{\partial r}{\partial \eta} \frac{\partial z}{\partial \xi}.$$ (6.83)

The mapping is one-to-one, so the inverse $T_\tau^{-1} : (r,z) \in \tau_{ijk} \mapsto (\xi,\eta) \in \hat{\tau}$ is well defined. The metrics of both mappings are related through

$$\frac{\partial \xi}{\partial x} = \frac{1}{J}\frac{\partial y}{\partial \eta}, \quad \frac{\partial \xi}{\partial y} = -\frac{1}{J}\frac{\partial x}{\partial \eta}$$

$$\frac{\partial \eta}{\partial x} = -\frac{1}{J}\frac{\partial y}{\partial \xi}, \quad \frac{\partial \eta}{\partial y} = \frac{1}{J}\frac{\partial x}{\partial \xi}$$

(6.84)

Using (6.84) and the chain rule, derivatives with respect to r and z of a given function $f = f(x,y) = \hat{f}(\xi,\eta)$ are related to the derivatives with respect to ξ and η through

$$\frac{\partial f}{\partial r} = \frac{1}{J}\left(\frac{\partial \hat{f}}{\partial \xi}\frac{\partial z}{\partial \eta} - \frac{\partial \hat{f}}{\partial \eta}\frac{\partial z}{\partial \xi} \right),$$

(6.85)

$$\frac{\partial f}{\partial z} = \frac{1}{J}\left(-\frac{\partial \hat{f}}{\partial \xi}\frac{\partial r}{\partial \eta} + \frac{\partial \hat{f}}{\partial \eta}\frac{\partial r}{\partial \xi} \right).$$

(6.86)

Finally, the metrics in (6.85)-(6.86) are easily computed with (6.80) and (6.81) and yield

$$\frac{\partial r}{\partial \xi} = \sum_{m=1}^{3} r_m \frac{\partial \hat{\lambda}_m}{\partial \xi}, \quad \frac{\partial r}{\partial \eta} = \sum_{m=1}^{3} r_m \frac{\partial \hat{\lambda}_m}{\partial \eta}$$

$$\frac{\partial z}{\partial \xi} = \sum_{m=1}^{3} z_m \frac{\partial \hat{\lambda}_m}{\partial \xi}, \quad \frac{\partial z}{\partial \eta} = \sum_{m=1}^{3} z_m \frac{\partial \hat{\lambda}_m}{\partial \eta}$$

(6.87)

The reference element with transformation (6.80)-(6.81) is extremely useful to perform a change of variable on the integrals appearing in (6.61), (6.66), (6.67), and (6.69). Note that derivatives with respect to the independent variables r and z are computed with (6.85)-(6.86).

Element matrixes (cf. (6.66), (6.67), and (6.69)) are computed through the reference element are assembled into global matrixes (cf. (6.56) and (6.57)). Boundary conditions, either Neumann or Dirichelet are applied at this point. The former are simply accounted with the computation of (6.61) at relevant nodes whereas the latter implies the reduction of the number of unknowns and corresponding back-substitution on the right hand sides of (6.56) and (6.57).

8. *Time marching scheme*

A time marching explicit scheme was used to determine the solutions U_j^{n+1}, W_j^{n+1}, and D_j^{n+1}, $j = 1,...,N$ at time t^{n+1} using known values at t^n, U_j^n, W_j^n, and D_j^n. Initial conditions at $t = 0$, U_j^0, W_j^0, and D_j^0, are provided (cf. (6.28)-(6.30)).

The sets of ordinary differential equations (6.56) and (6.57) are reduced to sets of algebraic equations relating $\mathbf{U}^{n+1}$ and $\mathbf{d}^{n+1}$ with $\mathbf{U}^n$ and $\mathbf{d}^n$. The former yields

$$\hat{\mathbf{K}}^{n+1}\mathbf{U}^{n+1} = \hat{\mathbf{F}}^{n,n+1}, \tag{6.88}$$

with

$$\hat{\mathbf{K}}^{n+1} = \mathbf{A}^{n+1} + \alpha_3 \mathbf{M}^{n+1}, \tag{6.89}$$

$$\hat{\mathbf{F}}^{n,n+1} = \mathbf{b}^{n+1} + \mathbf{M}^{n+1}\left(\alpha_3 \mathbf{U}^n + \alpha_4 \dot{\mathbf{U}}^n + \alpha_5 \ddot{\mathbf{U}}^n\right), \tag{6.90}$$

whereas the latter yields

$$\hat{\mathbf{K}}_d^{n+1}\mathbf{d}^{n+1} = \hat{\mathbf{F}}_d^{n,n+1}, \tag{6.91}$$

with

$$\hat{\mathbf{K}}_d^{n+1} = \mathbf{M}_d, \tag{6.92}$$

$$\hat{\mathbf{F}}_d^{n,n+1} = \mathbf{M}_d^n\mathbf{d}^n + \beta_1 \mathbf{b}_d^{n+1} + \beta_2 \mathbf{b}_d^n. \tag{6.93}$$

For (6.91), the time marching parameters are

$$\beta_1 = \alpha\Delta t, \qquad \beta_2 = (1-\alpha)\Delta t, \tag{6.94}$$

with constant α yielding different schemes: e.g. if $\alpha = 0$ yields the forward difference scheme, $\alpha = 1/2$ the Crank-Nicolson scheme, $\alpha = 2/3$ the Galerkin method, and $\alpha = 1$ the backward difference scheme. For the hyperbolic equation yielding (6.88), the time marching parameters are

$$\alpha_1 = \alpha\Delta t, \qquad \alpha_2 = (1-\alpha)\Delta t, \tag{6.95}$$

$$\alpha_3 = \frac{2}{\gamma(\Delta t)^2}, \qquad \alpha_4 = \frac{2}{\gamma(\Delta t)}, \qquad \alpha_5 = \frac{1-\gamma}{\gamma}, \tag{6.96}$$

similarly yielding several well-known schemes: e.g. with $\alpha = 1/2$ and $\gamma = 1/2$, the constant-average acceleration method, with $\gamma = 1/2$ the linear acceleration method, $\gamma = 8/5$ the Galerkin method, and $\gamma = 2$ the backward difference method. $\alpha = 1/2$ and $\gamma = 1/2$ was chosen for both systems of ordinary differential equations, yielding a stable scheme for the parabolic equation and a conditionally stable scheme for the hyperbolic problem [312,313].

Finally, some remarks are in order: (i) the calculation of $\hat{\mathbf{K}}^{n+1}$ and $\hat{\mathbf{F}}^{n,n+1}$ with $n = 0$ requires knowledge of initial conditions $\mathbf{U}^0$, $\dot{\mathbf{U}}^0$, and $\ddot{\mathbf{U}}^0$. The latter is unknown and is approximated with

$$\ddot{\mathbf{U}}^0 = \left[\mathbf{M}^1\right]^{-1}(\mathbf{b}^0 - \mathbf{A}^0\mathbf{U}^0); \tag{6.97}$$

and (ii) at the end of each time step, the new velocity vector $\dot{\mathbf{U}}^{n+1}$ and acceleration vector $\ddot{\mathbf{U}}^{n+1}$ are computed using the equations

$$\ddot{\mathbf{U}}^{n+1} = \alpha_3(\mathbf{U}^{n+1} - \mathbf{U}^n) - \alpha_4\dot{\mathbf{U}}^n - \alpha_5\ddot{\mathbf{U}}^n, \tag{6.98}$$

$$\dot{\mathbf{U}}^{n+1} = \dot{\mathbf{U}}^n + \alpha_1\ddot{\mathbf{U}}^{n+1} + \alpha_2\ddot{\mathbf{U}}^n, \tag{6.99}$$

with α_1 and α_2 defined by (6.95).

9. Newton-Raphson iteration method

The systems of equations obtained with the time marching technique are nonlinear. More particularly, $\hat{\mathbf{K}}^{n+1}$ and $\hat{\mathbf{F}}^{n,n+1}$ in (6.88) depend on $\mathbf{d}^{n+1}$ through the Young's modulus appearing in (6.59) and (6.61), and $\hat{\mathbf{F}}_d^{n,n+1}$ in (6.91) depend on not only on $\mathbf{d}^{n+1}$ but also on $\mathbf{U}^{n+1}$ through the functional $\mathfrak{D}(d,\boldsymbol{\varepsilon},\boldsymbol{\sigma})$ appearing in (6.64).

An iterative scheme is implemented to solve both nonlinear systems of algebraic equations. The matrixes were concatenated in a $3N$ by $3N$ system, i.e.

$$\left(\begin{bmatrix} \hat{\mathbf{K}}^{n+1}(\mathbf{d}^{n+1}) & \begin{matrix} 0 \\ 0 \end{matrix} \\ \begin{matrix} 0 & 0 \end{matrix} & [\hat{\mathbf{K}}_d^{n+1}] \end{bmatrix}\right) \left\{\begin{matrix} \{\mathbf{U}^{n+1}\} \\ \{\mathbf{d}^{n+1}\} \end{matrix}\right\} = \left\{\begin{matrix} \{\hat{\mathbf{F}}^{n,n+1}(\mathbf{d}^{n+1})\} \\ \{\hat{\mathbf{F}}_d^{n,n+1}(\mathbf{U}^{n+1},\mathbf{d}^{n+1})\} \end{matrix}\right\}, \tag{6.100}$$

which will be denominated

$$\left[\tilde{\mathbf{K}}(\tilde{\mathbf{U}})\right]\{\tilde{\mathbf{U}}\} = \{\tilde{\mathbf{F}}(\tilde{\mathbf{U}})\}. \tag{6.101}$$

The iterative scheme starts assuming that the solution $\tilde{\mathbf{U}}^{(r-1)}$ at the $(r-1)^{\text{th}}$ iteration is known. At $r = 1$, the beginning of the iteration, the solution $\tilde{\mathbf{U}}^{(0)}$ is chosen to be the solution of the at the previous time step, i.e.

$$\tilde{\mathbf{U}}^{(0)} = \left\{\begin{matrix} \{\mathbf{U}^n\} \\ \{\mathbf{d}^n\} \end{matrix}\right\}. \tag{6.102}$$

Using the solution from the $(r-1)^{\text{th}}$, the matrix $\tilde{\mathbf{K}}(\tilde{\mathbf{U}}^{(r-1)})$ and vector $\tilde{\mathbf{F}}(\tilde{\mathbf{U}}^{(r-1)})$ are computed. Since both were evaluated using estimated solution vector $\tilde{\mathbf{U}}^{(r-1)}$, it is expected that

$$\left[\tilde{\mathbf{K}}(\tilde{\mathbf{U}}^{(r-1)})\right]\{\tilde{\mathbf{U}}^{(r)}\} \neq \{\tilde{\mathbf{F}}(\tilde{\mathbf{U}}^{(r-1)})\}; \tag{6.103}$$

hence, a residual can be defined, i.e.

$$\mathbf{R} \equiv \left[\tilde{\mathbf{K}}(\tilde{\mathbf{U}}^{(r-1)})\right]\{\tilde{\mathbf{U}}^{(r)}\} - \{\tilde{\mathbf{F}}(\tilde{\mathbf{U}}^{(r-1)})\}. \tag{6.104}$$

A Picard iteration method of successive substitution was employed, i.e. $\tilde{\mathbf{U}}^{(r)}$ is directly obtained from

$$\left[\tilde{\mathbf{K}}(\tilde{\mathbf{U}}^{(r-1)})\right]\{\tilde{\mathbf{U}}^{(r)}\} = \{\tilde{\mathbf{F}}(\tilde{\mathbf{U}}^{(r-1)})\}. \tag{6.105}$$

A preconditioned conjugate gradient method was employed to obtain the solution of such system. Finally, the iteration proceeds until the difference between solutions from two consecutive iterations, measured with the Euclidean norm, is less than tolerance ε

$$\sqrt{\frac{\sum_{m=1}^{3N}\left(\tilde{U}_m^{(r)}-\tilde{U}_m^{(r-1)}\right)^2}{\sum_{m=1}^{3N}\left(\tilde{U}_m^{(r)}\right)^2}}\le\varepsilon\,, \tag{6.106}$$

where $\tilde{U}_m^{(r)}$ and $\tilde{U}_m^{(r-1)}$ are the mth components of the solutions at the rth and $(r-1)^{\text{th}}$ iterations, respectively. Once converged, $\tilde{\mathbf{U}}^{(r)}$ corresponds to the solutions of the problem at the next time step, i.e. $\mathbf{U}^{n+1}$ and $\mathbf{d}^{n+1}$.

E. Results

The solutions of radial and axial components of the linear momentum balance, (6.16) and (6.17) respectively, and equation governing degradation (6.4) are shown and discussed in this section. The dependent variables are $u_r(r,z,t)$, $u_z(r,z,t)$, and $d(r,z,t)$. Other quantities of interest such as the stress and the strain field are obtained through (6.11)-(6.14) and (6.10). The equation governing degradation as yet to be specified and the consequences of different choices is the main concern of this chapter.

1. Mesh generation and non-degraded solution

The finite cylinder was chosen to be constituted by degradable linear elastic-like material given in (6.2) with degradable Young's modulus (cf. (6.3)) and constant Poisson's ratio. The non-degraded Young's modulus E_0 was used to non-dimensionalize stress quantities and as PLLA is mostly incompressible [235,239], a nearly incompressible Poisson's ratio of $v=0.475$ was chosen. Time was also non-dimensionalized with τ_D, a characteristic time of degradation.

The finite cylinder was chosen to have a inner radius $R_i=1$ and a thickness of $h=R_i/2$, yielding an outer radius $R_o=1.5$. The length of the cylinder was chosen to be $2L=16h$. The study is restricted to motions that yield axial symmetry, thus only the top half of the cylinder (of length L) is chosen as the computational domain Ω (cf. (6.18)

spatial discretization of the finite cylinder (mesh I and mesh II)
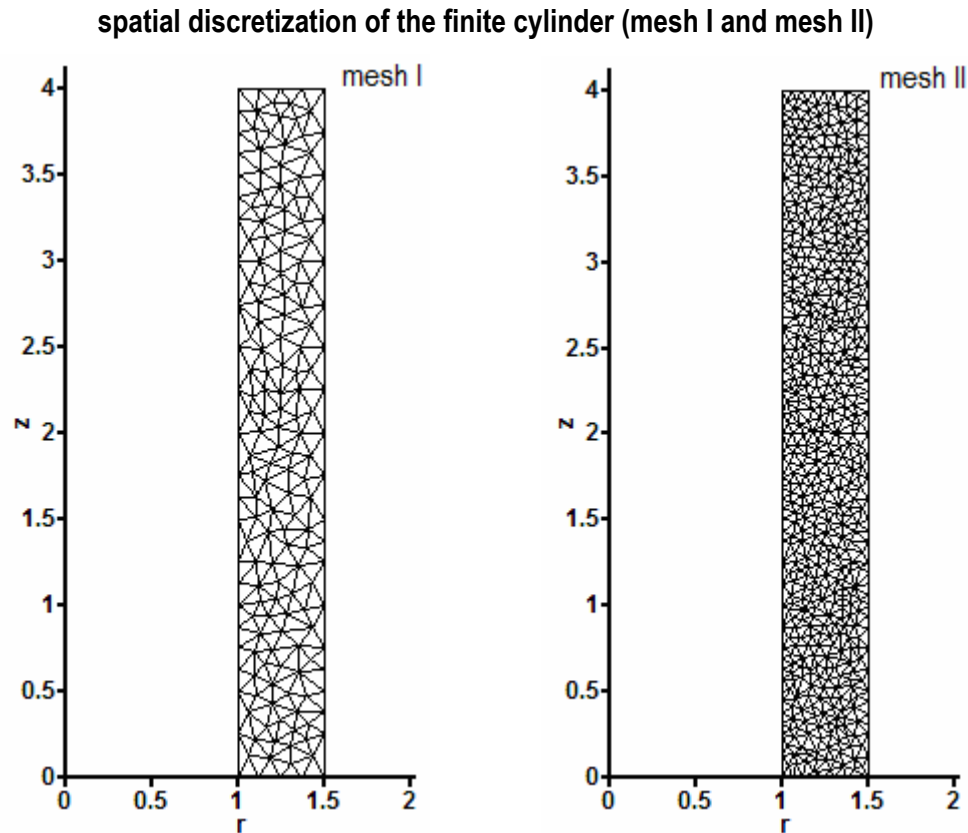
Fig. VI.1. Meshes used to discretize the circumferential section of the finite cylinder. Two meshes were used: mesh I has approximately 8 elements across the thickness, whereas mesh II was obtained with a refinement yielding approximately 16 across. Roughly speaking, each triangle was divided into four smaller triangles. Still, mesh generation is unstructured and both meshes are unrelated.

and symmetry boundary condition at $z = 0$, stated in (6.27)). Two unstructured meshes of triangular elements were generated with Triangle [315]. More precisely, N vertices $P_i = (r_i, z_i)$, $i = 1,..., N$ and M triangles $\tau_{ijk} = \{P_i, P_j, P_k\}$ were defined (cf. Table VI.1 and Fig. VI.1).

In order to obtain a deformation of an appreciable magnitude, it was observed that a transmural pressure of $\Delta P = 0.1 E_0$ would promote an increase of roughly 25% of the location of the inner surface at the central section of the cylinder (cf. Fig. VI.2 at $t = 3$), and hence, this value was chosen to be the representative maximum transmural

Table VI.1. Characteristics of the meshes used. Mesh independence was observed between mesh I and mesh II, hence mesh I was chosen due to its smaller computational load.

Mesh	# nodes	# elements
I	177	302
II	565	1021

pressure in this study. In order to evaluate the validity of the numerical algorithm developed and the computational method coded, a dynamic inflation cycle was subjected to a non-degraded linear elastic body discretized with mesh I and mesh II (shown in Fig. VI.2). $\Delta P(t)$ was chosen to be a continuous function with continuous first derivative (of time) as it was observed that sudden changes in pressure would promote oscillations in the cylinder. Nevertheless, sudden changes in pressure are never achieved realistically. The transmural pressure was achieved solely through inner pressurization, i.e. the outer surface is traction free ($P_o = 0$ in (6.25)) whereas the inner pressure matches the transmural pressure ($P_i(t) = \Delta P(t)$ in (6.24)). Finally, the top surface of the cylinder was chosen to be fixed (i.e. $\mathbf{u} = \mathbf{0}$ in (6.26)).

The method was validated in several ways: (i) if the top surface of the cylinder is subjected to a symmetry boundary condition with respect to the plane $z = L$, the infinite cylinder (solely with one spatial dimension, the radial) classical solution is recovered (not shown); (ii) if the fixed cylinder with L sufficiently large is considered, the one-dimensional solution was also recovered at most of the sections near the central section; (iii) the solution of the full dynamic problem concurred with the solution of the static problem for corresponding transmural pressure $\Delta P = \Delta P(t)$ at time t, meaning that the inertial term in the linear momentum balance (right hand side of (6.15)) is negligible; and finally (iv) the obtained displacements, strains, and stresses field were compared with corresponding quantities obtained with the solution of a full 3D-problem obtained with a finite element commercial package (ABAQUS) and concordance was observed.
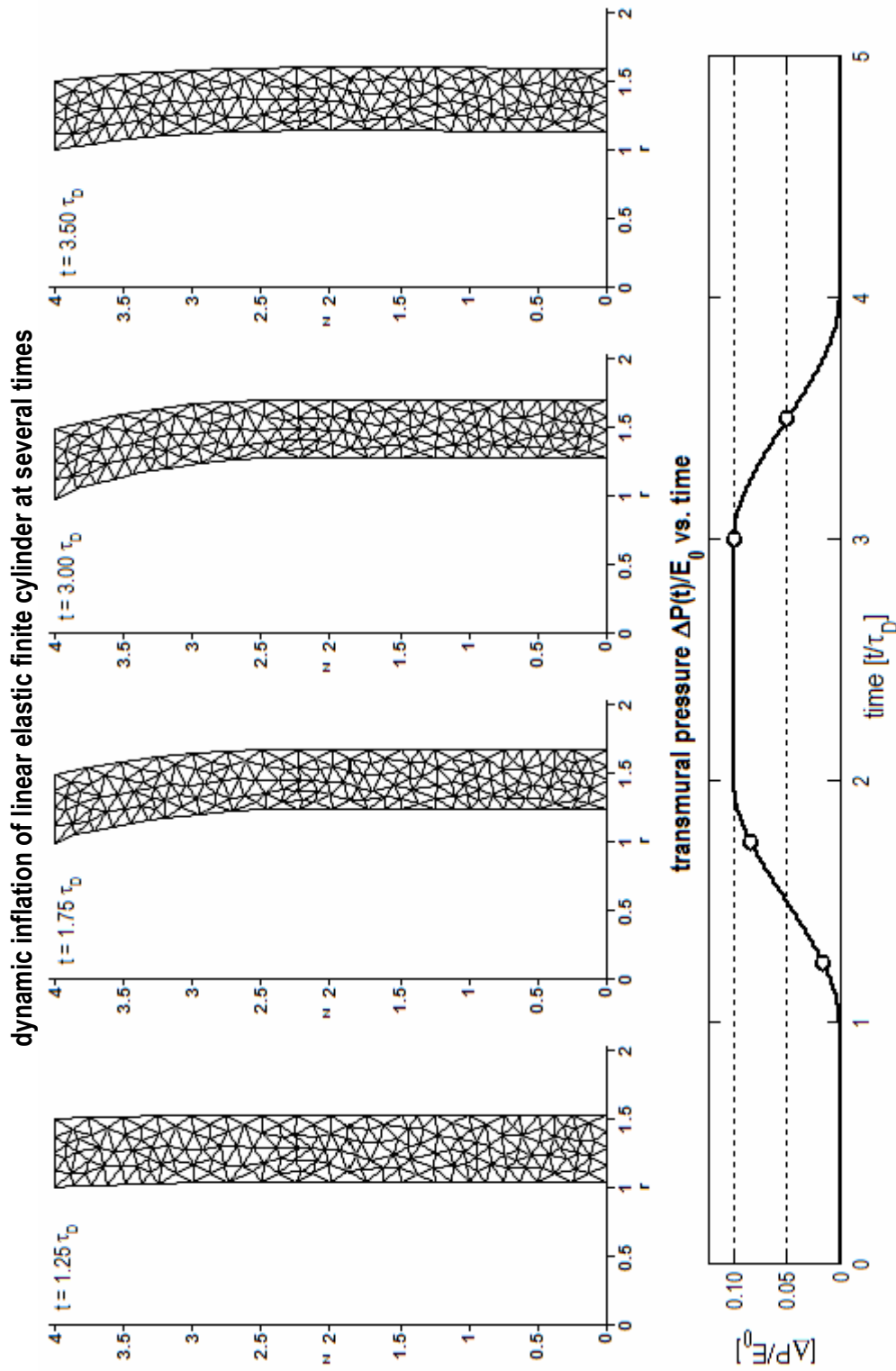
Fig. VI.2. Dynamic inflation of linear elastic finite cylinder at several times. As the inner pressure increases, the cylinder inflates. Due to the boundary conditions, the cylinder is held fixed at the top surface. Note that the amount of inflation is proportional to the transmural pressure; this is an expected feature of the linearized theory. The maximum pressure of $\Delta P/E_0 = 0.1$ was chosen such that it would promote a significant deformation to the cylinder.

linearized stress field in linear elastic finite cylinder at constant ΔP/ E₀ = 0.1
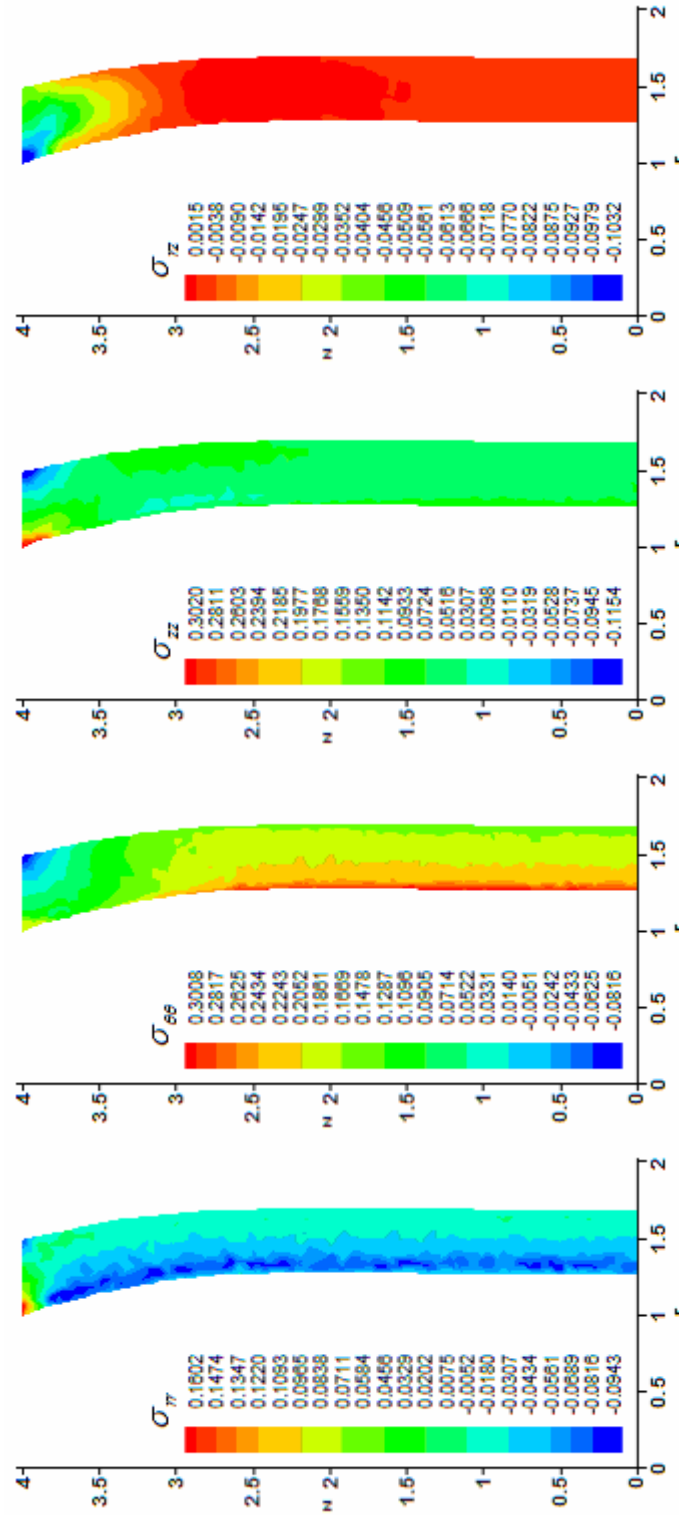
Fig. VI.3. Linearized stress field at the maximum transmural pressure in the linear elastic finite cylinder. Most of the cylinder responds almost like an cylindrical annulus (one of the linearized elasticity classical solutions) that is characterized by a σ_{zz} constant throughout the thickness and null σ_{rz}. The circumferential stress is positive as inflation imparts extension along this direction and the radial stress is mostly dominated by the boundary conditions: it matches the inner pressure at the inner surface and is zero at the outer surface. These conditions are observed for most of the locations far away from the top boundary condition. The effects of the boundary conditions are localized (St. Venant's principle) and hence the stress field degenerates from the classical solution near the top of the cylinder.

The solution obtained for this motion (the deformed shape is shown in Fig. VI.2 whereas the stress field is shown in Fig. VI.3) is characterized by two different regions: the stress field approximates the inflation of an infinite cylinder near the central surface, whereas near the top fixed part the influence of the boundary condition is appreciable.

Near the central section, axial location is somewhat negligible as the cylinder approaches the infinite cylinder solution: (i) u_z is small (but increases as the top surface is closer and the solution departs from the classical elasticity solution that assumes $\mathbf{u} = u_r(r)\mathbf{e}_r$); (ii) ε_{zz} is approximately zero (cf. (6.9) and (6.13)), as either $u_z \approx 0$ or $\partial u_r / \partial z \approx 0$, yielding a constant σ_{zz}; and finally (iii), $\varepsilon_{rz} \approx 0$ and $\sigma_{rz} \approx 0$. On the other hand, near the boundary condition, its effects are appreciable. The inner corner is under a state of traction (in all σ_{rr}, $\sigma_{\theta\theta}$, or σ_{zz}) whereas the reverse effect is observed at the outer corner. Shear stresses σ_{rz} also develop near this region as the material is distorted in the azimuthal direction. Lastly, note that at the inner surface $\sigma_{rr} = -\Delta P / E_0 = -0.1$ is prescribed by the boundary conditions. Finally, it must be remarked that the results presented in Fig. VI.2 and Fig. VI.3 are trivial and were obtained simply for validation of the computation setting developed in the previous section; they shown nothing less than the pure inflation of a linear elastic finite cylinder.

2. Measures of deformation

The equation governing degradation, specified above in a general sense

$$\frac{\partial d}{\partial t} = \mathfrak{D}(d, \boldsymbol{\varepsilon}, \boldsymbol{\sigma}) , \tag{6.4}$$

was not specified yet as it is expected that the form of $\mathfrak{D}(d, \boldsymbol{\varepsilon}, \boldsymbol{\sigma})$ plays an important role in the evolution of the degradation. The rate of increase of degradation is further assumed to be decomposed in

$$\frac{\partial d}{\partial t} = \mathfrak{D}_1(d, \boldsymbol{\varepsilon}, \boldsymbol{\sigma})d + \mathfrak{D}_0(\boldsymbol{\varepsilon}, \boldsymbol{\sigma}) , \tag{6.107}$$

i.e. a term with 1st order kinetics, $\mathfrak{D}_1$ (not precisely due to the possible dependence on d) and a term with 0th order, $\mathfrak{D}_0$, that depends solely on stress and strain. The case which $-\mathfrak{D}_1 = \mathfrak{D}_0$ yields the form

$$\frac{\partial d}{\partial t} = \frac{1}{\tau_D}(1-d)\mathfrak{D}(\boldsymbol{\varepsilon}, \boldsymbol{\sigma}), \qquad (6.108)$$

the linearized counterpart of (4.4) with inverse 1st order kinetics (phenomenologically derived above and corroborated by Rajagopal et al. [266]). τ_D is a characteristic time of degradation that will be used to non-dimensionalize time. This form will be thoroughly used in this study, which concentrates its effort on the form of $\mathfrak{D}(\boldsymbol{\varepsilon}, \boldsymbol{\sigma})$ and its dependence in strain and stress. It is also assumed that $\mathfrak{D}(\mathbf{0}, \mathbf{0}) = 0$, i.e. degradation does not increase if the body is in its natural stress free configuration. Obviously, a different setting could be used: e.g., a basal rate of hydrolysis could be used, e.g. $\mathfrak{D}(\mathbf{0}, \mathbf{0}) = D_0$ and changes in the rate of hydrolysis promoted by stress or strain could be accounted from that point. Nevertheless, in order to solely identify the role of stress and strain in degradation, $\mathfrak{D}(\mathbf{0}, \mathbf{0}) = 0$ was chosen in this study.

In order to develop a sound constitutive theory, one must think on what measures of strain or stress should be the rate of equation (6.108) dependent on. In order to have consistent theories, these measures should not only be frame indifferent (a classical requirement of the non-linear field theories of mechanics, cf. [206], although when dealing with the linearized theory of elasticity, this requirement should be alleviated since the inception of the theory is faulty by itself because not even the linearized strain tensor $\boldsymbol{\varepsilon}$ is frame indifferent), but also coordinate and geometry independent.

Coordinate independence is achieved by choosing measures that are independent of the coordinate system chosen for the representation of $\boldsymbol{\varepsilon}$ and $\boldsymbol{\sigma}$; geometry independence indicates that one should avoid measures of strain that are directly related with the geometries considered for the development of the theory. For example, by choosing in this particular case $\mathfrak{D}$ function of the circumferential strain $\varepsilon_{\theta\theta}$, one is

dilatation and distortion in linearized elastic finite cylinder at constant $\Delta P/E_0 = 0.1$
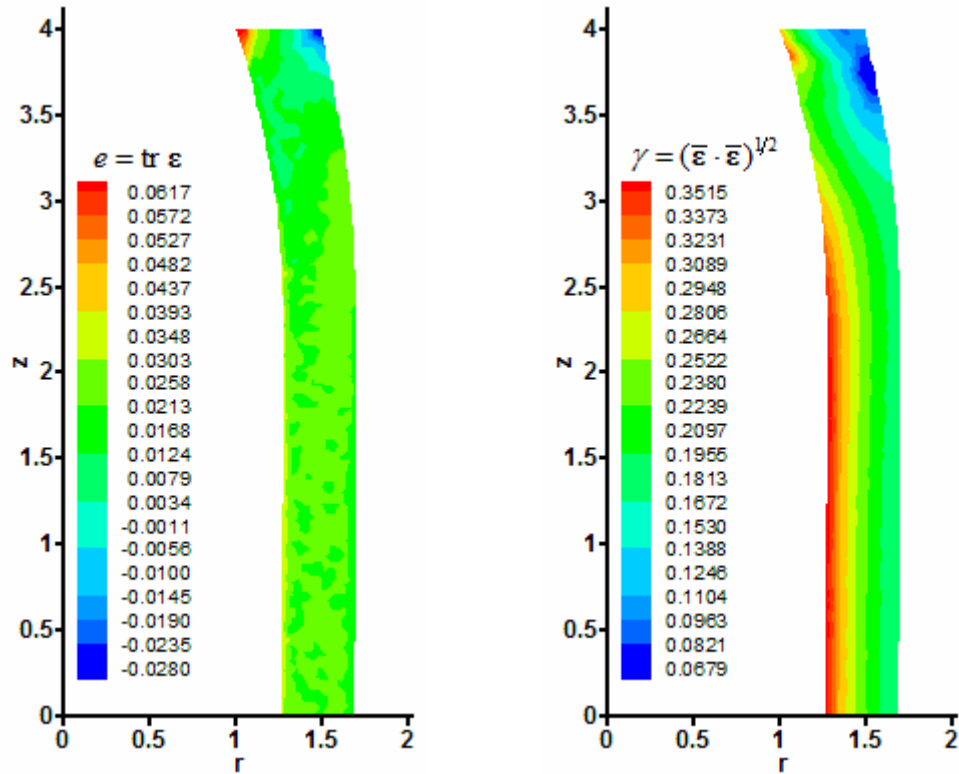
Fig. VI.4 Dilatation and distortion distribution in the finite cylinder at maximum inflation. Dilatation is defined as the 1st invariant of ε whereas the distortion is the norm of the deviatoric strain tensor. Both quantities are scalar measures of deformation. As the material is nearly incompressible, volume change is very small and hence the dilatation is approximately zero almost everywhere. On the other hand, the distortion is a strain measure, by definition, independent of volume change. Its maximum occurs at most of the inner surface as upon inflation, this region extends in the circumferential direction and contracts in the radial direction.

choosing a measure of strain that depends not only on this particular coordinate system but also is related to the body and the motion considered.

One immediate measure of deformation that can be obtained directly from the linearized strain is the dilatation, given by

$$e = \text{tr } \boldsymbol{\varepsilon}, \tag{6.109}$$

which is the 1st invariant of the linearized strain tensor (hence coordinate independent) and is a measure of change of volume per unit volume (shown in the left figure of Fig. VI.4). As the material is chosen in the first place to behave as a nearly incompressible material (with $\nu = 0.475$), the dilatation is appreciably small. In fact, in an incompressible material, $e = 0$ everywhere. Thus, the dilatation is clearly not a measure of deformation on which the rate of degradation of incompressible polymers should depend on.

The deviatoric strain tensor $\overline{\mathbf{\varepsilon}}$ is defined by

$$\overline{\mathbf{\varepsilon}} \equiv \mathbf{\varepsilon} - \frac{1}{3}(\text{tr } \mathbf{\varepsilon})\mathbf{1},\tag{6.110}$$

and is a measure of distortion independent of volume change. Note that by definition the 1st invariant of $\overline{\mathbf{\varepsilon}}$ is zero, i.e. $\text{tr } \overline{\mathbf{\varepsilon}} = 0$. A coordinate-independent scalar measure of distortion, γ, can be defined as the magnitude of the deviatoric strain tensor, given by

$$\gamma \equiv (\overline{\mathbf{\varepsilon}} \cdot \overline{\mathbf{\varepsilon}})^{1/2} = \sqrt{\text{tr } (\overline{\mathbf{\varepsilon}}^{\text{T}}\overline{\mathbf{\varepsilon}})}.\tag{6.111}$$

Henceforth, γ will be referred to as the distortion. For the inflation of the finite cylinder, the distortion is computed directly from (6.110) with (6.10) and is shown in the right figure of Fig. VI.4 for static inflation of the non-degradable counterpart for $\Delta P/E_0 = 0.1$). The distortion achieves a maximum throughout most of the inner wall of the cylinder. The less distorted regions are near the outer top corner.

3. *Inflation of finite cylinder that degrades through distortion*

If degradation is chosen to increase linearly with the amount of distortion, then $\mathfrak{D}(\mathbf{\varepsilon}, \mathbf{\sigma}) = \gamma$ and the equation governing degradation becomes
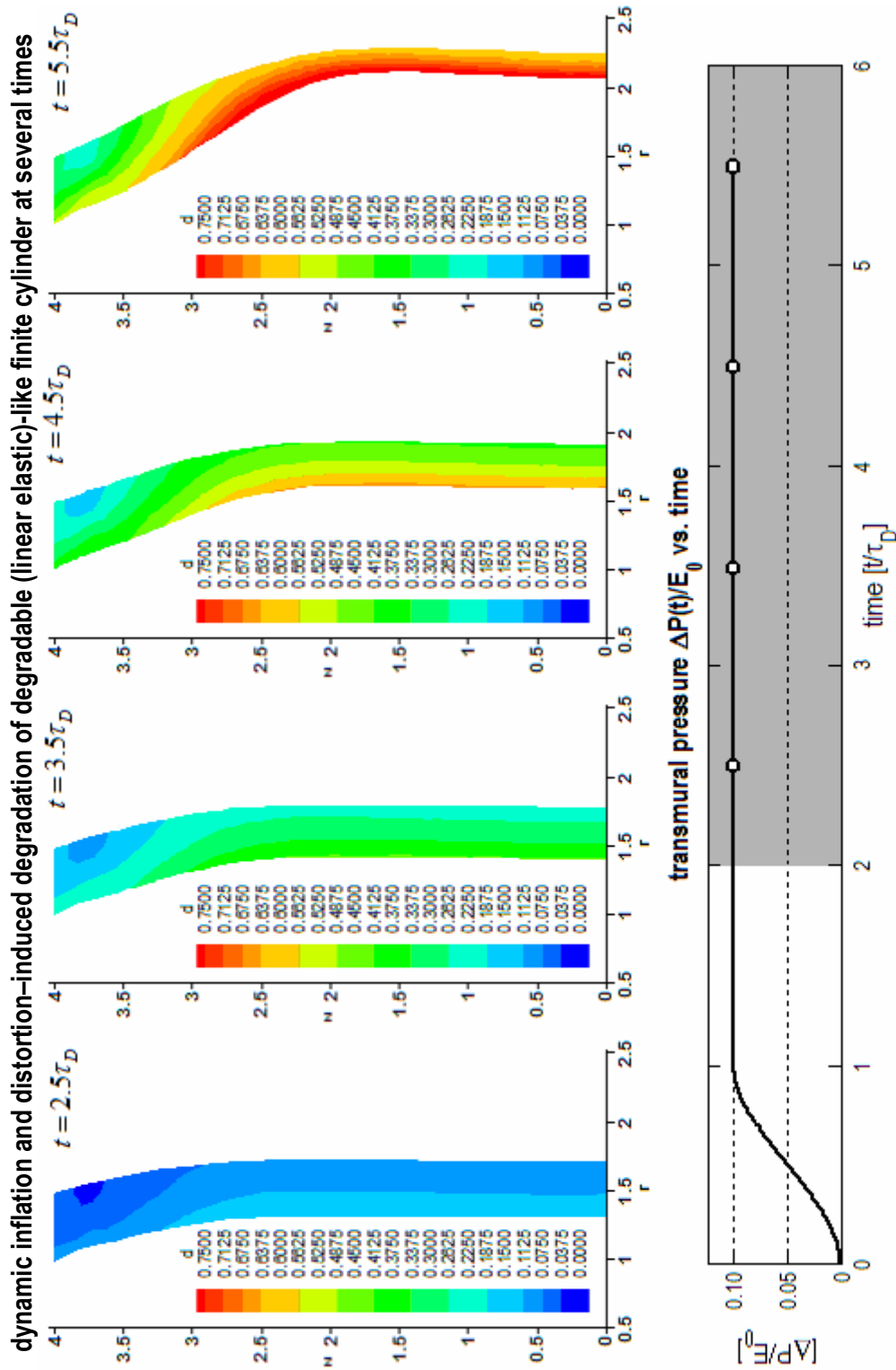
Fig. VI.5. Dynamic inflation and degradation of linear elastic cylinder that degrades linearly with distortion. Following the distribution of the distortion shown in Fig. VI.4, the cylinder degrades most near the inner surface where distortion achieves its maximum. As time proceeds, degradation proceeds outwards. Due to softening, the deformation that the same transmural pressure achieves increases, promoting more degradation towards a point when the numerical scheme breaks down.

$$\frac{\partial d}{\partial t} = \frac{1}{\tau_D}(1-d)\gamma,$$ (6.112)

where the right hand side is related with the dependent variables u_r and u_z through (6.111), (6.110), and (6.10). Equation (6.112) is solved simultaneously with equations (6.16) and (6.17) with initial and boundary conditions (6.24)-(6.30) following the numerical procedure described in the previous section. Input $\Delta P(t)$ was chosen to be

$$\Delta P(t)/E_0 = \begin{cases} 0.1\left[3(t/\tau_D)^2 - 2(t/\tau_D)^2\right] & t/\tau_D \leq 1 \\ 0.1 & t/\tau_D > 1 \end{cases},$$ (6.113)

and an activation criterion was set such that degradation is only active if $t/\tau_D \geq 2$, which inhibits degradation from occurring when the cylinder is being transiently loaded from $t/\tau_D = 0$ to $t/\tau_D = 1$ and a period of rest at the non-degraded deformed position from $t/\tau_D = 1$ to $t/\tau_D = 2$ (cf. bottom figure of Fig. VI.5, where the active degradation period is shown in gray).

The increase of degradation is ultimately related with the distribution of γ (cf. Fig. VI.4). Note that the distortion of the cylinder also changes with time as it softens and allows greater deformations. The region where the cylinder is less distorted is the region that degrades less (the region near the outer top corner, which degrades only 20% whereas near the inner wall at the central section, degradation achieves approximately 100%). As time proceeds, degradation increases in an inhomogeneous fashion from the inner wall to towards the outer wall. With the increase of degradation, the cylinder deforms to a greater extent upon the same constant transmural pressure, i.e. it creeps outwards. Due to deformation, the thickness decreases and ultimately it is unable to withstand the transmural pressure allowing such great inflations and causing the asymptotic increase of degradation. The behavior is concordant with the one shown in Fig. IV.9, Fig. V.7, and Fig. V.12.

**maximum shear strain and 2nd invariant of the deviatoric strain tensor
in linearized elastic finite cylinder at constant $\Delta P/E_0 = 0.1$**

Fig. VI.6. Maximum shear strain and 2nd invariant of the deviatoric strain tensor distribution in the finite cylinder at maximum inflation. Naturally, the maximum shear strain occurs at the inner top corner and its value is dramatically greater than everywhere else. The 2nd invariant of the deviatoric strain tensor is another common scalar strain measure. Its overall value is significantly greater than the maximum shear strain.

4. Principal directions of strain

Other measures of deformation can be obtained with the principal strains obtained with a spectral decomposition of the linearized strain tensor $\boldsymbol{\varepsilon}$. The principal strains $\varepsilon_1 \geq \varepsilon_2 \geq \varepsilon_3$ are the eigenvalues of $\boldsymbol{\varepsilon}$ and for this particular problem (cf. (6.10)) are given by

$$\varepsilon_1 = \frac{\varepsilon_{rr} + \varepsilon_{zz}}{2} + \sqrt{(\varepsilon_{rr} - \varepsilon_{zz})^2 + 4\varepsilon_{rz}^2} , \qquad (6.114)$$

$$\varepsilon_2 = \varepsilon_{\theta\theta} , \qquad (6.115)$$

$$\varepsilon_3 = \frac{\varepsilon_{rr} + \varepsilon_{zz}}{2} - \sqrt{(\varepsilon_{rr} - \varepsilon_{zz})^2 + 4\varepsilon_{rz}^2} . \qquad (6.116)$$

The maximum shear strain, γ^{max}, can be obtained with the principal strains through

$$\gamma^{max} = \frac{\varepsilon_1 - \varepsilon_3}{2} . \qquad (6.117)$$

Another common scalar measure can be obtained with the 2nd invariant of the deviatoric strain, $J_2^{\bar{\varepsilon}}$, which with respect to the principal strains is given by

$$J_2^{\bar{\varepsilon}} = \frac{(\varepsilon_1 - \varepsilon_2)^2 + (\varepsilon_1 - \varepsilon_3)^2 + (\varepsilon_2 - \varepsilon_3)^2}{6} . \qquad (6.118)$$

Both γ^{max} and $J_2^{\bar{\varepsilon}}$ are shown in Fig. VI.6 for static inflation under $\Delta P / E_0 = 0.1$. Their distribution follows a similar trend as the distortion: (i) both show maxima at the inner top corner where the material is most deformed; (ii) the magnitude of $J_2^{\bar{\varepsilon}}$ is slightly greater than the magnitude of γ^{max}. On the other hand, (iii) while the distortion was greatest at most of the inner wall, these two measures exhibit an average value near the central section.

The evolution of degradation was analyzed when its rate is considered to be linear with $J_2^{\bar{\varepsilon}}$, i.e. $\mathfrak{D}(\varepsilon, \sigma) = J_2^{\bar{\varepsilon}}$, and then

$$\frac{\partial d}{\partial t} = \frac{1}{\tau_D} (1 - d) J_2^{\bar{\varepsilon}} . \qquad (6.119)$$

Upon inflation, the finite cylinder degrades in a similar way as when degradation was chosen to increase linearly with distortion (the results for this case are shown in Fig. VI.7; the case with maximum shear is not shown but it was investigated: the
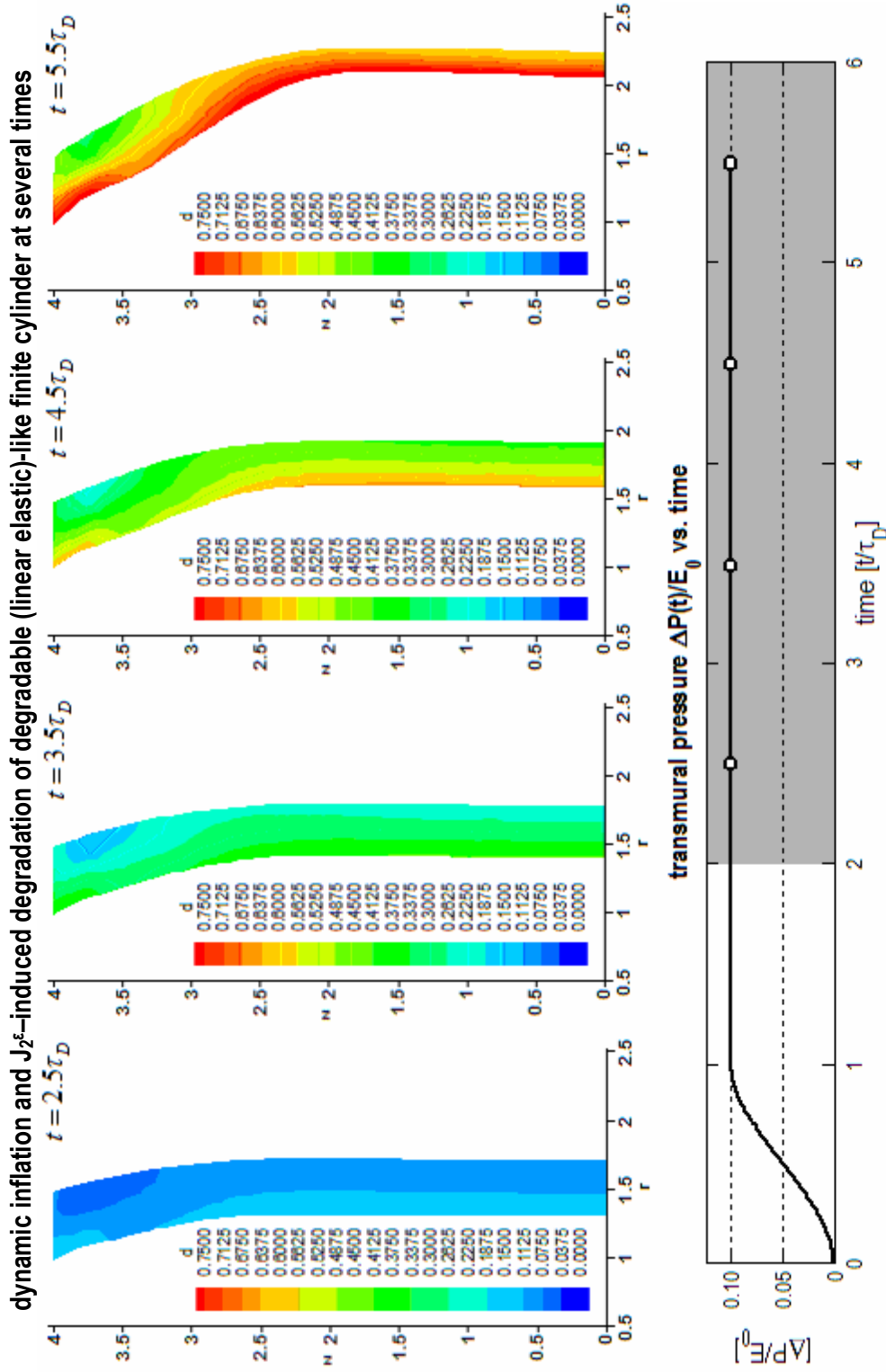
Fig. VI.7. Dynamic inflation and degradation of linear elastic cylinder that degrades linearly with the 2nd invariant of the deviatoric strain tensor. Following the distribution of the 2nd invariant of the deviatoric strain shown in Fig. VI.6, degradation occurs mostly where its value is greater, i.e. near the inner wall and at the inner top corner. Note the similarity between this and the previous case (cf. Fig. VI.5). Still, slight differences exist: the top outer corned degrades to a lesser extent.

cylinder degrades almost exclusively near the top inner corner). Note that near the fixed part, the cylinder degrades thoroughly and to a greater extent: this fact is due to the relative maximum in $J_2^{\bar{\varepsilon}}$. While the outer top corner remained almost non-degraded for degradation with distortion, in this case it degrades to a greater extent and hence imparts a different inflation profile to the cylinder.

5. Measures of stress

Similarly, degradation might increase due to existing stress in the material. The principal stresses $\sigma_1 \geq \sigma_2 \geq \sigma_3$ are related to the stress components (6.11)-(6.14) through

$$\sigma_1 = \frac{\sigma_{rr} + \sigma_{zz}}{2} + \sqrt{(\sigma_{rr} - \sigma_{zz})^2 + 4\sigma_{rz}^2} \,, \tag{6.120}$$

$$\sigma_2 = \sigma_{\theta\theta} \,, \tag{6.121}$$

$$\sigma_3 = \frac{\sigma_{rr} + \sigma_{zz}}{2} - \sqrt{(\sigma_{rr} - \sigma_{zz})^2 + 4\sigma_{rz}^2} \,. \tag{6.122}$$

Similarly, common scalar measures of the amount of stress are the maximum shear stress, τ^{max} (commonly used as a failure criterion for brittle material, the Tresca criterion), given by

$$\tau^{\mathrm{max}} = \frac{\sigma_1 - \sigma_3}{2} \,, \tag{6.123}$$

and the 2$^{\mathrm{nd}}$ invariant of the deviatoric stress, $J_2^{\bar{\sigma}}$ (related to the elastic energy of distortion and commonly used for the von Mises yield criterion), which is related to the principal stresses through

$$J_2^{\bar{\sigma}} = \frac{(\sigma_1 - \sigma_2)^2 + (\sigma_1 - \sigma_3)^2 + (\sigma_2 - \sigma_3)^2}{6} \,. \tag{6.124}$$

Both measures are shown in Fig. VI.8 for non-degraded cylinder subjected to a static inflation of $\Delta P / E_0 = 0.1$. Interestingly, the distribution of τ^{max} is comparable to the distribution of γ (cf. Fig. VI.4). On the other hand, the distribution of $J_2^{\bar{\sigma}}$ follows
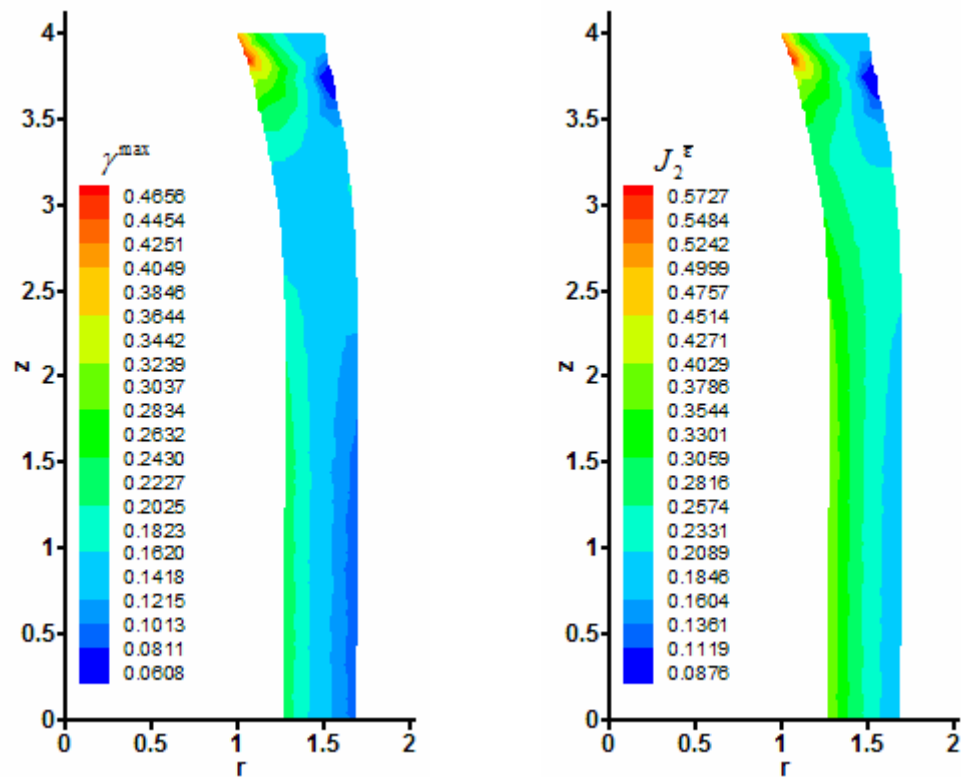
Fig. VI.8. Maximum shear stress and 2nd invariant of deviatoric stress tensor distribution in the finite cylinder under maximum inflation. Both quantities are common scalar measures of stress used in plasticity as yield conditions. The distribution of the maximum shear stress is very similar to the distortion (cf. Fig. VI.4). The 2nd invariant of the deviatoric stress tensor is proportional to the 2nd invariant of the deviatoric strain tensor (cf. Fig. VI.6). Indeed, they are related through (6.125).

directly the distribution of $J_2^{\bar{\varepsilon}}$. In fact, it can be shown that the deviatoric strain $\bar{\varepsilon}$ and the deviatoric stress $\bar{\sigma}$ are related through

$$\bar{\sigma} = 2\mu\bar{\varepsilon} ; \tag{6.125}$$

thus it follows that $J_2^{\bar{\sigma}}$ and $J_2^{\bar{\varepsilon}}$ are related. Nevertheless, it is important to remark that the case with increase of degradation linear with $J_2^{\bar{\sigma}}$, i.e. when $\mathfrak{D}(\varepsilon,\sigma) = J_2^{\bar{\sigma}}$ yielding
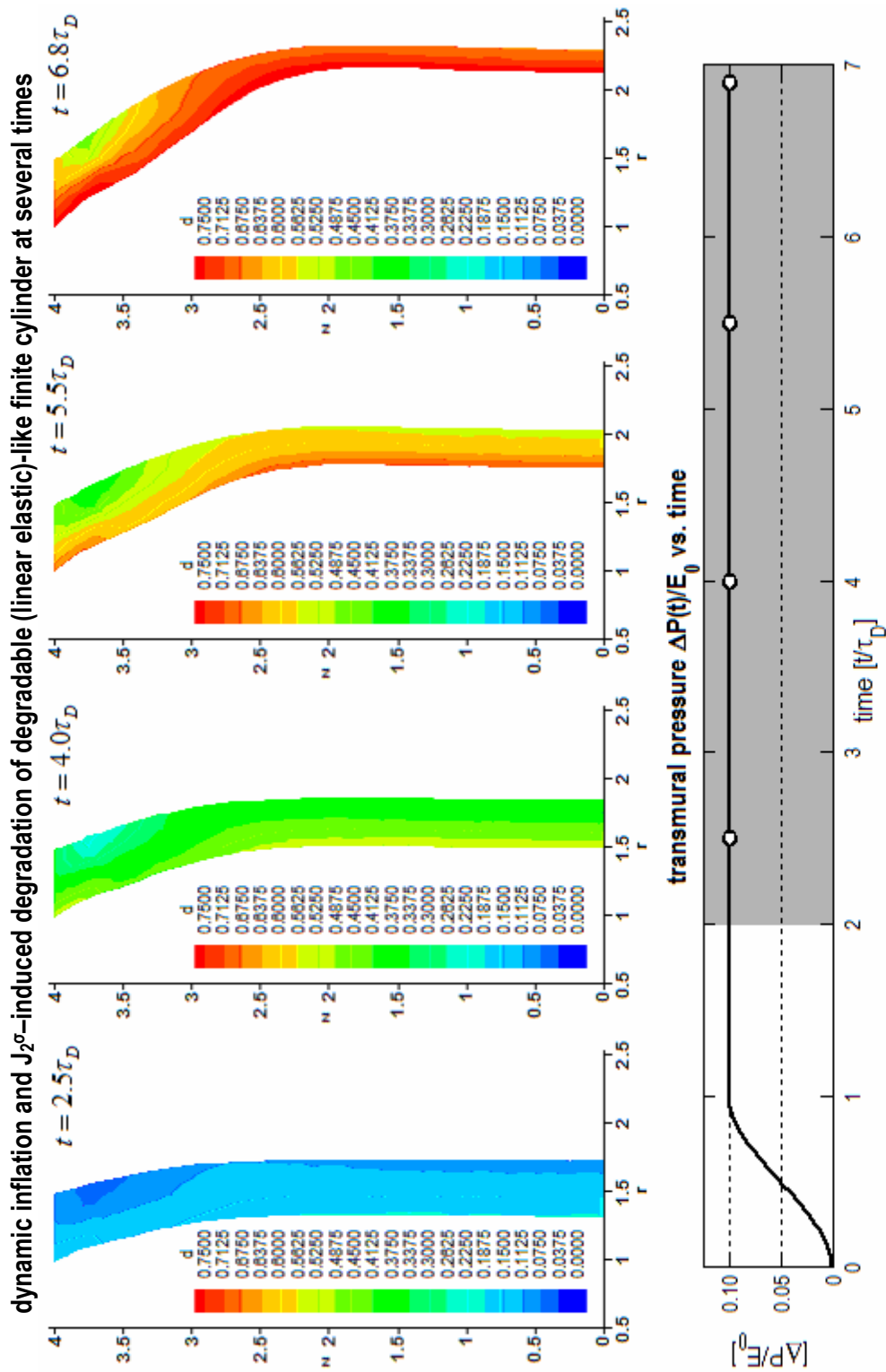
Fig. VI.9. Dynamic inflation and degradation of linear elastic cylinder that degrades linearly with the 2nd invariant of the deviatoric stress tensor. Although the 2nd invariant of the deviatoric stress is proportional to the 2nd invariant of the deviatoric strain, the evolution of degradation that each one yields is somewhat different. This is the case that promotes more extensive degradation to most of the cylinder and the same load promotes the greatest inflation along the height of the cylinder.

$$\frac{\partial d}{\partial t} = \frac{1}{\tau_D}(1-d)J_2^{\bar{\sigma}},$$

(6.126)

shows different characteristics than the previous studied case. This is due to the fact that in (6.119), the rate ($J_2^{\bar{\varepsilon}}$) is dependent solely on the current deformation, whereas if in (6.126) $J_2^{\bar{\sigma}}$ is substituted with (6.125), the rate will also take into account the mechanical property μ that decreases with degradation. Indeed, the degradation upon inflation following a rate that is linear with the energy of distortion $J_2^{\bar{\sigma}}$ (shown in Fig. VI.9) shows differences between the two previous analyzed cases (linear with γ, shown in Fig. VI.5, and linear with $J_2^{\bar{\varepsilon}}$, shown in Fig. VI.7): the cylinder is the most thoroughly degraded, and creep occurs to the most extent of the cylinder length.

6. Other measures of deformation

Other measures of deformation suitable for tubular structures were developed based on previous work of Criscione [316]. Four measures of deformation γ_i were considered and their linearized theory counterparts $\tilde{\gamma}_i$ are shown in Fig. VI.10 for static inflation of a non-degraded cylinder: (i) γ_1 is associated with dilatation strain and is given by

$$\gamma_1 = \ln J,$$

(6.127)

where J is the determinant of the deformation gradient, which with (2.35) and (6.9) yields

$$\begin{aligned}\tilde{\gamma}_1 &= \ln\left\{\left(1+\frac{u_r}{r}\right)\left[\left(1+\frac{\partial u_r}{\partial r}\right)\left(1+\frac{\partial u_z}{\partial z}\right)-\frac{\partial u_r}{\partial z}\frac{\partial u_z}{\partial r}\right]\right\}\\&= \ln\left(1+\frac{\partial u_r}{\partial r}+\frac{u_r}{r}+\frac{\partial u_z}{\partial z}\right)+o(\delta^2) = \ln(1+e)+o(\delta^2)\end{aligned}$$

(6.128)

Fig. VI.10. Distribution of other scalar measures of deformation in linear elastic finite cylinder under maximum inflation. Linearized versions of the scalar invariants for tubular structures developed by Criscione [316] were considered. The first invariant accounts volume change and due to incompressibility is approximately zero everywhere. The second is associated with axial strain and due to the particular motion considered (pure inflation) its maximum and minimum occur at the fixed surface: the inner corner is under axial extension whereas the outer corner, axial compression. The third invariant measures the inflation strain: due to the boundary condition, it is zero everywhere in the top surface (no inflation occurs there) whereas its overall distribution is very similar to the distortion presented before. Finally, the 4th invariant is related with telescopic shear. Telescopic shear occurs almost exclusively near the fixed boundary condition.

where e is the dilatation and due to nearly incompressibility of the material, its distribution is approximately zero everywhere in the cylinder (cf. first figure of Fig. VI.10); (ii) γ_2 is associated with axial strain and is given by

$$\gamma_2 = \frac{3}{2} \ln \lambda_z,$$ (6.129)

where $\lambda_z = J^{-1/3} \mathbf{z} \cdot \mathbf{FZ}$ (and $\mathbf{z}$ and $\mathbf{Z}$ are orthonormal basis vectors in the current and reference configurations corresponding to the axis of the cylinder, cf. [316] for details), its linearized counterpart is given by

$$\tilde{\gamma}_2 = \frac{3}{2} \ln \left[(1+e)^{-1/3} \left(1 + \frac{\partial u_z}{\partial z} \right) \right],$$ (6.130)

and its distribution (shown in the second figure of Fig. VI.10) is characterized by being approximately zero at most of the central part of the cylinder and strongly positive at the inner top corner and strongly negative at the outer top corner due to states of extension and compression respectively; (iii) γ_3 is associated with luminal inflation and is given by

$$\gamma_3 = 2 \ln \zeta,$$ (6.131)

where $\zeta = J^{-1/3} \lambda_z^{1/2} (\mathbf{q} \cdot \mathbf{FQ})$ ($\mathbf{q}$ and $\mathbf{Q}$ are orthonormal basis vectors in the current and reference configurations corresponding to the circumferential directions), its linearized counterpart is given by

$$\tilde{\gamma}_3 = 2 \ln \left[(1+e)^{-1/6} \left(1 + \frac{\partial u_z}{\partial z} \right)^{3/2} \frac{u_r}{r} \right],$$ (6.132)

and its distribution (shown in the third figure of Fig. VI.10) is directly related with the amount of circumferential extension that each portion of cylinder undergoes, i.e. strongly positive at the inner wall and zero at the top (fixed) surface; and finally, (iv) γ_4

is associated with axial or telescopic shear, a deformation wherein the inner wall is displaced axially relative to the outer wall, and is given by

$$\gamma_4 = \frac{\mathbf{z} \cdot \mathbf{FR}}{\mathbf{z} \cdot \mathbf{FZ}}, \tag{6.133}$$

where $\mathbf{R}$ is the orthonormal basis vector in the reference configuration corresponding to the radial direction, its linearized counterpart is given by

$$\tilde{\gamma}_4 = \frac{\dfrac{\partial u_z}{\partial r}}{1 + \dfrac{\partial u_z}{\partial z}}, \tag{6.134}$$

and its distribution (shown in the fourth figure of Fig. VI.10) is characterized by being zero at the central surface and increasing in magnitude (but negative) as the top surface is approached due to an increase in telescopic shear arising from the combined effects of inflation and the fixed boundary condition.

When degradation is considered to increase linearly with $\tilde{\gamma}_3$, i.e. due to the amount of inflation occurring, the equation governing equation becomes

$$\frac{\partial d}{\partial t} = \frac{1}{\tau_D}(1-d)\tilde{\gamma}_3. \tag{6.135}$$

With this, it is seen that due to the distribution of $\tilde{\gamma}_3$, the top surface does not undergo any degradation (as $\tilde{\gamma}_3 = 0$ at this location). The evolution of the cylinder (shown in Fig. VI.11) follows closely all the previous cases, i.e. degradation proceeds from the inner surface towards the outer surface, promoting the cylinder to creep while being fixed at the top. This case is the case that promotes less degradation on the outer top corner because the amount of inflation occurring around that region will always be constrained by the boundary condition. Due to that, the portion of length that creeps and is degraded the most is also the least in between all the cases considered (cf. Fig. VI.5, Fig. VI.7, and Fig. VI.9).
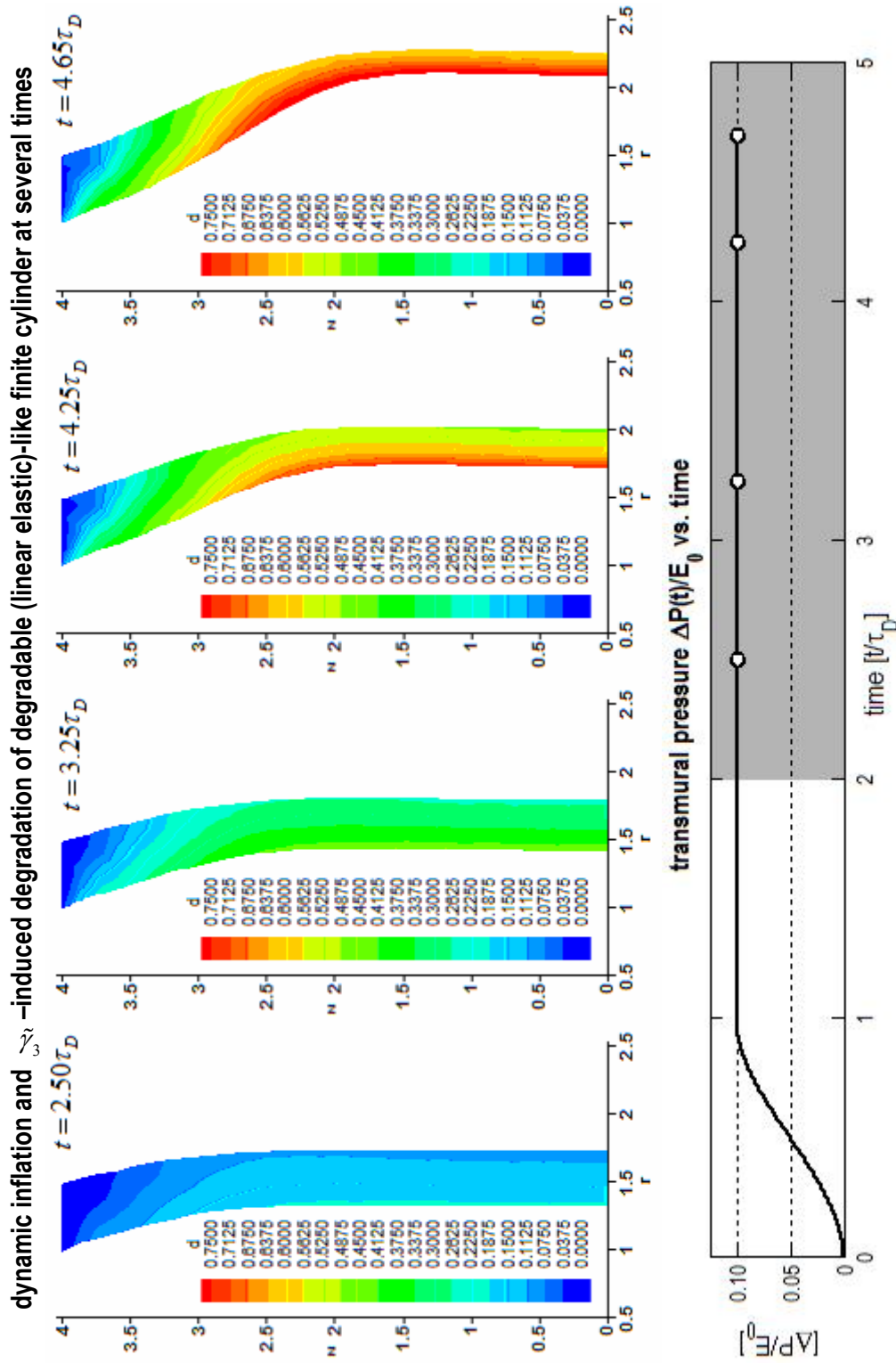
Fig. VI.11. Dynamic inflation and degradation of linear elastic cylinder that degrades linearly with a strain measure associated with luminal inflation. Although the distribution of $\tilde{\gamma}_3$ is similar to the distribution of distortion (cf. Fig. VI.4), the evolution of degradation with a rate linear in $\tilde{\gamma}_3$ yields is different. Note that the top surface does not inflate due to the boundary condition yielding the case that promotes least extensive degradation to most of the cylinder.
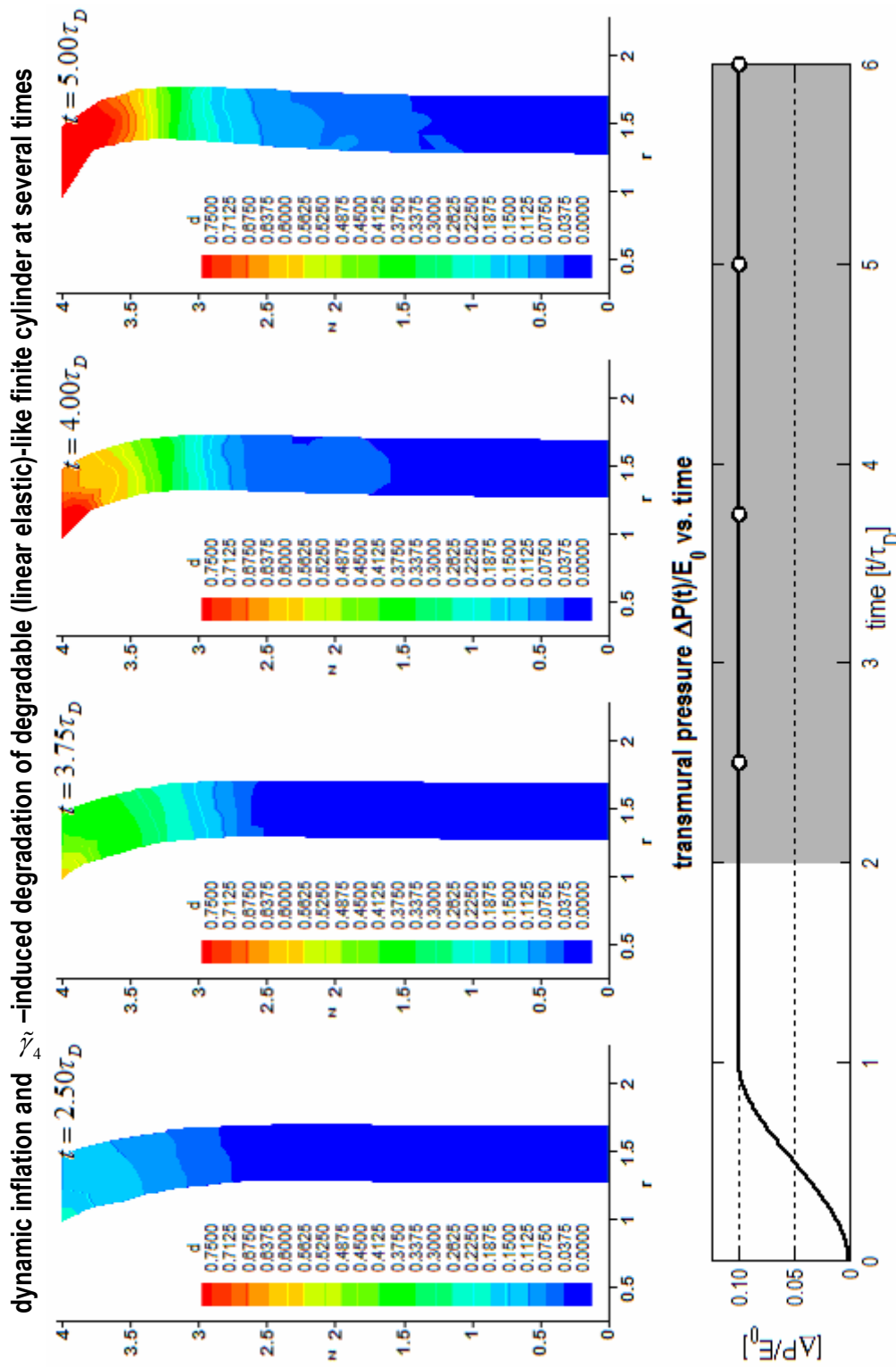
Fig. VI.12. Dynamic inflation and degradation of linear elastic cylinder that degrades linearly with a strain measure associated with axial shear. Degradation is mostly confined to the top part of the cylinder where axial shear is present due to the boundary condition. The evolution of degradation and the inflation of the cylinder during its course is dramatically different from all the previously studied cases.

On the other hand, when degradation is considered to increase linearly with the magnitude of $\tilde{\gamma}_4$, i.e. due to the amount of telescopic shear occurring upon inflation, the degradation governing equation becomes

$$\frac{\partial d}{\partial t} = \frac{1}{\tau_D}(1-d)\left|\tilde{\gamma}_4\right|, \tag{6.136}$$

and due to the remarkably different distribution of $\tilde{\gamma}_4$, the behavior of the degradable cylinder is remarkably different (shown in Fig. VI.12). Degradation increase is confined to only near the top surface because no appreciable telescopic shear occurs at most of its length (and indeed is zero at the central surface). As the material near the top part becomes softer, it is more prone to inflate and promote more degradation.

7. Response to inflation cycles

The last result presented in this chapter illustrates how the natural configuration of a degradable hyperelastic-like material does not evolve. The finite cylinder was subjected to two cycles in transmural pressure (cf. Fig. VI.13). Note that the cylinder recovers its initial shape after each inflation cycle with accompanied degradation. The stress free configuration is the same after any extent of degradation.

A reference configuration is characterized not only by the geometry (although considered locally) but also the material properties present in the stress representation from this reference configuration. Hence, degradation imparts changes in the response of the body not by an evolution of the reference configuration per se, but through an evolution of the mechanical properties associated with that reference configuration.

Lastly, note that this is a characteristic of degradable hyperelastic-like materials. If one considers either a viscoelastic or a degradable viscoelastic-like material, the natural configuration will evolve.
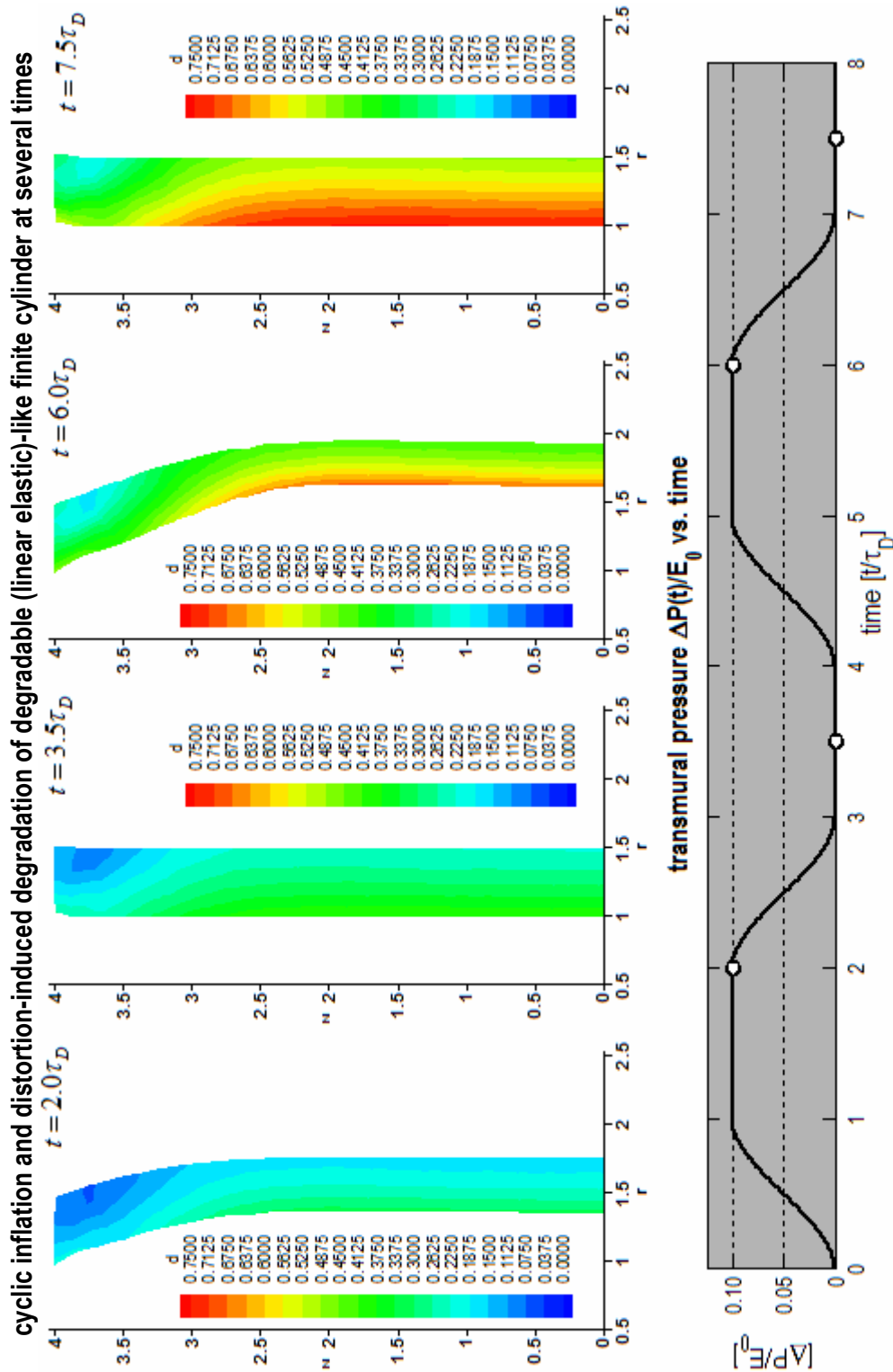
Fig. VI.13. Cyclic inflation and degradation of linear elastic cylinder that degrades linearly with the distortion. Note that no permanent set is induced in the degradable (linear elastic)-like material. Degradation is only responsible for the reduction of the material properties. At zero transmural pressure, the cylinder is not inflated, but after one or two cycles the Young's modulus is no longer constant throughout the body.

CHAPTER VII

BIODEGRADABLE STENTS

The ability to apply the analytical techniques developed previously to the design of implantable medical devices is hampered by the usual complex geometries encountered. In order to render real life applicability to these models they must be incorporated into a finite element formulation using the extendable capabilities of commercially available software packages, such that e.g. real stent geometries could be analyzed. The IBVP dealt with in the previous chapters (uniaxial extension and pure inflation of finite cylinder) serve as validation tools for such implementation.

A. ABAQUS user subroutines

The constitutive model that has been developed is implemented in finite element software ABAQUS/STANDARD through user subroutines. User subroutines are written in FORTRAN. This feature allows the user to define almost any constitutive model of arbitrary complexity into ABAQUS. The subroutines usually provide several kinematical quantities at the beginning and end of each step, such as the deformation gradient, and require some quantity, such as the stress, to be determined by the user's choice with the given inputs.

For a generic user material, UMAT is the subroutine most commonly used. The deformation gradient at the end of the step is provided as a guess; then the stress is computed and iterated until the converged solution is obtained. In estimating the value of the deformation gradient, ABAQUS uses the tangent modulus (defined as $\partial \Delta \mathbf{T} / \partial \Delta \mathbf{E}$). The tangent modulus must be supplied in the UMAT. An exact definition of the consistent tangent modulus is necessary to ensure quadratic convergence. However, it is often approximated in favor of a simpler algorithm and computation speed. This may result in the loss of quadratic convergence. In the current work, the tangent modulus that is the same as the elasticity matrix of the corresponding material under the approximation of infinitesimal deformation gradient is used (following [317]).

Other user subroutines allow other types of features. UHYPER is used to model incompressible hyperelastic materials: its inputs are the values of I_C and II_C and requires the user to specify the amount of stored energy and the corresponding derivatives with respect to the relevant stretch invariants. Furthermore, ABAQUS allows the definition of fields and state variables. A user defined subroutine USDFLD is called at each time increment and expects the computation of the defined fields following an algorithm provided by the user. Most of the possible variables on which such fields can depend on are either obtained directly or computed inside the subroutine.

B. Linear elastic material that degrades

The linear elastic material that degrades developed in the previous chapter was implemented in the first place in order to provide an enough simple case that would allow verification from an semi-analytical solution.

At the beginning of each time step, ABAQUS provides the strain tensor $\mathbf{E}$ and the corresponding increment $\mathbf{\Delta E}$. Using (2.38), the linearized strain tensors at the beginning and end of the time step, $\mathbf{\varepsilon}^t$ and $\mathbf{\varepsilon}^{t+\Delta t}$ are obtained. Simply through (2.122), the linearized stress at the end of the time step $\mathbf{\sigma}^{t+\Delta t}$ (one goal of the UMAT) is determined. The other goal is the tangent modulus which is simply given by

$$
\left(\tilde{\mathbb{C}} \right) = \begin{pmatrix} \lambda+2\mu & \lambda & \lambda & 0 & 0 & 0 \\ \lambda & \lambda+2\mu & \lambda & 0 & 0 & 0 \\ \lambda & \lambda & \lambda+2\mu & 0 & 0 & 0 \\ 0 & 0 & 0 & 2\mu & 0 & 0 \\ 0 & 0 & 0 & 0 & 2\mu & 0 \\ 0 & 0 & 0 & 0 & 0 & 2\mu \end{pmatrix},
\tag{7.1}
$$

where the notation $\left(\tilde{\mathbf{\sigma}} \right) = \left(\sigma_{11},\sigma_{22},\sigma_{33},\sigma_{12},\sigma_{13},\sigma_{23} \right)$ was used.

If the material is degradable, the mechanical properties λ and μ are functions of degradation. Choosing the Young's modulus the depreciable property (cf. (6.3)), λ and μ are computed from $E(d)$ and v, the Poisson's ratio, through (2.123) and (2.124).

spatial discretization of the finite cylinder
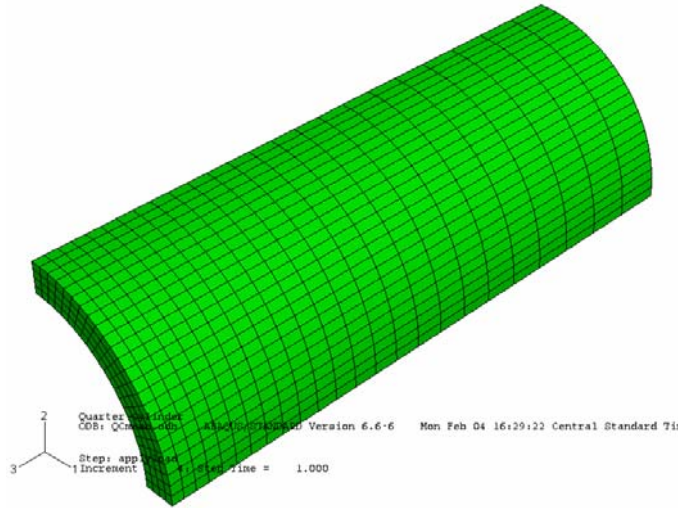
Fig. VII.1. Mesh used to discretized the finite cylinder domain in ABAQUS. Note that due to axis-symmetry, only the profile would be necessary (such as performed in the previous chapter). Nevertheless, the desire to analyze the full 3D performance of the user subroutines, on quarter of the cylinder with symmetry conditions on each side was modeled.

The UMAT allows state variables (defined in ABAQUS) to be associated with it. The degradation d is considered as a state variable and computed at the end of each time step. The equation governing degradation (6.108) is integrated as follows

$$\int_{t}^{t+\Delta t}\frac{\partial d}{\partial t}ds = d(t+\Delta t)-d(t) = \int_{t}^{t+\Delta t}\frac{1}{\tau_D}(1-d)\mathfrak{D}(\boldsymbol{\varepsilon},\boldsymbol{\sigma})ds , \qquad (7.2)$$

which yields the numerical scheme (with trapezoid integration rule)

$$d^{t+\Delta t} = \frac{d^t(t)+\dfrac{\Delta t}{\tau_D}\left[\mathfrak{D}(\boldsymbol{\varepsilon}^{t+\Delta t},\boldsymbol{\sigma}^{t+\Delta t})-(1-d^t)\mathfrak{D}(\boldsymbol{\varepsilon}^t,\boldsymbol{\sigma}^t)\right]}{1+\mathfrak{D}(\boldsymbol{\varepsilon}^{t+\Delta t},\boldsymbol{\sigma}^{t+\Delta t})} . \qquad (7.3)$$

Note that if $\mathfrak{D}(\boldsymbol{\varepsilon},\boldsymbol{\sigma})$ is chosen to be function of stress, equations (7.3) and (2.122) are nonlinear equations as $E = E(d)$. The distortion γ, defined as a scalar measure of

deformation is used in the form of $\mathfrak{D}(\varepsilon)$. The latter is given by (6.112) and the former by (6.111). Once $d^{t+\Delta t}$ is known, the stress field in the degradable body $\boldsymbol{\sigma}^{t+\Delta t}$ and tangent modulus of the iteration are given by (2.122) and (7.1).

1. Pure inflation of finite cylinder

A three-dimensional finite cylinder constituted by the material defined above was analyzed when subjected to pure inflation (i.e. inner pressure $P_i = P_i(t)$, traction free outer surface, symmetry at the central surfaced and fixed on the top). The mesh used to discretize the domain is shown in Fig. VII.1. When subjected to a transmural pressure, the cylinder deforms, promoting degradation (shown in Fig. VII.2). The case shown in Fig. VI.5 was recovered. With such comparison, one is able to ascertain the validity of the implementation.

2. A real stent geometry

Moore and co-workers modeled the finite deformation of a stent/artery system using nonlinear theories in commercially available finite element packages [30,318]. In that study, several stent design parameters of stents were investigated such as strut spacing, the radius of curvature at the crown junctions and their axial amplitude. The variation of these three stent design parameters yields a three-parameter family of stent geometries. Several were identified as best due to several scoring methods, such as stresses imparted in the artery wall or radial strength (cf. [30] for more details).

One of the designs proposed by Bedoya et al. [30] and shown in Fig. VII.3 was investigated under the present degradable model: (i) a depreciable Young's modulus of $E_0 = 3\,\text{GPa}$ in the virgin state, (ii) constant Poisson's ratio of $\nu = 0.475$ (nearly incompressible), (iii) a degradation process linear with distortion (cf. (6.112)). The stent was subjected to a constant outer radial pressure of $P_o = 1\,\text{atm}$, thought to be the effect of an artery wall pushing against the stent.
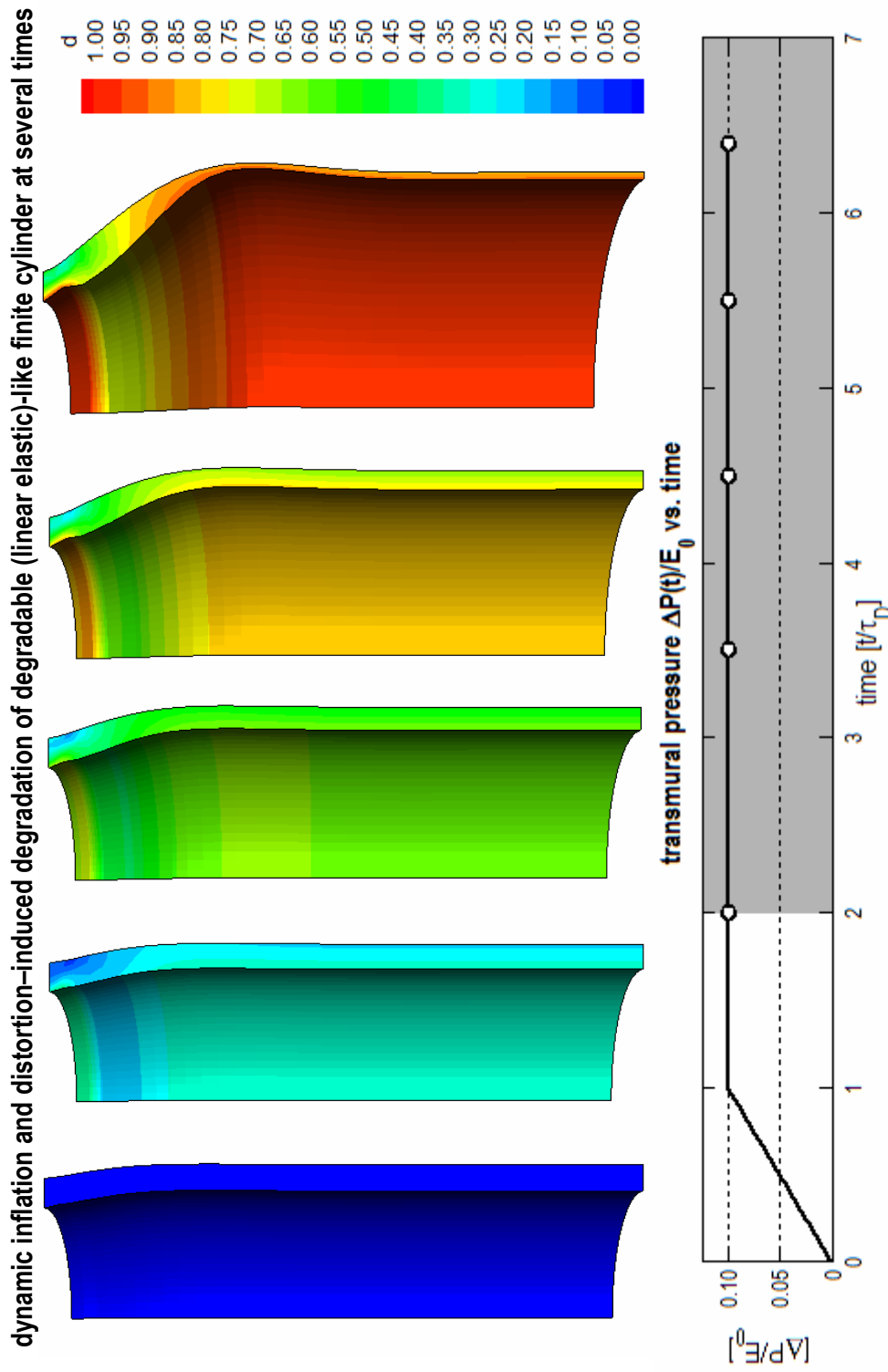
Fig. VII.2. Pure inflation of three-dimensional finite cylinder of degradable (linear elastic)-like material with degradation increasing linearly with distortion. The case shown in Fig. VI.5 was recovered. Hence, the implementation of the degradable (linear elastic)-like material was achieved with success. ABAQUS applies the transmural pressure with a linear increase. A "wait" step was prescribed before degradation was set active.

spatial discretization of the finite cylinder
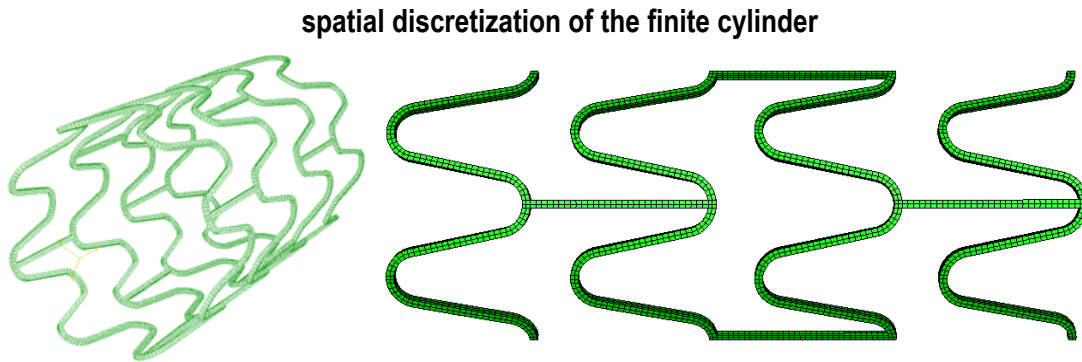
Fig. VII.3. Mesh used to discretize a real stent geometry (2B3) in ABAQUS. This geometry results from a 3-parameter family of stent geometries obtained from [30]. Three elements across the thickness were considered. Due to symmetry, only one quarter of the entire stent was modeled (on the right). On the left is shown the entire structure obtained through post processing.

As time increases, the deformation is responsible for promoting degradation to the particles of the stent (cf. Fig. VII.4). Some regions, such as the crowns, are subjected to greater deformations through bending occurring upon pressurization, and hence degrade to a greater extent. Degradation imparts mechanical properties reduction in the material and thus, the stent creeps inwards as it softens.

The deformation patterns of the biodegradable stent clearly differ from its non-degraded counterpart (shown in Fig. VII.4 corresponding to $t = 2$). Because most of the deformation is carried by the crowns, degradation occurs almost exclusively on those regions. As the stent is crimped by the external pressure, it promotes bending on the crown junction: a state of tension is seen in the convex side of each crown, whereas compression exists in the concave portion. Due to softening of these regions, the outer pressure is able to crimp the stent to a greater extent. Note that degradation proceeds from the crown junctions towards the middle of each segment in between crowns. Finally, note that by the time that the stent fails (surely before the numerical code, and most likely at the crown junctions), almost the entirety of the connector bars is mostly non-degraded.

Although a linearized theory and the linear material that degrade were employed,

Fig. VII.4. Real stent (2B3) made of degradable (linear elastic)-like material subjected to outer pressurization and distortion-induced degradation. As degradation and time proceeds, the cylinder degrades mostly at the crowns where a state of bending prevails. The connector bars remain mostly non-degraded. Note as the material softens, the same outer pressurization is responsible to creep the stent inwards.

the results seem phenomenologically sound. The deformation patterns of the stent upon outer pressurization and degradation clearly differ as time increases. Still, it is worth to remark that the main objective here is to prove feasibility of the incorporation of a degradation model into ABAQUS. These particular conditions were chosen as the first step towards that goal.

C. Degradable isotropic hyperelastic-like materials

In order to model incompressible isotropic hyperelastic materials, the user subroutine UHYPER was employed. UHYPER provides the used with the values of the invariants of the left Cauchy-Green stretch tensor, I_C, II_C, and III_C. Note that due to the constraint of incompressibility, $III_C = 1$. With these inputs, the subroutine must provide the amount of stored energy and the derivatives of the stored energy function with respect to the provided invariants as outputs. This task is extremely easy. For a neo-Hookean material, the former is computed from (2.102), whereas only $\partial W / \partial I_C$ is different from zero and corresponds to the shear modulus. More complicated stored energy functions such as the one proposed for non-degraded PLLA (cf. (3.21)) can be easily incorporated.

In order to have a hyperelastic material that degrades, the stored energy function is a function not only of deformation but also of the degradation parameter (cf. (4.10)). To achieve this in ABAQUS, the computation in the UHYPER subroutine simply takes into account the local value of the degradation, stored as a state variable (as in the previous case). When computing the value of the stored energy and its derivatives with respect to the invariants of $\mathbf{C}$, the algorithm obtains the local amount of degradation from the state variable at the current time step and updates the material properties (in the case of the neo-Hookean material that degrades, through (4.15) and (4.16)).

Lastly, the evolution of degradation is obtained at each location at the beginning of each time step through the user subroutine USDFLD. This user subroutine allows fields and state variables to be updated by the user. It is possible to obtain almost any

spatial discretization of the cylindrical fiber
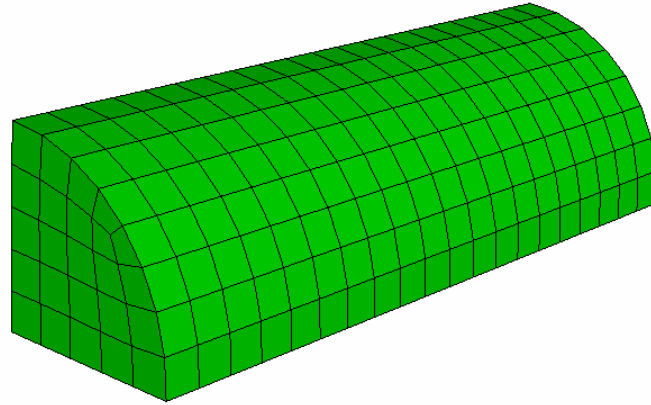
Fig. VII.5. Mesh used to discretize a cylindrical fiber. This geometry will be subjected to a state of uniaxial tension with the purpose of validation the implementation of the degradable neo-Hookean-like material in ABAQUS.

kinematical quantity. The deformation gradient $\mathbf{F}$ is obtained and through the computation of $\mathbf{C}$, the deformation dependent reaction rate can be obtained (cf. (4.11)). Using a similar measure of deformation (radius in the (I_C, II_C) plane), the evolution of degradation can be obtained by integration of (4.11) as performed in (7.2).

This subroutine is called at the beginning of each time step. It updates the value of one user defined field, the local deformation dependent reaction rate, and with the equation governing degradation, the state variable with the value of degradation at the end of the time step. This procedure was initially validated with the integration of a simple ODE independent of deformation and its accuracy was certificated. After the user defined field and state variable, ABAQUS resumes its algorithm with the computation of the stresses at the end of the time step through UHYPER, which already contains the newly updated information on the degradation.

1. Algorithm validation

In order to validate the algorithm, a degradable neo-Hookean-like material was implemented in ABAQUS under uniaxial extension when subjected to a constant
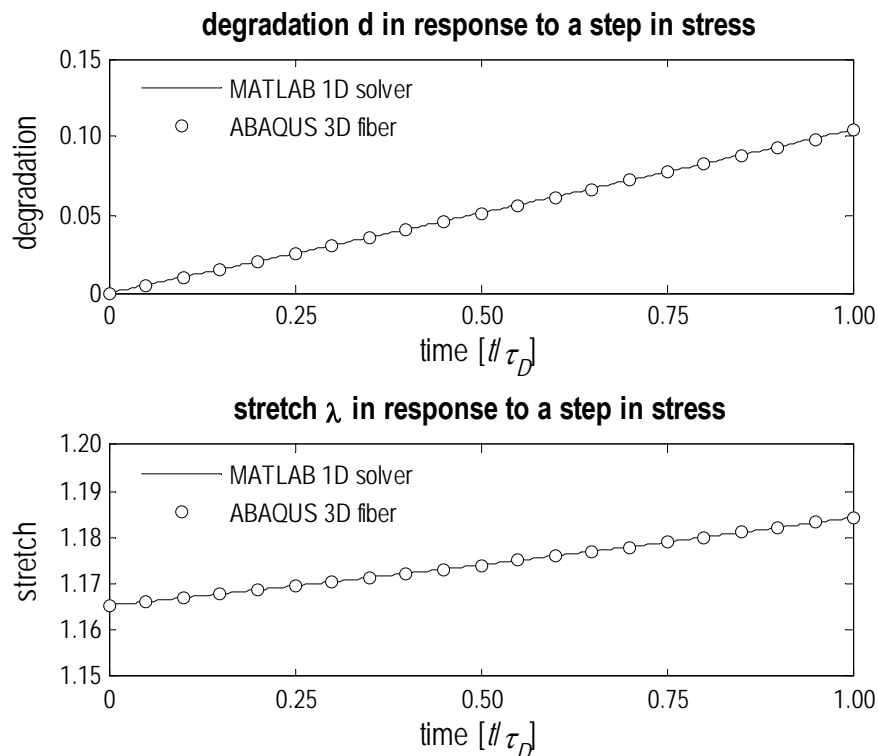
Fig. VII.6. Validation of the implementation of the degradable neo-Hookean-like material in ABAQUS. The results obtained for the uniaxial extension of a finite cylindrical fiber (shown in Fig. VII.5) yielded the cases shown in Fig. IV.8 and Fig. IV.9 (obtained analytical with one-dimensional modes). Implementation of degradable hyperelastic-like materials was achieved with success.

uniaxial stress (similar results as in Chapter IV.C.3). One quarter of a cylindrical fiber was used as computational domain and its mesh is shown in Fig. VII.5. The non-degraded shear modulus is $\mu_0 = 1$ GPa and the fiber will be subjected to a constant axial stress of $T_{33}/\mu_0 = 0.5$ to yield the lowest case shown in Fig. IV.8 and Fig. IV.9. The comparison between the results obtained with the MATLAB solver for the equations resulting from the 1D problem and the results obtained with the integration of the degradable behavior in ABAQUS through user subroutines for the full three-dimensional problem of a cylindrical fiber under the sate of uniaxial tension is shown in Fig. VII.6.

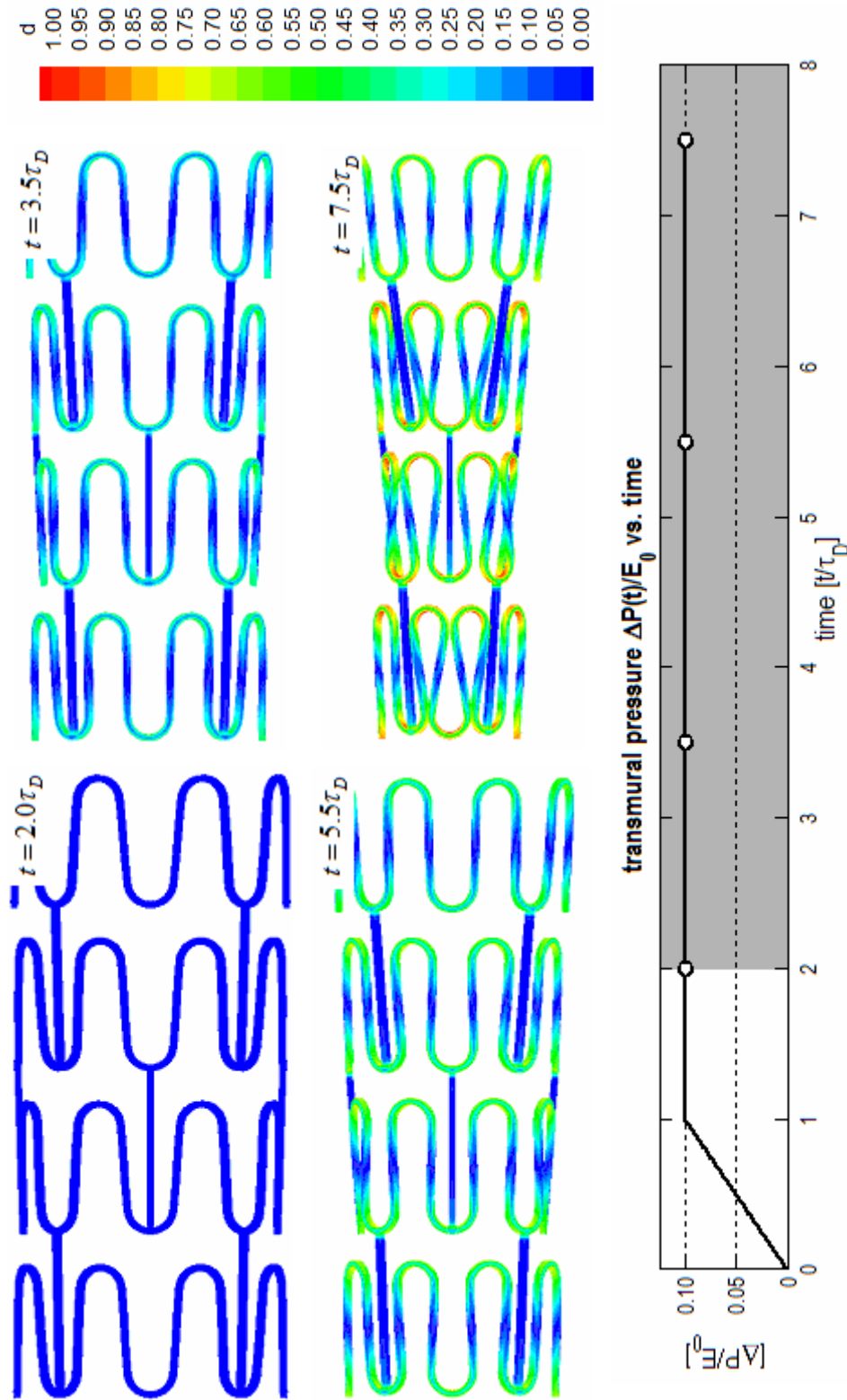**outer pressurization and deformation-induced degradation of degradable PLLA-like helical stent at several times**

Fig. VII.7. Helical stent of degradable PLLA-like material subjected to outer pressurization and deformation-induced degradation. TissueGen is currently interested in this class of stents due to the ease of manufacture. The top of the helical coil is pinned whereas the bottom is free. Due to the high profile of the stent, its radial strength is by far superior to the 2b3 stent. Due to the boundary condition, degradation occurs mostly near the fixed part of the helical coil. With pressure, the stent stretches in its length and shear is promoted along the helical coil, being the highest at the central fiber.

Concordance was obtained. Other cases were tested, such as prescribing a step in stretch. The amount of degradation promoted and the stress relaxation observed was also concordant with the results obtained with the integration of the constitutive model in ABAQUS (not shown).

2. *An helicoidal stent made of degradable PLLA*

The proposed stored energy function for non-degraded PLLA given in (3.21) with constants recorded in Table III.2 was integrated into the user subroutine UHYPER. With the knowledge of the current amount of degradation stored as a state variable, the amount of degradation promoted to the mechanical properties can be computed with (4.20) and (4.21)-(4.22) (cf. Fig. IV.5). Furthermore, the derivative of W with respect to I_C follows directly from (5.77). Lastly, with I_C provided by ABAQUS, the computation needed to implement this material into ABAQUS is trivial.

An helicoidal stent design is a design that is very easy to obtain with polymeric materials. A film of polymer can be spun around a cylindrical mandrel to obtain a cylindrical tube of controllable thickness. TissueGen (the company that supplied the polymer fibers for the experimental part of this research) is currently interested in such designs. The analysis of such design subjected to outer pressurization and strain-induced degradation is shown in Fig. VII.7. The boundary conditions considered were: (i) pinned on the top section of the helical coil, and (ii) normal pressure on the outer side surface. As the bottom of the structure is free, the strains in this region are mild and hence most of the degradation occurs near the fixed boundary condition. With pressure, a state of shear is promoted along the coil and degradation proceeds from the middle of the coil to the top and bottom surfaces. Finally, note that the crept displacement of such stent is very small and occurs mostly at the first ring.

3. *Real stent geometries with degradable PLLA*

Two real stent geometries were considered with the constitutive framework for

outer pressurization and deformation-induced degradation of degradable PLLA-like 2b3 stent at several times
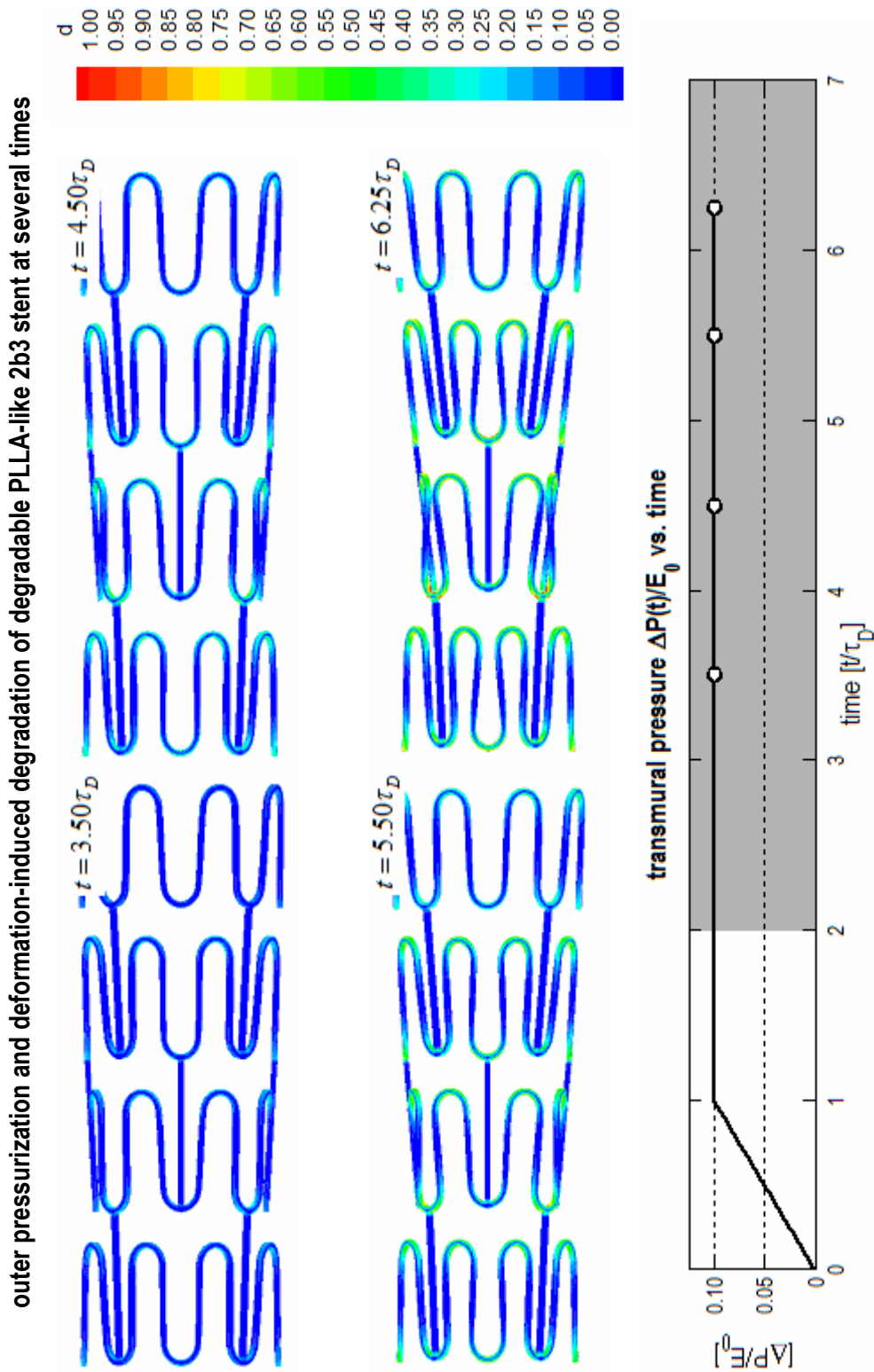
Fig. VII.8. Real stent (2B3) made of degradable PLLA-like material subjected to outer pressurization and deformation-induced degradation. Qualitatively similar results are obtained with the linearized theory (cf. Fig. VII.4); here, finite deformations are used. The stent is quite compliant and degradation occurs at a wide region close to the bent crowns. Degradation occurs at most of the struts forming the stent rings.

degradable hyperelastic-like materials: the previously analyzed 2B3 (cf. Fig. VII.8) and other showing a much greater radial strength, 1Z1 (shown in portion in Fig. VII.9). Whereas the former is able to deform to a great extent due to the curved crowns with a smaller angle, the latter is almost rigid even when increase the outer pressurization threefold.

Degradation of the 2B3 stent when considered to be made of degradable PLLA (constituted of degradable (linear elastic)-like material was shown in Fig. VII.4) shows similar characteristics. The cylinder creeps inwards as degradation proceeds, degradation is mostly confined to the crowns and the rings whereas the connector bars remain mostly non-degraded.

On the other hand, the 1Z1 stent shows a completely different behavior due to its inherent rigidity achieved through its design. Firstly, when subjected to outer pressurization, its deformation is negligible when compared with the one achieved by similar pressures on the 2B3. Secondly, due to the pointy crowns, strain concentration occurs mostly at those locations and hence degradation occurs almost exclusively at these corners. The connector bars and the rings remain mostly non-degraded and no significant change of diameter was observed even when the maximum degradation and zero stiffness was achieved at these delicate junctions leading the computational method to non-convergence.

Finally, it must be remarked that the adaptation of stainless steel stent designs to biodegradable stents can bring problems due to this localized degradation. When comparing both stent geometries, stent 2B3 suffers a much more distributed degradation. On the other hand, stent 1Z1 degrades exclusively at the crowns. If localized degradation promotes the failure of the material at these junction points, the struts of the former are mostly pristine whereas in the latter, degradation has taken its toll on these regions up to a certain extent. If the stent fails in this uncontrolled manner, non-degraded struts might promote embolic complications downstream.

outer pressurization and deformation-induced degradation of degradable PLLA-like 1z1 stent at several times
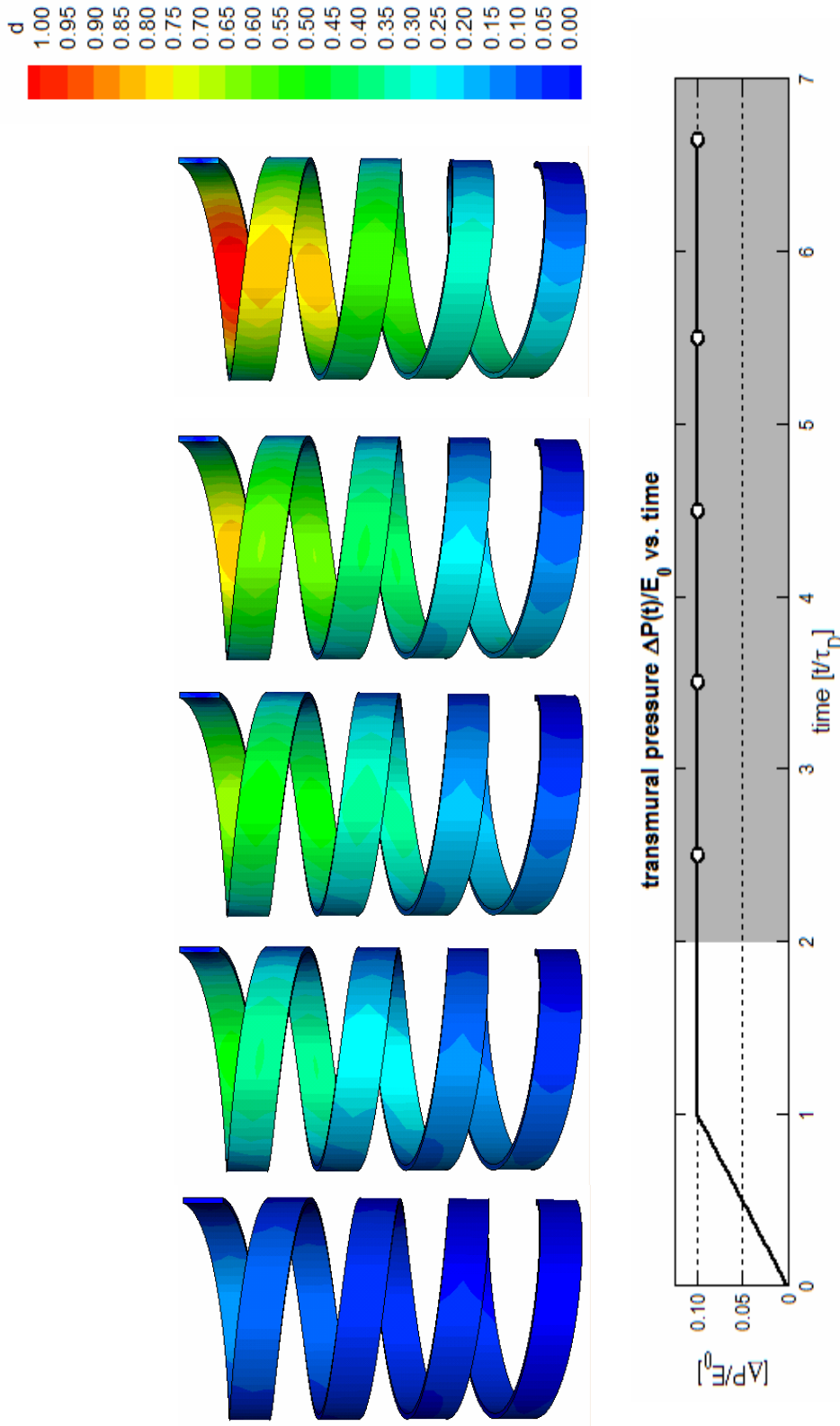

transmural pressure ΔP(t)/E$_0$ vs. time
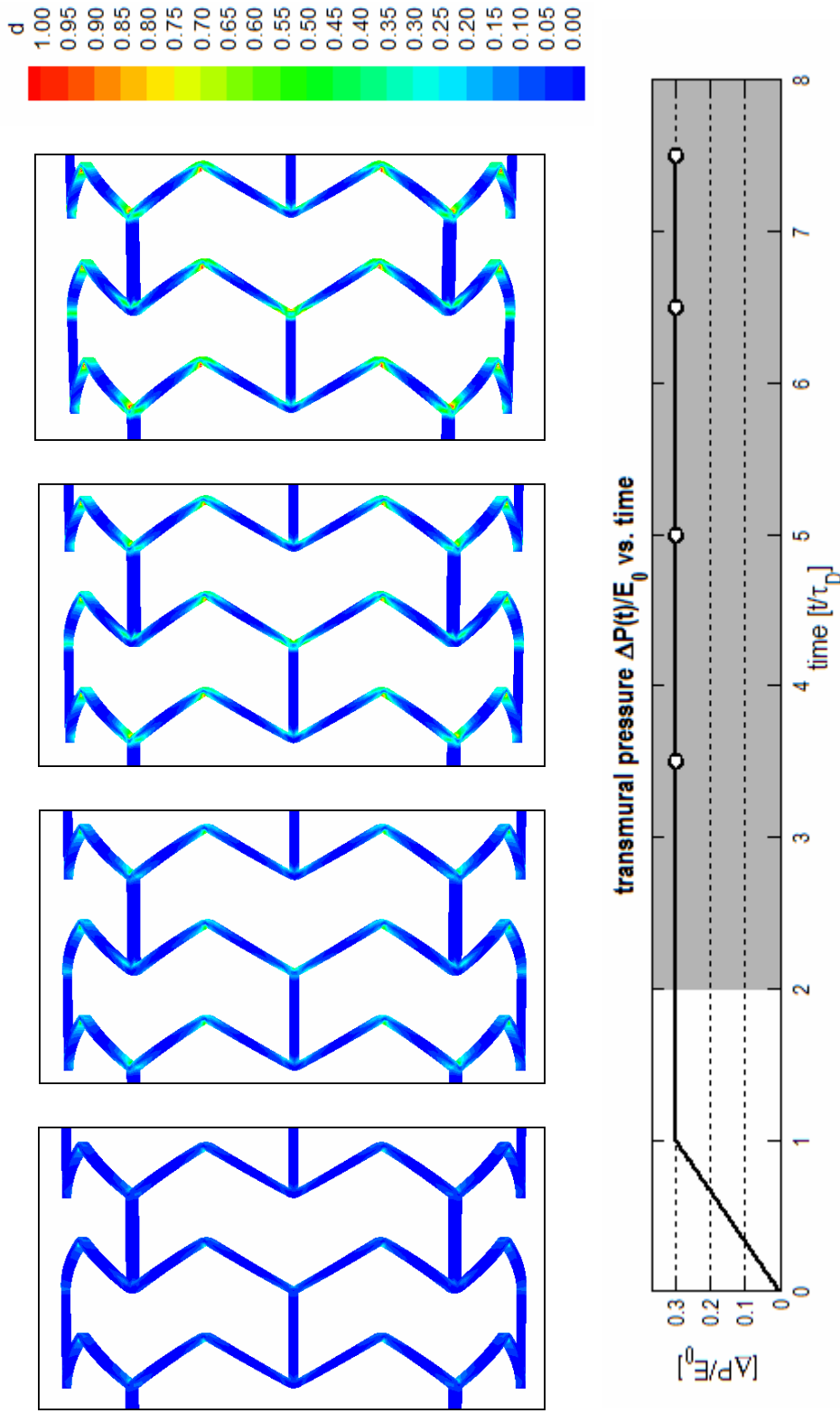
Fig. VII.9. Real stent (1Z1) made of degradable PLLA-like material subjected to outer pressurization and deformation-induced degradation. The 1Z1 stent is much stiffer than the 2B3; even with a three-fold increase in pressurization, its deformation is very small. Hence, most of the degradation is confined to the sharp crowns. If failure occurs at these sensible locations, most of the struts are still non-degraded and can provoke an embolism downstream.

CHAPTER VIII

EXPERIMENTS TOWARDS A MODEL FOR

BIODEGRADABLE POLY(L-LACTIC ACID)

The experimental portion of this research seeks to provide material parameters for biodegradable polymers undergoing biodegradation under physiologic loading. This process is complicated and lengthy as it should evolve together with the modeling efforts. Here is presented the starting point of this iterative process. Samples of FDA approved biodegradable PLLA were tested for their non-degraded mechanical properties in Chapter III. In this Chapter, similar experiments are conducted with samples that were degraded under tensile loading.

A. Materials and methods

A degradation chamber that allows degradation of fibers under tension was designed and constructed (shown in Fig. VIII.1). A heating pump (Polyscience Model 210, Niles, IL, USA) recirculates a pH 7.4 phosphate-buffered solution (Dulbecco's PBS, Invitrogen, Carlsbad, CA, USA) while maintaining the entire system at 37 ºC. The pH of the solution inside the degradation chamber is periodically monitored although the ratio of PBS in millimeters to polymer mass in grams is greater than 5000:1. The initial mass of each fiber was recorded with a digital scale (Mettler Toledo AL204, Columbus, OH, USA). In order to subject mechanical loads to the polymeric fibers inside the degradation chamber, a small metal crimp with a ring (8mm crimps, Crafts Etc!, Oklahoma City, OK, USA) was attached to each end of each fiber. In order to prevent degradation of these portions of the fibers, they were coated with water proof silicone (Sylgard, Dow Corning, Midland, MI, USA). Because this process is irreversible (it is impossible to remove the crimps without damaging the fibers), the total weight of the assembly was recorded. A total of 15 fibers (10 with two metal crimps each) were placed inside the degradation chamber and subjected to degradation.

degradation chamber used to degrade PLLA fibers under tension
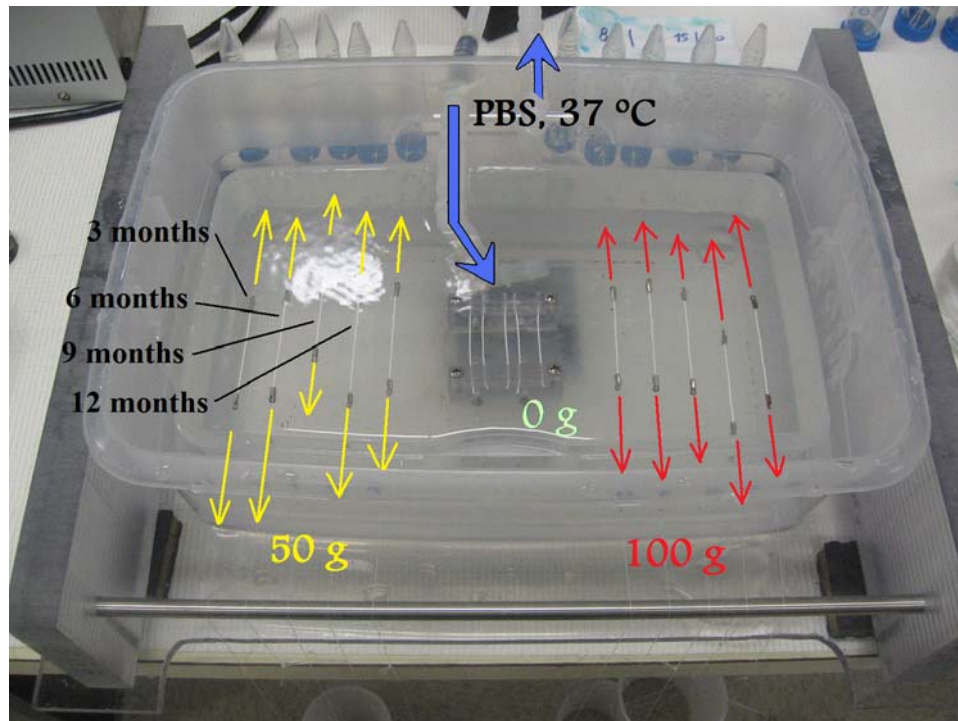
Fig. VIII.1. Degradation chamber used to degrade PLLA fibers under tension. Tensile loads were subjected to PLLA fibers through the attachment of deadweights. In order to have the fibers immersed in PBS at 37 ºC during the entire experimental time (12 months), a heating pump was used to recirculate the fluid. A rack was constructed to hold the fibers that were not subjected to any mechanical stimuli (shown in the middle).

During the entire course of degradation, 5 of the fibers were subjected to mechanical tension obtained with deadweights of 50 g, 5 other with 100 g, and the remaining 5 were not subjected to any mechanical stimuli (cf. Fig. VIII.1). The deadweights were attached to the metal crimps with monofilament nylon strings. The fibers that were not subjected to any mechanical stimuli were fixed in a polycarbonate rack constructed solely for this purpose (cf. center of Fig. VIII.1).

At each follow-up time (3 months, 6 months, and 9 months; but the experiment will be extended to 12 months) one fiber from each set was collected, dried, desiccated,

Table VIII.1. Summary of the fibers used in the experiment. The fibers supplied by TissueGen showed some variability either in diameter or length. Some of the fibers were also not perfectly straight and defects were observed with the naked eye. Defective and less perfect fibers were not used in the experiment.

fiber	mass (mg)	length (mm)	av. diam. (mm)	degradation conditions	mechanical tests			observations
					a	b	c	
18	27.7	61.8	0.903	none	SR 2%	SR 1%	SR 3%	sample 18c did not yield conclusive experiment
19	28.0	55.0	0.907	none	IER	IER	--	fiber#19 only yielded two samples
16	39.2	70.7	0.985	none	IER	IER	IER	
21	23.1	47.1	0.957	none	IER	IER	--	fiber#21 only yielded two samples
20	27.5	55.7	0.952	3mNL	IER	IER	SR1%	
4	31.3	65.0	0.963	3mSL	IER	IER	SR2%	sample 4c did not yield conclusive experiment
2	30.1	65.8	0.938	3mBL	IER	IER	SR1%	sample 2a did not yield conclusive experiment
3	29.2	62.6	0.948	4mBL	IER	IER	SR1%	fiber#3 broke after 4 months of degradation
15	29.9	63.8	0.967	6mNL	IER	SR1%	SR2%	
11	34.8	68.9	0.992	6mSL	IER	SR1%	SR2%	
10	34.4	63.0	0.992	6mBL	IER	IER	SR1%	sample 10a did not yield conclusive experiment
14	27.6	58.1	0.953	9mNL	IER	SR1%	IER	
7	32.7	65.6	1.005	9mSL	IER	IER	SR1%	
6	30.4	65.1	0.975	9mBL	IER	IER	SR1%	fiber #6 broke after 8 months of degradation and was re-attached, sample 6a did not yield conclusive experiment

Key: 3m – three months of degradation; 6m – six months; 9m – nine months; NL – fibers that were subjected to no tensile load; SL – fibers that were subjected to a tensile load originated by a deadweight of 50 g (SL: small load); BL – fibers that were subjected to a tensile load originated by a deadweight of 100g (BL: big load). IER – instantaneous elastic response: constant strain rate experiment till failure (5% strain/minute); SR1% - stress relaxation test in response to a step in strain of 1% during 10 minutes; SR2% - similar with a step in strain of 2%; SR3% - similar with a step in strain of 3%.

Table VIII.2. Mass reduction during the course of degradation. Mass loss was negligible and the difference in mass was much smaller than the experimental error associated with the technique. Fibers that were subjected to tensile loads were crimped and the difference measured was of the entire assembly. Hence, some caution should be taken with these results.

degradation conditions	3 months				6 months				9 months			
	fiber	initial (mg)	degraded (mg)	%	fiber	initial (mg)	degraded (mg)	%	fiber	initial (mg)	degraded (mg)	%
NL	20	27.5	27.6	1.00	15	29.9	29.9	1.00	14	27.6	27.2	0.99
SL	4	31.3	30.2	0.96	11	34.8	33.0	0.95	7	32.7	28.6	0.87
BL	2	30.1	26.6	0.88	10	34.4	30.5	0.89	6	30.4	NA	NA

And stored as described in Chapter III. Overall changes of the degraded fibers were measured (e.g. length, diameter, and mass). No appreciable change in length and diameter occurred. Mass reduction of non-crimped fibers was computed directly as the net difference before and after degradation. Mass reduction of crimped fibers was computed as the net difference between each assembly (fiber plus crimps, with the silicone removed to the most extent possible) before and after degradation. Percentage mass reduction was determined as a ratio between net difference and initial mass.

Each fiber was split into 3 samples (with the nomenclature of fiber number followed by sample, a, b, or c) for mechanical testing. Table VIII.1 synthesizes the conditions to which each fiber was subjected and the mechanical tests that were performed to each sample. Mechanical testing was performed as described in Chapter III and comprised of constant strain rate experiments at high strain rates (5 and 10%/min) for the determination of the instantaneous elastic response, and stress relaxation experiments to steps in strain (1% and 2% with 10 minutes of relaxation).

After mechanical testing, selected samples will undergo scanning electron microscopy (JSM 5900LV, JEOL, Peabody, MA, USA) and % crystallinity and glass transition temperature with DSC (as described in Chapter III). These results are not present at current time.

3 months instantaneous elastic response
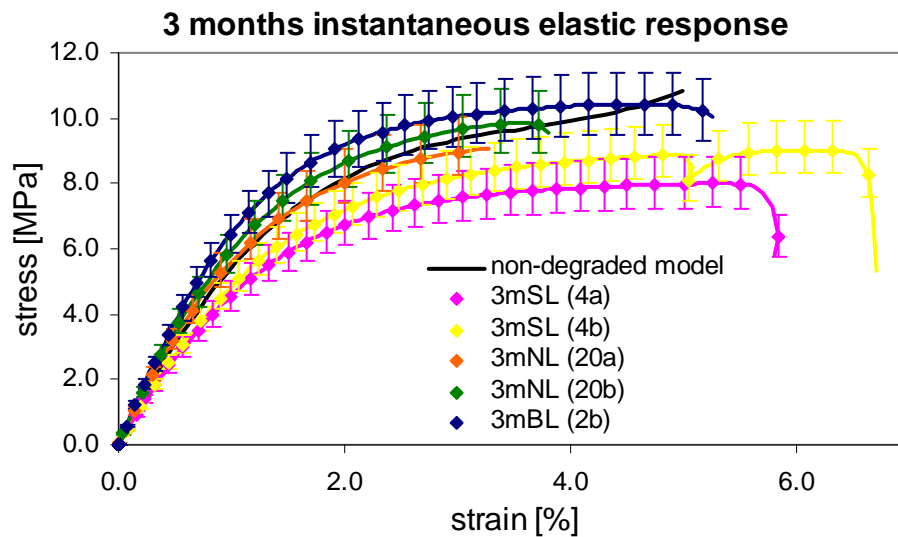
Fig. VIII.2. Three months instantaneous elastic response for several loading conditions. Degradation has not imparted significant changes in the instantaneous elastic response of PLLA. Fiber 4 (3mSL) showed a significantly softer mechanical response; that can possibly be attributed to a defective fiber.

B. Results

1. Mass loss

At each time point, the mass of the collected fibers was determined after drying and desiccation. The mass of the fibers that were subjected to tensile loads was measured together with the metal crimps as its removal is impossible and parts of the original part are trapped inside the crimp. Thus, the difference in weight recorded for such fibers is the difference between the initial and final assembly (two metal crimps plus the fiber). On the other hand, the mass of non-loaded fibers was determined directly. Percentage change in mass was considered as the ratio between the differences recorded and the initial mass of each fiber. Mass loss was negligible (cf. Table VIII.2). The fiber under no load did not change its mass at all during the 9 months degradation period. The fibers
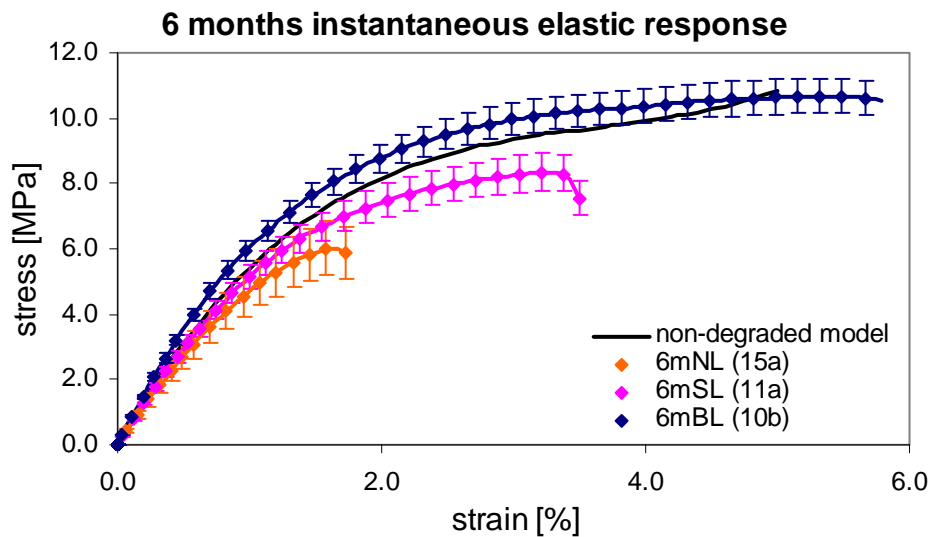
Fig. VIII.3. Six months instantaneous elastic response for several loading conditions. Data seems not to be conclusive as both 6mNL and 6mSL fibers failed under 5% strain and showed a somewhat reduced instantaneous elastic response. The slight increase in mechanical properties occurring in the BL fibers might be due to strain induced crystallization.

under load changed approximately 10%. Nevertheless, due to the uncertainty in the experimental method, this result should be observed very conservatively.

2. *Instantaneous elastic response*

Changes in the instantaneous elastic response are mild under all conditions at all time points (cf. Fig. VIII.2, Fig. VIII.3, and Fig. VIII.4 with the instantaneous elastic response at each collection point, 3 months, 6 months and 9 months, respectively; and Fig. VIII.5, Fig. VIII.6, and Fig. VIII.7 for each loading condition, no load, small load and big load, respectively).

Some fibers clearly showed much lower stress levels (e.g. 6mNL) and hint that changes in between fibers due to manufacturing or the existence of defects might play a more important role than changes due to degradation or even degradation conditions.
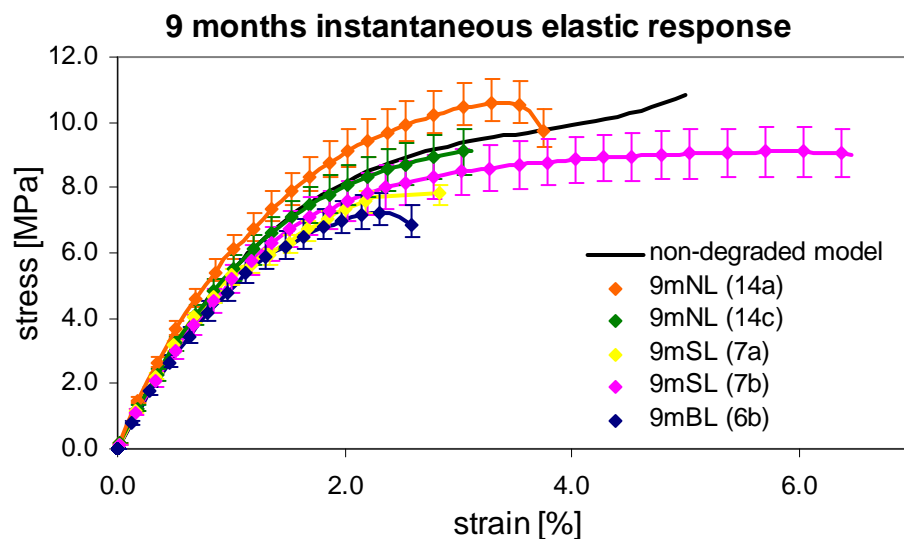
Fig. VIII.4. Nine months instantaneous elastic response for several loading conditions. Change in instantaneous elastic response, if any, was also very small. Nevertheless, degradation seems to be occurring to a greater extent in the loaded fibers.
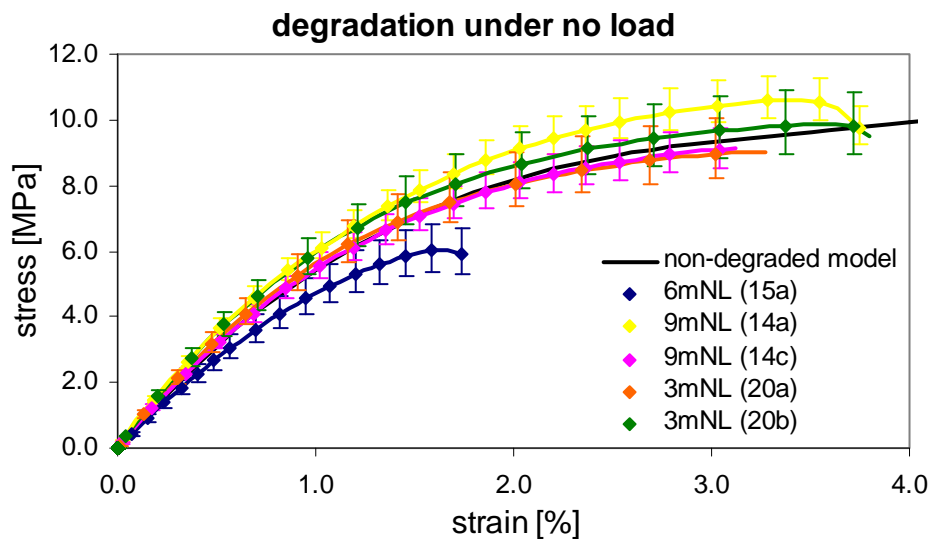
Fig. VIII.5. Instantaneous elastic response of fibers degraded under no load (NL) at several time points (3m, 6m, and 9m). Except the fiber at six months, degradation seems to be not occurring to an appreciable extend during the time course of the experiment.
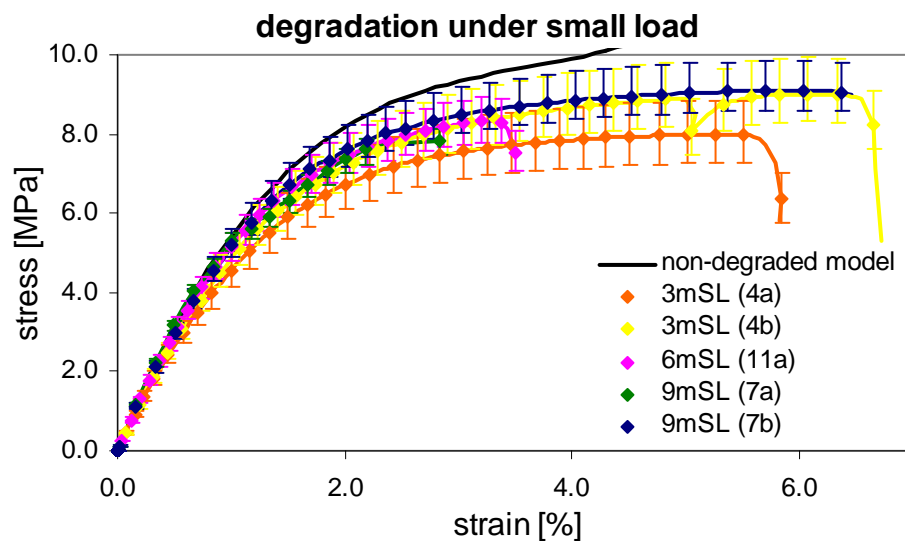
Fig. VIII.6. Instantaneous elastic response of fibers degraded under small load (SL) at several time points (3m, 6m, and 9m). Data is not conclusive as the responses are not much apart from each other.
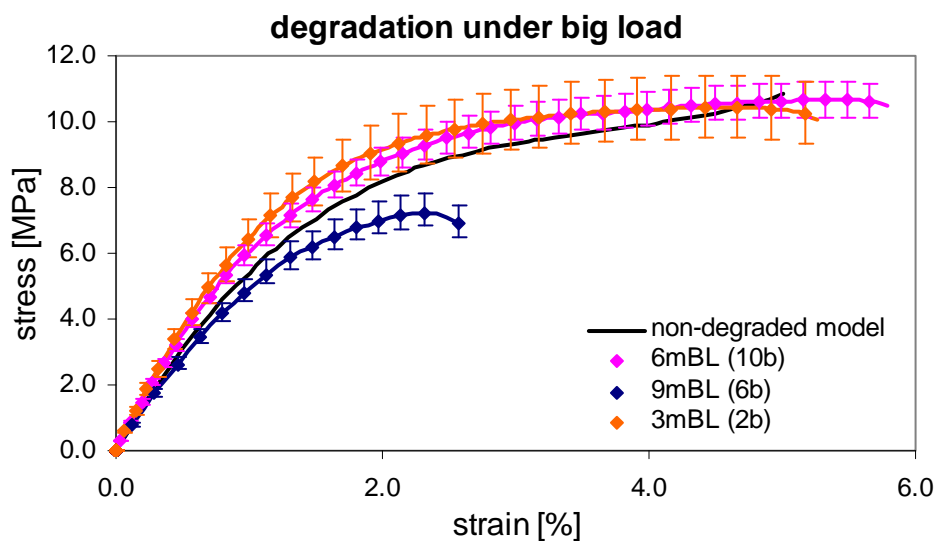
Fig. VIII.7. Instantaneous elastic response of fibers degraded under big load (BL) at several time points (3m, 6m, and 9m). Strain induced crystallization might play a role in the slight increase of mechanical properties observed under these conditions. The fiber at nine months might show degradation or might be apart due to defects. Twelve month data will provide more hints about the evolution of the IER.

Nevertheless, a decrease in mechanical properties (thought as lower stresses achieved with the same extension) can be observed either due to different loading conditions (cf. Fig. VIII.3) and due to the course of degradation (cf. Fig. VIII.7).

To conclude, the major feature of the instantaneous elastic response experiments is that a change in mechanical properties is observed but it seems to be small when compared with the non-degraded model (determined in Chapter III.C).

3.   Stress relaxation in response to steps in strain

Stress relaxation in response to 1% steps in strain shows even more inconclusive results: Fig. VIII.8, Fig. VIII.9, Fig. VIII.10, and Fig. VIII.11 show the stress relaxation responses at different time points whereas Fig. VIII.12, Fig. VIII.13, and Fig. VIII.14 show stress relaxation responses for each loading condition during the course of degradation.

At 9 months, the material seems to follow the same relaxation curve for all the loading conditions. At other time points, some differences are observed: either at 3 or 6 months, the relaxation curve corresponding to the unloaded fibers (3mNL and 6mNL) lie above the remaining ones (cf. Fig. VIII.9 and Fig. VIII.10). Also, if some tests are neglected (such as 6mSL and 6mBL in Fig. VIII.13 and Fig. VIII.14), a decrease in material properties (less stress for the same deformation) is observed in each loading condition as time increases.

Nevertheless, it must be remarked that just a reduced number of samples were tested under stress relaxation conditions, hence conclusions drawn from these results should be considered cautiously.

non-degraded stress relaxation response
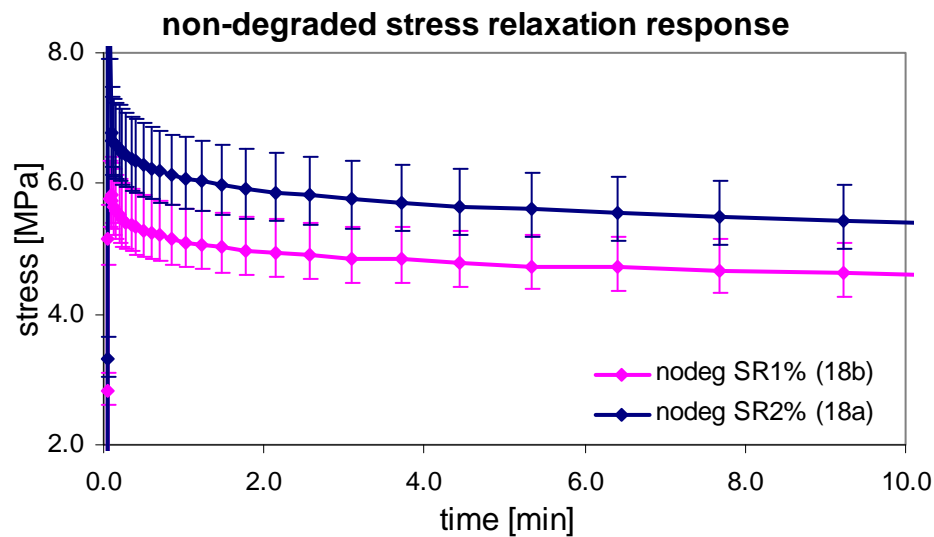
Fig. VIII.8. Stress relaxation response of non-degraded PLLA. Stress relaxation tests were performed during the initial analysis of non-degraded PLLA (with samples from a preliminary batch, shown in Fig. III.9). The batch of fibers used in the degradation experiment shows a slightly different stress relaxation response.

3 months stress relaxation response (SR1%)
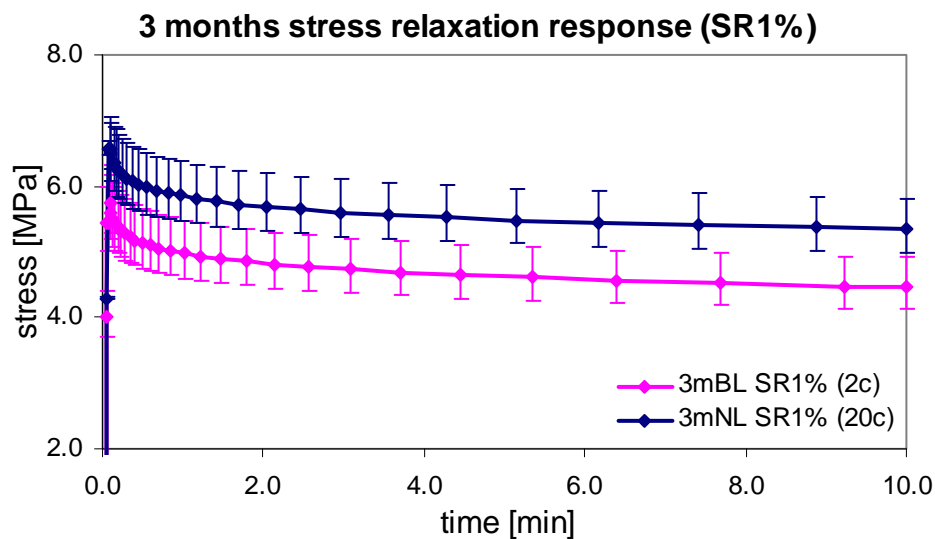
Fig. VIII.9. Stress relaxation in response to a step in strain (1%) of three months degraded PLLA under several loading conditions. Contrary to the IER results for similar degradation time (cf. Fig. VIII.2), the fiber that was subjected to load (3mBL) is under the unloaded counterpart (3mNL).

6 months stress relaxation response (SR1%)
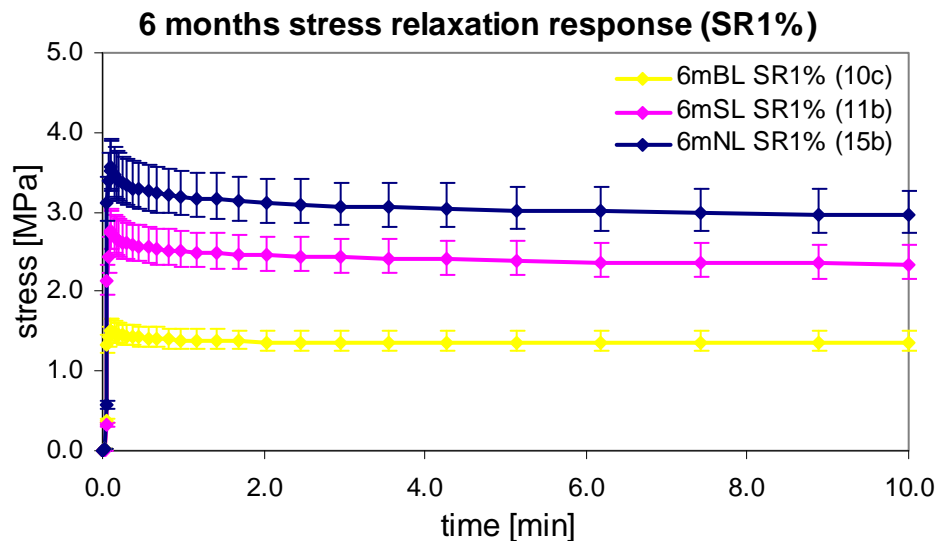
Fig. VIII.10. Stress relaxation in response to a step in strain (1%) of six months degraded PLLA under several loading conditions. A similar trend is observed. Nevertheless, the stresses achieved with the instantaneous step in strain are considerably lower than the previous case.

9 months stress relaxation response (SR1%)
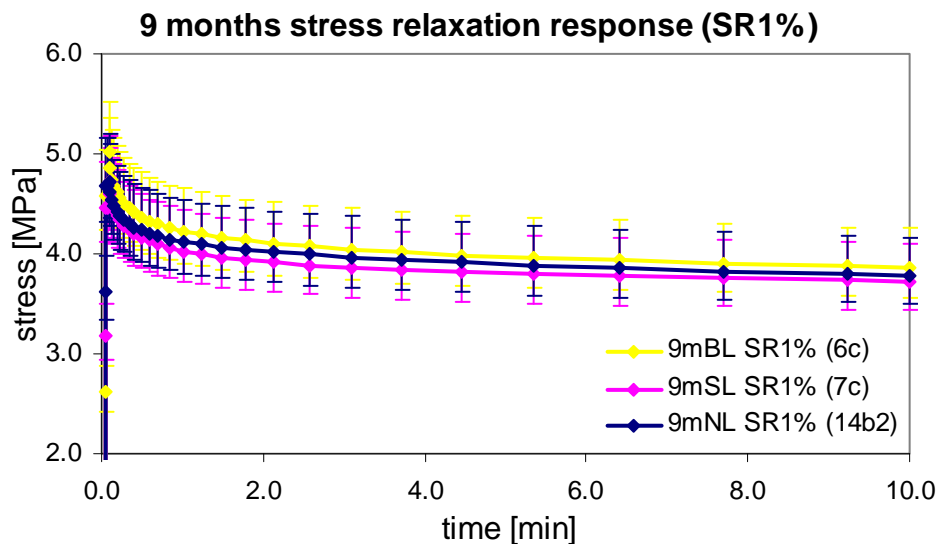
Fig. VIII.11 Stress relaxation in response to a step in strain (1%) of nine months degraded PLLA under several loading conditions. Interestingly, the response seems to be similar for all the loading conditions. The amount of stress is greater than the one observed at six months. The variability in between the fibers might play an important role in these experiments.
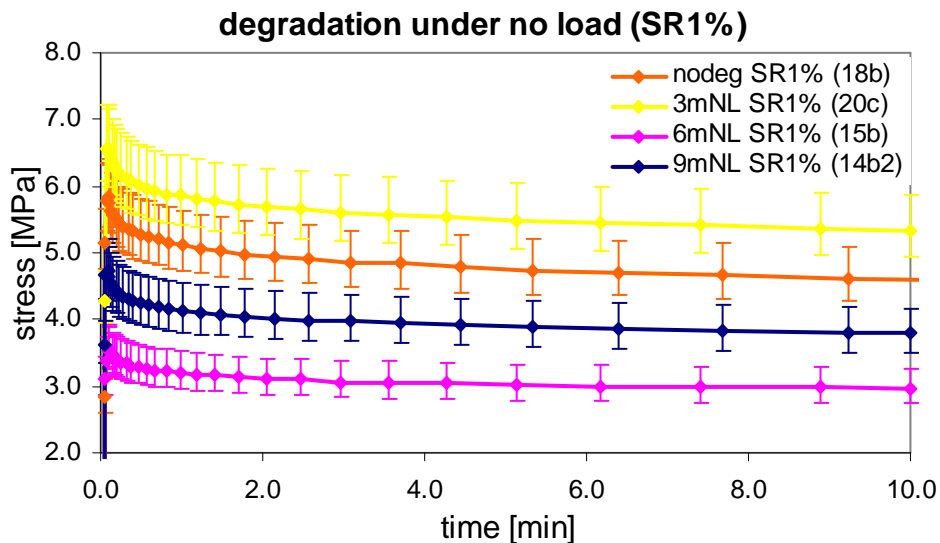
Fig. VIII.12. Stress relaxation in response to a step in stretch of fibers degraded under no load (NL) at several time points (non-degraded, 3m, 6m, and 9m). The experiments are not conclusive as no clear trend can be observed as the material degraded.
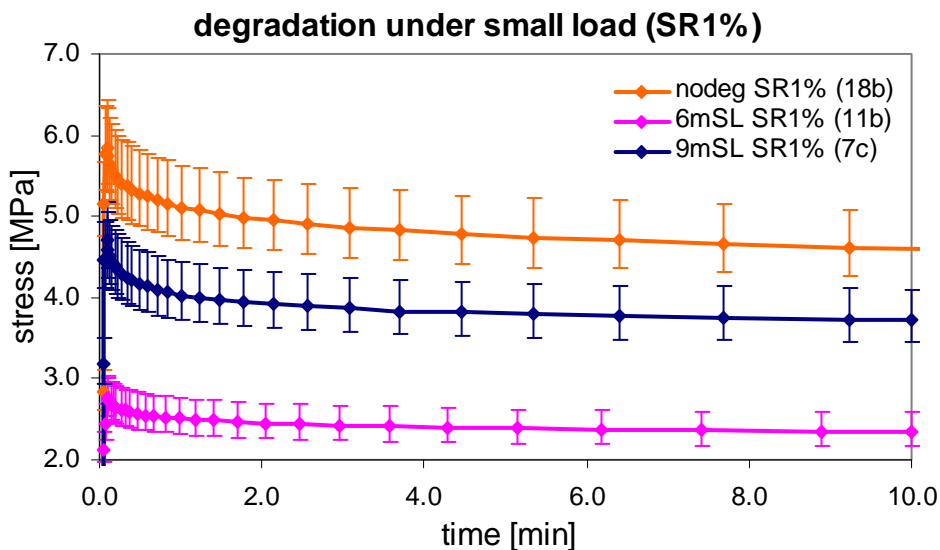
Fig. VIII.13. Stress relaxation in response to a step in stretch of fibers degraded under small load (SL) at several time points (non-degraded, 3m, and 9m). The experiment at 6 months is clearly outside the usual values. Although mechanical properties seem to decrease, it is impossible to draw any strong conclusion with only two curves.
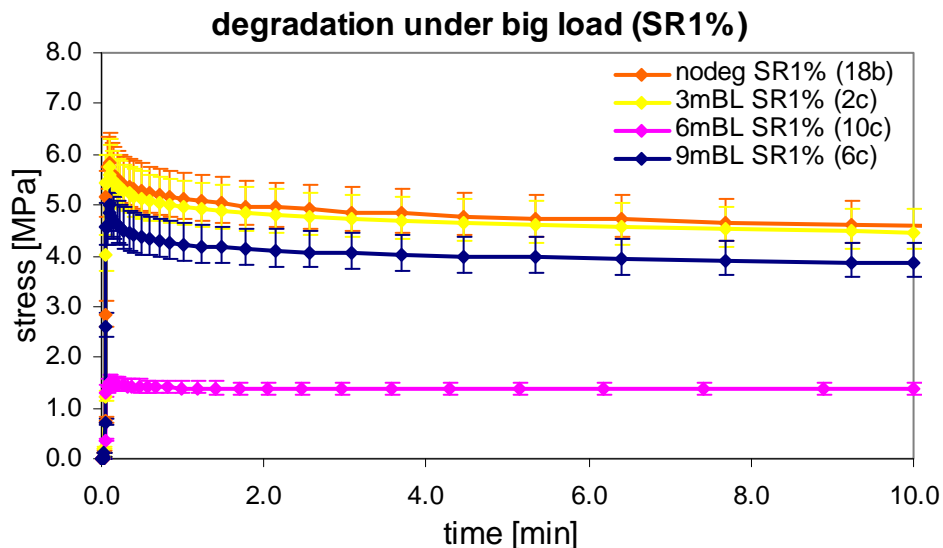
Fig. VIII.14. Stress relaxation in response to a step in strain (1%) of fibers degraded under big load (BL) at several time points (non-degraded, 3m, 6m, and 9m). If the experiment at 6 months is ignored, after an initial stage of just slight difference, the mechanical properties reduced to some extent after 9 month.

C. Discussion

Degradation and its effects on the mechanical properties of the material was not conclusively observed during the 9 months of the course of the experiment. Nevertheless, a trend and qualitative observations can be made.

Firstly, it must be remarked that a decrease in mechanical properties (thought of as a decrease in stress achieved with the same deformation, i.e. less force is necessary to extend the fiber) is observed in all but two samples tested: 3mNL SR1% (shown in Fig. VIII.12) and in the instantaneous elastic response on fibers subjected to big load (shown in Fig. VIII.7). The latter can be attributed to strain-induced crystallization whereas the former can be attributed to experimental variability, which is much more pronounced in the stress relaxation tests not only because of the narrow range of stresses measured but also due to the fact that a single test was performed.

Table VIII.3. Material constants of the degradable material obtained with reduction of selected data for illustrative purposes. The obtained results show that the best data reduction implies that μ_2 does not change with degradation. Furthermore, because $\beta_1 \approx 1$, $\mu_1 \approx 0$ as $d \rightarrow 1$. These results should be regarded as an illustration of the capabilities of the model. Accurate determination of the amount of degradation could be obtained as a change in molecular weight of the samples.

Degradable material constants		Sample degradation		
		9mNL (14c)	9mSL (7b)	9mBL (6b)
$\beta_1 = 0.99817$	$\beta_2 = 0$	$d = 0.0762$	$d = 0.2815$	$d = 0.5228$

On the other hand, a decrease (although in some cases not very significant) in mechanical response is observed in most of the figures. Several reasons can be listed towards this fact: (i) uncertainty inherent to the experimental technique (accounted with the error bars), (ii) not enough time was allowed to degradation have an appreciable effect, (iii) the loads might have been not large enough to promote significant differences between each degradation scheme, (iv) on the other hand, the loads could have been large enough to promote change in mechanical properties not due to degradation but due to other microstructure-changing mechanisms such as strain-induced crystallization in the loaded fibers, and finally (v) most important of all, the processing technique during the manufacturing of the fibers might have resulted in somewhat different fibers.

This last reason violates one of the postulates of the experimental hypothesis: all the fibers start at the same non-degraded condition. If so, the changes observed would be due to degradation and different degradation conditions. If not, changes that are occurring can be due to degradation but also due to the inherent difference in between the fibers. Each fiber started with properties different from each other (and that were not recorded individually) and changes are being inferred from a common non-degraded condition that all the fibers were assumed to share.

D. Reduction of selected data

In order to illustrate the capabilities of the proposed degradation model, experimental data of the instantaneous elastic response at 9 months (shown in Fig. VIII.4) was reduced. The non-degraded instantaneous elastic response is described by stored energy function (3.21) with material constants given in Table III.2. Material properties μ_1 and μ_2 were chosen to be functions of degradation (as described in section IV.C.2) as follows

$$\mu_1(d) = \mu_1^0(1 - \beta_1 d) \tag{8.1}$$

$$\mu_2(d) = \mu_2^0(1 - \beta_2 d) \tag{8.2}$$

where μ_1^0 and μ_2^0 are the material constants associated with the non-degraded response (when $d = 0$) and β_1 and β_2 are constants associated with the response at the maximum stage of degradation (as $d \to 1$).

Experimental results obtained with samples 14c (9mNL, nine months under no load), 7b (9mSL), and 6b (9mBL) were reduced simultaneously with the stored energy function and changing material properties function of degradation. Each curve shares all constants ($\mu_1^0, \mu_2^0, \beta_1$, and β_2) and is characterized by a certain level of degradation, i.e. d_{9mNL}, d_{9mSL}, and d_{9mBL} respectively.

The obtained results are summarized in Table VIII.3 and shown in Fig. VIII.15. The model is able to describe quite well the variety of responses as the material degrades. Note that the best fit obtained for this set of experimental data yields $\beta_2 = 0$, i.e. μ_2 is unchanged with degradation and only the first term of the stored energy function (3.21) decreases with degradation. Furthermore, due to that, the response of the material at the point of maximum degradation will be determined by the contribution of the second term (cf. Fig. III.16). Lastly, note that the values of degradation are somewhat large (above 50% in 9mBL) when compared with the slight differences instantaneous elastic response. These results should be regarded solely as an illustration of the
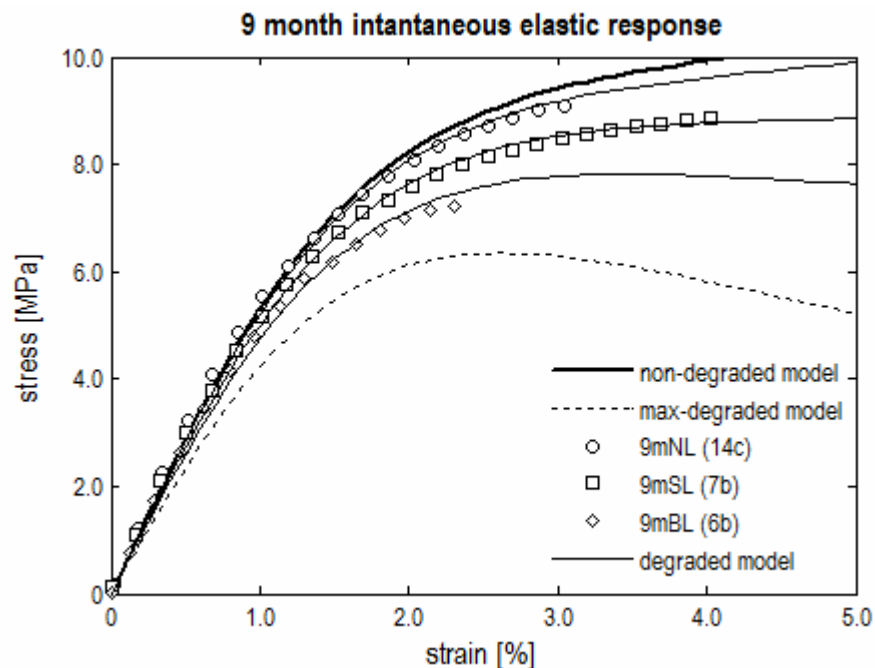
Fig. VIII.15. Instantaneous elastic response of the degradable material obtained with reduction of selected data for illustrative purposes. The results presented should be regarded only as an illustration of the capability of the presented model in describing the variety of responses as the material degrades.

capability of the model to describe the variety of responses during the course of degradation.

Lastly, the amount of degradation of each sample could be accurately determined as the loss of molecular weight. With different amounts of degradation corresponding to each degradation condition, the process of degradation described by the equation governing degradation (4.4) could be inferred. Furthermore, different forms of degradation (instead of the linear decreases with d used in (8.1) and (8.2)) could also be determined.

CHAPTER IX

CONCLUSIONS

A. Summary

The current work was focused on developing a constitutive model for describing the mechanical response of biodegradable polymers. The basis of the framework is phenomenological. Degradation, thought of as scission of bonds leading to reduction in molecular weight of the polymer, was captured with the introduction of a local scalar measure (the degradation parameter) describing the extent of bond scission. Degradation affects the response of the material and its evolution is governed by a governing equation describing the bond scission mechanism coupled to the linear momentum balance to yield the full description of the deformation and degradation of degradable bodies.

A particular class of biodegradable materials defined in this work is the class of degradable materials which response changes only due to decreases occurring in their material properties, i.e. their material constants become material functions of degradation. Several connections between the present model and existing theories were drawn, such as the theory of multiple natural configurations, materials with internal variables, aging material and damage mechanics, material divagation, strain-softening, and material clocks.

In order to understand the behavior of these materials under conditions relevant to stent design, several meaningful initial and boundary value problems were solved. Semi-inverse problems relevant either experimentally or directly applied to stents were considered, such as uniform uniaxial extension of fibers or inflation and extension of cylinders. Simple classes of degradable materials were chosen to illustrate the model, such as degradable hyperelastic-like or degradable viscoelastic-like materials, i.e. materials that in the absence (or at fixed levels) of degradation follow the classical hyperelastic or viscoelastic response, respectively.

The major features of the response of deformation-induced degradable bodies (when degradation occurs due to the presence of deformation) is that the increase of degradation confers stress relaxation, creep, and hysteresis to the response of the material, but arise from a completely different entropy producing mechanics than its classical viscoelastic counterparts. More precisely, as the material degrades due to the amount of deformation and the mechanical properties decrease, less force is necessary to maintain a given deformation or a constant force will promote a progressively greater deformation. These are two modes of the response of degradable materials: in the former, degradation increases asymptotically to its maximum value and the stress relaxes, whereas in the latter, more deformation promotes more degradation and vice versa.

A rigorous finite element setting accounting the degradation parameter and the equation governing degradation was developed and that allowed the solution of slightly more complicated problems. The time dependent inflation and extension of a finite cylinder, a problem with three dependent variables (2D in space and time) and three independent variables (two spatial displacements and the degradation parameter), was successfully solved.

Real stents have complicated geometries that do not allow semi-inverse solutions. Hence, in order to use the developed model as a tool for biodegradable stent design, the degradable material behavior was integrated with ABAQUS through the user subroutine capability. The integration of degradable materials in a finite element setting was achieved up to a certain generality and validated with the simpler geometries solved previously.

Stent deformation upon outer pressurization was found to be significantly different as degradation proceeded and highly dependent on stent design. Furthermore, it was seen that degradation is inhomogeneously distributed over the stent, and hence when the material fails at more delicate regions, other parts are still mostly non-degraded and might potentially cause embolic complications downstream. This is a clear indication of the problems that arise when one tries to simply adapt previous stainless steel stent

designs to biodegradable stents. Uniformity of degradation over the entire stent is a characteristic that should be pursued during biodegradable stent design stage. Biodegradable stent design must take into consideration that the failure of the material is eventually desired, must be achieved in a controlled manner, and its possible side effects must be accounted for.

The experimental portion of this work sought to provide material parameters for PLLA undergoing biodegradation under tensile loading. Experiments and modeling efforts should be concurrent and enhance each other. The experimental work performed represents the starting point of this iterative process.

Fibers of non-degraded PLLA were tested for their mechanical properties and suitable constitutive models were chosen to describe its one-dimensional response. PLLA was observed to be a nonlinear viscoelastic material. Nevertheless, it was possible to obtain an instantaneous elastic response as the response of the material seemed to be indifferent when high constant strain rates were considered. Stress relaxation tests were conducted and two viscoelastic models were employed to describe the stress relaxation response of the material: the quasilinear viscoelastic solid model and the Pipkin & Rogers single integral nonlinear viscoelastic solid. No significant improvement was achieved with the nonlinear model.

Similar PLLA fibers were then subjected to degradation under tension inside a degradation chamber designed solely for the purpose. Mechanical testing of degraded PLLA fibers was conducted in order to obtain the evolution of their response with degradation and time. Experimental data did not yield conclusive results after 9 months of degradation. Degradation seems to be occurring only within a negligible extent and changes in mechanical response are smaller than experimental uncertainty.

Three major factors can be listed as reasons for such: (i) the mechanical properties of the initially non-degraded fibers were assumed to be similar and due to manufacture or defects, this assumption might be invalid, (ii) the loads applied during degradation might have not been large enough to promote significant differences in the degradation conditions, and (iii) more time might be needed for degradation to be

experimentally observed. Nevertheless, a qualitative trend in mechanical properties reduction can be observed from the experimental data.

B. Recommendations for further work

The current work was first of its kind wherein degradation of polymeric materials was modeled within a three dimensional continuum mechanics framework. While the model captures the response of such materials in an acceptable manner, its derivation was based within phenomenological reasoning. The first step towards the improvement of such model is to confer it with a fully thermodynamic background. Rajagopal and co-workers have developed a thermodynamical framework that describes the mechanics of bodies capable of existing in multiple natural configurations based on the idea of evolving natural configuration and maximization of the rate of entropy production. Bond scission is per se an entropy producing mechanism. Specific choices for the stored energy function and the form of the rate of entropy production gives rise to different constitutive models which capture a diverse range of degradable material behavior. Inelastic behavior arising directly from balloon inflation during deployment seems to be another important feature to account for in future modeling efforts.

Other area of possible future work deals with polymer erosion. As the degrading polymer degrades, oligomers and monomers resulting from chain scission dissolve away from the polymer bulk. While degradation and material properties reduction occurs to an appreciable extent before erosion occurs (which is the range of validity of the current model), eroding polymers are open systems; hence the general procedure of continuum mechanics (every particle in the reference configuration is mapped onto all configurations at all times) is not suitable once erosion and mass loss become relevant.

Degradation of aliphatic polyesters occurs due to hydrolysis, hence the presence of water is the major requirement for degradation to occur. There are two ways to account the amount of swelling and water diffusion into the polymeric matrix. The first method is based on using mixture theory, while an alternative approach is based on a modification of the mass balance to include diffusion. In a similar way, drug release

from the polymeric matrix can be included; furthermore, experimental evidence supports the fact that changes in porosity due to degradation and erosion enhance drug elution.

The experimental part of this work is clearly short handed. Many more experiments are needed towards a full understanding of such materials. Changes in molecular weight distribution provide the clear picture of the extent of chain scission. Such data would even provide the perfect motivation to treat a polymeric system with multiple constituents, each corresponding to an interval in molecular weight.

Experiments performed for longer periods of time, with fast degrading polymers, and under other kinds of degradation conditions could be pursued in order to gain a better understanding of the underlying physical mechanisms associated with polymer degradation. On the other hand, in order to understand the mechanics of biodegradable implants, real geometries with implantable polymeric systems should be tested. The usage of amorphous degradable polymers might be useful in the separation of changes in mechanical properties due to crystallization and due to degradation. Still, there is the need to design suitable experimental devices that subject polymers to constant stretch (and measure force) or constant stress (and measure stretch) during the entire course of degradation.

Lastly, more work can be performed on the analysis of real stent geometries made of biodegradable polymer with the integration of biodegradable material models into ABAQUS. It is of the utmost importance not only to realize that the response of biodegradable stents is of a completely different nature than their stainless steel counterparts but also to understand how such response changes over degradation. Only after these initial steps, successful biodegradable stent design can be achieved.

REFERENCES

[1] C.T. Dotter, Transluminal angioplasty: A long view, Radiology 135 (1980) 561-564.

[2] M.J. Lipinski, W.F. Fearon, V.F. Froelicher, G.W. Vetrovec, The current and future role of percutaneous coronary intervention in patients with coronary artery disease, J. Interv. Cardiol. 17 (2004) 283-294.

[3] S. Glagov, Intimal hyperplasia, vascular modeling, and the restenosis problem, Circulation 89 (1994) 2888-2891.

[4] D.W. Muller, S.G. Ellis, E.J. Topol, Experimental models of coronary artery restenosis, J. Am. Coll. Cardiol. 19 (1992) 418-432.

[5] G.S. Roubin, J.S. Douglas, Jr., S.B. King, 3rd, S.F. Lin, N. Hutchison, R.G. Thomas, A.R. Gruentzig, Influence of balloon size on initial success, acute complications, and restenosis after percutaneous transluminal coronary angioplasty. A prospective randomized study, Circulation 78 (1988) 557-565.

[6] J.S. Douglas, Jr., S.B. King, 3rd, G.S. Roubin, Influence of the methodology of percutaneous transluminal coronary angioplasty on restenosis, Am. J. Cardiol. 60 (1987) 29B-33B.

[7] I.J. Sarembock, P.J. LaVeau, S.L. Sigal, I. Timms, J. Sussman, C. Haudenschild, M.D. Ezekowitz, Influence of inflation pressure and balloon size on the development of intimal hyperplasia after balloon angioplasty. A study in the atherosclerotic rabbit, Circulation 80 (1989) 1029-1040.

[8] P. Libby, D. Schwartz, E. Brogi, H. Tanaka, S.K. Clinton, A cascade model for restenosis. A special case of atherosclerosis progression, Circulation 86 (1992) III47-III52.

[9] J.W. Currier, D.P. Faxon, Restenosis after percutaneous transluminal coronary angioplasty: Have we been aiming at the wrong target?, J. Am. Coll. Cardiol. 25 (1995) 516-520.

[10] G.S. Mintz, J.J. Popma, A.D. Pichard, K.M. Kent, L.F. Satler, C. Wong, M.K. Hong, J.A. Kovach, M.B. Leon, Arterial remodeling after coronary angioplasty: A serial intravascular ultrasound study, Circulation 94 (1996) 35-43.

[11] U. Sigwart, J. Puel, V. Mirkovitch, F. Joffre, L. Kappenberger, Intravascular stents to prevent occlusion and restenosis after transluminal angioplasty, N. Engl. J. Med. 316 (1987) 701-706.

[12] J. Al Suwaidi, P.B. Berger, D.R. Holmes, Jr., Coronary artery stents, JAMA 284 (2000) 1828-1836.

[13] J.C. Palmaz, Balloon-expandable intravascular stent, AJR. Am. J. Roentgenol. 150 (1988) 1263-1269.

[14] R.A. Schatz, Introduction to intravascular stents, Cardiol. Clin. 6 (1988) 357-372.

[15] P.W. Serruys, P. Dejaegere, F. Kiemeneij, C. Macaya, W. Rutsch, G. Heyndrickx, H. Emanuelsson, J. Marco, V. Legrand, P. Materne, J. Belardi, U. Sigwart, A. Colombo, J.J. Goy, P. Vandenheuvel, J. Delcan, M.A. Morel, A comparison of balloon-expandable-stent implantation with balloon angioplasty in patients with coronary-artery disease, N. Engl. J. Med. 331 (1994) 489-495.

[16] D.L. Fischman, M.B. Leon, D.S. Baim, R.A. Schatz, M.P. Savage, I. Penn, K. Detre, L. Veltri, D. Ricci, M. Nobuyoshi, M. Cleman, R. Heuser, D. Almond, P.S. Teirstein, R.D. Fish, A. Colombo, J. Brinker, J. Moses, A. Shaknovich, J. Hirshfeld, S. Bailey, S. Ellis, R. Rake, S. Goldberg, A randomized comparison of coronary-stent placement and balloon angioplasty in the treatment of coronary-artery disease, N. Engl. J. Med. 331 (1994) 496-501.

[17] R.A. Schatz, D.S. Baim, M. Leon, S.G. Ellis, S. Goldberg, J.W. Hirshfeld, M.W. Cleman, H.S. Cabin, C. Walker, J. Stagg, M. Buchbinder, P.S. Teirstein, E.J. Topol, M. Savage, J.A. Perez, R.C. Curry, H. Whitworth, J.E. Sousa, F. Tio, Y. Almagor, R. Ponder, I.M. Penn, B. Leonard, S.L. Levine, R.D. Fish, J.C. Palmaz, Clinical-experience with the Palmaz-Schatz coronary stent - initial results of a multicenter study, Circulation 83 (1991) 148-161.

[18] G.S. Mintz, R. Hoffmann, R. Mehran, A.D. Pichard, K.M. Kent, L.F. Satler, J.J. Popma, M.B. Leon, In-stent restenosis: The Washington Hospital Center experience, Am. J. Cardiol. 81 (1998) 7E-13E.

[19] R.S. Schwartz, Neointima and arterial injury: Dogs, rats, pigs, and more, Lab. Invest. 71 (1994) 789-791.

[20] R.S. Schwartz, Pathophysiology of restenosis: Interaction of thrombosis, hyperplasia, and/or remodeling, Am. J. Cardiol. 81 (1998) 14E-17E.

[21] M. Jaff, M. Dake, J. Pompa, G. Ansel, T. Yoder, Standardized evaluation and reporting of stent fractures in clinical trials of noncoronary devices, Catheter. Cardiovasc. Interv. 70 (2007) 460-462.

[22] A. Kamura, T. Kawasaki, N. Koga, T. Inoue, K. Node, Fracture of a sirolimus-eluting stent with migration, Int. J. Cardiol. In Press, Corrected Proof.

[23] E.R. Edelman, C. Rogers, Pathobiologic responses to stenting, Am. J. Cardiol. 81 (1998) 4E-6E.

[24] S. Robaina, B. Jayachandran, Y. He, A. Frank, M.R. Moreno, R.T. Schoephoerster, J.E. Moore, Jr., Platelet adhesion to simulated stented surfaces, J. Endovasc. Ther. 10 (2003) 978-986.

[25] C. Rogers, E.R. Edelman, Endovascular stent design dictates experimental restenosis and thrombosis, Circulation 91 (1995) 2995-3001.

[26] A. Farb, D.K. Weber, F.D. Kolodgie, A.P. Burke, R. Virmani, Morphological predictors of restenosis after coronary stenting in humans, Circulation 105 (2002) 2974-2980.

[27] J.J. Wentzel, D.M. Whelan, W.J. van der Giessen, H.M. van Beusekom, I. Andhyiswara, P.W. Serruys, C.J. Slager, R. Krams, Coronary stent implantation changes 3-d vessel geometry and 3-d shear stress distribution, J. Biomech. 33 (2000) 1287-1295.

[28] J.J. Wentzel, R. Krams, J.C. Schuurbiers, J.A. Oomen, J. Kloet, W.J. van Der Giessen, P.W. Serruys, C.J. Slager, Relationship between neointimal thickness and shear stress after Wallstent implantation in human coronary arteries, Circulation 103 (2001) 1740-1745.

[29] J. Moore, Jr., J.L. Berry, Fluid and solid mechanical implications of vascular stenting, Ann. Biomed. Eng. 30 (2002) 498-508.

[30] J. Bedoya, C.A. Meyer, L.H. Timmins, M.R. Moreno, J.E. Moore, Effects of stent design parameters on normal artery wall mechanics, J. Biomech. Eng. 128 (2006) 757-765.

[31] S. Glagov, C.K. Zarins, N. Masawa, C.P. Xu, H. Bassiouny, D.P. Giddens, Mechanical functional role of non-atherosclerotic intimal thickening, Front. Med. Biol. Eng. 5 (1993) 37-43.

[32] A.M. Lincoff, E.J. Topol, S.G. Ellis, Local drug delivery for the prevention of restenosis. Fact, fancy, and future, Circulation 90 (1994) 2070-2084.

[33] D.M. Whelan, H.M. van Beusekom, W.J. van der Giessen, Mechanisms of drug loading and release kinetics, Semin. Interv. Cardiol. 3 (1998) 127-131.

[34] T.L. Lambert, V. Dev, E. Rechavia, J.S. Forrester, F. Litvack, N.L. Eigler, Localized arterial wall drug delivery from a polymer-coated removable metallic stent. Kinetics, distribution, and bioactivity of forskolin, Circulation 90 (1994) 1003-1011.

[35] Y.K. Ahn, M.H. Jeong, J.W. Kim, S.H. Kim, J.H. Cho, J.G. Cho, C.S. Park, S.W. Juhng, J.C. Park, J.C. Kang, Preventive effects of the heparin-coated stent on restenosis in the porcine model, Catheter. Cardiovasc. Interv. 48 (1999) 324-330.

[36] A.M. Lincoff, J.G. Furst, S.G. Ellis, R.J. Tuch, E.J. Topol, Sustained local delivery of dexamethasone by a novel intravascular eluting stent to prevent restenosis in the porcine coronary injury model, J. Am. Coll. Cardiol. 29 (1997) 808-816.

[37] T. Yamawaki, H. Shimokawa, T. Kozai, K. Miyata, T. Higo, E. Tanaka, K. Egashira, T. Shiraishi, H. Tamai, K. Igaki, A. Takeshita, Intramural delivery of a specific tyrosine kinase inhibitor with biodegradable stent suppresses the restenotic changes of the coronary artery in pigs in vivo, J. Am. Coll. Cardiol. 32 (1998) 780-786.

[38] Y.W. Ye, C. Landau, J.E. Willard, G. Rajasubramanian, A. Moskowitz, S. Aziz, R.S. Meidell, R.C. Eberhart, Bioresorbable microporous stents deliver recombinant adenovirus gene transfer vectors to the arterial wall, Ann. Biomed. Eng. 26 (1998) 398-408.

[39] D.I. Axel, W. Kunert, C. Goggelmann, M. Oberhoff, C. Herdeg, A. Kuttner, D.H. Wild, B.R. Brehm, R. Riessen, G. Koveker, K.R. Karsch, Paclitaxel inhibits arterial smooth muscle cell proliferation and migration in vitro and in vivo using local drug delivery, Circulation 96 (1997) 636-645.

[40] S.O. Marx, T. Jayaraman, L.O. Go, A.R. Marks, Rapamycin-fkbp inhibits cell-cycle regulators of proliferation in vascular smooth-muscle cells, Circ. Res. 76 (1995) 412-417.

[41] R. Gallo, A. Padurean, T. Jayaraman, S. Marx, M. Rogue, S. Adelman, J. Chesebro, J. Fallon, V. Fuster, A. Marks, J.J. Badimon, Inhibition of intimal thickening after balloon angioplasty in porcine coronary arteries by targeting regulators of the cell cycle, Circulation 99 (1999) 2164-2170.

[42] F. Saia, A. Marzocchi, P.W. Serruys, Drug-eluting stents. The third revolution in percutaneous coronary intervention, Ital. Heart J. 6 (2005) 289-303.

[43] E. Grube, U. Gerckens, R. Muller, L. Bullesfeld, Drug eluting stents: Initial experiences, Z. Kardiol. 91 (2002) 44-48.

[44] M.C. Morice, P.W. Serruys, J.E. Sousa, J. Fajadet, E. Ban Hayashi, M. Perin, A. Colombo, G. Schuler, P. Barragan, G. Guagliumi, F. Molnar, R. Falotico, A randomized comparison of a sirolimus-eluting stent with a standard stent for coronary revascularization, N. Engl. J. Med. 346 (2002) 1773-1780.

[45] J.W. Moses, M.B. Leon, J.J. Popma, P.J. Fitzgerald, D.R. Holmes, C. O'Shaughnessy, R.P. Caputo, D.J. Kereiakes, D.O. Williams, P.S. Teirstein, J.L. Jaeger, R.E. Kuntz, Sirolimus-eluting stents versus standard stents in patients with stenosis in a native coronary artery, N. Engl. J. Med. 349 (2003) 1315-1323.

[46] J. Schofer, M. Schluter, A.H. Gershlick, W. Wijns, E. Garcia, E. Schampaert, G. Breithardt, Sirolimus-eluting stents for treatment of patients with long atherosclerotic lesions in small coronary arteries: Double-blind, randomised controlled trial (e-sirius), Lancet 362 (2003) 1093-1099.

[47] D. Ardissino, C. Cavallini, E. Bramucci, C. Indolfi, A. Marzocchi, A. Manari, G. Angeloni, G. Carosio, E. Bonizzoni, S. Colusso, M. Repetto, P.A. Merlini, Sirolimus-eluting vs uncoated stents for prevention of restenosis in small coronary arteries: A randomized trial, JAMA 292 (2004) 2727-2734.

[48] E. Grube, S. Silber, K.E. Hauptmann, R. Mueller, L. Buellesfeld, U. Gerckens, M.E. Russell, Taxus i: Six- and twelve-month results from a randomized, double-blind trial on a slow-release paclitaxel-eluting stent for de novo coronary lesions, Circulation 107 (2003) 38-42.

[49] K. Tanabe, P.W. Serruys, E. Grube, P.C. Smits, G. Selbach, W.J. van der Giessen, M. Staberock, P. de Feyter, R. Muller, E. Regar, M. Degertekin, J.M. Ligthart, C. Disco, B. Backx, M.E. Russell, Taxus III trial: In-stent restenosis treated with stent-based delivery of paclitaxel incorporated in a slow-release polymer formulation, Circulation 107 (2003) 559-564.

[50] G.W. Stone, S.G. Ellis, D.A. Cox, J. Hermiller, C. O'Shaughnessy, J.T. Mann, M. Turco, R. Caputo, P. Bergin, J. Greenberg, J.J. Popma, M.E. Russell, One-year clinical results with the slow-release, polymer-based, paclitaxel-eluting taxus stent: The Taxus IV trial, Circulation 109 (2004) 1942-1947.

[51] P.A. Lemos, P.W. Serruys, R.T. van Domburg, F. Saia, C.A. Arampatzis, A. Hoye, M. Degertekin, K. Tanabe, J. Daemen, T.K. Liu, E. McFadden, G. Sianos, S.H. Hofma, P.C. Smits, W.J. van der Giessen, P.J. de Feyter, Unrestricted utilization of sirolimus-eluting stents compared with conventional bare stent implantation in the "Real world": The rapamycin-eluting stent evaluated at Rotterdam Cardiology Hospital (research) registry, Circulation 109 (2004) 190-195.

[52] R. Zahn, C.W. Hamm, S. Schneider, U. Zeymer, C.A. Nienaber, G. Richardt, M. Kelm, B. Levenson, T. Bonzel, U. Tebbe, G. Sabin, J. Senges, Incidence and predictors of target vessel revascularization and clinical event rates of the sirolimus-eluting coronary stent (results from the prospective multicenter german Cypher stent registry), Am. J. Cardiol. 95 (2005) 1302-1308.

[53] A.T. Ong, P.W. Serruys, J. Aoki, A. Hoye, C.A. van Mieghem, G.A. Rodriguez-Granillo, M. Valgimigli, K. Sonnenschein, E. Regar, M. van der Ent, P.P. de Jaegere, E.P. McFadden, G. Sianos, W.J. van der Giessen, P.J. de Feyter, R.T. van Domburg, The unrestricted use of paclitaxel- versus sirolimus-eluting stents for coronary artery disease in an unselected population: One-year results of the Taxus-stent evaluated at Rotterdam Cardiology Hospital (t-search) registry, J. Am. Coll. Cardiol. 45 (2005) 1135-1141.

[54] A. Kastrati, A. Dibra, S. Eberle, J. Mehilli, J. Suarez de Lezo, J.J. Goy, K. Ulm, A. Schomig, Sirolimus-eluting stents vs paclitaxel-eluting stents in patients with coronary artery disease: Meta-analysis of randomized trials, JAMA 294 (2005) 819-825.

[55] E. Grube, L. Buellesfeld, Rapamycin analogs for stent-based local drug delivery. Everolimus- and tacrolimus-eluting stents, Herz 29 (2004) 162-166.

[56] E. Grube, L. Buellesfeld, Everolimus for stent-based intracoronary applications, Rev. Cardiovasc. Med. 5 Suppl 2 (2004) S3-8.

[57] M.A. Beijk, J.J. Piek, Xience V everolimus-eluting coronary stent system: A novel second generation drug-eluting stent, Expert Rev. Med. Devices 4 (2007) 11-21.

[58] H. Storger, E. Grube, M. Hofmann, F. Schwarz, J. Haase, Clinical experiences using everolimus-eluting stents in patients with coronary artery disease, J. Interv. Cardiol. 17 (2004) 387-390.

[59] H. Honda, T. Meguro, K. Takizawa, S. Isoyama, Use of everolimus-eluting stent with a bioresorbable polymer coating for treatment of recurrent in-stent restenosis, J. Invasive Cardiol. 17 (2005) 112-115.

[60] Y. Tsuchiya, A.J. Lansky, R.A. Costa, R. Mehran, C. Pietras, Y. Shimada, S. Sonoda, E. Cristea, M. Negoita, G.D. Dangas, J.W. Moses, M.B. Leon, P.J. Fitzgerald, R. Muller, H. Storger, K.E. Hauptmann, E. Grube, Effect of everolimus-eluting stents in different vessel sizes (from the pooled future i and ii trials), Am. J. Cardiol. 98 (2006) 464-469.

[61] J.A. Ormiston, M.W. Webster, G. Armstrong, First-in-human implantation of a fully bioabsorbable drug-eluting stent: The BVS poly-l-lactic acid everolimus-eluting coronary stent, Catheter. Cardiovasc. Interv. 69 (2007) 128-131.

[62] S. Tanimoto, P.W. Serruys, L. Thuesen, D. Dudek, B. de Bruyne, B. Chevalier, J.A. Ormiston, Comparison of in vivo acute stent recoil between the bioabsorbable everolimus-eluting coronary stent and the everolimus-eluting cobalt chromium coronary stent: Insights from the Absorb and Spirit trials, Catheter. Cardiovasc. Interv. 14 (2007) 14.

[63] L. Buellesfeld, E. Grube, Abt-578-eluting stents. The promising successor of sirolimus- and paclitaxel-eluting stent concepts?, Herz 29 (2004) 167-170.

[64] D.E. Kandzari, M.B. Leon, Overview of pharmacology and clinical trials program with the zotarolimus-eluting Endeavor stent, J. Interv. Cardiol. 19 (2006) 405-413.

[65] S. Korovesis, E. Giazitzoglou, D.G. Katritsis, Subacute thrombosis following implantation of zotarolimus-eluting stent, Hellenic J. Cardiol. 47 (2006) 310-312.

[66] J. Fajadet, W. Wijns, G.J. Laarman, K.H. Kuck, J. Ormiston, T. Munzel, J.J. Popma, P.J. Fitzgerald, R. Bonan, R.E. Kuntz, Randomized, double-blind, multicenter study of the endeavor zotarolimus-eluting phosphorylcholine-encapsulated stent for treatment of native coronary artery lesions: Clinical and angiographic results of the Endeavor II trial, Circulation 114 (2006) 798-806.

[67] D.E. Kandzari, M.B. Leon, J.J. Popma, P.J. Fitzgerald, C. O'Shaughnessy, M.W. Ball, M. Turco, R.J. Applegate, P.A. Gurbel, M.G. Midei, S.S. Badre, L. Mauri, K.P. Thompson, L.A. LeNarz, R.E. Kuntz, Comparison of zotarolimus-eluting and sirolimus-eluting stents in patients with native coronary artery disease: A randomized controlled trial, J. Am. Coll. Cardiol. 48 (2006) 2440-2447.

[68] A. Jeremias, B. Sylvia, J. Bridges, A.J. Kirtane, B. Bigelow, D.S. Pinto, K.K. Ho, D.J. Cohen, L.A. Garcia, D.E. Cutlip, J.P. Carrozza, Jr., Stent thrombosis after successful sirolimus-eluting stent implantation, Circulation 109 (2004) 1930-1932.

[69] I. Iakovou, T. Schmidt, E. Bonizzoni, L. Ge, G.M. Sangiorgi, G. Stankovic, F. Airoldi, A. Chieffo, M. Montorfano, M. Carlino, I. Michev, N. Corvaja, C. Briguori, U. Gerckens, E. Grube, A. Colombo, Incidence, predictors, and outcome of thrombosis after successful implantation of drug-eluting stents, JAMA 293 (2005) 2126-2130.

[70] J.R. Nebeker, R. Virmani, C.L. Bennett, J.M. Hoffman, M.H. Samore, J. Alvarez, C.J. Davidson, J.M. McKoy, D.W. Raisch, B.K. Whisenant, P.R. Yarnold, S.M. Belknap, D.P. West, J.E. Gage, R.E. Morse, G. Gligoric, L. Davidson, M.D. Feldman, Hypersensitivity cases associated with drug-eluting coronary stents: A review of available cases from the research on adverse drug events and reports (RADAR) project, J. Am. Coll. Cardiol. 47 (2006) 175-181.

[71] M. Joner, A.V. Finn, A. Farb, E.K. Mont, F.D. Kolodgie, E. Ladich, R. Kutys, K. Skorija, H.K. Gold, R. Virmani, Pathology of drug-eluting stents in humans: Delayed healing and late thrombotic risk, J. Am. Coll. Cardiol. 48 (2006) 193-202.

[72] R. Virmani, F. Liistro, G. Stankovic, C. Di Mario, M. Montorfano, A. Farb, F.D. Kolodgie, A. Colombo, Mechanism of late in-stent restenosis after implantation of a paclitaxel derivate-eluting polymer stent system in humans, Circulation 106 (2002) 2649-2651.

[73] S.H. Duda, B. Pusich, G. Richter, P. Landwehr, V.L. Oliva, A. Tielbeek, B. Wiesinger, J.B. Hak, H. Tielemans, G. Ziemer, E. Cristea, A. Lansky, J.P. Beregi, Sirolimus-eluting stents for the treatment of obstructive superficial femoral artery disease: Six-month results, Circulation 106 (2002) 1505-1509.

[74] S.H. Duda, M. Bosiers, J. Lammer, D. Scheinert, T. Zeller, A. Tielbeek, J. Anderson, B. Wiesinger, G. Tepe, A. Lansky, C. Mudde, H. Tielemans, J.P. Beregi, Sirolimus-eluting versus bare nitinol stent for obstructive superficial femoral artery disease: The Sirocco II trial, J. Vasc. Interv. Radiol. 16 (2005) 331-338.

[75] D.N. Ku, D.P. Giddens, C.K. Zarins, S. Glagov, Pulsatile flow and atherosclerosis in the human carotid bifurcation. Positive correlation between plaque location and low oscillating shear stress, Arterosclerosis 5 (1985) 293-302.

[76] J.E. Moore, Jr., C. Xu, S. Glagov, C.K. Zarins, D.N. Ku, Fluid wall shear stress measurements in a model of the human abdominal aorta: Oscillatory behavior and relationship to atherosclerosis, Atherosclerosis 110 (1994) 225-240.

[77] X. He, D.N. Ku, Pulsatile flow in the human left coronary artery bifurcation: Average conditions, J. Biomech. Eng. 118 (1996) 74-82.

[78] K. Rhee, J.M. Tarbell, A study of the wall shear rate distribution near the end-to-end anastomosis of a rigid graft and a compliant artery, J. Biomech. 27 (1994) 329-338.

[79] C.P. Cheng, N.M. Wilson, R.L. Hallett, R.J. Herfkens, C.A. Taylor, In vivo MR angiographic quantification of axial and twisting deformations of the superficial femoral artery resulting from maximum hip and knee flexion, J. Vasc. Interv. Radiol. 17 (2006) 979-987.

[80] V.A. DePalma, R.E. Baier, J.W. Ford, V.L. Glott, A. Furuse, Investigation of three-surface properties of several metals and their relation to blood compatibility, J. Biomed. Mater. Res. 6 (1972) 37-75.

[81] C.M. Agrawal, K.F. Haas, D.A. Leopold, H.G. Clark, Evaluation of poly(L-lactic acid) as a material for intravascular polymeric stents, Biomaterials 13 (1992) 176-182.

[82] W.J. van der Giessen, H.M.M. van Beusekom, C.D. van Houten, L.J. van Woerkens, P.D. Verdouw, P.W. Serruys, Coronary stenting with polymer-coated and uncoated self-expanding endoprostheses in pigs, Coron. Artery Dis. 3 (1992) 631-640.

[83] J.G. Murphy, R.S. Schwartz, K.C. Huber, D.R. Holmes, Jr., Polymeric stents: Modern alchemy or the future?, J. Invasive Cardiol. 3 (1991) 144-148.

[84] T. Peng, P. Gibula, K.-d. Yao, M.F.A. Goosen, Role of polymers in improving the results of stenting in coronary arteries, Biomaterials 17 (1996) 685-694.

[85] I.K. De Scheerder, K.L. Wilczek, E.V. Verbeken, J. Vandorpe, P.N. Lan, E. Schacht, H. De Geest, J. Piessens, Biocompatibility of polymer-coated oversized metallic stents implanted in normal porcine coronary arteries, Atherosclerosis 114 (1995) 105-114.

[86] O.F. Bertrand, R. Sipehia, R. Mongrain, J. Rodes, J.C. Tardif, L. Bilodeau, G. Cote, M.G. Bourassa, Biocompatibility aspects of new stent technology, J. Am. Coll. Cardiol. 32 (1998) 562-571.

[87] D.R. Holmes, A.R. Camrud, M.A. Jorgenson, W.D. Edwards, R.S. Schwartz, Polymeric stenting in the porcine coronary artery model: Differential outcome of exogenous fibrin sleeves versus polyurethane-coated stents, J. Am. Coll. Cardiol. 24 (1994) 525-531.

[88] P.W. Serruys, H. Emanuelsson, W. van der Giessen, A.C. Lunn, F. Kiemeney, C. Macaya, W. Rutsch, G. Heyndrickx, H. Suryapranata, V. Legrand, J.J. Goy, P. Materne, H. Bonnier, M.C. Morice, J. Fajadet, J. Belardi, A. Colombo, E. Garcia, P. Ruygrok, P. de Jaegere, M.A. Morel, Heparin-coated Palmaz-Schatz stents in human coronary arteries. Early outcome of the Benestent-II pilot study, Circulation 93 (1996) 412-422.

[89] M.N. Babapulle, M.J. Eisenberg, Coated stents for the prevention of restenosis: Part ii, Circulation 106 (2002) 2859-2866.

[90] S. Silber, J. Hamburger, E. Grube, M. Pfisterer, J. Belardi, J. Webb, K. Zmudka, C. Nienaber, K. Hauptman, W. Rutsch, K. Dawkins, J. Drzewiecki, J. Koglin, A.

Colombo, Direct stenting with Taxus stents seems to be as safe and effective as with predilatation. A post hoc analysis of Taxus II, Herz 29 (2004) 171-180.

[91]   J.G. Murphy, R.S. Schwartz, W.D. Edwards, A.R. Camrud, R.E. Vlietstra, D.R. Holmes, Jr., Percutaneous polymeric stents in porcine coronary arteries. Initial experience with polyethylene terephthalate stents, Circulation 86 (1992) 1596-1604.

[92]   W.J. van der Giessen, C.J. Slager, H.M. van Beusekom, D.S. van Ingen Schenau, R.A. Huijts, J.C. Schuurbiers, W.J. de Klein, P.W. Serruys, P.D. Verdouw, Development of a polymer endovascular prosthesis and its implantation in porcine arteries, J. Interv. Cardiol. 5 (1992) 175-185.

[93]   W.J. van der Giessen, C.J. Slager, E.J. Gussenhoven, H.M. van Beusekom, R.A. Huijts, J.C. Schuurbiers, R.A. Wilson, P.W. Serruys, P.D. Verdouw, Mechanical features and in vivo imaging of a polymer stent, Int. J. Card. Imaging 9 (1993) 219-226.

[94]   W.J. van der Giessen, A.M. Lincoff, R.S. Schwartz, H.M. van Beusekom, P.W. Serruys, D.R. Holmes, Jr., S.G. Ellis, E.J. Topol, Marked inflammatory sequelae to implantation of biodegradable and nonbiodegradable polymers in porcine coronary arteries, Circulation 94 (1996) 1690-1697.

[95]   T.A. Fischell, Polymer coatings for stents. Can we judge a stent by its cover?, Circulation 94 (1996) 1494-1495.

[96]   I.K. De Scheerder, K.L. Wilczek, E.V. Verbeken, J. Vandorpe, P.N. Lan, E. Schacht, J. Piessens, H. De Geest, Biocompatibility of biodegradable and nonbiodegradable polymer-coated stents implanted in porcine peripheral arteries, Cardiovasc. Intervent. Radiol. 18 (1995) 227-232.

[97]   J. Zidar, A. Lincoff, R. Stack, Biodegradable stents, in: E.J. Topol, (Ed), Textbook of interventional cardiolology, WB Saunders, Philadelphia, 1994, pp. 787-802.

[98]   H. Tamai, K. Igaki, E. Kyo, K. Kosuga, A. Kawashima, S. Matsui, H. Komori, T. Tsuji, S. Motohara, H. Uehata, Initial and 6-month results of biodegradable poly-L-lactic acid coronary stents in humans, Circulation 102 (2000) 399-404.

[99]   D.P. Faxon, Vascular stents, Rev. Cardiovasc. Med. 2 (2001) 106-107.

[100]   A. Colombo, E. Karvouni, Biodegradable stents: "Fulfilling the mission and stepping away", Circulation 102 (2000) 371-373.

[101]   G. Wills, Cincinnatus: George Washington and the enlightenment, 1st edition, Doubleday, Garden City, NY, 1984.

[102]   T. Kimura, H. Yokoi, Y. Nakagawa, T. Tamura, S. Kaburagi, Y. Sawada, Y. Sato, H. Yokoi, N. Hamasaki, H. Nosaka, et al., Three-year follow-up after implantation of metallic coronary-artery stents, N. Engl. J. Med. 334 (1996) 561-566.

[103] A. Kastrati, D. Hall, A. Schomig, Long-term outcome after coronary stenting, Curr. Contr. Trials C. 1 (2000) 48-54.

[104] E. Therasse, G. Soulez, P. Cartier, L. Passerini, P. Roy, L. Bruneau, L. Gaboury, Infection with fatal outcome after endovascular metallic stent placement, Radiology 192 (1994) 363-365.

[105] R. Blindt, K.M. Hoffmeister, H. Bienert, Pfannschmitt, G. Bartsch, H. Thissen, D. Klee, J. Vom Dahl, Development of a new biodegradable intravascular polymer stent with simultaneous incorporation of bioactive substances, Int. J. Artif. Organs 22 (1999) 843-853.

[106] M.E. Staab, D.R. Holmes, R.S. Schwartz, Polymers, in: U. Sigwart, (Ed), Endoluminal stenting, WB Saunders, London, 1996, pp. 34-44.

[107] T. Hayashi, Biodegradable polymers for biomedical uses, Prog. Polym. Sci. 19 (1994) 663-702.

[108] N. Grabow, M. Schlun, K. Sternberg, N. Hakansson, S. Kramer, K.P. Schmitz, Mechanical properties of laser cut poly(L-lactide) micro-specimens: Implications for stent design, manufacture, and sterilization, J. Biomech. Eng. 127 (2005) 25-31.

[109] T. Valimaa, S. Laaksovirta, T.L. Tammela, P. Laippala, M. Talja, T. Isotalo, A. Petas, K. Tarri, P. Tormala, Viscoelastic memory and self-expansion of self-reinforced bioabsorbable stents, Biomaterials 23 (2002) 3575-3582.

[110] I. Uurto, J. Mikkonen, J. Parkkinen, L. Keski-Nisula, T. Nevalainen, M. Kellomaki, P. Tormala, J.P. Salenius, Drug-eluting biodegradable poly-D/L-lactic acid vascular stents: An experimental pilot study, J. Endovasc. Ther. 12 (2005) 371-379.

[111] S.H. Su, R.Y. Chao, C.L. Landau, K.D. Nelson, R.B. Timmons, R.S. Meidell, R.C. Eberhart, Expandable bioresorbable endovascular stent. I. Fabrication and properties, Ann. Biomed. Eng. 31 (2003) 667-677.

[112] E.M. Hietala, U.S. Salminen, A. Stahls, T. Valimaa, P. Maasilta, P. Tormala, M.S. Nieminen, A.L. Harjula, Biodegradation of the copolymeric polylactide stent. Long-term follow-up in a rabbit aorta model, J. Vasc. Res. 38 (2001) 361-369.

[113] M. Unverdorben, A. Spielberger, M. Schywalsky, D. Labahn, S. Hartwig, M. Schneider, D. Lootz, D. Behrend, K. Schmitz, R. Degenhardt, M. Schaldach, C. Vallbracht, A polyhydroxybutyrate biodegradable stent: Preliminary experience in the rabbit, Cardiovasc. Intervent. Radiol. 25 (2002) 127-132.

[114] C.M. Agrawal, H.G. Clark, Deformation characteristics of a bioabsorbable intravascular stent, Invest. Radiol. 27 (1992) 1020-1024.

[115] M. Zilberman, K.D. Nelson, R.C. Eberhart, Mechanical properties and in vitro degradation of bioresorbable fibers and expandable fiber-based stents, J. Biomed. Mater. Res. B 74 (2005) 792-799.

[116] N. Grabow, H. Martin, K.P. Schmitz, The impact of material characteristics on the mechanical properties of a poly(L-lactide) coronary stent, Biomed. Tech. (Berl). 47 Suppl 1 Pt 1 (2002) 503-505.

[117] J.P. Nuutinen, C. Clerc, P. Tormala, Theoretical and experimental evaluation of the radial force of self-expanding braided bioabsorbable stents, J. Biomater. Sci. Polym. Ed. 14 (2003) 677-687.

[118] B. Heublein, R. Rohde, V. Kaese, M. Niemeyer, W. Hartung, A. Haverich, Biocorrosion of magnesium alloys: A new principle in cardiovascular implant technology?, Heart 89 (2003) 651-656.

[119] C. Di Mario, H. Griffiths, O. Goktekin, N. Peeters, J. Verbist, M. Bosiers, K. Deloose, B. Heublein, R. Rohde, V. Kasese, C. Ilsley, R. Erbel, Drug-eluting bioabsorbable magnesium stent, J. Interv. Cardiol. 17 (2004) 391-395.

[120] M. Peuster, P. Wohlsein, M. Brugmann, M. Ehlerding, K. Seidler, C. Fink, H. Brauer, A. Fischer, G. Hausdorf, A novel approach to temporary stenting: Degradable cardiovascular stents produced from corrodible metal - results 6-18 months after implantation into new zealand white rabbits, Heart 86 (2001) 563-569.

[121] J.D. Bier, P. Zalesky, S.T. Li, H. Sasken, D.O. Williams, A new bioabsorbable intravascular stent: In vitro assessment of hemodynamic and morphometric characteristics, J. Interv. Cardiol. 5 (1992) 187-194.

[122] A. Lauto, M. Ohebshalom, M. Esposito, J. Mingin, P.S. Li, D. Felsen, M. Goldstein, D.P. Poppas, Self-expandable chitosan stent: Design and preparation, Biomaterials 22 (2001) 1869-1874.

[123] M. Vert, Aliphatic polyesters: Great degradable polymers that cannot do everything, Biomacromolecules 6 (2005) 538-546.

[124] M. Labinaz, J.P. Zidar, R.S. Stack, H.R. Phillips, Biodegradable stents: The future of interventional cardiology?, J. Interv. Cardiol. 8 (1995) 395-405.

[125] H. Tamai, K. Igaki, T. Tsuji, E. Kyo, K. Kosuga, A. Kawashima, S. Matsui, H. Komori, S. Motohara, H. Uehata, E. Takeuchi, A biodegradable poly-L-lactic acid coronary stent in the porcine coronary artery, J. Interv. Cardiol. 12 (1999) 443-449.

[126] T. Tsuji, H. Tamai, K. Igaki, E. Kyo, K. Kosuga, T. Hata, M. Okada, T. Nakamura, H. Komori, S. Motohara, H. Uehata, Biodegradable polymeric stents, Curr. Interv. Cardiol. Rep. 3 (2001) 10-17.

[127] T. Tsuji, H. Tamai, K. Igaki, E. Kyo, K. Kosuga, T. Hata, T. Nakamura, S. Fujita, S. Takeda, S. Motohara, H. Uehata, Biodegradable stents as a platform to drug loading, Int. J. Cardiovasc. Intervent. 5 (2003) 13-16.

[128] M. Zilberman, N.D. Schwade, R.C. Eberhart, Protein-loaded bioresorbable fibers and expandable stents: Mechanical properties and protein release, J. Biomed. Mater. Res. B 69 (2004) 1-10.

[129] T.L. Tammela, M. Talja, Biodegradable urethral stents, BJU Int. 92 (2003) 843-850.

[130] T. Isotalo, M. Talja, T. Valimaa, P. Tormala, T.L. Tammela, A bioabsorbable self-expandable, self-reinforced poly-L-lactic acid urethral stent for recurrent urethral strictures: Long-term results, J. Endourol. 16 (2002) 759-762.

[131] I. Uurto, A. Kotsar, T. Isotalo, J. Mikkonen, P.M. Martikainen, M. Kellomaki, P. Tormala, T.L. Tammela, M. Talja, J.P. Salenius, Tissue biocompatibility of new biodegradable drug-eluting stent materials, J. Mater. Sci. - Mater. Med. 18 (2007) 1543-1547.

[132] H. Laufman, T. Rubel, Synthetic absorbable sutures, Surg. Gynecol. Obstet. 145 (1977) 597-608.

[133] W.S. Pietrzak, M.L. Verstynen, D.R. Sarver, Bioabsorbable fixation devices: Status for the craniomaxillofacial surgeon, J. Craniofac. Surg. 8 (1997) 92-96.

[134] R. Langer, Drug delivery and targeting, Nature 392 (1998) 5-10.

[135] S. Levenberg, R. Langer, Advances in tissue engineering, in: G.P. Schatten, (Ed), Current topics in developmental biology, vol. 61, Current topics in developmental biology 61, Elsevier Academic Press Inc, San Diego, 2004, pp. 113-134.

[136] M. Vert, S.M. Li, G. Spenlehauer, P. Guerin, Bioresorbability and biocompatibility of aliphatic polyesters, J. Mater. Sci. - Mater. Med. 3 (1992) 432-446.

[137] G. Khang, J.M. Rhee, J.K. Jeong, J.S. Lee, M.S. Kim, S.H. Cho, H.B. Lee, Local drug delivery system using biodegradable polymers, Macromol. Res. 11 (2003) 207-223.

[138] K.A. Athanasiou, C.M. Agrawal, F.A. Barber, S.S. Burkhart, Orthopaedic applications for PLA-PGA biodegradable polymers, Arthroscopy 14 (1998) 726-737.

[139] J.C. Middleton, A.J. Tipton, Synthetic biodegradable polymers as orthopedic devices, Biomaterials 21 (2000) 2335-2346.

[140] R.M. Ottenbrite, A.C. Albertsson, G. Scott, Discussion on degradation terminology, in: M. Vert, J. Feijen, A.C. Albertsson, G. Scott, E. Chiellini, (Eds),

Biodegradable polymers and plastics, The Royal Society of Chemisty, Cambridge, 1992, pp. 73-92.

[141] W.S. Pietrzak, D.R. Sarver, M.L. Verstynen, Bioabsorbable polymer science for the practicing surgeon, J. Craniofac. Surg. 8 (1997) 87-91.

[142] A. Gopferich, Polymer degradation and erosion: Mechanisms and applications, Eur. J. Pharm. Biopharm. 4 (1996) 1-11.

[143] A. Gopferich, Mechanisms of polymer degradation and elimination, in: A.J. Domb, J. Kost, D.M. Wiseman, (Eds), Handbook of biodegradable polymers, Drug targeting and delivery, Harwood Academic Publishers, Australia, 1997, pp. 451-471.

[144] N.A. Weir, F.J. Buchanan, J.F. Orr, D.F. Farrar, G.R. Dickson, Degradation of poly-L-lactide: Part 2: Increased temperature accelerated degradation, P. I. Mech. Eng. H 218 (2004) 321-330.

[145] W. Schnabel, Polymer degradation, Macmillan Publishing, New York, 1981.

[146] D.J. Harmon, H.L. Jacobs, Degradation of natural rubber during mill mastication, J. Appl. Polym. Sci. 10 (1966) 253-257.

[147] D. Campbell, A. Peterlin, Free-radical formation in uniaxially stressed nylon, J. Polym. Sci. Pol. Lett. 6 (1968) 481-485.

[148] L.R.G. Treloar, Physics of rubber elasticity, 2nd, Clarendon Press, Oxford, 1958.

[149] N.A. Weir, F.J. Buchanan, J.F. Orr, G.R. Dickson, Degradation of poly-l-lactide: Part 1: In vitro and in vivo physiological temperature degradation, P. I. Mech. Eng. H 218 (2004) 307-319.

[150] W.L. Hawkins, Polymer degradation, Polymer degradation and stabilization, Springer-Verlag, Berlin, 1984, pp. 3-34.

[151] S.A. Ali, S.P. Zhong, P.J. Doherty, D.F. Williams, Mechanisms of polymer degradation in implantable devices. 1. Poly(caprolactone), Biomaterials 14 (1993) 648-656.

[152] S.A. Ali, P.J. Doherty, D.F. Williams, Mechanisms of polymer degradation in implantable devices. 2. Poly(DL-lactic acid), J. Biomed. Mater. Res. 27 (1993) 1409-1418.

[153] X.S. Wu, N. Wang, Synthesis, characterization, biodegradation, and drug delivery application of biodegradable lactic/glycolic acid polymers. Part ii: Biodegradation, J. Biomater. Sci. Polym. Ed. 12 (2001) 21-34.

[154] R.A. Miller, J.M. Brady, D.E. Cutright, Degradation rates of oral resorbable implants (polylactates and polyglycolates): Rate modification with changes in PLA/PGA copolymer ratios, J. Biomed. Mater. Res. 11 (1977) 711-719.

[155] S.H. Hyon, K. Jamshidi, Y. Ikada, Effects of residual monomer on the degradation of DL-lactide polymer, Polym. Int. 46 (1998) 196-202.

[156] G.L. Siparsky, K.J. Voorhees, F.D. Miao, Hydrolysis of polylactic acid (PLA) and polycaprolactone (PCL) in aqueous acetonitrile solutions: Autocatalysis, J. Environ. Polym. Deg. 6 (1998) 31-41.

[157] Y. Zhang, S. Zale, L. Sawyer, H. Bernstein, Effects of metal salts on poly(DL-lactide-co-glycolide) polymer hydrolysis, J. Biomed. Mater. Res. 34 (1997) 531-538.

[158] T. Ivanova, N. Grozev, I. Panaiotov, J.E. Proust, Role of the molecular weight and the composition on the hydrolysis kinetics of monolayers of poly(alpha-hydroxy acid)s, Colloid Polym. Sci. 277 (1999) 709-718.

[159] C. Booth, The mechanical degradation of polymers, Polymer 4 (1963) 471-478.

[160] A.B. Bestul, Evidence for mechanical shear degradation of high polymers, J. Phys. Chem. 61 (1957) 418-421.

[161] J.D. Culter, J.L. Zakin, G.K. Patterson, Mechanical degradation of dilute-solutions of high polymers in capillary tube flow, J. Appl. Polym. Sci. 19 (1975) 3235-3240.

[162] J.F.S. Yu, J.L. Zakin, G.K. Patterson, Mechanical degradation of high molecular-weight polymers in dilute-solution, J. Appl. Polym. Sci. 23 (1979) 2493-2512.

[163] N.D. Miller, D.F. Williams, The in vivo and in vitro degradation of poly(glycolic acid) suture material as a function of applied strain, Biomaterials 5 (1984) 365-368.

[164] C.C. Chu, Strain-accelerated hydrolytic degradation of synthetic absorbable sutures, in: C.W. Hall, (Ed), Surgical research, recent developments: Proceedings of the First Annual Scientific Session of the Academy of Surgical Research, Pergamon Press, San Antonio, 1985, pp. 111-115.

[165] S.P. Zhong, P.J. Doherty, D.F. Williams, The effect of applied strain on the degradation of absorbable suture in vitro, Clin. Mater. 14 (1993) 183-189.

[166] M. Deng, J. Zhou, G. Chen, D. Burkley, Y. Xu, D. Jamiolkowski, T. Barbolt, Effect of load and temperature on in vitro degradation of poly(glycolide-co-L-lactide) multifilament braids, Biomaterials 26 (2005) 4327-4336.

[167] M.J. Wiggins, J.M. Anderson, A. Hiltner, Effect of strain and strain rate on fatigue-accelerated biodegradation of polyurethane, J. Biomed. Mater. Res. A 66A (2003) 463-475.

[168] M.J. Wiggins, J.M. Anderson, A. Hiltner, Biodegradation of polyurethane under fatigue loading, J. Biomed. Mater. Res. A 65A (2003) 524-535.

[169] J.A. Tamada, R. Langer, Erosion kinetics of hydrolytically degradable polymers, Proc. Natl. Acad. Sci. U. S. A. 90 (1993) 552-556.

[170] F.V. Burkersroda, L. Schedl, A. Gopferich, Why degradable polymers undergo surface erosion or bulk erosion?, Biomaterials 23 (2002) 4221-4231.

[171] D.S. Katti, S. Lakshmi, R. Langer, C.T. Laurencin, Toxicity, biodegradation and elimination of polyanhydrides, Adv. Drug Deliver. Rev. 54 (2002) 933-961.

[172] S.M. Li, S. McCarthy, Further investigations on the hydrolytic degradation of poly(DL-lactide), Biomaterials 20 (1999) 35-44.

[173] H. Pistner, D.R. Bendix, J. Muhling, J.F. Reuther, Poly(L-lactide) - a long-term degradation study in vivo. 3. Analytical characterization, Biomaterials 14 (1993) 291-298.

[174] S.M. Li, M. Vert, Morphological-changes resulting from the hydrolytic degradation of stereocopolymers derived from L-lactides and DL-lactides, Macromolecules 27 (1994) 3107-3110.

[175] J.M. Schakenraad, M.J. Hardonk, J. Feijen, I. Molenaar, P. Nieuwenhuis, Enzymatic activity toward poly(L-lactic acid) implants, J. Biomed. Mater. Res. 24 (1990) 529-545.

[176] H. Pistner, R. Gutwald, R. Ordung, J. Reuther, J. Muhling, Poly(L-lactide) - a long-term degradation study in vivo. 1. Biological results, Biomaterials 14 (1993) 671-677.

[177] K.T. Nguyen, S.H. Su, A. Sheng, D. Wawro, N.D. Schwade, C.F. Brouse, P.E. Greilich, L. Tang, R.C. Eberhart, In vitro hemocompatibility studies of drug-loaded poly-(L-lactic acid) fibers, Biomaterials 24 (2003) 5191-5201.

[178] R. Gutwald, H. Pistner, J. Reuther, J. Muhling, Biodegradation and tissue-reaction in a long-term implantation study of poly(L-lactide), J. Mater. Sci. - Mater. Med. 5 (1994) 485-490.

[179] D.F. Williams, Biodegradation of surgical polymers, J. Mater. Sci. 17 (1982) 1233-1246.

[180] M. Vert, S. Li, H. Garreau, J. Mauduit, M. Boustta, G. Schwach, R. Engel, J. Coudane, Complexity of the hydrolytic degradation of aliphatic polyesters, Angew. Markomol. Chemie 247 (1997) 239-253.

[181] T.Q. Nguyen, Kinetics of mechanochemical degradation by gel permeation chromatography, Polym. Degrad. Stabil. 46 (1994) 99-111.

[182] T.Q. Nguyen, H.H. Kausch, GPC data interpretation in mechanochemical polymer degradation, Int. J. Polym. Anal. Ch. 4 (1998) 447-470.

[183] W. Kuhn, The kinetics of the decomposition of high molecular chains, Ber. Deut. Chem. Ges. 63 (1930) 1503-1509.

[184] E.W. Montroll, R. Simha, Theory of depolymerization of long chain molecules, J. Chem. Phys. 8 (1940) 721-727.

[185] O. Saito, On the effect of high energy radiation to polymers. 1. Cross-linking and degradation, J. Phys. Soc. Jpn. 13 (1958) 198-206.

[186] K.W. Scott, Criteria for random degradation of linear polymers, J. Polym. Sci. Pol. Sym. (1974) 321-334.

[187] M. Ballauff, B.A. Wolf, Degradation of chain molecules. 1. Exact solution of the kinetic-equations, Macromolecules 14 (1981) 654-658.

[188] A.M. Kotliar, S. Podgor, Evaluation of molecular size distributions and molecular weight averages resulting from random crosslinking and chain-scission processes, J. Polym. Sci. 55 (1961) 423-436.

[189] A.M. Emsley, R.J. Heywood, Computer modeling of the degradation of linear-polymers, Polym. Degrad. Stabil. 49 (1995) 145-149.

[190] A.V. Shyichuk, V.S. Lutsjak, A determination of rates ratio of simultaneous cross-linking and scission from MWD shape, Eur. Polym. J. 31 (1995) 631-634.

[191] V. Bellenger, M. Ganem, B. Mortaigne, J. Verdu, Lifetime prediction in the hydrolytic aging of polyesters, Polym. Degrad. Stabil. 49 (1995) 91-97.

[192] D. Browarzik, A. Koch, Application of continuous kinetics to polymer degradation, J. Macromol. Sci. - Pure Appl. Chem. A33 (1996) 1633-1641.

[193] J.E.J. Staggs, Modelling random scission of linear polymers, Polym. Degrad. Stabil. 76 (2002) 37-44.

[194] J.S. Yoon, H.J. Jin, I.J. Chin, C. Kim, M.N. Kim, Theoretical prediction of weight loss and molecular weight during random chain scission degradation of polymers, Polymer 38 (1997) 3573-3579.

[195] S.M. Bose, Y. Git, Mathematical modelling and computer simulation of linear polymer degradation: Simple scissions, Macromol. Theor. Simul. 13 (2004) 453-473.

[196] A. Joshi, K.J. Himmelstein, Dynamics of controlled release from bioerodible matrices, J. Control. Release 15 (1991) 95-104.

[197] A.G. Thombre, Theoretical aspects of polymer biodegradation: Mathematical modeling of drug release and acid-catalyzed poly(ortho-ester) biodegradation, in: M. Vert, J. Feijen, A.C. Albertsson, G. Scott, E. Chiellini, (Eds), Biodegradable polymers and plastics, The Royal Society of Chemisty, Cambridge, 1992, pp. 214-225.

[198] R.P. Batycky, J. Hanes, R. Langer, D.A. Edwards, A theoretical model of erosion and macromolecular drug release from biodegrading microspheres, J. Pharm. Sci. 86 (1997) 1464-1477.

[199] V. Lemaire, J. Belair, P. Hildgen, Structural modeling of drug release from biodegradable porous matrices based on a combined diffusion/erosion process, Int. J. Pharm. 258 (2003) 95-107.

[200] S. Prabhu, S. Hossainy, Modeling of degradation and drug release from a biodegradable stent coating, J. Biomed. Mater. Res. A 80A (2007) 732-741.

[201] A. Gopferich, R. Langer, Modeling polymer erosion, Macromolecules 26 (1993) 4105-4112.

[202] A. Gopferich, Erosion of composite polymer matrices, Biomaterials 18 (1997) 397-403.

[203] A. Gopferich, Bioerodible implants with programmable drug release, J. Control. Release 44 (1997) 271-281.

[204] J. Siepmann, A. Gopferich, Mathematical modeling of bioerodible, polymeric drug delivery systems, Adv. Drug Deliver. Rev. 48 (2001) 229-247.

[205] C. Truesdell, K.R. Rajagopal, An introduction to the mechanics of fluids, Birkhäuser, Boston, 2000.

[206] C.A. Truesdell, A first course in rational continuum mechanics, 2nd edition, Academic Press, Boston, 1991.

[207] C. Truesdell, W. Noll, The non-linear field theories of mechanics, 3rd edition, Springer-Verlag, Berlin, New York, 2004.

[208] C.A. Truesdell, R.A. Toupin, The classical field theories, in: S. Flügge, (Ed), Handbuch der physik III/1, Springer, Berlin, 1960, pp. 226–793.

[209] W. Jaunzemis, Continuum mechanics, Macmillan, New York, 1967.

[210] P. Chadwick, Continuum mechanics: Concise theory and problems, 2nd edition, Dover Publications, Mineola, NY, 1999.

[211] M.E. Gurtin, An introduction to continuum mechanics, Academic Press, New York, 1981.

[212] W.S. Slaughter, The linearized theory of elasticity, Birkhäuser, Boston, 2002.

[213] C.A. Truesdell, Essays in the history of mechanics, Springer-Verlag, Berlin, 1968.

[214] K.R. Rajagopal, The elasticity of elasticity, Z. Agnew. Math. Phys. 58 (2007) 309-317.

[215] A.V. Tobolsky, Structure and properties of polymers, Interscience, New York, 1965.

[216] A. Wineman, K.R. Rajagopal, Mechanical response of polymers: An introduction, Cambridge University Press, Cambridge, 2000.

[217] J.D. Ferry, Viscoelastic properties of polymers, Wiley, New York, 1961.

[218] A. Wineman, Nonlinear viscoelastic membranes, Comput. Math. Appl. 53 (2007) 168-181.

[219] A.C. Pipkin, T.G. Rogers, A non-linear integral representation for viscoelastic behaviour, J. Mech. Phys. Solids 16 (1968) 59-72.

[220] A.S. Wineman, Large axially symmetric stretching of a nonlinear viscoelastic membrane, Int. J. Solids Struct. 8 (1972) 775-790.

[221] F.L. Dai, K.R. Rajagopal, A.S. Wineman, Nonuniform extension of a nonlinear viscoelastic slab, Int. J. Solids Struct. 29 (1992) 911-930.

[222] F.L. Dai, K.R. Rajagopal, Proportional shearing of a nonlinear viscoelastic layer, Int. J. Nonlinear Mech. 28 (1993) 57-68.

[223] F. Dai, A study on torsion of a nonlinear viscoelastic slab about noncoincident axes, Int. J. Solids Struct. 30 (1993) 3451-3465.

[224] Y.C. Fung, Stress-strain history relations of soft tissues in simple elongation, in: Y.C. Fung, N. Perrone, M. Anliker, (Eds), Biomechanics, its foundations and objectives, Prentice-Hall, Englewood Cliffs, NJ, 1972, pp. 181-208.

[225] J.M. Huyghe, D.H. Vancampen, T. Arts, R.M. Heethaar, The constitutive behavior of passive heart-muscle tissue - a quasi-linear viscoelastic formulation, J. Biomech. 24 (1991) 841-849.

[226] S.L.Y. Woo, G.A. Johnson, B.A. Smith, Mathematical-modeling of ligaments and tendons, J. Biomech. Eng. - T. ASME 115 (1993) 468-473.

[227] W. Yang, T.C. Fung, K.S. Chian, C.K. Chong, Viscoelasticity of esophageal tissue and application of a QLV model, J. Biomech. Eng. 128 (2006) 909-916.

[228] L.J. Dortmans, A.A. Sauren, E.P. Rousseau, Parameter estimation using the quasi-linear viscoelastic model proposed by Fung, J. Biomech. Eng. 106 (1984) 198-203.

[229] R. Quintanilla, G. Saccomandi, The importance of the compatibility of nonlinear constitutive theories with their linear counterparts, J. Appl. Mech. - T. ASME 74 (2007) 455-460.

[230] Z.L. Zhou, Creep and recovery of nonlinear viscoelastic materials of the differential type, Int. J. Eng. Sci. 29 (1991) 1661-1672.

[231] Z.L. Zhou, Creep and stress-relaxation of an incompressible viscoelastic material of the rate type, Int. J. Solids Struct. 28 (1991) 617-630.

[232] P.J. Flory, Principles of polymer chemistry, Cornell Univeristy Press, Ithaca, NY, 1953.

[233] I.M. Ward, Mechanical properties of solid polymers, Wiley-Interscience, New York, 1971.

[234] F. Rodriguez, C. Cohen, C. Ober, L.A. Archer, Principles of polymer systems, 5th edition, Taylor & Francis, New York, 2003.

[235] D. Garlotta, A literature review of poly(lactic acid), J. Polym. Environ. 9 (2001) 63-84.

[236] R.G. Sinclair, The case for polylactic acid as a commodity packaging plastic, J. Macromol. Sci. - Pure Appl. Chem. A33 (1996) 585-597.

[237] M.H. Hartmann, High molecular weight polylactic acid polymers, in: D.L. Kaplan, (Ed), Biopolymers from renewable resources, Springer-Verlag, Berlin, 1998, pp. 367-411.

[238] H. Benninga, A history of lactic acid making: A chapter in the history of biotechnology, Kluwer Academic Publishers, Boston, 1990.

[239] J. Lunt, Large-scale production, properties and commercial applications of polylactic acid polymers, Polym. Degrad. Stabil. 59 (1998) 145-152.

[240] G.B. Kharas, F. Sanchez-Riera, D.K. Severson, Polymers of lactic acid, in: D.P. Mobley, (Ed), Plastics from microbes, Hanser-Gardner, Munich, 1994, pp. 93-137.

[241] R.E. Drumright, P.R. Gruber, D.E. Henton, Polylactic acid technology, Adv. Mater. 12 (2000) 1841-1846.

[242] K. Jamshidi, S.H. Hyon, Y. Ikada, Thermal characterization of polylactides, Polymer 29 (1988) 2229-2234.

[243] J.R. Dorgan, H. Lehermeier, M. Mang, Thermal and rheological properties of commercial-grade poly(lactic acid)s, J. Polym. Environ. 8 (2000) 1-9.

[244] G. Perego, G.D. Cella, C. Bastioli, Effect of molecular weight and crystallinity on poly(lactic acid) mechanical properties, J. Appl. Polym. Sci. 59 (1996) 37-43.

[245] H. Tsuji, H. Takai, S.K. Saha, Isothermal and non-isothermal crystallization behavior of poly(l-lactic acid): Effects of stereocomplex as nucleating agent, Polymer 47 (2006) 3826-3837.

[246] P. De Santis, A.J. Kovacs, Molecular conformation of poly(L-lactic acid), Biopolymers 6 (1968) 299-306.

[247] H.M. De Oca, I.M. Ward, Structure and mechanical properties of poly(L-lactic acid) crystals and fibers, J. Poly. Sci. Pol. Phys. 45 (2007) 892-902.

[248] D. Sawai, T. Yokoyama, T. Kanamoto, M. Sungil, S.H. Hyon, L.P. Myasnikova, Crystal transformation and development of tensile properties upon drawing of poly(L-lactic acid) by solid-state coextrusion: Effects of molecular weight, Macromol. Symp. 242 (2006) 93-103.

[249] K. Takahashi, D. Sawai, T. Yokoyama, T. Kanamoto, S.H. Hyon, Crystal transformation from the alpha- to the beta-form upon tensile drawing of poly(L-lactic acid), Polymer 45 (2004) 4969-4976.

[250] D. Sawai, K. Takahashi, T. Imamura, K. Nakamura, T. Kanamoto, S.H. Hyon, Preparation of oriented beta-form poly(L-lactic acid) by solid-state extrusion, J. Poly. Sci. Pol. Phys. 40 (2002) 95-104.

[251] W. Hoogsteen, A.R. Postema, A.J. Pennings, G. Tenbrinke, P. Zugenmaier, Crystal-structure, conformation, and morphology of solution-spun poly(L-lactide) fibers, Macromolecules 23 (1990) 634-642.

[252] A.C. Renouf-Glauser, J. Rose, D.F. Farrar, R.E. Cameron, The effect of crystallinity on the deformation mechanism and bulk mechanical properties of plla, Biomaterials 26 (2005) 5771-5782.

[253] J.F. Mano, Study of the segmental dynamics in semi-crystalline poly(lactic acid) using mechanical spectroscopies, Macromol. Biosci. 5 (2005) 337-343.

[254] C. Migliaresi, D. Cohn, A. Delollis, L. Fambri, Dynamic mechanical and calorimetric analysis of compression-molded PLLA of different molecular-weights - effect of thermal treatments, J. Appl. Polym. Sci. 43 (1991) 83-95.

[255] L. Fambri, A. Pegoretti, R. Fenner, S.D. Incardona, C. Migliaresi, Biodegradable fibres of poly(L-lactic acid) produced by melt spinning, Polymer 38 (1997) 79-85.

[256] Y. Furuhashi, Y. Kimura, N. Yoshie, H. Yamane, Higher-order structures and mechanical properties of stereocomplex-type poly(lactic acid) melt spun fibers, Polymer 47 (2006) 5965-5972.

[257] N.A. Weir, F.J. Buchanan, J.F. Orr, D.F. Farrar, A. Boyd, Processing, annealing and sterilisation of poly-L-lactide, Biomaterials 25 (2004) 3939-3949.

[258] J.R. Sarasua, A.L. Arraiza, P. Balerdi, I. Maiza, Crystallinity and mechanical properties of optically pure polylactides and their blends, Polym. Eng. Sci. 45 (2005) 745-753.

[259] J.D. Humphrey, Cardiovascular solid mechanics: Cells, tissues, and organs, Springer, New York, 2002.

[260] K.D. Nelson, A. Romero, P. Waggoner, B. Crow, A. Borneman, G.M. Smith, Technique paper for wet-spinning poly(L-lactic acid) and poly(DL-lactide-co-glycolide) monofilament fibers, Tissue Eng. 9 (2003) 1323-1330.

[261] J.F. Mano, J.L.G. Ribelles, N.M. Alves, M.S. Sanchez, Glass transition dynamics and structural relaxation of PLLA studied by DSC: Influence of crystallinity, Polymer 46 (2005) 8258-8265.

[262] P.D. van de Witte, P. J., J.W.A. van den Berg, J. Feijen, Phase behavior of polylactides in solvent-nonsolvent mixtures, J. Poly. Sci. Pol. Phys. 34 (1996) 2553-2568.

[263] R.S. Rivlin, D.W. Saunders, Large elastic deformations of isotropic materials. 7. Experiments on the deformation of rubber, Philos. Tr. R. Soc. S.-A 243 (1951) 251-288.

[264] J.C. Criscione, Rivlin's representation formula is ill-conceived for the determination of response functions via biaxial testing, J. Elasticity 70 (2003) 129-147.

[265] A.G. James, A. Green, G.M. Simpson, Strain energy functions of rubber. 1. Characterization of gum vulcanizates, J. Appl. Polym. Sci. 19 (1975) 2033-2058.

[266] K.R. Rajagopal, A.R. Srinivasa, A.S. Wineman, On the shear and bending of a degrading polymer beam, Int. J. Plasticity 23 (2007) 1618-1636.

[267] K.R. Rajagopal, A.S. Wineman, A constitutive equation for nonlinear solids which undergo deformation induced microstructural changes, Int. J. Plasticity 8 (1992) 385-395.

[268] K.R. Rajagopal, A.R. Srinivasa, On the thermomechanics of materials that have multiple natural configurations - part i: Viscoelasticity and classical plasticity, Z. Agnew. Math. Phys. 55 (2004) 861-893.

[269] A. Wineman, Torsion of an elastomeric cylinder undergoing microstructural changes, J. Elasticity 62 (2001) 217-237.

[270] K.R. Rajagopal, A.R. Srinivasa, Mechanics of the inelastic behavior of materials--part 1, theoretical underpinnings, Int. J. Plasticity 14 (1998) 945-967.

[271] K.R. Rajagopal, A.R. Srinivasa, Mechanics of the inelastic behavior of materials. Part ii: Inelastic response, Int. J. Plasticity 14 (1998) 969-995.

[272] K.R. Rajagopal, A.R. Srinivasa, A thermodynamic frame work for rate type fluid models, J. Non-Newton. Fluid 88 (2000) 207-227.

[273] K.R. Rajagopal, A.R. Srinivasa, On the inelastic behavior of solids - part 1: Twinning, Int. J. Plasticity 11 (1995) 653-678.

[274] K.R. Rajagopal, A.R. Srinivasa, Inelastic behavior of materials. Part ii. Energetics associated with discontinuous deformation twinning, Int. J. Plasticity 13 (1997) 1-35.

[275] K.R. Rajagopal, A.R. Srinivasa, On the thermomechanics of shape memory wires, Z. Agnew. Math. Phys. 50 (1999) 459-496.

[276] K. Kannan, K.R. Rajagopal, Simulation of fiber spinning including flow-induced crystallization, J. Rheol. 49 (2005) 683-703.

[277] I.J. Rao, K.R. Rajagopal, A thermodynamic framework for the study of crystallization in polymers, Z. Agnew. Math. Phys. 53 (2002) 365-406.

[278] I.J. Rao, J.D. Humphrey, K.R. Rajagopal, Biological growth and remodeling: A uniaxial example with possible application to tendons and ligaments, CMES-Comp. Model. Eng. 4 (2003) 439-455.

[279] J.M. Krishnan, K.R. Rajagopal, Thermodynamic framework for the constitutive modeling of asphalt concrete: Theory and applications, J. Mater. Civil Eng. 16 (2004) 155-166.

[280] J.S. Soares, J.E. Moore, Jr., K.R. Rajagopal, Theoretical modeling of cyclically loaded biodegradable cylinders, in: F. Mollica, L. Preziosi, K.R. Rajagopal, (Eds), Modeling biological materials, Modeling and simulation in science, engineering and technology, Birkhauser, Boston, 2007, pp. 125-177.

[281] J.S. Soares, J.E. Moore, K.R. Rajagopal, Constitutive framework for biodegradable polymers with applications to biodegradable stents, ASAIO J. (2008) in press.

[282] S. Baek, A.R. Srinivasa, Diffusion of a fluid through an elastic solid undergoing large deformation, Int. J. Nonlinear Mech. 39 (2004) 201-218.

[283] A. Wineman, Some comments on the mechanical response of elastomers undergoing scission and healing at elevated temperatures, Math. Mech. Solids 10 (2005) 673-689.

[284] A. Wineman, J. Shaw, Combined deformation- and temperature-induced scission in a rubber cylinder in torsion, Int. J. Nonlinear Mech. 42 (2007) 330-335.

[285] J.A. Shaw, A.S. Jones, A.S. Wineman, Chemorheological response of elastomers at elevated temperatures: Experiments and simulations, J. Mech. Phys. Solids 53 (2005) 2758-2793.

[286] A. Wineman, J.H. Min, Inhomogeneity in a sheared elastomeric layer as a result of thermally induced scission and healing, Math. Mech. Solids 9 (2004) 17-35.

[287] A. Wineman, J. Shaw, A correspondence principle for scission-induced stress relaxation in elastomeric components, J. Appl. Mech. - T. ASME 71 (2004) 769-773.

[288] H.E. Huntley, A.S. Wineman, K.R. Rajagopal, Chemorheological relaxation, residual stress, and permanent set arising in radial deformation of elastomeric hollow spheres, Math. Mech. Solids 1 (1996) 267-299.

[289] H.E. Huntley, A.S. Wineman, K.R. Rajagopal, Stress softening, strain localization and permanent set in the circumferential shear of an incompressible elastomeric cylinder, IMA J. Appl. Math. 59 (1997) 309-338.

[290] J.C. Simo, J.W. Ju, Strain-based and stress-based continuum damage models. 1. Formulation, Int. J. Solids Struct. 23 (1987) 821-840.

[291] B.D. Coleman, M.E. Gurtin, Thermodynamics with internal state variables, J. Chem. Phys. 47 (1967) 597-613.

[292] D.C. Stouffer, A.S. Wineman, Linear viscoelastic materials with environmental dependent properties, Int. J. Eng. Sci. 9 (1971) 193-212.

[293] D.C. Stouffer, A.S. Wineman, Constitutive representation for linear aging, environmental-dependent viscoelastic materials, Acta Mech. 13 (1972) 31-53.

[294] D.C. Stouffer, A.M. Strauss, Continuum theory of degrading elastic solids with application to stress-corrosion, Int. J. Eng. Sci. 14 (1976) 915-924.

[295] D.C. Stouffer, A.M. Strauss, Theory of material divagation, Int. J. Eng. Sci. 16 (1978) 1019-1028.

[296] K.R. Rajagopal, A.S. Wineman, A note on viscoelastic materials that can age, Int. J. Nonlinear Mech. 39 (2004) 1547-1554.

[297] K. Kannan, A note on aging of a viscoelastic cylinder, Comput. Math. Appl. 53 (2007) 324-328.

[298] R.W. Ogden, D.G. Roxburgh, A pseudo-elastic model for the Mullins effect in filled rubber, P. Roy. Soc. Lond. A Mat. 455 (1999) 2861-2877.

[299] C.O. Horgan, G. Saccomandi, Constitutive modelling of rubber-like and biological materials with limiting chain extensibility, Math. Mech. Solids 7 (2002) 353-371.

[300] C.O. Horgan, R.W. Ogden, G. Saccomandi, A theory of stress softening of elastomers based on finite chain extensibility, P. Roy. Soc. Lond. A Mat. 460 (2004) 1737-1754.

[301] M.F. Beatty, The Mullins effect in a pure shear, J. Elasticity 59 (2000) 369-392.

[302] M.F. Beatty, S. Krishnaswamy, A theory of stress-softening in incompressible isotropic materials, J. Mech. Phys. Solids 48 (2000) 1931-1965.

[303] A.E. Zuniga, M.F. Beatty, A new phenomenological model for stress-softening in elastomers, Z. Agnew. Math. Phys. 53 (2002) 794-814.

[304] B. Bernstein, A. Shokooh, The stress clock function in viscoelasticity, J. Rheol. 24 (1980) 189-211.

[305] A. Wineman, J.H. Min, The pressurized cylinder problem for nonlinear viscoelastic materials with a strain clock, Math. Mech. Solids 1 (1996) 393-409.

[306] A.S. Wineman, Branching of strain histories for nonlinear viscoelastic solids with a strain clock, Acta Mech. 153 (2002) 15-21.

[307] U. Saravanan, K.R. Rajagopal, On the role of inhomogeneities in the deformation of elastic bodies, Math. Mech. Solids 8 (2003) 349-376.

[308] U. Saravanan, K.R. Rajagopal, Inflation, extension, torsion and shearing of an inhomogeneous compressible elastic right circular annular cylinder, Math. Mech. Solids 10 (2005) 603-650.

[309] R. Lazarov, Math 610: Numerical methods for PDE's, Texas A&M University, College Station, TX 2007.

[310] E.B. Becker, G.F. Carey, J.T. Oden, Finite elements: An introduction, Prentice-Hall, Englewood Cliffs, NJ, 1981.

[311] A. Ern, J.-L. Guermond, Eléments finis : Théorie, applications, mise en oeuvre, Springer, Berlin, 2002.

[312] J.N. Reddy, An introduction to the finite element method, 2nd edition, McGraw-Hill, New York, 1984.

[313] J.N. Reddy, An introduction to nonlinear finite element analysis, Oxford University Press, Oxford, 2004.

[314] D. Kincaid, W. Cheney, Numerical analysis: Mathematics of scientific computing, 3rd edition, Brooks/Cole Publishing, Pacific Grove, CA, 2002.

[315] J.R. Shewchuck, Triangle: A two-dimensional quality mesh generator and Delaunay triangulator, http://www.cs.cmu.edu/~quake/triangle.html (2002).

[316] J.C. Criscione, A constitutive framework for tubular structures that enables a semi-inverse solution to extension and inflation, J. Elasticity 77 (2004) 57-81.

[317] S.C. Prasad, Constitutive modeling of creep of single crystal superalloys, Ph.D. Dissertation, Texas A&M University, College Sation, TX, 2005.

[318] L.H. Timmins, M.R. Moreno, C.A. Meyer, J.C. Criscione, A. Rachev, J.E. Moore, Jr., Stented artery biomechanics and device design optimization, Med. Biol. Eng. Comput. 45 (2007) 505-513.

VITA

João Filipe da Silva Soares, Ph.D. was born in Lisboa, Portugal. He obtained his Licenciatura degree in aerospace engineering at the Instituto Superior Técnico da Univesidade Técnica de Lisboa in 2002. He came to College Station, Texas in the Summer of 2003 to pursue his doctorate degree with Dr. K. R. Rajagopal at Texas A&M University. The author can be reached at joao@tamu.edu and his permanent address is:

João Silva Soares
Rua José Gomes Ferreira, 23 – 6ºdto
2675-394 Odivelas
Portugal